2010

Bioluminescent mouse models of prostate cancer progression and therapy

Robert Ulf Svensson
University of Iowa

BIOLUMINESCENT MOUSE MODELS OF PROSTATE CANCER PROGRESSION AND THERAPY

by

Robert Ulf Svensson

An Abstract

Of a thesis submitted in partial fulfillment
of the requirements for the Doctor of
Philosophy degree in Molecular Physiology and Biophysics
in the Graduate College of
The University of Iowa

May 2010

Thesis Supervisor: Associate Professor Michael D. Henry

ABSTRACT

Prostate cancer is the most common visceral neoplasm and second leading cause of cancer death in US men. It is a complex heterogeneous and multi-factorial disease whose mechanistic basis is poorly understood. Furthermore, treatment options for advanced metastatic prostate cancer are limited and do not impart significant survival benefits, highlighting the need for novel and more effective therapeutic strategies. To this end we examined the use of RNAi therapy based on the systemic delivery of optimized small interfering RNAs (siRNAs) targeting the androgen receptor (AR). siRNA treatment induced massive cell death *in vitro* but was unable to induce tumor regression or improve survival in an animal model of advanced human prostate cancer due to inefficient cellular delivery and uptake of siRNAs at metastatic sites. To explore further, we developed a bioluminescent animal model that enables the high throughput screening of siRNA pharmacodynamic and biodistribution properties. Systemically delivered siRNAs, although potent, were only effective at inhibiting gene expression in the liver.

Reliable and tractable animal models of prostate cancer are needed in order to help better understand the molecular mechanisms of disease progression. Here we describe an improvement on the previously characterized *Pten* mutant model of prostate cancer by incorporation of a luciferase reporter allele. Specifically, the cancer initiating event is coupled to activation of firefly luciferase from the endogenous *ROSA26* promoter in the same prostate epithelial cells. Additionally, we have extensively backcrossed our model onto the albino C57BL6TYRC2J and BALB/c backgrounds which enhances bioluminescence imaging (BLI) sensitivity. Consistent with previous studies, we show that progression of prostate cancer from 3-12 weeks is rapid and correlates with an increase in bioluminescence. However, longitudinal BLI from 12-40 weeks reveals a plateau in bioluminescence signal that is correlated with a halt in cellular proliferation as evidenced by Ki67 staining at necropsy. In contrast to other studies, prostate cancer never

progressed beyond a high grade prostatic intraepithelial neoplasm (HGPIN). Furthermore, we demonstrate for the first time that cancer progression is accompanied by increased inflammation, characterized by enhanced recruitment of myeloid derived suppressor cells (MDSCs). We further demonstrate the utility of B6-Luc mice in monitoring response to prostate cancer therapy.

Relatively few established risk factors for prostate cancer have been identified. Obesity has been linked to increased mortality rates in prostate cancer patients. Using B6-Luc mice we demonstrate that obesity induced a prostatic inflammatory response characterized by increased expression of *IL-6* and *IL-1β*. However, the effects of obesity on prostate cancer progression were inconclusive due to the small number of animals enrolled in the study. Taken together, we have developed novel model systems that will enable the mechanistic basis of prostate cancer progression and response to therapy to be evaluated in the appropriate experimental context.

Abstract Approved: _____
Thesis Supervisor

_____
Title and Department

_____
Date

BIOLUMINESCENT MOUSE MODELS OF PROSTATE CANCER PROGRESSION AND THERAPY

by

Robert Ulf Svensson

A thesis submitted in partial fulfillment
of the requirements for the Doctor of
Philosophy degree in Molecular Physiology and Biophysics
in the Graduate College of
The University of Iowa

May 2010

Thesis Supervisor: Associate Professor Michael D. Henry

Graduate College
The University of Iowa
Iowa City, Iowa

CERTIFICATE OF APPROVAL

_____

PH.D. THESIS

_____

This is to certify that the Ph.D. thesis of

Robert Ulf Svensson

has been approved by the Examining Committee
for the thesis requirement for the Doctor of Philosophy
degree in Molecular Physiology and Biophysics at the May 2010 graduation.

Thesis Committee: _____
Michael D. Henry, Thesis Supervisor

_____
Kevin P. Campbell

_____
Adam Dupuy

_____
Robert Piper

_____
Peter Mohler

To Irina.

ACKNOWLEDGMENTS

I would like to thank Michael Henry for his enthusiasm, guidance and great mentorship over the past 5 years. I would also like to thank Henry lab members, both past and present, for all their help and fruitful discussion overs the years. I would also like to thank the members of my thesis committee for their advice throughout my thesis. Finally I would like to thank Kamal Rahmouni for his expert advice during collaboration, Tom Moninger and the central microscopy research facility for their expertise, Jessica Haverkamp for assistance with flow cytometry, Oskar Rokhlin and Michael Cohen for their expert assistance and all the administrative members of the Department of Molecular Physiology and Biophysics for their hard work.

TABLE OF CONTENTS

LIST OF TABLES vii

LIST OF FIGURES viii

CHAPTER

I. INTRODUCTION 1

Prostate Cancer 1
Prostate Cancer Epidemiology 3
Mouse Models of Prostate Cancer 7
Small Animal Imaging in Cancer 10
Prostate Cancer Therapy 12
Hormone Refractory Prostate Cancer 14
RNAi and siRNA Therapeutics 16
Relevance and Focus of the Project 19

II. ANDROGEN RECEPTOR TARGETED SIRNA THERAPY FOR ADVANCED PROSTATE CANCER 21

Introduction 20
Materials and Methods 24
Bioluminescene Imaging 24
Mouse models of prostate cancer 24
Cell culture and generation of luciferase expressing cell lines 25
Cell viability assays 25
Design and generation of siRNAs 25
AR western blots 26
siRNA treatments 27
Results 27
Design and *in vitro* potency of AR siRNAs 27
Formulation of AR siRNAs using cholesterol, liposomes or atelocollagen 28
Efficacy of formulated siRNAs *in vivo* 29
Discussion 31

III. ASSESSING SIRNA PHARMACODYNAMICS IN A LUCIFERASE EXPRESSING MOUSE 41

Introduction 41
Materials and Methods 43
Animals 43
Bioluminscence imaging 43
In vitro and in vivo liposomal siRNA treatments 44
RNA and protein preparation from tissues 45
Quantitative RTPCR of luciferase mRNA and luciferase activity assay 46
Lymphocyte purification and adoptive transfer 46
Statistical analyses 46
Results 47

Generation of a ubiquitous luciferase-expressing mouse 47
FLASH mice can be used as donors for immune cell trafficking and transplantation studies 48
FLASH mice are suitable for studying the pharmacodynamics of systemically delivered siRNAs.....49
Discussion.....51

IV. CHEMOTHERAPEUTIC AGENTS UPREGULATE THE CYTOMEGALOVIRUS PROMOTER: IMPLICATIONS FOR BIOLUMINESCENCE IMAGING OF TUMOR RESPONSE TO THERAPY 61

Introduction.....61
Materials and Methods 63
Cell culture and generation of luciferase expressing cell lines 63
Drug treatments 63
Bioluminescence imaging 64
Caspase 3 assay and cell viability assays 65
Quantitative-RTPCR of luciferase mRNA 65
Luciferase activity assay.....66
Subcutaneous tumor model 66
P38MAPK western blot.....67
Statistical analyses.....67
Results.....68
Treatment of luciferase expressing cells with apoptosis inducing agents results in a transient increase in bioluminescence.....68
Bioluminescence can be induced by translation-independent and translation dependent mechanisms 70
Doxorubicin treatment of subcutaneous luciferase expressing xenograft tumors leads to a transient increase in bioluminesence *in vivo* 73
Inhibition of the p38MAPK pathway blocks doxorubicin and staurosporine induced bioluminescence in 22Rv1-CMV cells 74
Discussion.....75

V. CHARACTERIZATION OF A NOVEL MOUSE MODEL OF PROSTATE CANCER.....92

Introduction.....92
Materials and Methods 95
Mouse Strains and Genotyping 95
Bioluminescence Imaging 95
RNA and protein preparation from tissues.....96
PCR and luciferase activity assay.....96
Immunofluorescence and antibodies 96
Haematoxylin, Eosin and Massons Trichrome staining.....97
Senescence associated β-Galactosidase stain 98
2- Deoxyglucose uptake 98
Rapamycin treatment of B6-Luc mice 98
Castrations of B6-Luc mice.....99
FACS analysis of inflammatory subsets.....99
Results.....100
Generation of a novel model of prostate cancer.....100
Bioluminescence in B6-Luc mice is restricted to the prostate 100

BLI of cancer progression in B6-Luc and Balbc-Luc mice 101
Pathologic changes in *Pten* $^{-/-}$ and *Pten* $^{+/-}$ B6-Luc and Balbc-Luc mice 103
Pten $^{-/-}$ B6-Luc mice respond to androgen deprivation and develop rare neuoroendocrine features 104
Aged *Pten* $^{-/-}$ B6-Luc display focal loss of glycosylated dystroglycan 106
Myeloid derived suppressor cells (MDSCs) are recruited to prostates of *Pten* $^{-/-}$ B6-Luc mice.....107
Pten $^{-/-}$ B6-Luc mice respond to Rapamycin treatment 108
Discussion.....109

VI. DIET INDUCED OBESITY AND PROSTATE CANCER PROGRESSION 139

Introduction.....139
Materials and Methods 142
Mouse Strains and Genotyping 142
Bioluminescence Imaging 142
Diet induced obesity 143
Plasma biomarker analysis 143
Histological and immunfluorscence assays.....143
Results.....144
Generation of study cohorts.....144
High fat diet induces obesity in B6-Luc mice 145
Diet induced obesity increases levels of plasma biomarkers 146
Bioluminescence intensity is not significantly different between control vs high fat fed B6-Luc mice.....146
Diet induced obesity enhances production of pro-inflammatory cytokines but does not affect cancer progression in B6-Luc mice 147
Discussion.....148

VII. SUMMARY AND FUTURE DIRECTIONS.....160

REFERENCES 179

LIST OF TABLES

Table

2.1. Doxorubicin and paclitaxel-induced increase in bioluminescence is accompanied by an induction of apoptosis and a loss in cell viability 84

5.2 Table showing numbers of mice used for each experiment.....138

LIST OF FIGURES

Figure

2.1. siRNAs effectively reduce AR expression in prostate cancer cell lines....36

2.2. siRNAs targeting AR induce cell death in AR positive but not AR negative prostate cancer cell lines....37

2.3. Liposomal si-Luc is effective at inhibiting luciferase expression in the absence of transfection reagent....38

2.4. Atelo-Luc and Lipo-Luc are ineffective at inhibiting luciferase expression *in vivo*....39

2.5. Formulated siRNAs are unable to induce tumor regression or improve survival in a mouse model of advanced prostate cancer....40

3.1. Generation of ubiquitous luciferase expressing mice....55

3.2. FLASH mice exhibit ubiquitous luciferase expression....56

3.3. Imaging adoptively transferred FLASH lymphocytes *in vivo*....57

3.4. Longitudinal BLI of adoptively transferred lymphocytes....58

3.5. Liposomal siRNA efficacy in FLASH mice....59

3.6. Assessing pharmacodynamics of si-Luc *in vivo*....60

4.1. AR siRNAs induce an increase in bioluminescence in 22Rv1 cells that is inversely correlates with cell viability....81

4.2. Staurosporine induces a transient increase in bioluminescence in luciferase expressing prostate carcinoma cells....82

4.3. Doxorubicin, staurosporine and paclitaxel induce a transient increase in bioluminescence in luciferase expressing prostate carcinoma cells....83

4.4. Chemotherapeutics doxorubicin and paclitaxel induce a transient increase in bioluminescence in 22Rv1-CMVluc and PC3-CMVluc cells but not 22Rv1-SV40luc cells....85

4.5. Trichostatin-A (TSA) induces bioluminescence and AR gene expression in cells engineered to express luciferase and AR from the CMV promoter....86

4.6. Bioluminescence can be induced by translation-independent and translation-dependent mechanisms....87

4.7. Doxorubicin treatment increases luciferase mRNA and protein in 22Rv1-CMVluc cells but not 22Rv1-SV40luc cells....88

4.8. Doxorubicin treatment of 22Rv1-CMVluc subcutaneous xenograft tumors leads to a transient increase in luciferase expression *in vivo* 89

4.9. Doxorubicin treatment of 22RV1-SV40luc subcutaneous xenograft tumors does not affect luciferase expression *in vivo* 90

4.10. Inhibition of the p38MAPK pathway blocks the doxorubicin and staurosporine-induced increase in bioluminescence....91

5.1. Generating a novel mouse model of spontaneous prostate cancer 117

5.2. Prostate specific bioluminescence in B6-Luc mice 118

5.3. Loss of *Pten* expression in epithelial cells of *Pten* -/- B6-Luc mice 119

5.4. Induction of pAKT473 in *Pten* -/- B6-Luc mice 120

5.5. Bioluminescence imaging of prostate cancer progression in B6-Luc and Balbc-Luc mice....121

5.6. Ki67 positive proliferative levels in 6 week old B6-Luc mice 122

5.7. Ki67 positive proliferation levels in 25 week old B6-Luc mice.....123

5.8. Senescence associated β-Gal activity and metabolic activity of B6-Luc mice. 124

5.9. Pathologic changes in *Pten* -/- B6-Luc mice 125

5.10. Pathologic changes in *Pten* -/- Balbc-Luc mice....126

5.11. Focal HGPIN is evident in 6 month old *Pten* +/- B6-Luc mice 127

5.12. Spontaneous tumor development in 18 month old *Pten* +/- Balbc-Luc mice.....128

5.13. Response to castration and development of castrate resistance in B6-Luc mice....129

5.14. Early emergence of castrate resistance in B6-Luc mice 130

5.15. Localization of *Foxa2* positive cells in castrate resistant B6-Luc mice 131

5.16. Localization of *Chromogranin A* positive cells in castrate resistant B6-Luc mice....132

5.17. Focal loss of glycosylated α-DG expression in B6-Luc mice 133

5.18. Increased numbers of basal cells in *Pten* -/- B6-Luc mice 134

5.19. MDSCs are recruited to the prostate lobes of *Pten* -/- B6-Luc mice....135

5.20. *Pten* -/- B6-Luc respond to rapamycin therapy 136

5.21. Rapamycin reduces pS6 expression in *Pten* -/- B6-Luc mice 137

6.1. Generation of B6-Luc study cohorts....153

6.2. Diet induced obesity in B6-Luc mice 154

6.3. High fat diet increases plasma leptin and insulin levels in B6-Luc mice 155

6.4. BLI of prostate cancer progression in high fat fed and control B6-Luc mice 156

6.5. Increased stromal response and epithelial cell proliferation in high fat fed mouse #1480 157

6.6. Increased expression of *IL-6* and *IL-1β* in diet induced obesity 158

6.7. No differences in Ki67 or pAKT473 expression in diet induced obesity 159

7.1. Recruitment of MDSCs in prostates of aged POET-3 *Pten* +/- mice & increased infiltration during acute prostatitis 174

7.2. Pathological changes in prostates of induced POET-3 *Pten* +/- mice 175

7.3. BLI of prostate cancer progression during diet induced obesity in *Pten* -/- B6-Luc animals 176

7.4. Leptin receptor mRNA expression and effects of leptin on prostate cancer cell growth 177

7.5. Construction and efficacy of AAV8-Leptin *in vitro* and *in vivo* 178

CHAPTER I

INTRODUCTION

Prostate Cancer

Prostate cancer is the most common visceral neoplasm in men in most western populations and is the second leading cause of cancer death among men in the USA (Jemal, Siegel et al. 2009). It is estimated that there are currently around 2 million American men living with prostate cancer (American Cancer Society). About 1 man in 6 will be diagnosed with prostate cancer during their lifetime and 1 in 35 will die from the disease (Jemal, Siegel et al. 2009). Prostate cancer was responsible for an estimated 27360 deaths in U.S men during 2009 (Jemal, Siegel et al. 2009). Despite prostate cancer's high morbidity, death rates have continually declined since the 1990's. However, it is unclear weather this decline is due to the use of early detection tests for prostate cancer or other factors such as improvements in treatment or lifestyle changes (Edwards, Ward et al. 2010). Prostate cancer can be found early through the use of the Prostate Specific Antigen test (PSA test) or the Digital Rectal Exam (DRE) (Borley and Feneley 2009). Unfortunately, neither the PSA test nor the DRE are 100% accurate and it is thought that prostate cancer is generally an over-treated disease in males because high PSA levels alone do not give doctors enough information to distinguish between prostate cancer and other complications such as prostatitis or benign prostatic hyperplasia (BPH) (Shariat, Scardino et al. 2008; Welch and Albertsen 2009).

Prostate cancer is a complex multifactorial disease that displays extensive heterogeneity (Mackinnon, Yan et al. 2009). In most cases, prostate cancer is slow growing and takes many years to develop into a detectable tumor. However, because of its heterogeneous growth patterns some patients will experience a more rapidly growing

and aggressive prostate cancer. It is very difficult to ascertain whether a prostate cancer will become clinically aggressive or remain indolent throughout a man's lifetime, complicating treatment options (Gittes 1991). Despite these difficulties, some progress has been made on trying to determine the morphological lesions that may act as potential precursor lesions. The most likely precursor lesion to prostate cancer is prostatic intraepithelial neoplasia (PIN) (Foster, Burns et al. 2000). PIN is a proliferative lesion characterized by cytological abnormalities within the prostatic ducts and is classified as either low grade (LG) or high grade (HG) based on the degree of cytological changes (Sakr and Partin 2001). HGPIN increases in frequency with age and is associated with prostate cancer, otherwise termed prostatic adenocarcinoma (Sakr, Grignon et al. 1996). It has not been well established whether HGPIN is a significant predictor of subsequent prostate cancer as studies are conflicting. Some clinicopatholgical evidence suggests that HGPIN can act as an independent risk factor for prostate cancer (Haggman, Macoska et al. 1997; Merrimen, Jones et al. 2009). Prostate cancer was diagnosed in significantly more men with HGPIN on initial biopsy than in those with benign prostates even after taking into account age, PSA levels and sign out pathologist. However, other studies find no relationship between the two but note that HGPIN is still a useful marker for clinically significant prostate adenocarcinoma (Delatour and Mai 2008).

Most prostate cancers are adenocarcinomas due to the glandular nature of the prostate. Adenocarcinomas of the prostate are graded based on their degree of differentiation and aggressiveness. The most widely used grading scheme in the US is the Gleason system which is based entirely on the architectural growth patterns of the prostatic carcinoma (Mellinger, Gleason et al. 1967; Gleason and Mellinger 1974). Five basic grade patterns are used to generate a Gleason score ranging from 2-10 by combining the most common (primary and secondary) patterns of cancer within the specimen (Gleason and Mellinger 1974). The higher the Gleason score, the worse the prognosis. For prostate cancer, the grade information is used with prostate cancer stage to

group cases into an overall category. The stages of prostate cancer refer to the size of the tumor and how far it has spread. The most common staging system is the TNM system which evaluates the size of the tumor (T) and the degree of lymph node (N) and distant metastasis (M) (Wallace, Chisholm et al. 1975). These are grouped into four stages (I-IV). Localized prostate cancer refers to a tumor that remains confined to the prostate and are graded as either stage I or stage II depending on how advanced the tumors are. During regional prostate cancer, the tumor has spread beyond the prostate capsule and into nearby tissues such as the seminal vesicles or nearby muscles. This is referred to as stage III prostate cancer. In metastatic prostate cancer the tumor has spread to nearby lymph nodes or to other parts of the body such as bones, liver or the lungs. Metastatic prostate cancer is referred to as stage IV prostate cancer and is the most common cause of death in prostate cancer patients (Scher 2003). Unfortunately, the cellular and molecular pathways that contribute to the genesis and progression of prostate cancer remain poorly understood.

Prostate Cancer Epidemiology

Prostate cancer etiology remains obscure with a large number of putative risk factors and relatively few established risk factors (Hsing and Chokkalingam 2006) . Age is the strongest established risk factor for prostate cancer. The incidence of prostate cancer rises exponentially with age, more so than any other disease (Parkin, Pisani et al. 1999). Prostate cancer is very uncommon in men under the age of 50 (~0.1% of all cases). Over 85% of prostate cancers are diagnosed in men over age 65 (Patel and Klein 2009). Another poorly understood risk factor is ethnicity. Prostate cancer incidence and mortality rates are highest in African American men and lowest in men on the Asian continent, specifically Chinese, Indian and Japanese men (Hsing and Chokkalingam 2006; Patel and Klein 2009). African American males are more than twice as likely to die

from prostate cancer as white men (Hsing and Chokkalingam 2006). Additionally, migratory studies have found that Japanese men who migrate to the US continent have increased risk of developing prostate cancer within one generation (Gronberg 2003). The reasons for these ethnical differences are not known and it is thought to involve a complex interplay between genetic, environmental and lifestyle differences associated with prostate cancer. Studies have also indicated that hereditary factors may be responsible for prostate cancer. Men with a first degree male relative with prostate cancer have a 2-3 fold increase risk of prostate cancer (Spitz, Currier et al. 1991).

Many putative risk factors ranging from infection to environmental susceptibility and inflammation have also been implicated in prostate cancer development and progression. There continues to be considerable debate about the role of diet on prostate cancer risk due to many contradicting studies. Although western diets, which are typically high in fats and low in grains, fruits and vegetables, have been associated with a higher risk of prostate cancer, it is extremely difficult to determine the 'smoking gun' or direct cancer initiator. Fat intake is the most frequently studied dietary risk factor for prostate cancer. Most studies have reported a positive association between monounsaturated and animal fats with increased prostate cancer risk (West, Slattery et al. 1991; Bairati, Meyer et al. 1998). Researchers have found that diets high in vegetable and fruits may be helpful in preventing prostate cancer (Chan, Lok et al. 2009). Consumption of tomatoes, cauliflower, broccoli and green tea seemed to impose a decreased risk for prostate cancer (Ma and Chapman 2009). The effect of tomatoes has largely been attributed to the anti-oxidant effect of lycopenes (Krek, Grun et al. 2005). Excessive dietary calcium may infer an increased risk of prostate cancer (Gao, LaValley et al. 2005; Severi, English et al. 2006). However, studies have been contradictory and recent data suggests that in older Americans a high intake of calcium has a significant impact on risks for some cancers but no risk for prostate cancer (Park, Mitrou et al. 2007).

Approximately 20% of all adult human cancers result from chronic inflammation (De Marzo et al. 1999). Growing evidence suggests a role for chronic inflammation in prostate cancer. Furthermore, epidemiological studies have noted that users of anti-inflammatory agents such as aspirin or non steroidal anti-inflammatory drugs (NSAIDs) have a reduced risk of prostate cancer (Jacobs et al. 2005). Chronic inflammation can be induced by a number of stimuli including infectious agents, trauma, urine reflux and dietary factors (De Marzo et al 1999). Chronic inflammation is thought to promote tumor onset through a number of mechanisms including the production of DNA damaging agents such as peroxynitrites; the production of pro-angiogenic factors and the production of matrix metalloproteases. Recent data also suggests that defective anti-tumor immunity through activation of myeloid derived suppressor cells (MDSCs) offers a unique mechanism of tumor promotion (Youn, Nagaraj et al. 2008). Several studies have correlated the presence of inflammatory cytokines, chemokines and growth factors with prostate cancer. However, a direct relationship between prostate cancer and inflammation has yet to be demonstrated due to limitations in the field (Haverkamp et al. 2008). A thorough understanding of prostate specific inflammation and the development of animal models that allow inflammation to be studied directly in the prostate will allow us to further understand the dynamic role of prostate inflammation and its impact on prostate cancer development and progression.

Recent studies suggest that obesity may also be a risk factor for prostate cancer (Andersson, Wolk et al. 1997; Calle, Rodriguez et al. 2003) as well as many other cancers such as breast and colon. Studies examining whether obesity acts a risk factor for prostate cancer development have reported mixed results. In some cases, obesity has been associated with reduced risk of prostate cancer (Giovannucci, Rimm et al. 2003). However, more of a consensus seems to be apparent on the effects of obesity on prostate cancer progression. Obesity has consistently been related to more aggressive prostate cancers and increased risk of death from prostate cancer. Several large cohort studies by

the American Cancer Society, namely the cancer prevention studies, have identified increased rates of death in obese prostate cancer patients (Rodriguez, Patel et al. 2001). A study of 135000 construction workers in Sweden found similar results. Men in the highest body mass index (BMI) category were 40% more likely to die of prostate cancer than the men in the lowest BMI category (Andersson, Wolk et al. 1997). Another study followed 752 men aged 40-64 and newly diagnosed with prostate cancer. In a nine year follow up, men who had been obese before prostate cancer diagnosis were 2.6 times more likely than men with a normal BMI to die of prostate cancer (Gong, Agalliu et al. 2007). Obesity has also been associated with an increased rate of progression and metastasis after therapy suggesting it may contribute to the acquisition of androgen independent prostate cancer (Amling, Riffenburgh et al. 2004; Freedland, Aronson et al. 2004; Strom, Wang et al. 2005). Furthermore, the prevalence of obesity correlates with prostate cancer risk across populations. However, these observations may be explained in part by detection bias making the association between obesity and prostate cancer complex (Freedland and Aronson 2005).

Experiments in mouse models of prostate cancer have attempted to validate the epidemiological findings and establish a relationship between obesity and prostate cancer in an experimental context. However, most have focused on the role of caloric restriction and how it may hinder prostate cancer progression. An isocaloric low fat diet was found to significantly slow tumor growth of LAPC-4 cells in a xenograft model of prostate cancer (Ngo, Barnard et al. 2003). A low fat diet was also able to delay the development of invasive prostatic adenocarcinoma in a spontaneous mouse model of prostate cancer (Kobayashi, Barnard et al. 2008). Another study demonstrated that a reduction in body fat and lean mass, without changing food intake, can significantly delay carcinogenesis (Huffman, Johnson et al. 2007). Few studies to date have actually tested directly the effects of obesity on prostate cancer progression in animal models. Leung *et al* found no

effect of high fat diet on the promotion of induced prostate carcinogenesis in the noble rat model (Leung, Benzie et al. 2002).

Although the mechanisms of how obesity might promote prostate cancer progression are unknown, several have been proposed. Increased adiposity leads to increased production of adipokines such as leptin. A sizeable number of studies have indicated that leptin may potentiate the growth and migratory properties of cancer cells (Onuma, Bub et al. 2003; Somasundar, Yu et al. 2003). Clinical studies have also shown that increased serum leptin was associated with larger and higher grade prostate tumors (Stattin, Soderberg et al. 2001). Several other pro-inflammatory adipocyte secreted factors such as *TNFα* and *IL-6* , levels of which are elevated in obese patients, have also been implicated in prostate cancer progression (Rajala and Scherer 2003). Decreased levels of testosterone that are associated with obesity may also promote the development of lethal androgen independent prostate cancer. However, in order to validate these epidemiological findings in an appropriate experimental context, future studies are needed in suitable animal models.

Mouse Models of Prostate Cancer

Studying the cellular and molecular mechanisms of prostate cancer progression in humans is difficult. Therefore, model organisms are needed in order to help better understand and treat this disease. The development of genetically engineered mouse models (GEM) of prostate cancer has greatly improved our ability to study disease progression and enhanced the pre-clinical assessment of novel therapeutic agents (Singh and Johnson 2006). However, it is important to understand the differences in comparative anatomy and histology between rodents and humans when interpreting data from GEM models. Both mouse and humans have similar epithelial cell types (luminal, basal and neuroendocrine) in their prostates but their ratio and distribution varies (Roy-Burman,

Wu et al. 2004). There are also significant differences in the stroma. The human prostate has a dense stroma composed of muscle and fibrous tissue compared to the mouse which has a very modest stromal compartment. The human prostate is a single alobular structure that is divided into three zones; central, peripheral and transitional (McNeal 1988). The mouse prostate consists of four paired lobes, anterior, dorsal, lateral and ventral that are situated at the base of bladder and surround the urethra. However, some of the zones in the human prostate are considered analogous to murine prostate lobes. The dorsal lateral prostate is considered most similar to the human peripheral zone and the central zone is considered analogous to the mouse anterior prostate. Despite some apparent differences, both species harbor functionally equivalent prostate glands. However, unlike the mouse, the human prostate is prone to spontaneously develop prostate pathology. Therefore in order for mice to develop prostate cancer they must be genetically altered. Alternatively, mice can be used to model prostate cancer by injecting them with human prostate cancer cells. Such xenograft models have been central in our ability to understand prostate cancer and important for developing therapies for its treatment. However, xenograft models are typically based on the propagation of human cancer cell lines in immunocompromised mice. Because of this, they do not recapitulate conditions of the tumor microenvironment and do not account for influence of the immune system during cancer progression. For these reasons and others, GEM models offer several advantages over xenograft models of prostate cancer (Sharpless and Depinho 2006). The last decade has seen the development of a number of GEM models of prostate cancer (Roy-Burman, Wu et al. 2004; Kasper 2005). Typically these are generated through either overexpression of an oncogene or deletion of a tumor suppressor gene via the use of prostate specific promoter. The availability of several prostate specific promoters in theory allows for virtually any gene to be overexpressed or deleted. However, genes that are usually altered in human prostate cancers are the candidate choices. Examples such as members of the fibroblast growth factor family (FGF) and FGF receptors (FGFR) have

been overexpressed in the mouse prostate epithelium in an attempt to model human prostate cancer (Song, Wu et al. 2002; Freeman, Welm et al. 2003). Overexpression in these models was sufficient to induce phenotypic changes in both the epithelium and stromal compartment. However, pathologic changes did not progress beyond HGPIN indicating that additional oncogenic events may be required. The serine threonine protein kinase *AKT* is also commonly overexpressed in human prostate cancers and was therefore targeted for overexpression in the mouse. Using a constitutively active form of *AKT*, Majumder *et al* demonstrated that mice developed pathological features consistent with PIN that never progressed to invasive carcinoma or metastasis (Majumder, Yeh et al. 2003). Alternatively, GEM models have also utilized overexpression of viral oncogenes, chosen due to their ability to inhibit critical tumor supressor genes. One of the first viral oncogene overexpression models involved expression of viral *SV40* large T antigen in the prostate via the prostatic steroid binding protein C31 gene (Maroulakou, Anver et al. 1994). Large T antigen functions by inhibiting activity of *p53* and Retinoblastoma (*Rb*), two well studied and frequently mutated genes in human cancer. Male transgenic mice developed prostate neoplasias that eventually progressed to an adenocarcinoma and metastasized. Since then other models have been developed through prostate specific expression of viral oncoproteins. Transgenic adenocarcinoma of the mouse prostate (TRAMP) mice used the rat probasin promoter to drive expression of both large and small T antigens in the prostate epithelium (Greenberg, DeMayo et al. 1995; Gingrich, Barrios et al. 1997). A similar model, the LADY, was designed used a smaller version of the promoter and only expressed the large T antigen in the same compartment (Kasper, Sheppard et al. 1998). Although both models have been useful in analyzing various parameters of disease progression they also display some limitations in their ability to accurately model human prostate cancer. For example, viral oncoproteins are not naturally associated with human prostate cancer and the neuoroendocrine differentiation that they develop is not a phenotype commonly observed in most human prostate cancers.

Perhaps the most reliable GEM model for prostate cancer is the phosphatase and tensin homologue (*Pten*) knockout model. *Pten* is one of the most frequently mutated tumor suppressor genes in cancer and its conditional deletion in prostate epithelial cells *in vivo* was found to recapitulate many of the steps observed in progression of human prostate cancers (Wang, Gao et al. 2003). Mice developed histopathological features like PIN right through to distant metastases in a relatively rapid time frame. Because prostate cancer in these mice develops into an adenocarcinoma with 100% penetrance, this model is believed to be one of the most biologically relevant. Although such models offer a unique opportunity to study prostate cancer progression, because tumor growth cannot be assessed directly in visceral prostate tissue often postmortem studies using large cohorts of mice are needed. Thus, such a study is neither efficient nor cost effective. However, imaging techniques can be applied to overcome this problem. Advances in small animal imaging techniques such as bioluminescence imaging (BLI), magnetic resonance imaging (MRI) and positron emission tomography (PET) have enabled effective non invasive visualization of tumor growth and response to therapy *in vivo* (Gross and Piwnica-Worms 2005). The application of BLI to GEM models of prostate cancer is now becoming popular and will allow researchers unique opportunities to study carcinogenesis (Contag, Spilman et al. 1997). However, in order for GEM models to be more widely used for cancer progression and prevention studies, refinements are still needed (Pienta, Abate-Shen et al. 2008).

Small Animal Imaging in Cancer

The increasing number of studies performed in animal models has stimulated the development of novel molecular imaging modalities adapted to circumvent the constraints of routine methodologies. Thus, novel these novel methods allow the researcher to study non invasive longitudinal dynamic processes in living specimens

(Gross and Piwnica-Worms 2005). Several imaging strategies can be employed that enable cancer growth and progression to be visualized non invasively.

Nuclear imaging modalities such as positron emission tomography (PET) and single photon emission computed tomography (SPECT) are highly sensitive and quantitative. These strategies are based on imaging decaying radionuclides that are administered to the patient. During the decaying process energy is released in the form of gamma rays that are then detected by sophisticated imaging equipment. In mice, PET and SPECT have been used to monitor the efficacy of gene therapy vectors, expression of extracellular receptors and trafficking of lymphocytes (Tjuvajev, Finn et al. 1996; MacLaren, Gambhir et al. 1999; Melder, Munn et al. 2002). However, such processes demand expensive and highly sophisticated instrumentation and often dedicated facilities with committed personnel (Gross and Piwnica-Worms 2005).

Magnetic resonance imaging (MRI) allows for the sensitive detection of soft tissue pathologies due to its excellent soft tissue contrast properties. MRI utilizes a magnetic field to align spinning protons (usually hydrogen atoms). A radio frequency pulse is then used to change the alignment and their return to baseline is recorded as a change in electromagnetic flux. The timing parameters of pulse and recording are altered resulting in differences in magnetic contrast that can be used to construct an image. High resolution MRI has been successfully used to visualize tumor size and metastatic burden in mice (Gillies, Bhujwalla et al. 2000).

Optical imaging techniques such as fluorescence and bioluminescence provide simple and cost effective strategies to image fundamental biological processes *in vivo*. In fluorescence imaging, the energy from an external source of light is absorbed and immediately re-emitted at a longer wavelength of lower energy. Fluorescent reporters do not require a substrate molecule, providing them with an advantage over other optical reporters. However, fluorescence imaging is not quantitative and tissue penetrance is

poor. Nonetheless, fluorescence imaging has been used successfully to detect tumor growth *in vivo* (Kaneko, Yano et al. 2001).

Bioluminescence imaging (BLI) involves the detection of photons of light from cells expressing a luciferase enzyme. The oxidation of a substrate molecule by luciferase in the presence of magnesium and ATP generates photons of light than can be captured using a sensitive charge coupled device camera (CCD). BLI is a sensitive, simple to execute and cost efficient means to monitor biological processes non invasively (Gross and Piwnica-Worms 2005). Luciferase reporters can be introduced into either transplantable cell lines or genetically modified cancer prone mice and is therefore becoming a popular choice of imaging modality. Furthermore, genetic manipulation of the luciferase reporter or modification of the substrate continues to advance the potential of BLI in small animals (Shah, Tung et al. 2005; Wehrman, von Degenfeld et al. 2006; Wurdinger, Badr et al. 2008). BLI is not likely to be used in human patients because stable expression of the luciferase reporter is required but BLI has enabled, and will continue to facilitate, the efficient monitoring of a number of biological processes such as primary tumor growth and response to therapy in animal models.

Prostate Cancer Therapy

Modern methods of detection and treatment options have improved the prognosis for prostate cancer patients. Because 90% of prostate cancers are detected in the local and regional stages, the cure rate for prostate cancer is very high (Jemal, Siegel et al. 2009). The 5 yr survival rate (percentage of patients who live at least 5 yrs after prostate cancer diagnosis) is nearly 100% for patients with localized cancer compared with 31% for patients with metastasized cancer at diagnosis (Jemal, Siegel et al. 2009). Different types of treatment are available for prostate cancer patients (Sriprasad, Feneley et al. 2009). Those in good health are usually offered surgery as a treatment for prostate cancer.

Routine surgeries for early stage cancers usually involve radical prostatectomy in an attempt to remove the prostate, surrounding tissue and seminal vesicles. Typically this is performed either through an incision in the abdominal wall (retropubic prostatectomy) (Walsh, Lepor et al. 1983) or perineum (perineal prostatectomy) (Young 1905). Removal of the lymph nodes (lymphadenectomy) may be done at the same time. Men who are unsuitable for a radical prostatectomy, due to age or illness, may be offered a transurethral resection of the prostate (TURP). Following prostatectomy an imaging test, such as the ProstaScint scan, may be performed to locate recurrent prostate cancer. Complications arising from surgery for prostate cancer involve impotence and urine leakage (Klein, Ciezki et al. 2009; Magheli and Burnett 2009). Recent studies have shown that patients who underwent surgery for prostate cancer had longer survival rates compared to other methods of treatment such as radiotherapy or watchful waiting; a process that involves closely monitoring a patients condition without treatment until symptoms develop (Merglen, Schmidlin et al. 2007).

Radiation therapy is a treatment that may be offered for both early stage and advanced prostate cancers. As the name suggests, it uses high doses of radiation to kill the cancer cells and is often used on patients who are not amenable to surgery. Radiation therapy involves either external beam radiation, where a machine that rotates around the body will blast radiation toward the tumor or internal beam radiation therapy (Brachytherapy) where radiation is delivered inside the body using seeds, needles or catheters that are placed into the prostate tumor. Studies have shown an increased risk of bladder cancer and/or rectal cancer in males treated with radiation therapy (Shirodkar, Kishore et al. 2009)

Hormone therapy is a treatment option that involves either reducing the levels or blocking the action of hormones that are critical for the viability of the cancer cells. Much of this work was pioneered by Nobel prize winner Charles Hugging during the 1940s when he discovered the relationship between the endocrine system and the prostate gland

(Huggins and Hodges 1972). Hormone therapy may be used in conjunction with other therapies and is often used for advanced late stage prostate cancer that has spread to secondary sites throughout the body. Androgens, mostly produced by the testis, are the main hormones that enable prostate cancers to grow. Much focus is on trying to inhibit androgen production, via luteinizing releasing hormone antagonists or orchiectomy, or to block their mode of action through the use of antiandrogens such as flutamide (Labrie, Dupont et al. 1982; Lukka, Waldron et al. 2006). Androgen ablation therapy is the mainstay of therapy for progressive prostate cancer, as first described by Huggins over 30 years ago (Huggins 1967). However, despite initial responsiveness to hormone deprivation therapy, overtime most patients will relapse into hormone refractory prostate cancer for which there is no cure.

Hormone Refractory Prostate Cancer

For localized prostate cancer, surgery and/or radiation therapy can be curative. However, patients that present with locally advanced or metastatic prostate cancer require hormone deprivation to suppress tumor growth because prostate cancers require androgens for growth and survival. Despite initial responsiveness, most patients relapse into an incurable hormone refractory prostate cancer within 18-24 months (Attar, Takimoto et al. 2009). During this transition the tumor becomes insensitive to androgens (androgen independent prostate cancer - AIPC) resulting in death of the patient within a few years of diagnosis. Much focus is on trying to determine the mechanisms of AIPC development and recent data has shed light on the androgen receptor (AR) as a key player in this process (Feldman and Feldman 2001). Testosterone, the main circulating androgen, is produced by the testes, circulates in the blood where it is bound to albumin or sex hormone binding globulin (SHBG) and enters prostate cells where it is converted into dhihydrotestosterone (DHT) before binding to the AR. The AR is a member of the

steroid-thyroid-retinoid nuclear receptor family that when bound to DHT will enter the nucleus and act as transcription factor for a number of target genes that contain androgen response elements (AREs) in their promoters. The activated AR DNA complex then recruits co-activators or co-repressors to stimulate or inhibit gene transcription (McKenna, Lanz et al. 1999). Because mutations in the AR are more frequently found in metastatic prostate cancers compared to primary tumors, researchers believe that androgen ablation therapy provides selective pressure to target the androgen signaling pathway (Taplin, Bubley et al. 1995; Marcelli, Ittmann et al. 2000). Several mechanisms by which prostate cancers may circumvent androgen ablation through the AR have been postulated (Feldman and Feldman 2001).

Despite being incurable, AIPC is not untreatable. With insufficient response rates, chemotherapy was once thought to play an insignificant role for the treatment of metastatic AIPC. However, two recent studies using antimicrotubular agents for chemotherapy have demonstrated a small but significant survival benefit for patients with AIPC (Petrylak, Tangen et al. 2004; Tannock, de Wit et al. 2004). The studies, named SWOG 9916 and TAX 327, reported on the efficacy of a DNA damaging agent, mitoxantrone, plus the immunosuppressant prednisone and the combination of docetaxel, a microtubule stabilizing agent, with either estramustine or prednisone, respectively. In both studies, docetaxel based therapy proved superior to mitoxantrone plus prednisone in terms of response rate and for the first time demonstrated a survival benefit by significantly reducing the risk of death by 20-24% at 3 years. Based on these data, the FDA has approved docetaxel plus prednisone as the current standard treatment for AIPC. However, despite significant improvements in pain palliation, quality of life and small benefits in survival, resistance to chemotherapy can still develop.

Given the complexity of mechanisms underlying APIC development and common resistance to therapy seen using small molecule inhibitors, novel therapeutic strategies are needed. One such novel therapeutic strategy may be RNA interference (RNAi). RNAi is

a powerful and natural method of gene inhibition that that utilizes endogenous cellular machinery to either inhibit transcription or translation of mRNAs. RNAi therapy offers several advantages over current therapeutic modalities and is described below.

RNAi and siRNA Therapeutics

In 1998 Andrew Fire and Craig Mello described a process where double stranded RNA (dsRNA) was able to inhibit the expression of complementary genes in the roundworm *Caenorhabditis elegans* (Fire, Xu et al. 1998). Hence, the process was termed RNA interference (RNAi). Unknown at the time, RNAi had actually been observed before this in plants as a phenomenon of cosuppression (Napoli, Lemieux et al. 1990) where it has since been postulated that RNAi evolved as an antiviral defense mechanism. RNAi exploits a natural, complex pathway that regulates gene expression. Long dsRNAs are processed by the endoribonuclease Dicer into short 21bp duplexes with 2 base 3' overhangs called small interfering siRNAs (siRNAs) (Bernstein, Caudy et al. 2001). siRNAs enter a protein complex called RISC (RNA induced silencing complex) by which one strand of the duplex, the passenger strand, is cleaved and discarded (Matranga, Tomari et al. 2005; Rand, Petersen et al. 2005). The other 'guide strand' mediates the degradation of sequence specific mRNAs that are complementary to it (Ameres, Martinez et al. 2007). Argonaute 2 (Slicer) mediates cleavage of the target RNA (Rand, Ginalski et al. 2004). The biochemistry of RNAi has been extensively studied and well characterized since its original discovery.

Since the discovery that siRNAs can silence genes in mammalian cells (Elbashir, Harborth et al. 2001) there has been rapid progress toward its development as a therapeutic application. However, in order to design siRNAs as potent triggers of RNAi *in vivo*, many considerations must be taken into place. To be useful as drugs, siRNAs must be delivered to the cytoplasm of the cells where the specific gene target is

expressed. Delivery of the siRNA to intended tissues and cell types is the main hurdle to the successful development of siRNA therapeutics. In order for an siRNA to reach its intended gene target it faces many challenges from multiple hurdles in the extracellular environment and various barriers for intracellular uptake. siRNAs must navigate the vascular system while avoiding filtration, phagocytosis and enzymatic degradation (Xie, Woodle et al. 2006). Naked siRNAs are extremely unstable in the bloodstream and degraded rapidly (Soutschek, Akinc et al. 2004). Therefore siRNAs must be made more drug like through the use of chemical modifications to the backbone, sugars and ribose oligonucleotide bases in an attempt to increase stability in the serum and improve their pharmacokinetic properties (Bumcrot, Manoharan et al. 2006).

RNAi mediated gene silencing can be highly specific. Nevertheless, two major concerns for siRNA specificity are 'off target effects' due to silencing of mRNAs that share sequence homology with target genes and 'immune stimulation' due to activation of the innate immune system to administered siRNAs (Bridge, Pebernard et al. 2003; Jackson, Bartz et al. 2003). Thankfully, much of the chemistry behind their mode of action has been elucidated and with the careful design and modification of siRNAs, many of these problems can be negated. However, effective delivery to target tissues and cells now remains the most challenging hurdle in the development of RNAi therapy. The mode of siRNA administration is dependent on the intended target tissue and its accessibility. The route of delivery will affect the total dose needed and the effective tissue distribution. Localized siRNA delivery offers several advantages including lower dose requirements and potentially higher bioavailability (Behlke 2006). Direct localized delivery may also reduce unwanted side effects. Several reports have demonstrated efficacy of locally delivered siRNAs. Intranasal or intratracheal administration results in efficient gene silencing in the lungs (Bitko, Musiyenko et al. 2005). Direct instillation of siRNAs into the CNS has been used to silence specific neuronal mRNA targets in multiple regions (Thakker, Natt et al. 2004; Luo, Zhang et al. 2005). Another example

where local delivery has been successful is intraocular injection of siRNAs. Delivery of siRNA specific to VEGF , injected into the subretinal space, resulted in significant reduction of angiogenesis in a mouse model of retinal neovascularization (Reich, Fosnot et al. 2003). Subconjunctivital administration of siRNAs targeting transforming growth factor Beta (TGF-B) reduced the inflammatory cell infiltration and collagen deposition in a wound induced mouse model of ocular inflammation (Nakamura, Siddiqui et al. 2004). These proof of concept studies have facilitated the development of siRNA therapy for clinical trials for age related macular degeneration (AMD). The first clinical trial was initiated in 2004 by Acuity Pharmaceuticals and has now progressed to phase III under the control of Opko Health. Direct intratumoral delivery of siRNAs has also been used to monitor the effects of gene inhibition on tumor growth in several xenograft mouse models of cancer (Song, Zhu et al. 2005; McNamara, Andrechek et al. 2006).

Systemic administration of siRNAs enables a much broader tissue distribution. Intravenous (i.v) administration is often considered the broadest, however alternative routes such as intraperitoneal (i.p) or subcutaneous can also be achieved. Because systemically delivered siRNAs face a number of challenges typically not associated with local delivery, efforts are focused on trying to maximize their pharmacokinetic properties and enhance their cellular uptake. Silencing of genes *in vivo* has been achieved in a number of disease contexts in a variety of ways. For application to oncology, several studies have reported anti-tumoral efficacy of systemically delivered siRNAs. Liposomal delivery of siRNAs targeting the *EphA2* gene resulted in up to 50% reduction of tumor size in a mouse model of ovarian cancer (Landen, Chavez-Reyes et al. 2005). Cationic liposomes containing siRNAs against *RAF1* were able to silence the expression of Raf1 in tumors and inhibit tumor growth in a xenograft model of prostate cancer (Pal, Ahmad et al. 2005). Atelocollagen siRNA particles have also demonstrated anti tumoral efficacy in a mouse model of prostate cancer (Takeshita, Minakuchi et al. 2005). Other notable experiments in models of hypercholesteremia and viral infection (Hepatitis B and

Influenza) have demonstrated promising proof of concept studies for the use of systemic RNAi therapy (Uprichard, Boyd et al. 2005; Zimmermann, Lee et al. 2006).

Clearly the potency and target selectivity, even down to single nucleotide polymorphisms, of siRNA duplexes gives this potential therapy a large advantage over traditional pharmaceutical agents. Combined with high throughput production and their ability to target virtually any gene, siRNA therapy is quickly moving to forefront as a major class of new therapeutics.

Relevance and focus of my project

Prostate cancer is a complex heterogeneous disease whose mechanistic basis is poorly understood. Understanding how prostate cancers transition from indolent to life threatening is of utmost importance so prostate cancers can be avoided or better treated. Furthermore, AIPC is incurable and advances in therapeutic intervention are needed. Hence, the goal of my work was to span the spectrum of prostate cancer by assessing the use of systemic siRNA therapy for AIPC and finally to develop a spontaneous animal model of prostate cancer that will aid in dissecting the mechanistic basis for disease progression.

In this thesis, I first examined the use of AR targeted siRNA therapy in an animal model of human AIPC. Treatment of cell lines *in vitro* with AR siRNAs was sufficient to induce apoptosis and reduce viability. However, *in vivo* administration of AR targeted siRNAs was unable to reduce tumor growth or improve survival in an animal model. We determined that delivery of systemic siRNAs was the main hurdle to success of this therapy. To further assess this, I developed an animal model (FLASH) that would specifically allow the pharmacodynamic properties of systemically delivered siRNAs to be assessed in a high throughput manner. Using FLASH mice I analyzed the biodistribution and pharmacodynamic properties of liposomal siRNAs.

Next, I developed and characterized a novel mouse model of spontaneous prostate cancer (B6-Luc mice). I developed this model in an attempt to improve on previously developed mouse models of prostate cancer. Specifically, I incorporated a firefly luciferase reporter allele that allowed us to monitor prostate cancer progression non invasively using BLI. Using this model, I was able to show that prostate cancer progression is unique in this model compared to other similar models. Furthermore, I show that this model will be useful for the pre-clinical testing of new drugs aimed at combating prostate cancer.

Relatively few risk factors for prostate cancer progression have been established. Obesity is a potential risk factor that has been linked to increased mortality rates in prostate cancer patients. My final project involved examining the effects of diet induced obesity on prostate cancer progression in B6-Luc mice. I was able to show that diet induced obesity induced a prostatic inflammatory response in B6-Luc mice. However, obesity did not effect prostate cancer progression in this model. Future studies are aimed at utilizing larger cohorts of mice for similar studies.

This research has provided novel model systems that will aid in the general development of prostate cancer therapeutics, from siRNA therapy to chemotherapy. Furthermore, this research will allow us to dissect the mechanistic basis for prostate cancer and to identify specific factors that promote progression to advanced disease.

CHAPTER II

ANDROGEN RECEPTOR TARGETED SIRNA THERAPY FOR ADVANCED PROSTATE CANCER

Introduction

Androgen deprivation therapy remains the first line therapy for locally advanced or metastatic prostate cancer since its original inception (Huggins 1967). Despite initial responsiveness, subjects typically relapse into androgen independent prostate cancer (AIPC) within 18-24 months (Attar, Takimoto et al. 2009). AIPC is a lethal form of prostate cancer for which there is no cure. There are several mechanisms by which AIPC can develop (Feldman and Feldman 2001). Understanding the pathways and mechanisms behind AIPC development is of utmost importance for the developing therapies for this lethal form of prostate cancer.

Efforts are focused on trying to understand the mechanisms behind AIPC development. The frequent mutation rate of the androgen receptor (AR) in metastatic prostate cancer has led researchers to believe that androgen deprivation therapy provides a select pressure to target the androgen signaling axis (Taplin, Bubley et al. 1995; Marcelli, Ittmann et al. 2000). The AR may be involved in the development of AIPC in a number of ways (Chen, Welsbie et al. 2004; Attar, Takimoto et al. 2009). Amplification of the AR may allow it to become hypersensitive to castrate levels of androgens (Visakorpi, Hyytinen et al. 1995; Gregory, Johnson et al. 2001). Missense mutations in the AR gene may facilitate the AR to become inappropriately activated by various non androgen steroids and androgen antagonists (Buchanan, Greenberg et al. 2001). Alternatively, the AR may be converted into an outlaw receptor and become activated by ligand independent mechanisms, such as growth factor activated or receptor tyrosine

kinase activated pathways (Culig, Hobisch et al. 1994). Because expression of the AR is critical in these cases, AR antagonists such as bicalutamide, have been developed in an attempt to inhibit its activity. However, responses to these treatments are usually partial and transient, with AR activity becoming resistant to antagonism through a number of mechanisms (Kawata, Ishikura et al.; Colabufo, Pagliarulo et al. 2008). Therefore, new therapies are needed in order to efficiently target and inhibit activity of the AR. One such therapy might be RNAi. Recent studies have demonstrated efficacy of siRNA therapy in mouse models of cancer (Song, Wang et al. 2002; Dassie, Liu et al. 2009). However, the use of systemically delivered siRNAs targeting the AR in animal models of advanced prostate cancer are lacking.

RNAi is a highly promising technology for the treatment of cancer. Therapeutics based on RNAi offer a powerful method of gene inhibition and offer several advantages over traditional pharmacological agents. In particular, cancer cells may accumulate key mutations rendering them insensitive to small molecule inhibition. Alternatively many attractive therapeutic targets may be un druggable. The principal advantage of RNAi is that all targets can be inhibited. Furthermore, lead compounds can be rapidly identified and optimized and easily synthesized on a large scale and RNAi offers a more selective and potent method of inhibition (Bumcrot, Manoharan et al. 2006). Because endogenous RNAi is mediated by siRNAs, much attention has focused on developing systemically delivered synthetic siRNAs to target disease causing genes *in vivo*. However, systemic siRNA therapy is challenged by the method of delivery and stability *in vivo*. Because siRNAs are extremely hydrophilic and unstable in the serum as a result of serum nucleases and rapid excretion, they must be made more drug like through the use of chemical modifications to the backbone, sugars and ribose oligonucleotide bases. This has been achieved by the introduction of a phosphothiorate backbone (P=S) linkage at the 3' end for exonuclease resistance and 2' methylpurine modifications (2'-OMe) for

endonuclease resistance (Choung, Kim et al. 2006). Such modifications enhanced plasma stability and increased *in vitro* potency.

In an attempt to overcome systemic delivery problems, siRNAs have been conjugated to targeting molecules (Soutschek, Akinc et al. 2004; McNamara, Andrechek et al. 2006). Conjugation is especially attractive for siRNA based therapy because conjugates can be placed onto the passenger strand without disrupting the activity of the guide strand. Conjugation to cholesterol has been successfully used to achieve *in vivo* silencing in animal models of hypercholesteremia (Soutschek, Akinc et al. 2004). Similar studies have been performed using siRNAs that were encapsulated within liposomes (Zimmermann, Lee et al. 2006). Such formulations are favored for systemic siRNA therapy because they significantly enhanced pharmacokinetic properties. Additionally, siRNAs have also been encapsulated into atelocollagen particles (Ochiya, Takahama et al. 1999). Systemic delivery of atelocollagen-siRNA complexes was effective at inhibiting tumor growth, particularly at metastatic bone lesions, in a mouse model of prostate cancer (Takeshita, Minakuchi et al. 2005). Taken together, these data demonstrate the powerful utility of systemic siRNA therapy in pre-clinical models.

In this study we demonstrate the efficacy of chemically modified and formulated siRNAs for inhibition of the AR in advanced prostate cancer. Specifically, we formulated AR siRNAs with either cholesterol conjugation or encapsulation within liposomes or atelocollagen. We show that targeting the AR *in vitro* leads to apoptotic cell death in AR positive 22Rv1 cells but nor AR negative PC3 cells. Efficacy of cholesterol conjugated and atelocollagen formulated siRNAs was only demonstrated using transfection reagent lipofectamine. However, liposomal siRNA complexes were able to induce target gene inhibition without the need for any transfection reagents. Systemic delivery of formulated AR-siRNA complexes was unable to inhibit tumor growth or improve survival in an *in vivo* mouse model of advanced prostate cancer. Future studies are aimed at targeted delivery of siRNAs.

Materials and Methods

Bioluminescence Imaging

All BLI was performed using an IVIS 100 imaging system (Caliper Life Sciences). BLI of cells was performed by addition of D-luciferin (Caliper Life Sciences) to the cell culture medium at a final concentration of 150μg/mL. Samples were then imaged using a 15cm field of view with exposure times varying from 1-15 seconds. Photon flux was calculated using Living Image software (version 2.5) and represented as photons/sec/cm^2/sr. Bioluminescence values were then represented as percent photon flux of untreated or vehicle control values. For BLI of mice, mice were first anesthetized in a chamber with 3% isoflurane. D-luciferin was then administered to each mouse via intraperitoneal injection at a dose of 150mg/kg and left to incubate for 8 minutes while being maintained on 3% isoflurane. Mice were then imaged using a 20cm field of view and an exposure time of 1 second. Bioluminescence values were calculated by measuring photons/sec/cm^2/sr in the region of interest surrounding the bioluminescence signal from the tumor with the lower signal threshold set to 5% of the maximum signal value.

Mouse models of prostate cancer

All animal procedures were performed with approval from the University of Iowa Animal Care and Use Committee. In order to generate a mouse model of advanced prostate cancer, 22Rv1-Luc cells were injected into the left ventricles of SCID mice as previously described (Drake, Gabriel et al. 2005). In order to generate subcutaneous tumors, 24 male athymic *nu/nu* mice (NCI) were injected into the periscapular subcutis with 2 x 10^6 22Rv1-luc cells (12 mice) while being maintained on 3% isoflurane. Mice

were returned to their housing and closely monitored for body weight and general health status

Cell culture and generation of luciferase expressing cell lines

All cell lines were obtained from the American Type Culture Collection. 22Rv1-Luc cell lines have been described previously (Drake, Gabriel et al. 2005). 22RV1 and LNCaP cells were cultured in RPMI 1640 medium and PC3 cells were cultured in DMEM medium. All cell culture media was supplemented with 10% FBS (Hyclone), 1% non-essential amino acids; media for luciferase expressing cell lines was also supplemented with 400μg/ml Geneticin (G418). All cells were cultured at 37°C in an atmosphere containing 5% CO_2.

Cell viability assays

Cell viability was determined using a cell proliferation reagent WST-1 (Roche) according to manufacturer's instructions and as previously described [REF]. Values from treated cells were divided by those from non-treated control values and represented as % control value. Each data point represents the mean ± SEM.

Design and generation of siRNAs

We designed 13 different 21nt siRNAs in exons 4-6 of the human AR mRNA. These were screened for their ability to reduce AR protein expression. From this initial screen we chose 5 siRNAs that demonstrated most potent inhibition of AR. The sequence of AR siRNAs are as follows: AR4 sense strand, cuGGGAAAGucAAGcccAuT*T; antisense strand, AUGGGCUUGACUUUCCcAGTsT; AR10 sense strand cuGuGcAAGuGcccAAGAuT*T; antisense strand, AUCUUGGGcACUUGcAcAGT*T;

The sequence of si-Luc is as follows sense strand, cuuAcGcuGAGuAcuucGAT*T; antisense strand, UCGAAGUACUCAGCGUAAGT*T. Lower case letters represent 2'-*O-methyl*-nucleotides. The asterisks denote phosphorothioate linkages. We prepared cholesterol modified versions of these as previously described (Soutschek, Akinc et al. 2004). Cholesterol modified siRNAs were screened for target efficacy by transfection of 2nM, 10nM, 50nM, 100nM and 200nM into both LNCaP and 22Rv1 cells (see below). In addition to cholesterol moiety we prepared 2 different versions (M1 and M2) that contained modifications to the double stranded RNA as previously described (Soutschek, Akinc et al. 2004). We also prepared liposomal and atelocollagen encapsulated siRNAs as previously described (Ochiya, Takahama et al. 1999; Minakuchi, Takeshita et al. 2004; Akinc, Zumbuehl et al. 2008). The liposomal preparation contains novel lipidoid $98N_{12}$-5, a polyethylene glycol lipid (PEG-DMG) and cholesterol.

AR western blots

Cell lysates were prepared 48hrs post transfection and AR expression was analyzed by western blot. Control lysates were prepared from cells receiving Lipofectamine (LF) only. Protein concentrations were calculated using a BioRad Dc Protein Assay. Equal amounts of protein were electrophoresed in a 12% SDS polyacrylamide gel and transferred onto PVDF membranes. Membranes were blotted with anti AR antibody (Millipore PG-21) or β-actin antibody (Sigma A1978), incubated with HRP-conjugated goat anti-rabbit IgG (Jackson 111-035-003) and signal was detected by enhanced chemiluminescence.

siRNA treatments

In vitro: Cholesterol-si; For initial screening, LNCaP and 22Rv1 cells were transfected with AR siRNAs in lipofectamine (LF) either 50nM chol-AR4 M1 siRNA or LF alone according to manufacurers instructions. Cells were analyzed 48hrs post transfection for AR expression by western blot. For cytotoxic analysis, 22Rv1 and PC3 cells were transfected with either 50NM chol-AR4, 50nM chol-AR10, 50nM chol-ARMM or left untreated and analyzed for cell viability at days 3 and 5 post transfection using a WST assay. For BLI analysis chol-si-Luc siRNAs were transfected in the absence of lipofectamine. $5x10^4$ 22Rv1-Luc cells were treated with a dose response of si-Luc. We performed BLI assays using an IVIS100 to measure luciferase signal 48hrs post transfection.

Liposomal-si; For BLI analysis, cells were treated as above

Atelocollagen-si; For BLI analysis, cells were treated as above

In vivo: Cholesterol-si; On day 25 post 22Rv1-Luc injection mice received their first dose (50mg/kg) of siRNA either AR-4, AR-10, AR-Mismatch (ARMM) or PBS via intravenous tail vein injection. Dosing continued twice a week for a period of 3 weeks. Mice were imaged weekly by BLI and general health was monitored closely.

Liposomal-si; 10mg/kg every 3 days for 2 weeks beginning 3 weeks after IC injection:

Atelocollagen-si; 10mg/kg, 1 injection every 3 days (3 injections total) beginning 3 weeks after IC injection

Results

Design and *in vitro* potency of AR siRNAs

We designed 13 different 21nt siRNAs in exons 4-6 of the human AR mRNA with different backbone modifications and screened each in a dose response for their

ability to reduce AR protein expression in human prostate cancer cell lines LNCap and 22Rv1 (Figure 2.1). From this screen we identified AR4 as the most potent siRNA *in vitro*. AR4 was then chemically modified to enhance pharmacokinetic properties by the addition of a phosphophiorate linkage (P=S) and 2' OMe groups as previously described (Soutschek, Akinc et al. 2004). Modified (M1) and unmodified (M2) versions of AR4 were analyzed for their efficacy in reducing AR protein levels in LNCap cells by densitometry western blots (Fig 2.1B). Modified AR4 siRNAs were potent at reducing AR expression in the presence of lipofectamine, but only moderately active in the absence of any transfection reagent. Next, we tested for the cytotoxic effects of AR inhibition using AR4, AR10 and control AR Mismatch (ARMM) siRNAs in AR positive luciferase expressing 22Rv1-Luc cells and AR negative PC3 cells (Figure 2.2). Both AR4 and AR10 were able to induce apoptosis and significantly decrease cell viability as measured using a WST assay (Figure 2.2A). However, we noticed a paradoxical increase in bioluminescence in AR4 and AR10 treated cells that was inversely correlated with cell death (Figure 2.2C). The reasons for this involve regulation of the CMV promoter used to express high levels of luciferase in 22Rv1 cells and are discussed in further detail in Chapter IV of this thesis. AR4 and AR10 treatment of AR negative PC3 cells had no effect on cell viability indicating that cytotoxic effects seen in 22Rv1 cells are a direct result of AR inhibition (Figure 2.2B).

Formulation of AR siRNAs using cholesterol, liposomes or atelocollagen

AR4 and luciferase targeted siRNAs (si-Luc) were formulated either by conjugation to a cholesterol moiety on the sense strand (Soutschek, Akinc et al. 2004) or encapsulated into liposomes (Akinc, Zumbuehl et al. 2008) or atelocollagen particles (Ochiya, Takahama et al. 1999) in an attempt to overcome systemic delivery problems *in*

vivo. Because these formulations are intended to enhance the cellular uptake of siRNAs, we tested the ability of formulated siRNAs targeting luciferase (si-Luc) to inhibit luciferase expression in 22Rv1-Luc cells in the absence of any transfection reagents (Figure 2.3A-C). Luciferase targeted siRNAs were chosen for this assay because of our ability to rapidly screen their pharmacodynamic properties via bioluminescence imaging (BLI) using an IVIS100 imaging system. Only liposomal si-Luc was able to significantly decrease bioluminescence in 22Rv1-Luc cells in the absence of any transfection reagent (Figure 2.3B). Although Cholesterol si-Luc was able to slightly reduce bioluminescence in a dose dependent manner, the magnitude never reached statistical significance (Figure 2.3C). Atelocollagen si-Luc was completely inactive in the absence of transfection reagent (Figure 2.3A).

Efficacy of formulated siRNAs *in vivo*

Previous studies have demonstrated the efficacy of systemically delivered formulated siRNAs in mice and non human primates. Furthermore, atelocollagen siRNAs have shown *in vivo* potency in a mouse model of human prostate cancer (Takeshita, Minakuchi et al. 2005). We have developed a mouse model of advanced human prostate cancer (AIPC) based on the intra-cardiac injection of luciferase expressing 22Rv1-Luc cells (Drake, Gabriel et al. 2005). 22Rv1 cells express a mutant AR and are consequently androgen independent, therefore providing an excellent source to model human AIPC. Expression of luciferase in this model allows us to assess tumor growth, distribution and response to therapy using BLI in a highly sensitive IVIS100 imaging system. BLI revealed that 22Rv1 cells were able to disseminate and colonize both soft tissue and bone in a distribution pattern similar to metastatic foci documented clinically. A previous study had demonstrated that in a similar mouse model, atelocollagen siRNAs were particularly effective at inhibiting gene expression in metastatic bone lesions (Takeshita, Minakuchi

et al. 2005). Therefore, we tested whether liposomal and atelocollagen encapsulated siRNAs were able to inhibit luciferase expression at metastatic tumor sites in our mouse model and in subcutaneous 22Rv1-Luc tumors in athymic nude mice (Figure 2.4A-D). In contrast to previously reported studies, we did not see any efficacy of atelocollagen si-Luc at metastatic tumor sites (Figure 2.4A & C). Liposomal si-Luc also failed to inhibit luciferase expression in subcutaneous 22Rv1 tumors (Figure 2.4B & D). Figures 2.4C and 2.4D are representative images captured from the IVIS 100 demonstrating lack of efficacy of *in vivo* siRNA treatment.

In order to determine the *in vivo* potency of AR inhibition using formulated AR siRNAs, we injected SCID mice with 1x10^5 22Rv1-Luc cells and let them form tumors for 4 Weeks. Success of intra-cardiac injection was determined as previously described (Drake, Gabriel 2005). Mice were assigned into treatment groups and dosed with either 50mg/kg of cholesterol AR-siRNA, 10mg/kg Liposomal AR-siRNA or10mg/kg Atelocollagen si-RNA. We also injected mice with 50mg/kg ARMM as a control group. The dosing regimen for each treatment group was as follows: Chol-AR; 50mg/kg every 3 days for 2 weeks beginning 3 weeks after IC injection: Lipo-AR; 10mg/kg every 3 days for 2 weeks beginning 3 weeks after IC injection: Atelo-AR; 10mg/kg, 1 injection every 3 days (3 injections total) weeks beginning 3 weeks after IC injection.

To monitor for effects of AR-siRNA treatment on tumor growth, we performed BLI weekly. At the same time, mice were also assessed for cytotoxic effects of systemic siRNA delivery by recording body weights. Mice did not lose any significant body weight during the treatment period. Figure 2.5 demonstrates that none of the siRNA treatments were able to inhibit tumor growth as assessed by longitudinal BLI. Furthermore, AR-siRNAs did not improve survival as shown by kaplan meir analysis (Figure 2.5D). Taken together, although siRNA mediated inhibition of AR *in vitro* was sufficient to induce cell death, systemic delivery failed to inhibit tumor growth or improve survival in a mouse model of advanced prostate cancer. These data confirm the

AR as an attractive therapeutic target for the treatment of advanced prostate cancer but also underscore the need for novel delivery methods to facilitate anti tumor efficacy of systemically delivered siRNAs.

Discussion

Here we demonstrate the utility of siRNA mediated AR inhibition for advanced prostate cancer. We designed potent siRNAs targeting the AR that were chemically modified and formulated in an attempt to improve their pharmacokinetic properties *in vivo*. Specifically, siRNAs containing phosphophiorate (P=S) and 2'-OMe modifications were either conjugated to a cholesterol moiety or encapsulated within liposomes or atelocollagen particles. Transfection of AR-siRNAs into human prostate cancer cells expressing AR induced cell death via apoptosis and had no effect on cell viability of AR negative prostate cancer cells. In an attempt to extend these findings *in vivo* we tested the ability of AR-siRNAs to induce tumor regression in an animal model of advanced prostate cancer developed in our laboratory. Treatment of AIPC tumor bearing mice with cholesterol, liposomal or atelocollagen siRNAs was unable to inhibit tumor growth or improve survival.

siRNA therapy offers several advantages over current therapeutic modalities. Clearly our data demonstrate that potent gene silencing of AR is sufficient to induce cell death in AR positive prostate cancers. However, the need for transfection reagents using cholesterol conjugation or atelocollagen particles underscores the importance of cellular uptake for maximal siRNA efficacy. Conjugation to cholesterol was previously shown to achieve *in vivo* silencing. Intravenous injection of siRNA-Cholesterol duplexes targeting apoliporotein B (ApoB) in mice, silenced ApoB mRNA by 55% in the liver and 70% in the jejunum (Soutschek, Akinc et al. 2004). Uptake of cholesterol conjugated siRNAs was demonstrated to be dependent of HDL and LDL lipoprotein particles (Wolfrum, Shi

et al. 2007). Internalization of cholesterol siRNAs is accomplished by receptor mediated endocytosis of the LDL or HDL receptors and because of this, cholesterol siRNAs have shown maximal efficacy in the liver and jejunum. Unfortunately, tumor growth in our model cannot be directed to a particular tissue, so it remains unclear whether cholesterol siRNAs were capable of inducing apoptosis in metastatic liver tumors. Furthermore, it is unclear whether the human prostate cancer cells used in this study express the necessary lipoprotein receptors required for cholesterol intake. Although the precise mechanism of liposomal siRNA uptake is yet to be elucidated, it is thought to be mediated through endocytosis (Love, Mahon et al.). This may explain why liposomal siRNAs were effective at inhibiting luciferase expression in cell cultures without the need for transfection reagents. However, we did not see a similar effect *in vivo*. In order to achieve such an effect, we may need to alter the dose and regimen of treatment. It may be possible to further optimize the *in vivo* pharmacokinetic properties of liposomal siRNA delivery by adjusting the biophysical parameters such as particle size, nature of PEGylation and formulation composition in an attempt to improve the *in vivo* efficacy (Akinc, Goldberg et al. 2009). Previous studies have demonstrated that intravenous injection of siRNAs formulated into stable nucleic acid lipid particles (SNALPs) silenced ApoB in both mice and non human primates by more than 90% (Zimmermann, Lee et al. 2006). Furthermore, a single injection of 2.5mg/kg SNALP-siRNA was able to silence ApoB for at least 11 days. Again, silencing was limited to the livers of animals used in this study. Although atelocollagen siRNAs have demonstrated efficacy in a mouse model of prostate cancer, we were unable to recapitulate such an effect. It was previously demonstrated that systemic delivery of atelocollagen-siRNA complexes targeting EZH2 and p110α was effective at inhibiting tumor growth, particularly at metastatic bone lesions, in a mouse model of prostate cancer (Takeshita, Minakuchi et al. 2005). Interestingly, in our study, atelocollagen siRNA treatment of cell cultures was completely ineffective at inhibiting luciferase expression in the absence of transfection reagents. The

mechanism of uptake of atelocollagen is yet to be discovered. Atelocollagen is obtained by cleaving the telopeptides from Collagen I to reduce its immunogenicity. Integrins have been implicated as collagen receptors; therefore it is plausible that atelocollagen may interact with a collagen receptor such as Integrin α2β1. It is unknown whether the particular collagen receptor required for atelocollagen internalization is expressed in the cell lines used in this study. Future studies could be aimed at addressing this question.

We chemically modified siRNAs in an attempt to improve their pharmacokinetic properties ranging from enhanced stability, protection from serum nucleases, no 'off targeting' and increased cellular uptake. Protection from nucleases was accomplished by introducing a phosphothiorate backbone (P=S) linkage at the 3' end for exonuclease resistance and 2' methylpurine modifications (2'-OMe) for endonuclease resistance. Other important considerations such as siRNA specificity and immunogenicity must also be considered when designing siRNAs. Transcriptional profiling and bioinformatic analyses have revealed that siRNAs have the potential to silence a number of off target genes often in the 3' UTRs of mRNA (Jackson, Bartz et al. 2003; Qiu, Adema et al. 2005; Jackson, Burchard et al. 2006). It was determined that the seed region of the siRNA is what determines its specificity (Birmingham, Anderson et al. 2006; Jackson, Burchard et al. 2006). Specifically the critical nucleotides were found to be in positions 2-8 from the 5' end of the guide strand (Boese, Leake et al. 2005). In an attempt to avoid the seed region off targeting effect, it was determined that nucleotides 2-8 of the guide strand must be unique only to the intended target. It was also discovered that chemical modifications of the nucleotides of the seed region can substantially reduce off targeting (Jackson, Burchard et al. 2006). In addition to silencing off target genes, siRNAs could also cause problems by triggering immune and inflammatory responses. These may involve the interferon response through recognition by toll like receptor (TLR) pathways (Hornung, Guenthner-Biller et al. 2005) Indeed it has been demonstrated that siRNAs can engage TLRs in plasmacytoid dendritic cells resulting in an interferon response characterized by

inflammatory cytokine production (Bridge, Pebernard et al. 2003; Hornung, Guenthner-Biller et al. 2005). TLR activation seems to be sequence specific; with GU rich regions being an important trigger and the interferon response is only mediated by dsRNA that are longer than 30nt offering a window for the development of candidate siRNAs for clinical use. Although we did not assess the possibility of interferon induction in our model, previous work has demonstrated that such systemically siRNAs did not induce a host immune response.

Taken together these data demonstrate that delivery remains the main hurdle to the successful development of RNAi therapeutics. Although the formulations used in this study favor systemic distribution, they do not allow for tissue specific targeting. Such an option would be very attractive due to expression of tumor specific antigens on cancer cells. The use of targeted siRNA delivery has garnered a lot of attention since the discovery of RNAi and some progress has been made on its feasibility *in vivo*. Antibody-protamine fusion proteins containing an siRNA targeting MDM2 or VEGF and the Fab fragment of an HIV envelope antibody were developed to mediate specific uptake in cells expressing the HIV envelope protein (Song, Zhu et al. 2005). Injection of these complexes, either intratumorally or intravenously *in vivo*, inhibited subcutaneous tumor growth of B16 cells in mice. The use of RNA aptamers to bind with high affinity and specificity to target molecules has also demonstrated success in *in vivo* models. Aptamer-siRNA chimeras were developed to target prostate specific membrane antigen (PSMA), a tumor antigen that is overexpressed in some prostate cancers (Dassie, Liu et al. 2009). In order to demonstrate *in vivo* efficacy, the aptamers were first chemically modified to enhance circulating half life and improve processing of the siRNA by the cellular machinery. Intravenous injection of optimized chimeras induced regression of PSMA expressing tumors in nude mice.

In conclusion, we have demonstrated the feasibility of AR targeted siRNA therapy for prostate cancer *in vitro* but were unable to achieve *in vivo* silencing in an

animal model of advanced human prostate cancer. Future studies are aimed at developing targeted siRNA therapies in an attempt to overcome the systemic delivery problems associated with this study.

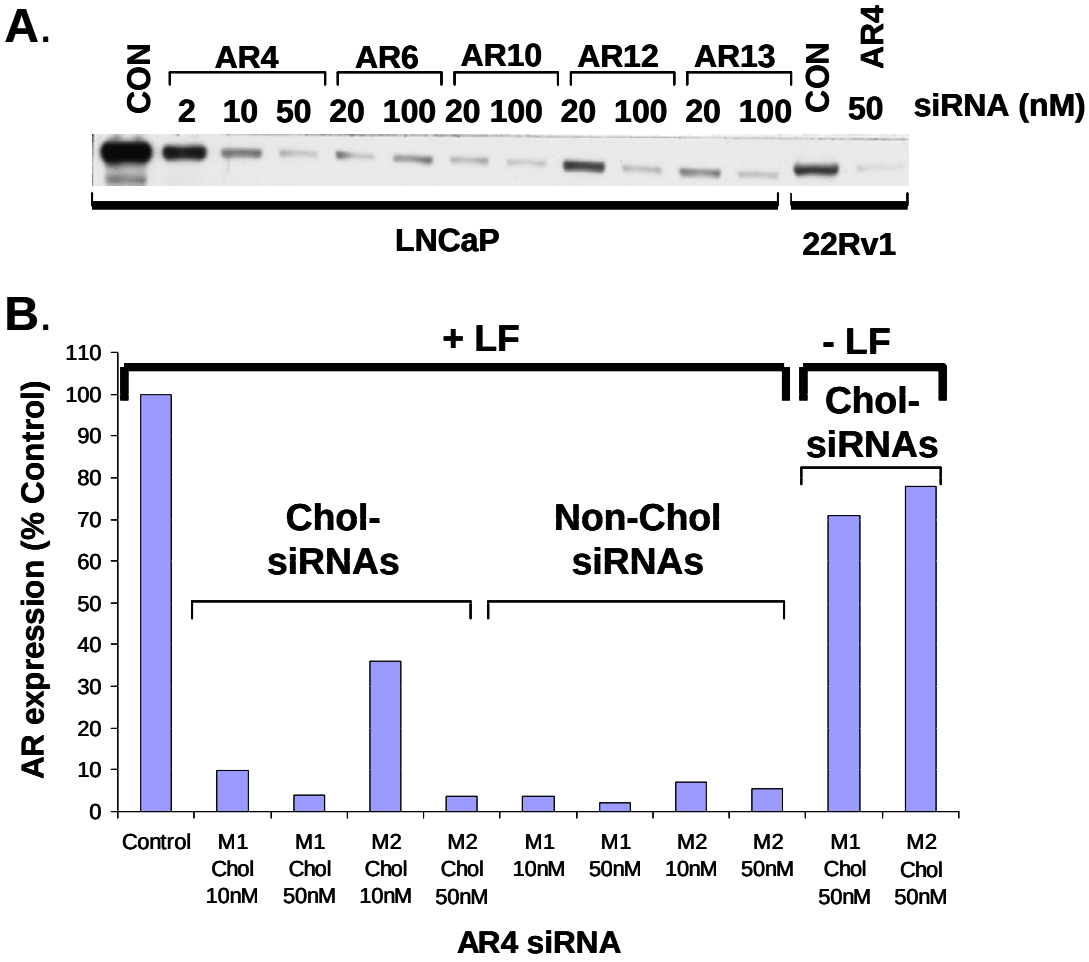

Figure 2.1: siRNAs effectively reduce AR expression in prostate cancer cell lines. (A) Dose-response analysis of AR4, AR6, AR12, AR13 in LNCaP and AR4 in 22Rv1 cells. siRNAs at the concentrations indicated were transfected using Lipofectamine 2000 (LF) according to the manufacturers instructions. Cell lysates were prepared 48h post-transfection and AR expression was analyzed by Western blot. (B) Modified and unmodified versions of AR4 (see text for description) were analyzed at the indicated concentrations for potency at reducing AR expression in LNCaP cell. These were introduced either with or without LF. AR expression was measured by densitometry from Western blots. In both experiments Control lysates were prepared from cells transfected with LF only. In separate experiments transfection with siRNA directed against luciferase did not affect AR expression.

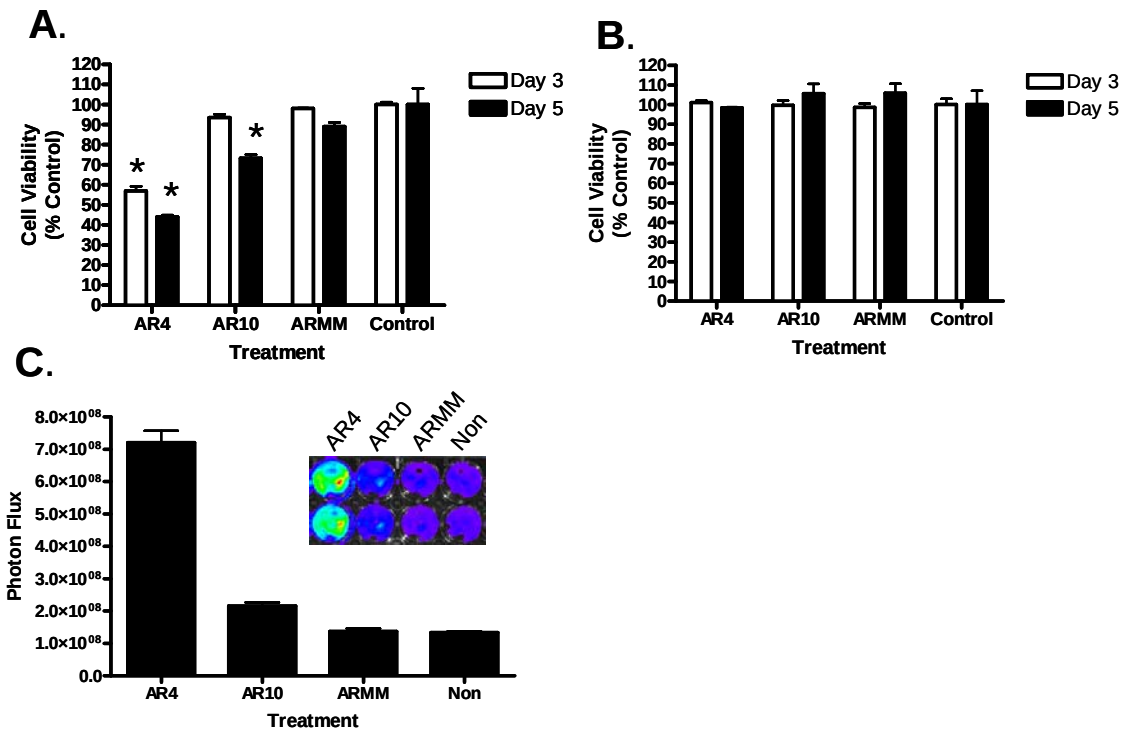

Figure 2.2: siRNAs targeting AR induce cell death in AR positive but not AR negative prostate cancer cell lines. (A) 22Rv1 cells were treated with either AR4, AR10, ARMM or left untreated for 3 and 5 days and cell viability was determined using a WST assay. Significant differences between si-AR and control treated cells denoted by asterisks;*p<0.05, **p<0.01 ***p<0.001 Error bars represent mean + SEM .(B) AR negative PC3 cells were treated same as above. (C) AR4 siRNA induces an increase in bioluminescence in 22Rv1 cells 3 days after treatment.

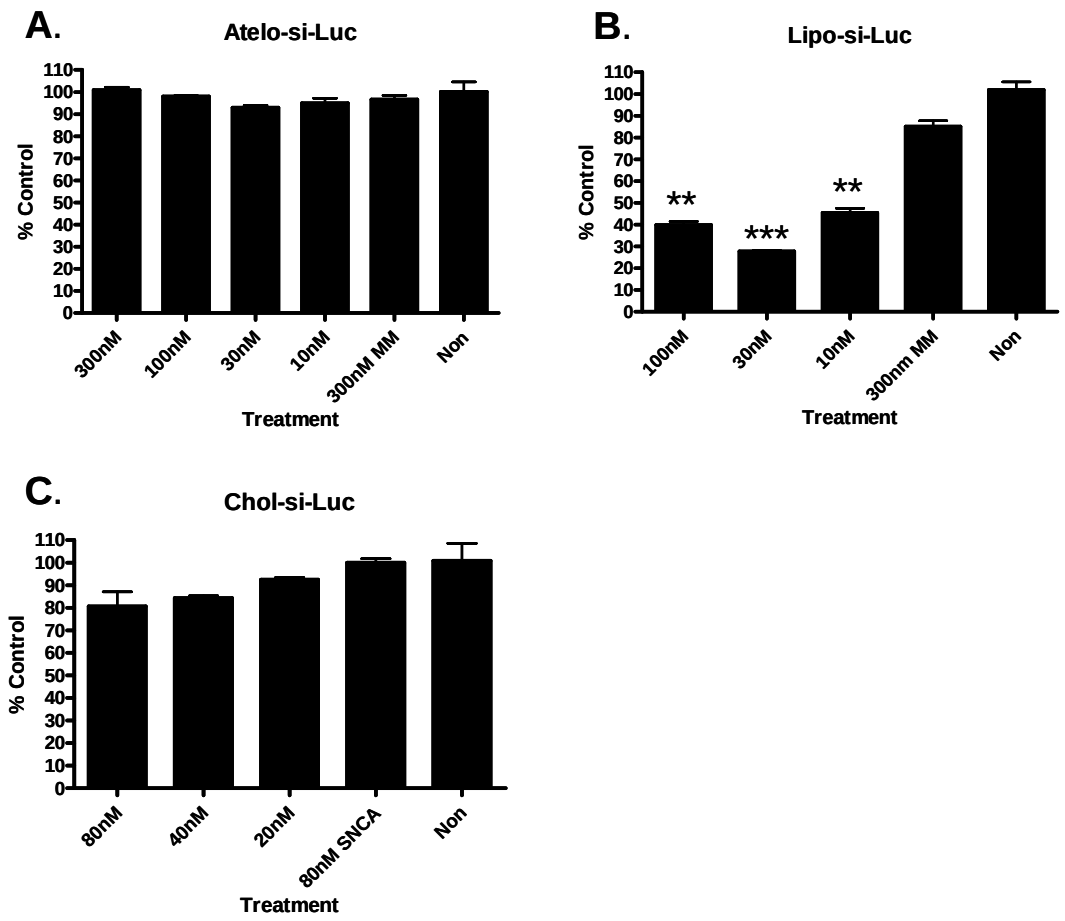

Figure 2.3: Liposomal si-Luc is effective at inhibiting luciferase expression in the absence of transfection reagent. A dose response analysis of either Atelo si-Luc (A), Lipo si-Luc (B) or Chol si-Luc (C) was performed for their ability to inhibit luciferase expression and reduce bioluminescence in 22Rv1-Luc cells in the absence of lipofectamine 2000. Only Lipo si-Luc was able to significantly reduce bioluminescence in the absence of lipofectamine. Significant differences between si-AR and control treated cells denoted by asterisks;*$p<0.05$, **$p<0.01$ ***$p<0.001$. Error bars represent mean + SEM

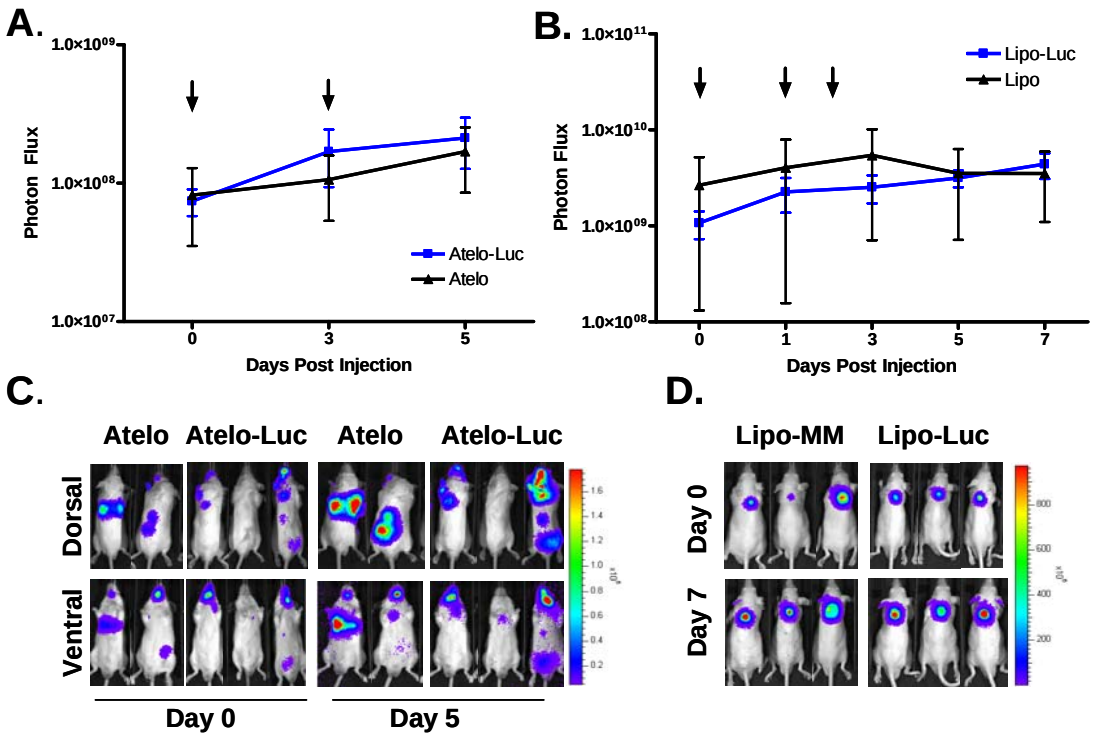

Figure 2.4: Atelo-Luc and Lipo-Luc are ineffective at inhibiting luciferase expression *in vivo*. (A) Mice bearing 22Rv1-Luc tumors were injected with either Atelo-Luc or Atelo alone and assessed for bioluminescence on days 3 and 5 post injection. Arrows denote treatment regimen. Error bars represent mean + SEM (n= 10). Images in C are representative of both treatments from day 0 and day 5. (B) Mice bearing 22Rv1-Luc subcutaneous tumors were injected with either Lipo-Luc or Lipo-MM and assessed for bioluminescence on days 1, 3, 5 and 7 post injection. Arrows denote treatment regimen. Error bars represent mean + SEM (n=10) . Images in D are representative of both treatments from day 0 and day 7.

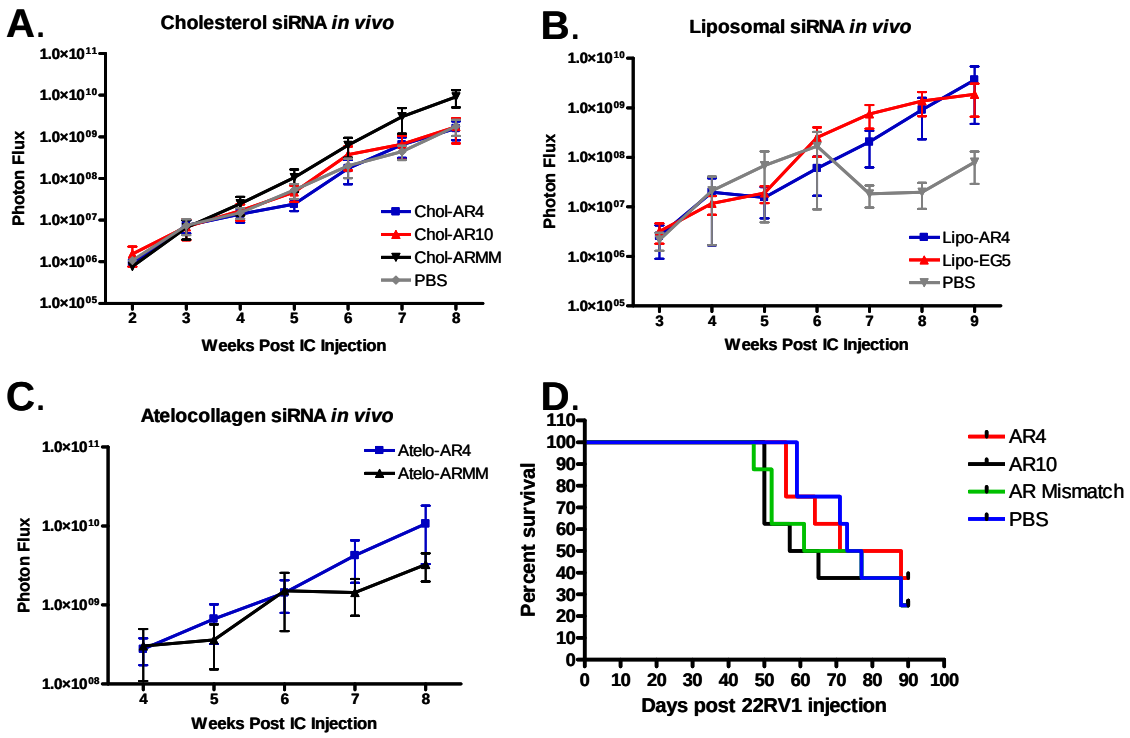

Figure 2.5: Formulated siRNAs are unable to induce tumor regression or improve survival in a mouse model of advanced prostate cancer. (A) Mice bearing 22Rv1-Luc tumors for 3 weeks were injected with either (A) chol-AR4, chol-AR10, chol-ARMM; (B) Lipo-AR4, Lipo-EG5 or PBS; and (C) Atelo-AR or Atelo-ARMM. Mice in each treatment group were assessed for tumor growth via BLI weekly. Error bars in A-C represent mean + SEM (n=10) (D) Kaplan Meier survival data cholesterol-si treatment demonstrating no improvement in survival.

CHAPTER III

ASSESSING SIRNA PHARMACODYNAMICS IN A LUCIFERASE EXPRESSING MOUSE

Introduction

Systemic delivery of small interfering RNA (siRNA) to target cells and organs remains a significant barrier to the successful development of this new class of therapeutics for many possible indications. A variety of approaches to this problem are currently under intensive investigation including means to augment the pharmacokinetic and distribution properties of siRNAs as well as strategies to effect cell-type specific uptake of siRNAs *in vivo*, for review see (de Fougerolles, Vornlocher et al. 2007). The ability to evaluate these strategies rapidly in preclinical models should facilitate the selection and optimization of the best approaches. New developments in small animal molecular imaging have significantly impacted modern therapeutic development (Willmann, van Bruggen et al. 2008) Among these is bioluminescence imaging (BLI) (Contag, Spilman et al. 1997). Bioluminescence imaging (BLI) involves the sensitive detection of photons from cells expressing a luciferase enzyme. Luciferase mediated oxidation of the luciferin substrate in the presence of ATP, oxygen and Mg^{2+} generates bioluminescence which is detected using a sensitive charged-coupled device camera. BLI offers several advantages over alternative molecular imaging techniques in that it is relatively simple to execute, is cost effective and enables non-invasive serial imaging over time without harm to the experimental animal.

Several transgenic mouse models have been engineered to express a luciferase enzyme. Expression of luciferase can be restricted to certain tissues or cell types through the use of tissue specific promoters, e.g. (Huang, Ma et al. 1997; Carlsen, Moskaug et al.

2002; Wilsbacher, Yamazaki et al. 2002), and engineered luciferase enzymes can be activated in response to certain molecular processes, e.g. (Luker, Sharma et al. 2002; Rehemtulla, Taneja et al. 2004; Gross and Piwnica-Worms 2005). Luciferase can also be ubiquitously expressed in an animal through the use of a constitutive promoter (Lyons, Meuwissen et al. 2003; Cao, Wagers et al. 2004). Constitutive promoters, such as the β-actin promoter, have been used to drive luciferase expression in these transgenic mice. Higher luciferase expression may generate more signal; allowing for more sensitive detection *in vivo*. In each case BLI has provided novel insights into a number of biological processes such as gene regulation, apoptosis, transplantation, cell trafficking and spontaneous tumorigenesis (Carlsen, Moskaug et al. 2002; Laxman, Hall et al. 2002; Liao, Zhong et al. 2007). BLI is also routinely used to assess tumor response to therapy in both xenograft and syngeneic transplant models (Sweeney, Mailander et al. 1999; Rehemtulla, Stegman et al. 2000; Svensson, Barnes et al. 2007). Such models provide an attractive means to screen the effects of novel anti-neoplastic agents. They also offer the opportunity to examine site-specific effects of compounds and have been particularly useful when studying the effects of local and systemic siRNA delivery (Takeshita, Minakuchi et al. 2005).

In order to develop a facile screen to study the pharmacodynamics of systemically-delivered siRNAs we generated a mouse strain that has robust ubiquitous expression of luciferase from an endogenous promoter. We utilized the conditional activation of pGL3 luciferase from *ROSA26*-LSL-Luc mice developed by Safran *et al* (Safran, Kim et al. 2003) through ectopic expression of Cre recombinase in oocytes under the control of the probasin promoter (Wu, Wu et al. 2001). We demonstrate that luciferase expression is detected in all tissues examined including lymphocytes which can be serially imaged over time when adoptively transferred into naïve mice. Using our mouse model we demonstrate that we can efficiently assess pharmacodynamic properties of a novel liposomal siRNA formulation targeting luciferase. We show that a single bolus

dose of this siRNA targets luciferase knockdown to the liver, largely avoiding other tissues for up to 16 days, demonstrating the potential therapeutic application of liposomal siRNA therapy.

Materials and Methods

Animals

All animal procedures were performed with approval from the University of Iowa Animal Care and Use Committee and by the authors' Institutional Review Board. Pb-Cre4^{+} mice (obtained from the NIH Mouse Models of Human Cancer Consortium) were mated with *ROSA26*-LSL-Luc mice (gift from William Kaelin) and backcrossed onto the C57BL6^{TYRC2J} (albino C57BL6; Jackson labs, Bar Harbor, Maine) background for 6 generations. N6 Pb-Cre4^{+}, *ROSA26*-LSL-Luc $^{fl/fl}$ male mice were then mated to N6 PbCre4+, *ROSA26*-LSL-Luc $^{fl/fl}$ female mice. Offspring were genotyped by PCR for the presence of the Pb-Cre4^{+} and *ROSA26*-LSL-Luc alleles using gene specific primers and imaged in an IVIS100 imaging system to assess bioluminescence.

Bioluminescence Imaging

All BLI was performed in an IVIS100 imaging system (Caliper Life Sciences, Alameda, California). For BLI of mice, D-luciferin (Gold Biotechnology, St Louis, Missouri) was administered to each mouse via intraperitoneal or intravenous injection at a dose of 150mg/kg. Animals were then anesthetized in a chamber with 3% isoflurane and immediately placed onto the imaging platform while being maintained on 3% isoflurane. Mice were then imaged after 2 min of substrate injection using a 20cm field of view and an exposure time of 1s and serially imaged every 4 min for a total period of 50

min. Bioluminescence values were calculated by measuring photon flux (photons/sec) in the region of interest surrounding the bioluminescence signal emanating from the mice. For BLI of protein lysates, samples were imaged using a 10cm field of view and an exposure time of 10s. For BLI of lymphocytes, cells were imaged using a 10cm field of view and an exposure time of 5 min. Bioluminescence values were calculated by measuring photons/sec for each sample.

In vitro and *in vivo* liposomal siRNA treatments

The liposomal formulation comprising the novel lipidoid $98N_{12}$-5, a polyethylene glycol lipid (PEG-DMG) and cholesterol has been described ((Akinc, Zumbuehl et al. 2008)). The sequence of si-FVII has been described (Akinc, Zumbuehl et al. 2008) and the sequence of si-Luc is as follows: sense strand, cuuAcGcuGAGuAcuucGAT*T; antisense strand, UCGAAGUACUCAGCGUAAGT*T. Lower case letters represent 2'-*O-methyl*-nucleotides. The asterisks denote phosphorothioate linkages. The siRNAs were synthesized by Alnylam Pharmaceuticals (Cambridge, Massachusetts) as described (Akinc, Zumbuehl et al. 2008). si-Luc was used to test luciferase inhibition in FLASH mouse embryonic fibroblasts (MEFS). MEFS were isolated from E13 embryos using the following protocol. Isolated embryos were eviscerated, washed in PBS and minced using scissors and scalpels. Following enzymatic dissociation (Trypsin/EDTA for 30min at 37°C) embryonic tissue was mixed with 18 ml of DMEM (Invitrogen, Carlsbad, California) supplemented with 10% FBS (Hyclone, South Logan, Utah), 1% non-essential amino acids (Invitrogen), 1% penicillin/streptomycin and left for 10 min to let clumps fall. Supernatant was then plated into 10cm dishes and incubated at 37°C in an atmosphere containing 5% CO_2. MEFS were then grown to confluence and frozen stocks (8% DMSO) were prepared. For *in vitro* siRNA treatment, MEFS were seeded into 24 well plates at $1x10^5$ cells/well. Following overnight culture, a dose response of liposomal

siRNA (10nM, 30nM, 90nM and 270nM si-Luc and 270nM si-FVII) was added in triplicate to the MEFS along with a non treated control. Fresh media was added 24h later. 72h post siRNA treatment, D-luciferin (150µg/mL) was added to each well and BLI was performed. Cell viability for each treatment was determined using a cell proliferation reagent WST-1 (Roche, Nutley, New Jersey) according to manufacturer's instructions. For *in vivo* administration of siRNAs, 5mg/kg siRNA were injected via lateral tail vein injection into FLASH mice. Following euthanasia, organs were removed and analyzed using an *in vitro* luciferase assay. Photon flux for si-Luc treated mice were compared to si-FVII treated mice and data represented as % FVII control (set at 100%)

RNA and protein preparation from tissues

Tissues from FLASH mice were removed and either flash frozen in liquid nitrogen for subsequent protein preparation or immediately placed (100mg) into 1ml of TRIZOL (Invitrogen) for RNA preparation. For RNA extraction, samples in TRIZOL were homogenized using a Powergen125 Teflon homogenizer (Fisher Scientific, Pittsburgh, Pennsylvania). Samples were then subjected to RNA extraction under manufacturers conditions. Purified RNA preparations were subjected to DNaseI treatment to remove any contaminating genomic DNA. For protein preparation, frozen tissues were homogenized into a powder using a mortar and pestle. Samples were then suspended in 1X Reporter Lysis Buffer (Buffer RLB, Promega, Madison, Wisconsin) and frozen overnight at -80°C. Samples were then subjected to three freeze thaw cycles (37°C – LN_2) and centrifuged at 13000rpm for 7.5 min. Supernatants were analyzed for protein quantity using a Biorad (Hercules, California) protein assay using manufacturers conditions.

Quantitative-RTPCR of luciferase mRNA and luciferase activity assay

RNA samples were subjected to quantitative-RT-PCR as previously described (Svensson, Barnes et al. 2007). Protein samples (150μg) were subjected to an *in vitro* luciferase activity assay as previously described (Svensson, Barnes et al. 2007)

Lymphocyte purification and adoptive transfer

Single cell suspensions from spleen and lymph node were resuspended in 0.83% NH_4Cl (in 1 mM Trizma Base) for erythrocyte lysis. Cells were washed, counted and resuspended at $2x10^8$/ml in bead buffer (PBS with 0.1% BSA and 0.02% NaN_3). B cells were depleted by incubation with BioMag Goat anti-mouse IgG and Goat anti-mouse IgM paramagnetic beads (Polysciences Inc, Warrington, Pennsylvania). Following B cell depletion, the remaining cells were again resuspended at $2x10^8$/ml in bead buffer and incubated with either BioMag SelectaPur CD8a paramagnetic beads for generation of enriched CD4(+) T cells, BioMag SelectaPur CD4 paramagnetic beads for generation of enriched CD8(+) T cells or a combination of the two for NK cell enrichment. B cell enrichment was performed by incubation with a combination of BioMag SelectaPur CD4 and CD8a paramagnetic beads. Viability of enriched cell fractions exceeded 95% and purity was greater than 80%. Cells were washed repeatedly and resuspended in PBS for BLI and adoptive transfer. For adoptive transfer $1x10^7$ cells/mouse (C57BL6^{TYRC2J}) were injected via the lateral tail vein.

Statistical analyses

All statistical analyses utilized ANOVA with Bonferroni post-test**.**

Results

Generation of a ubiquitous luciferase-expressing mouse

In order to generate a mouse that ubiquitously expresses luciferase we crossed male *ROSA26*-LSL-Luc and female Pb-Cre4^{+} mice (Wu, Wu et al. 2001; Safran, Kim et al. 2003). Pb-Cre4^{+} mice contain a Cre-recombinase transgene under control of the rat probasin promoter where expression is restricted to prostatic epithelium in male mice. However, it has been documented that female mice which harbor the Pb-Cre4 transgene have ectopic expression of Cre-recombinase in oocytes (Wu, Wu et al. 2001). *ROSA26*-LSL-Luc mice are a strain in which a pGL3 luciferase cDNA preceded by a LoxP-Stop-LoxP (LSL) is inserted into the ubiquitously expressed *ROSA26* locus [REF]. Using these two strains of mice we took advantage of the ectopic oocyte expression of Cre and crossed female mice containing the Pb-Cre4 transgene that were also homozygous for the *ROSA26*-LSL-Luc allele (R26-LSL-Luc $^{fl/fl}$) with male mice that were similarly positive for Pb-Cre4^{+} and R26-LSL-Luc $^{fl/fl}$ (Figure 3.1). Cre expression in the oocyte (see inset in Fig. 3.1) should lead to recombination of the LSL-Luc allele such that the stop codon upstream of luciferase is removed and luciferase becomes expressed from the endogenous *ROSA26* promoter. If this recombination occurs in the zygote, each daughter cell will contain 2 active copies of the luciferase allele and the result will be a mouse that has ubiquitous expression of the luciferase enzyme. To confirm this, we performed BLI on the offspring from this cross (Figure 3.2A). BLI of 4 week old animals revealed that the majority of mice were positive for luciferase expression. However, we also produced some Pb-Cre4^{+} mice that did not have ubiquitous luciferase expression indicating that not all of the oocytes had ectopic expression of Cre-recombinase. We found that Cre-recombinase was ectopically active in ~93% of the offspring (N=43 mice). For convenience, we designated these mice as FLASH (Firefly Luciferase Activated

Systemically in Homozygotes). *Ex vivo* imaging confirmed that luciferase was expressed in all tissues examined (Figure 3.2A). We found that intravenous injections of D-luciferin (150mg/kg) increased maximal signal output by ~5-fold compared to intraperitoneal injections (Figure 3.2B). Maximal signal output using intravenous injection of D-luciferin occurred immediately post administration whereas optimal imaging for intraperitoneal injections occurred ~15-20 min post D-luciferin administration as has been described previously in other models (Wu, Sundaresan et al. 2001). In order for us to examine whether luciferase was expressed homogeneously we prepared RNA and protein from lysates from a panel of tissues from both male and female FLASH mice and performed qRT-PCR for luciferase and an *in vitro* luciferase activity assay. qRT-PCR for luciferase revealed that luciferase transcript was most abundant in the testes (Figure 3.2C). Similarly, BLI of protein lysates from FLASH mice revealed that luciferase is expressed uniformly in all tissues examined except for the testes which have a higher expression level (Figure 3.2D). The reasons for the latter are unclear, however original characterization of the ROSAβgeo26 mouse documented that *ROSA26* was highly active in the testes (Zambrowicz, Imamoto et al. 1997).

FLASH mice can be used as donors for immune cell trafficking and transplantation studies

Conventional BLI strategies to image immune cell trafficking or tissue transplantation require purification of the desired cell types and transduction with a luciferase reporter using a variety of gene transfer techniques (Edinger, Cao et al. 2003; Baumjohann and Lutz 2006; Kim, Hung et al. 2007). Gene transfer efficiency remains an obstacle and stable reporter expression can be variable over time. The use of a transgenic mouse that has active ubiquitous luciferase expression may bypass some of these limitations. In order to test whether we could use FLASH mice as a universal donor we

purified $CD4^+$, $CD8^+$, B Cells and NK cells from FLASH mice and performed *ex vivo* imaging (Figure 3.3A). All four cell types produced detectable luciferase expression higher than in previous studies (Cao, Wagers et al. 2004). Signal output from these cells was relatively uniform ranging from 1.1-2.7 photons/sec. To determine whether we could image these cells *in vivo* we adoptively transferred $1x10^7$ $CD4^+$ T cells into albino C57BL6 mice ($C57BL6^{TYRC2J}$ mice). BLI of mice 24h post adoptive transfer revealed robust bioluminescence signal in all mice. Focal signals were detected in vicinity of the spleen, cervical lymph nodes, mesenteric lymph nodes, and inguinal lymph nodes (Figure 3.3B). *Ex vivo* imaging confirmed the location of $CD4^+$ T cell engraftment (Figure 3.3C). Longitudinal analyses of $CD4^+$, $CD8^+$ and NK cell adoptive transfer into SCID mice revealed that bioluminescence signal was increased 60 days post adoptive transfer (Figure 3.4). These data demonstrate that cells derived from FLASH mice can be transplanted and sensitively imaged *in vivo*.

FLASH mice are suitable for studying the pharmacodynamics of systemically-delivered siRNAs

In order to determine whether FLASH mice could be used to assess the pharmacodynamics of systemically-delivered siRNAs, we first examined whether a liposomal formulation of luciferase targeted siRNA (si-Luc) (Akinc, Zumbuehl et al. 2008) could inhibit the expression of luciferase in mouse embryonic fibroblasts (MEFS) isolated from FLASH mice (Figure 3.5A). This experiment demonstrated that we are able to reduce luciferase protein levels by ~90% using a 90nM dose of si-Luc *in vitro*. Importantly, a 270nM dose of control siRNA targeting Factor VII (si-FVII) did not reduce luciferase expression levels. To determine the efficacy of si-Luc *in vivo* we treated FLASH mice with either si-Luc or si-FVII via single bolus intravenous injection (5mg/kg). *Ex vivo* BLI of liver and lung 3 days post injection revealed that the si-Luc was

able to reduce the expression of luciferase in the liver compared to si-FVII treated mice (Figure 3.5B). We also detected a slight decrease in *ex vivo* bioluminescence from the lungs of si-Luc treated mice. We prepared RNA and protein from these tissues and tested whether the reduced levels of luciferase expression seen *ex vivo* could be confirmed using quantitative RT-PCR and an *in vitro* luciferase activity assay. Luciferase RNA and protein are reduced by ~90% in the livers of mice treated with si-Luc compared to si-FVII control treated mice (Figure 3.5C). Although there may be a trend toward reduced luciferase RNA and protein in the lungs of si-Luc treated mice, this did not reach statistical significance. However it is still possible that liposomal si-Luc exerts minor effects in the lung. In order to establish that we could sensitively measure differences in luciferase activity in the linear range in these various tissues, we prepared protein lysates from a panel of tissues and performed an *in vitro* luciferase activity assay on a wide range of protein concentrations (Figure 3.5D). In all tissues examined there was a high correlation (R^2=0.99) between light output and protein concentration. These data demonstrate the utility of FLASH mice for analyzing siRNA efficacy *in vivo*.

In order to characterize the pharmacodynamic properties of liposomal si-Luc we injected mice once either by intravenous tail vein injection or intraperitoneal injection with 5mg/kg of si-Luc or si-FVII. We then harvested tissue 3 days post injection and performed a luciferase activity assay. Intravenous administration of liposomal-formulated siRNAs is far superior in reducing luciferase expression in the liver (Figure 3.6A). We next sought to test whether we could achieve greater inhibition of luciferase expression in heterozygous mice that only contain 1 copy of the luciferase reporter allele (fl/wt mice). We treated both homozygous (fl/fl) and heterozygous (fl/wt) FLASH mice with si-Luc or si-FVII and prepared protein lysates 4 days post-injection (Figure 3.6B). Inhibition of luciferase expression was not significantly different between fl/wt and fl/fl FLASH mice indicating that changes in the levels of luciferase expression within a two-fold range do not affect RNAi efficacy in this model. To determine whether there are any gender-

specific differences in RNAi between male FLASH mice and female FLASH mice we treated both males and females with either si-Luc or si-FVII (Figure 3.6C). Levels of luciferase inhibition in the livers of treated male and female mice were not statistically different and we were not able to inhibit luciferase in any other tissue in female FLASH mice. To test further the pharmacodynamic properties of liposomal si-Luc we performed a time course of luciferase inhibition in FLASH mice. We treated mice with liposomal-formulated siRNAs and prepared protein lysates from a panel of tissues at days 4, 8 and 16 post-injection. Luciferase expression in the liver slowly increases from ~20% at day 4 to ~50% at day 16 post-injection (Figure 3.6D). These data show that a single injection of siRNA is able to reduce luciferase expression in the liver significantly for 16 days, but we did not observe any significant decreases in any other tissues examined. Hence, we have demonstrated the utility of FLASH mice for assessment of pharmacodynamic properties of *in vivo* administered siRNAs.

Discussion

Here we describe the development of a mouse strain that contains robust ubiquitous expression of a firefly luciferase reporter allele from the endogenous *ROSA26* promoter. By taking advantage of ectopic germline expression of Cre in the Pb-Cre4 transgenic mouse, we activated luciferase expression in all tissues of *ROSA26*-LSL-Luc mice. While we have not definitively demonstrated that luciferase is expressed in every cell in these mice, the amount of luciferase activity in a variety of organ homogenates and the similar levels of luciferase activity on a per cell basis in several lymphocyte populations suggests that expression is ubiquitous and uniform in all cells except the testis where higher expression levels were observed. Previously developed mouse models aimed at generating luciferase expressing mice involved transgenic approaches. Expression of luciferase in these models may be variable due to position effects,

transgene silencing or promoter expression in murine tissues. For example, although it is difficult to compare directly, the LucRep mouse developed by Lyons et al (Lyons, Meuwissen et al. 2003)apparently demonstrates less signal than FLASH mice when subjected to similar imaging conditions.. Moreover, in FLASH mice, luciferase is expressed from an endogenous promoter (*ROSA26*) in its normal genomic context, which is probably a more stable configuration for expressing consistent levels of luciferase through many generations of mice. The *ROSA26* promoter was originally discovered by random retroviral gene trapping in embryonic stem cells (Friedrich and Soriano 1991). Since then it has been targeted for genetic manipulation offering researchers novel methods to study temporal and tissue specific gene expression (Soriano 1999; Safran, Kim et al. 2003; Gu and Cole 2007).

Luciferase expression was detected in all tissues examined and at higher levels in lymphocytes than previously described mouse models (Cao, Bachmann et al. 2005). The level of expression was sufficiently robust to measure the trafficking of 10^7 $CD4^+$ cells to various lymphoid organs in living animals. Our mouse model has several advantages as universal donors for analyzing cell trafficking or tissue transplantation. Previous studies aimed at imaging trafficking of immune cells via BLI were performed using purified subsets of cells that had been engineered to express luciferase *in vitro*. Inherent problems with these studies include transfection efficiencies, promoter expression in cells and stable reporter expression over time (Mandl, Schimmelpfennig et al. 2002; Cao, Bachmann et al. 2005). Cells derived from FLASH mice already contain endogenous expression of luciferase from a constitutively active promoter and mitigate the need for any transduction of transfection of reporter constructs. Nuclear imaging strategies (SPECT and PET) have also been employed to image immune cell migration non-invasively (Baumjohann and Lutz 2006; Radu, Shu et al. 2008). Although these techniques are quantitative they also demand sophisticated instrumentation and are

relatively expensive and less sensitive. BLI of a luciferase reporter provides robust, cost effective and sensitive means to image these processes *in vivo*.

We also describe the use of FLASH mice to analyze the pharmacodynamics of systemically-delivered siRNAs. siRNA therapy is rapidly emerging as an approach for the treatment of a variety of human diseases (de Fougerolles, Vornlocher et al. 2007). The availability of animal models that enable high throughput screening of siRNA delivery, efficacy and safety would greatly facilitate the progression of siRNA therapy into clinical trials. Traditional assays to determine siRNA efficacy *in vivo* involve preparation of RNA and protein for quantitative RT-PCR and western blot analysis. Here we describe an alternative method using an *in vitro* luciferase activity assay. We demonstrate that a single intravenous injection of a liposomal-formulated siRNA targeting luciferase was able to reduce the levels of luciferase mRNA and protein by ~90% in the liver without significantly affecting expression in other tissues. Previous studies using the same liposomal siRNA formulation targeting ApoB and FVII documented similar levels of target inhibition in the liver (John, Constien et al. 2007; Akinc, Zumbuehl et al. 2008). We found that intravenous injections were far superior in inhibiting luciferase expression in the liver relative to intraperitoneal injections. This suggests that siRNA delivery efficacy is driven primarily by c_{max} in the liver. Reduction of luciferase expression was relatively durable, evident even 16 days after injection. Ongoing efforts are aimed at harnessing this powerful method of gene inhibition for certain liver associated diseases (Zimmermann, Lee et al. 2006). We were not able to inhibit luciferase significantly in any other tissues analyzed. Liposomal-formulated siRNAs used in this study are not targeted by ligand attachment, but this formulation has been optimized to target delivery to the liver (Akinc, Zumbuehl et al. 2008). Efforts continue to develop ligand-based tissue- and tumor-specific delivery (Song, Zhu et al. 2005; McNamara, Andrechek et al. 2006). The primary advantages of this model are that siRNA efficacy can be determined against a uniformly expressed and non-essential target

in all tissues. One drawback of the approach described here is that the ubiquitous expression of luciferase precludes evaluation of tissue-specific effects in living animals. However, it may be possible to transplant target cells of interest, as we have shown here for lymphoid cells, into non-bioluminescent hosts so that effects of siRNAs specifically on those cells can be evaluated *in vivo*. We believe that FLASH mice offer the opportunity to screen such formulations rapidly for targeting efficacy. The ability to determine the pharmacodynamics of novel siRNA formulations rapidly in FLASH mice will aid in their progression as potential therapeutics.

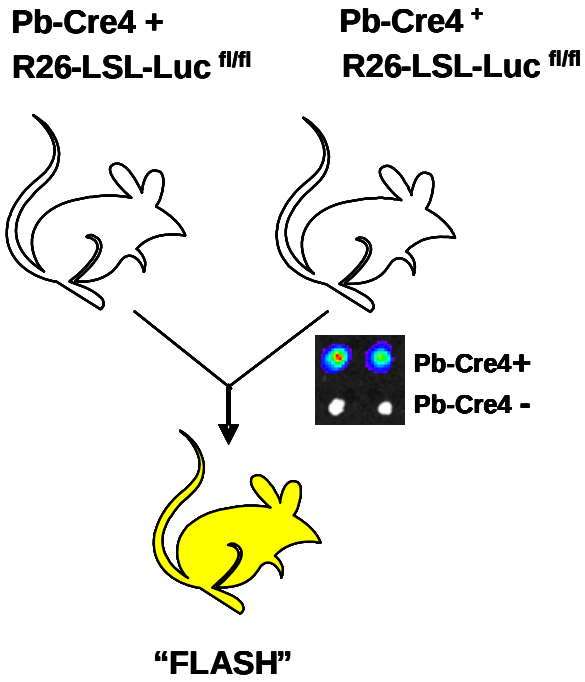

Figure 3.1: Generation of ubiquitous luciferase expressing mice. Pb-Cre4+, R26-LSL-Luc $^{fl/fl}$ male mice were mated with Pb-Cre4+, R26-LSL-Luc $^{fl/fl}$ female mice to generate ubiquitous luciferase expressing FLASH mice. Inset panel shows ovaries from both Pb-Cre4 positive and negative mice demonstrating that Pb-Cre4 is ectopically expressed in oocytes.

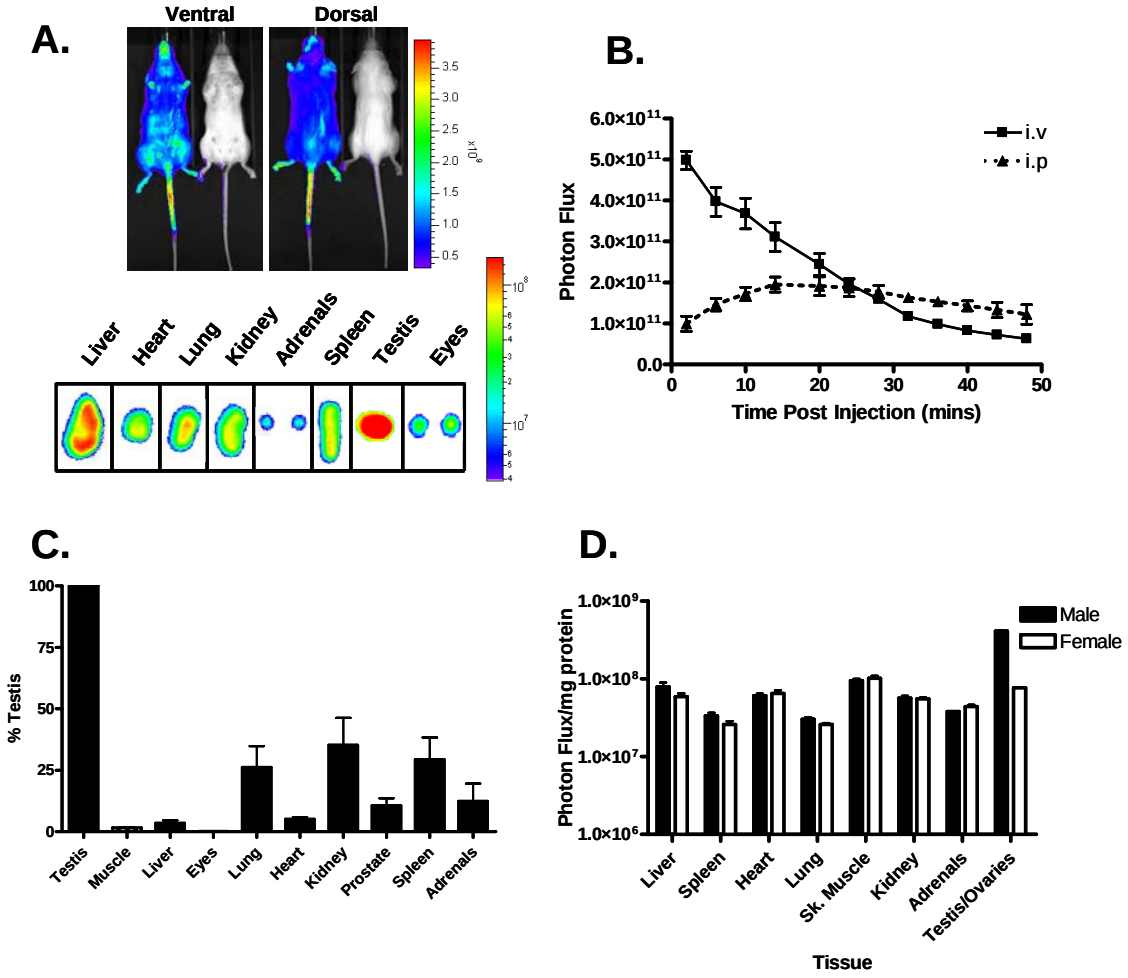

Figure 3.2: FLASH mice exhibit ubiquitous luciferase expression. (**A**) BLI of FLASH mice demonstrates intense signal from a mouse that demonstrated germline recombination of *ROSA26*-LSL-Luc (left) whereas a littermate that did not exhibit recombination showed no signal (right). Panels show *ex vivo* bioluminescent images of FLASH tissues (scale bar not shown). (**B**) Bioluminescence kinetics of intravenous vs. intraperitoneal injections of substrate D-Luciferin. Y-axis represents bioluminescence as photon flux (photons/sec) for whole body bioluminescence values. Error bars represent mean + SEM (n=4). (**C**) Quantitative RT-PCR for luciferase in various FLASH tissues. (**D**) Luciferase expression in a panel of FLASH tissues using an *in vitro* luciferase assay. Values are expressed as photon flux (photons/sec) per mg of protein. Error bars represent mean + SEM (n=3)

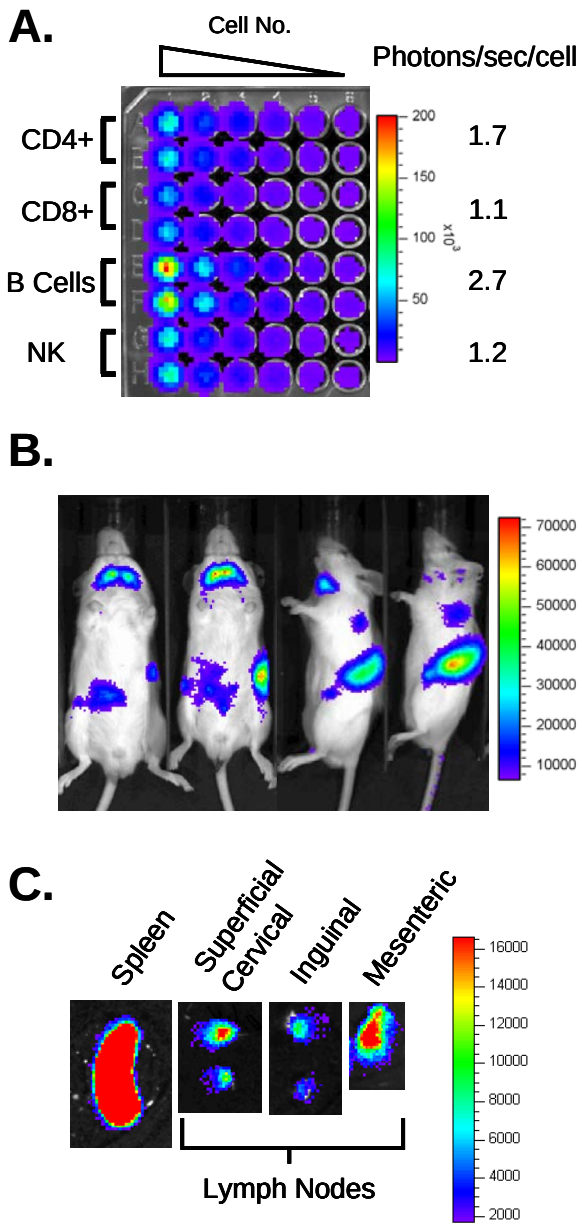

Figure 3.3: Imaging adoptively transferred FLASH lymphocytes *in vivo*. (**A**) $CD4^+$ T cells, $CD8^+$ T cells, B cells and NK cells were isolated from FLASH mice and imaged for bioluminescence intensity *in vitro*. Scale bar represents photons/sec/cm^2/sr. Average photon flux was calculated for each cell type as photons/sec/cell. (**B**) $1x10^7$ $CD4^+$ T cells were adoptively transferred via intravenous tail vein injection into albino C57BL6 mice ($C57BL6^{TYRC2J}$ mice) and imaged 24h post transfer. Focal signals of bioluminescence appear in areas that correspond to spleen, mesenteric, superficial cervical and inguinal lymph nodes. (**C**) *Ex vivo* BLI confirms the locations of $CD4^+$ T cell engraftment in various lymphoid organs. Scale bars in b and c represent photons/sec/cm^2/sr

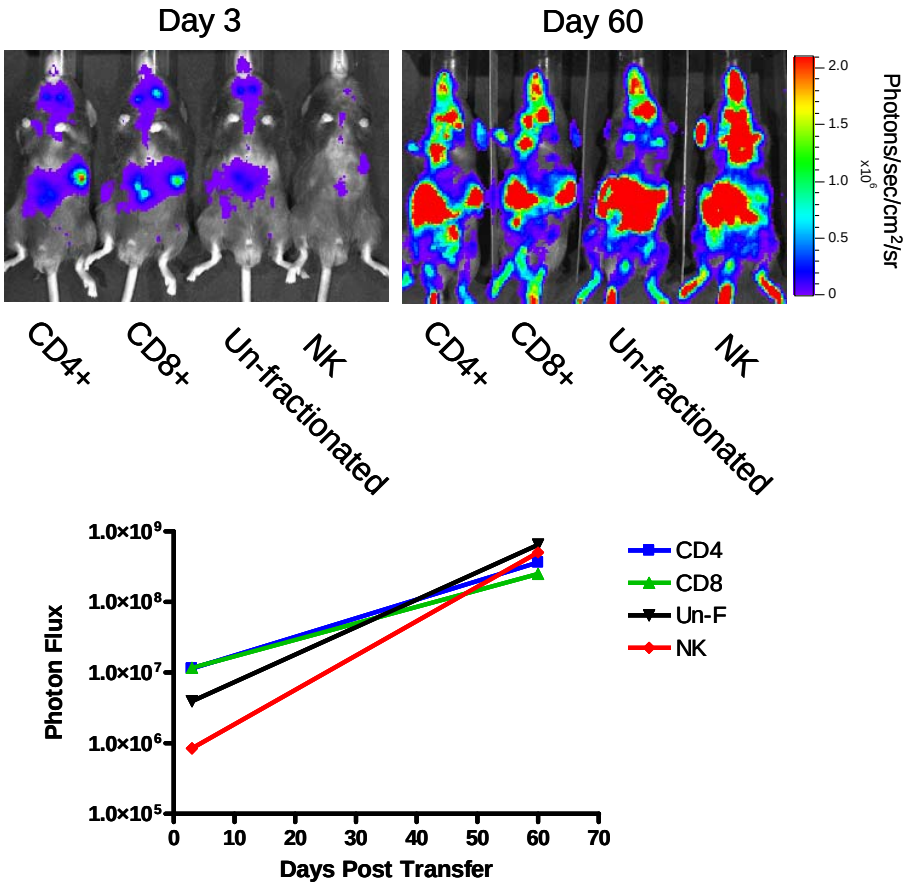

Figure 3.4: Longitudinal BLI of adoptively transferred lymphocytes. SCID mice were injected via the lateral tail vein with 10^7 CD4+, CD8+, NK cells or un-fractionated (Un-f) cells and imaged via BLI at days 3 and 60 post transfer. Scale bar in upper panel represents photons/sec/cm^2/sr and in lower graph represents whole body photon flux (photons/sec) for individual mice.

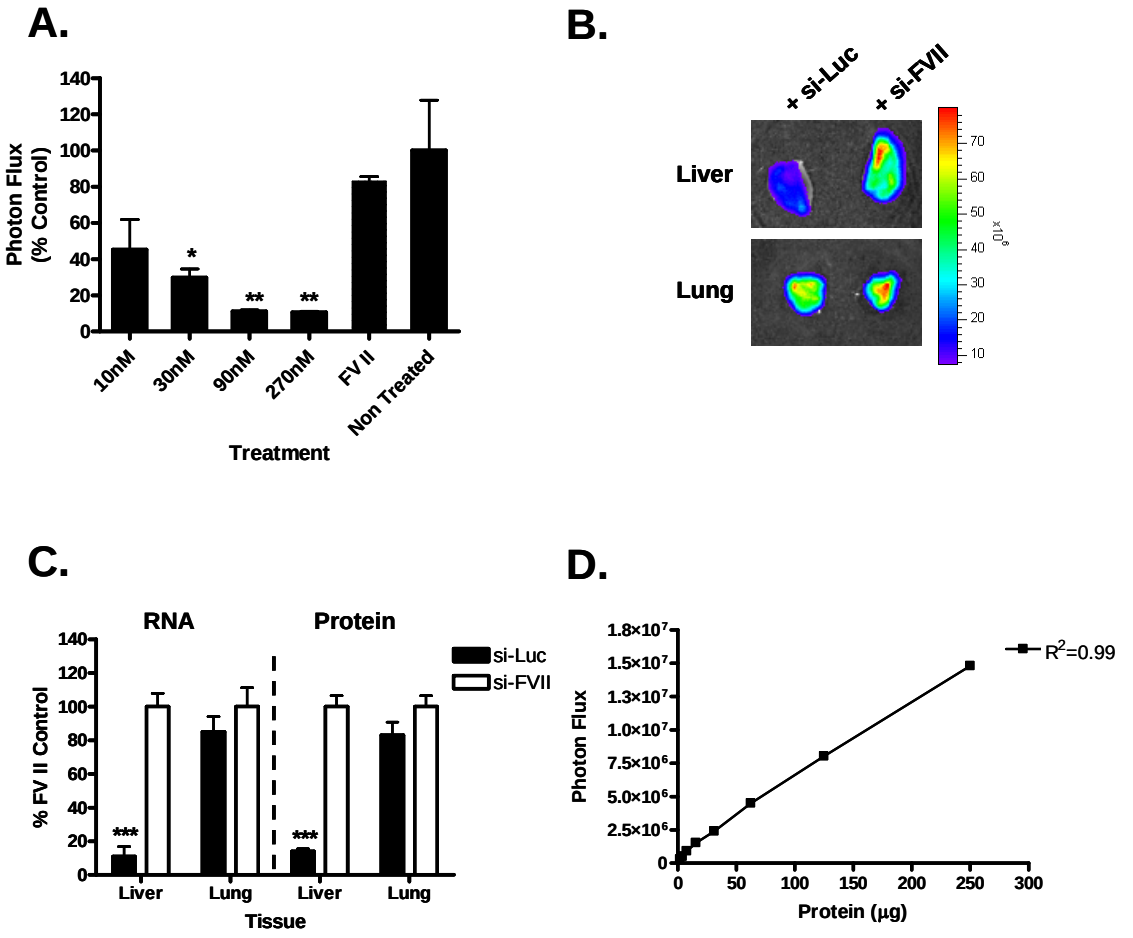

Figure 3.5: Liposomal siRNA efficacy in FLASH mice. (**A**) FLASH MEFS were treated with either 10nM, 30nM, 90nM or 270nM of si-Luc, 270nM of si-FVII or left untreated. BLI and cell viability assays were performed 72h post treatment. Y-axis represents bioluminescence as photon flux (photons/sec) normalized to cell viability. Significant differences between si-Luc and non-treated MEFS denoted by asterisks;*p<0.05, **p<0.01 ***p<0.001. Error bars represent mean + SEM (n=3). (**B**) FLASH mice were injected with either si-Luc or si-FVII and *ex vivo* BLI was performed on liver and lung tissue 72h post injection. Scale bar represents photons/sec/cm^2/sr. (**C**) Luciferase expression levels were quantified using q-RTPCR and an *in vitro* luciferase activity assay from the liver and lungs of si-Luc and si-FVII treated FLASH mice. Y-axis represents RNA and protein levels as a % of si-FVII treated control mice. Error bars represent mean + SEM (n=3). Significant differences between si-Luc and si-FVII treated animals denoted by asterisks;*p<0.05, **p<0.01 ***p<0.001. (**D**) Linear relationship between luciferase and total protein concentration from the liver of a FLASH mouse. Y-axis represents photon flux (photons/sec).

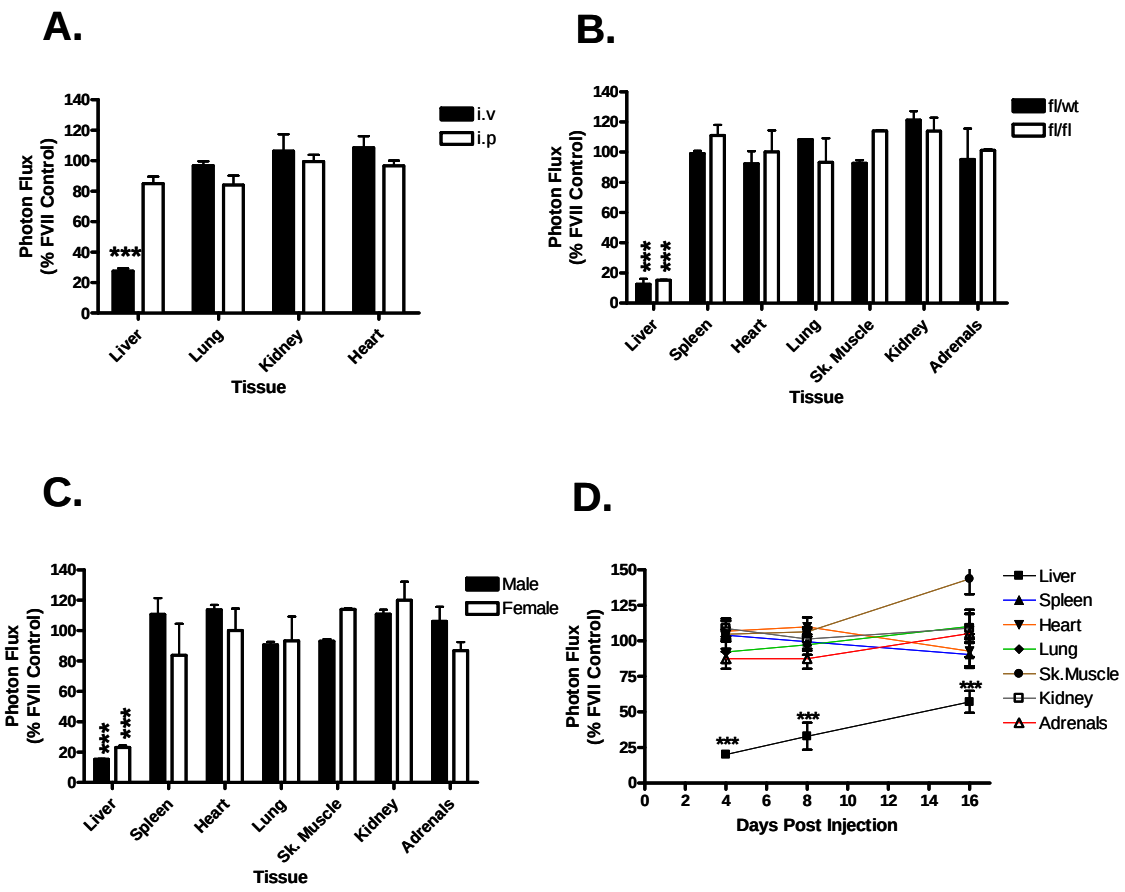

Figure 3.6: Assessing pharmacodynamics of si-Luc *in vivo*. (**A**) FLASH mice were injected intravenously or intraperitoneally with si-Luc or si-FVII (5mg/kg, single bolus i. v) and tissues were analyzed for luciferase expression 72h post injection. (**B**) si-Luc efficacy evaluated in various tissues in FLASH heterozygous (fl/wt) mice 72h post injection. (**C**) Comparison of si-Luc efficacy in male and female FLASH mice 72h post injection. (**D**) Timecourse of si-Luc efficacy in FLASH mice. Y-axes in a, b, c and d represent photon flux (photons/sec) of si-Luc treatment as a % of si-FVII control. Significant differences between si-Luc and si-FVII treated animals denoted by asterisks;*p<0.05, **p<0.01 ***p<0.001. Error bars for a, b, c and d represent mean + SEM (n=3).

CHAPTER IV

CHEMOTHERAPEUTIC AGENTS UPREGULATE THE CYTOMEGALOVIRUS PROMOTER: IMPLICATIONS FOR BIOLUMINESCENCE IMAGING OF TUMOR RESPONSE TO THERAPY

Introduction

The development of small animal imaging techniques, including bioluminescence imaging (BLI), has greatly impacted our ability to study the biology of cancer as well as to evaluate tumor response to therapy (Gross and Piwnica-Worms 2005). BLI is based on detection of photons generated from cells expressing a luciferase enzyme (Contag, Spilman et al. 1997). The light-generating reaction also requires a substrate molecule (e.g. luciferin) as well as ATP, oxygen and Mg^{++} so that signal can only be generated in viable cells. Expression of luciferase may be accomplished through stable expression in cancer cell lines used for transplantable tumor models or by transgenic expression of luciferase in genetically modified cancer-prone mice (Edinger, Sweeney et al. 1999; Vooijs, Jonkers et al. 2002).

One application of this approach has been to use BLI to monitor response to therapy (Sweeney, Mailander et al. 1999; Rehemtulla, Stegman et al. 2000). While constitutive expression of luciferase can report on cytotoxic effects of therapy, expression of luciferase in various reporter strategies can show that particular biological mechanisms are engaged by drug treatment, see for examples (Laxman, Hall et al. 2002; Luker, Pica et al. 2003; Gross and Piwnica-Worms 2005). Implementation of these approaches requires that the light signal is correlated with parameters, such as cell viability, pathway activation/inhibition etc, for which photon emission is a surrogate measurement. This has been well documented in the previously cited studies. However, as this technology has

emerged there have been questions about how certain features of the tumor microenvironment may influence bioluminescence signal generation, such as hypoxia, cellular metabolism and distribution of substrate (Lee, Byun et al. 2003; Rudin, Rausch et al. 2005; Schroeder, Yuan et al. 2005). It is thus important to remain aware of these and other possibilities as the use of BLI in cancer models is further developed and implemented.

In xenograft and syngeneic transplant models, expression of luciferase is achieved through stable transfection or transduction of a vector for luciferase expression. Generally, strong promoters in mammalian cells such as cytomegalovirus (CMV), simian virus-40 (SV40) and others have been used for constitutive expression of luciferase (Contag 2000; Rehemtulla, Stegman et al. 2000; Scatena, Hepner et al. 2004). Higher luciferase expression may generate more signal allowing for more sensitive detection of cells *in vivo*. However, it is important to remember that these promoters, while expressed well in many cell types, may nonetheless be regulated by various biological influences. In cells engineered to express CMV-driven luciferase, we show that treatment with chemotherapeutic agents doxorubicin and paclitaxel results in a transient increase in bioluminescence even though the cells are undergoing apoptosis and are less viable than control cells. We find that this is a result of increased steady state luciferase mRNA and protein. Upregulation of luciferase is dependent on the activation of the p38MAPK pathway, which is known to regulate several transcription factors capable of influencing the CMV promoter. Additionally, we find that low doses of staurosporine are capable of inducing bioluminescence through the same mechanism in cells expressing CMV-luciferase; however, at high doses, induction occurs in both CMV- and SV40-luciferase cell lines through a mechanism that does not require protein synthesis. We are able to recapitulate our *in vitro* results *in vivo* using a mouse xenograft model. The data presented here have important implications when using BLI to monitor the response of tumor cells to cancer therapy both in cell culture and in animal hosts.

Materials and Methods

Cell culture and generation of luciferase expressing cell lines

All cell lines were obtained from the American Type Culture Collection. 22RV1, LNCaP and 4T1 cells were cultured in RPMI 1640 medium and PC3, NIH/3T3 and MDA-MB-231 cells were cultured in DMEM medium. All cell culture media was supplemented with 10% FBS (Hyclone), 1% non-essential amino acids; media for luciferase expressing cell lines was also supplemented with 400µg/ml Geneticin (G418). All cells were cultured at 37°C in an atmosphere containing 5% CO_2. Generation of CMV luciferase expressing 22Rv1-CMVluc (22Rv1.Luc.PN2) cells was previously described (Drake, Gabriel et al. 2005). PC3-CMVluc, MDA.MB.231-CMVluc, 4T1-CMVluc and NIH3T3-CMVluc cells were generated using the same method. Generation of SV40 luciferase expressing 22Rv1-SV40luc (22Rv1.Luc.1.17) cells was previously described (Henry, Wen et al. 2004). Generation of CMV androgen receptor-overexpressing PC3 cells and SFFV-driven LNCaP cells were previously described [REF]. For transient transfection experiments MDA.MB.231 cells were transfected with either pCDNA3.1-luc (CMV-Luc: pGEM luciferase (Promega) subcloned into pCDNA3.1 (invitrogen)) or pGL3 (SV40 Luc-Promega) plasmids using Lipofectamine 2000 (Invitrogen) according to manufacturers instructions.

Drug treatments

For doxorubicin and paclitaxel treatment, cells were seeded at 2 x 10^5 / well in 24-well plates for caspase 3 assays or 1 x 10^5 / well in 48-well plates for bioluminescence and WST assays. 24 hrs later, media was removed and replaced with fresh media (500µl for 24 well plates and 250µl for 48 well plates) for non-treated controls or media

containing a dose range of doxorubicin (100nM, 400nM, 750nM, 1000nM; Sigma) or paclitaxel (30nM, 90nM, 300nM, 900nM; Sigma). For MDA.MB.231 cells transiently expressing luciferase, paclitaxel was added 48hrs after transfection. For staurosporine treatment, cells were seeded in 48 well plates at 1.5 x 10^5 / well. The next day cells were incubated for 30 minutes in 250µL fresh media containing 150□g/mL D-luciferin. 100µL of the appropriate dilution of STS was then added directly to cells to final concentrations of 4µM, 250nM, or 60nM and control cells received 100µL of 0.4% DMSO to make a total volume of 350µl/well. For cycloheximide treatment, 22Rv1-CMVluc cells were seeded at 1 x 10^5 / well in a 48-well plate. The next day cells were pretreated with 10µg/ml cycloheximide (Sigma) or vehicle control (H_2O) for 2 hrs. D-luciferin was then added to cells at a final concentration of 150µg/mL for 20 mins. Cells were then treated with 4□M or 60nM staurosporine or 0.4% DMSO in a total volume of 350µl/well. For p38 MAPK inhibition cells were treated with a dose range of SB203580 (3µM, 10µM or 30µM; Sigma) either alone or in combination with 400nM doxorubicin (22Rv1-CMVluc) or 90nM paclitaxel (PC3-CMVluc) for a period of 48 hrs. 0.1% DMSO was used as a vehicle control. Treated cells were analyzed (see below) at various timepoints for bioluminescence, cell viability (WST assay) and caspase 3 activity. Media was not changed throughout any of the treatment periods. For the experiments shown in Supplemental figure 2, cells were either treated with 100ng/ml Trichostatin-A (Sigma) or with media for 24 hours before western blots were performed as previously described (Rokhlin, Taghiyev et al. 2002).

Bioluminescence imaging

All BLI was performed using an IVIS 100 imaging system (Caliper Life Sciences). BLI of cells was performed by addition of D-luciferin (Caliper Life Sciences) to the cell culture medium at a final concentration of 150µg/mL. Samples were then

imaged using a 15cm field of view with exposure times varying from 1-15 seconds. Photon flux was calculated using Living Image software (version 2.5) and represented as photons/sec/cm^2/sr. Bioluminescence values were then represented as percent photon flux of untreated or vehicle control values.

Caspase 3 assay and cell viability assays

Assays for caspase 3 activity were performed using a commercially available colorimetric caspase 3 assay kit (Sigma #CASP-3-C). Cells were seeded at 2 x 10^5 / well in 24 well plates for 24 hrs at 37°C and then exposed to either apoptotic stimuli, vehicle control or left untreated. At each time point caspase 3 activity was measured following the manufacturer's instructions. Treated cells were compared to non treated or vehicle control cells and values were represented as mean ± SEM percent of control value. Cell viability was determined using a cell proliferation reagent WST-1 (Roche) according to manufacturer's instructions. Values from treated cells were divided by those from non-treated control values and represented as % control value. Each data point represents the mean ± SEM.

Quantitative-RTPCR of luciferase mRNA

pGEM *Luciferase* forward primer: 5'-CCGCGTACGTGATGTTCACC-3';
pGEM *Luciferase* reverse primer: 5'-GAGGATGGAACCGCTGGAGA-3'.
pGL3 *Luciferase* forward primer: 5'-CGCGGTCGGTAAAGTTGTTC-3';
pGL3 *Luciferase* reverse primer: 5'-CCCGGTATCCAGATCCACAA-3'.
Human *GAPDH* forward primer: 5'-CCATGTTCGTCATGGGTGTG-3';
Human *GAPDH* reverse primer: 5'CAGGGGTGCTAAGCAGTTGG-3'.

Total RNA isolation was performed using RNEasy tissue kit (Qiagen) and reverse transcription was carried out using iScript cDNA synthesis kit (BioRad). The resulting cDNAs were used as PCR template using CYBR Green I (Invitrogen) and data was collected on iCycler thermal cycler (BioRad). Experimental values were normalized to GAPDH values. Relative expression values were calculated using a comparative Ct method (Pfaffl 2001).

Luciferase activity assay

Lysates of staurosporine-treated, doxorubicin-treated or untreated cells were prepared by adding 500µL of lysate buffer (250mM sucrose, 25mM HEPES, 1mM EDTA; pH 7.2) to monolayers growing in 6 well plates and homogenizing by pipetting. Protein concentrations were calculated using a BioRad Dc Protein Assay. Equal amounts of protein (averaging 37µg/well/assay) were added at a volume of 50µL to 96 well plates, mixed with 100µL assay buffer (15mM $MgCl_2$, 150µg/mL D-luciferin, 1µg/mL ATP, 1M Tris-HCl; pH 7.4) and imaged in an IVIS 100.

Subcutaneous tumor model

All animal procedures were performed with approval from the University of Iowa Animal Care and Use Committee. 24 male athymic *nu/nu* mice (NCI) were injected into the periscapular subcutis with either 2 x 10^6 22Rv1-CMVluc cells (12 mice) or 2 x 10^6 22Rv1-SV40luc cells (12 mice) while being maintained on 3% isoflurane. Mice were returned to their housing and closely monitored for body weight and general health status. After 13 days of tumor development mice were imaged using the IVIS 100 and tumor volumes were measured using calipers and calculated using the equation ½[L x W^2]. For each cell line mice were randomly divided into two groups (n=6) (designated PBS and

doxorubicin), each group having similar average bioluminescence intensities as determined by t-test. Mice in the PBS group then received 200μL of PBS and mice in the doxorubicin group received 200μL of doxorubicin 8mg/kg (200μL@1mg/ml) via intravenous tail vein injection. Mice were imaged and tumor volumes were recorded at 1, 2, 3, 4, 5, 6, 10 and 23 days post treatment. Body weight was measured at the same time intervals. For BLI of mice, mice were first anesthetized in a chamber with 3% isoflurane. D-luciferin was then administered to each mouse via intraperitoneal injection at a dose of 150mg/kg and left to incubate for 8 minutes while being maintained on 3% isoflurane. Mice were then imaged using a 20cm field of view and an exposure time of 1 second. Bioluminescence values were calculated by measuring photons/sec/cm^2/sr in the region of interest surrounding the bioluminescence signal from the tumor with the lower signal threshold set to 5% of the maximum signal value.

P38MAPK western blot

Lysates were prepared from cells treated with or without lipopolysaccharide or 400nM doxorubicin for a period of 5 minutes. Protein concentrations were calculated using a BioRad Dc Protein Assay. Equal amounts of protein were electrophoresed in a 12% SDS polyacrylamide gel and transferred onto PVDF membranes. Membranes were blotted with phospho p38 MAPK antibody (Biosource 44-684G) or β-actin antibody (Sigma A1978), incubated with HRP-conjugated goat anti-rabbit IgG (Jackson 111-035-003) and signal was detected by enhanced chemiluminescence.

Statistical analyses

All statistical analyses were performed using ANOVA with Bonferroni post tests.

Results

Treatment of luciferase expressing prostate cancer cells with apoptosis-inducing agents results in a transient increase in bioluminescence.

Our original observation occurred when we treated luciferase expressing 22Rv1 cells with AR targeted siRNAs (Chapter II). We noticed that cells treated with AR siRNAs, despite undergoing apoptosis and losing viability, had higher levels of bioluminescence intensity 3 days after treatment when examined in an IVIS100 imaging system (Figure 4.1). The effect was transient because bioluminescence was lower than control treated cells 6 days after treatment. To determine whether the effect was specific to AR inhibition or a result of apoptosis we next examined the effects of chemotherapeutic agents doxorubicin, a DNA-damaging agent; paclitaxel, a microtubule-stabilizing agent; and staurosporine, a potent protein kinase inhibitor, on luciferase-expressing human prostate cancer cell lines (Figures 4.2, 4.3, 4.4 and Table 1). These cell lines have been engineered to stably express luciferase either via retroviral transduction with CMV-driven luciferase (CMVluc) or stable transfection with SV40 driven luciferase (SV40luc) and are designated as 22Rv1-CMVluc, PC3-CMVluc and 22Rv1-SV40luc. As expected, in all three cell lines, doxorubicin, paclitaxel and staurosporine elicited apoptotic cell death and a consequent loss of cell viability as measured by caspase 3 activity and WST viability assay, respectively (Figures 4.2C, 4.2B and Figure 4.4). High dose staurosporine (4μM) rapidly caused significant induction of apoptosis by 2h (Figure 4.2C) and a significant loss of cell viability 6-8hrs post treatment. Lower doses of staurosporine (60nM and 250nM) induced a slight, but significant induction of caspase 3 and reduction of cell viability by 24h (Figure 4.4D). Similarly, doxorubicin and paclitaxel treatment resulted in peak caspase 3 activity between 24-48hrs and cell

viability significantly decreased 48hrs after treatment (Figure 4.4B and Figures 4.3 B,C,E,F,H,I).

We also measured bioluminescence from these cell lines and, surprisingly, we found increased signal upon staurosporine treatment of all three cell lines and upon doxorubicin and paclitaxel treatment of 22Rv1-CMVluc and PC3-CMVluc cells (Figures 4.2 A-D, Figure 4.3, Figure 4.4A-B and Table 1). The increase in bioluminescence signal in response to doxorubicin and paclitaxel occurred even as these cells were undergoing apoptotic cell death and a loss in cell viability (Figure 4.4B, Figure 4.3B, C, E and Table 1). In contrast, we only observed an increase in bioluminescence in 22Rv1-SV40luc cells treated with a high 4μM dose of staurosporine (Figure 4.2A), whereas we observed increases with 4μM and lower doses of 60nM and 250nM in both 22Rv1-CMVluc and PC3-CMVluc cells (Figure 4.2A-D). Bioluminescence induction in response to 4μM staurosporine was characteristically rapid, peaking within 1hr of treatment (Figure 4.2C) and preceding peak induction of apoptosis, whereas the increase in bioluminescence signal from the 60nM staurosporine-treated CMVluc cell lines became maximal only after 24 hr similar to the time course for induction of apoptosis (Figure 4.2D). In 22Rv1-CMVluc cells all three agents induced an increase in bioluminescence to levels significantly higher than control values, ranging from 150%-250%. With the exception of doxorubicin treatment, we saw similar effects in PC3-CMVluc cells (Figure 4.2A, B, and Figure 4.4A). At later time points, (~120hrs with doxorubicin and paclitaxel) cells treated with any of the three agents exhibited decreases in bioluminescence to levels below that of untreated control values (Figure 4.4B, Figure 4.3B,C,E,F,H,I and Table 1). Thus, each agent is able to induce a transient increase in bioluminescence and in some cases, this occurs during a period in which these agents induce apoptosis and a loss in cell viability. We also noticed similar effects when cells were treated with the histone deacetylase inhibitor Trichostatin A (TSA). TSA was able to induce bioluminescence in both 22Rv1-CMVluc and PC3-CMVluc cell lines (Figure 4.5). This effect was also not

limited to the expression of luciferase as TSA treatment induced AR expression in PC3 cells engineered to express AR from the CMV promoter. However, TSA was unable to induce AR expression in cells engineered to express AR from the SFFV promoter (Figure 4.5B).

To determine whether the increase in bioluminescence in response to apoptotic inducing agents was specific for human prostate carcinoma cell lines, we examined human breast carcinoma (MDA.MB.231) mouse mammary carcinoma (4T1) and mouse fibroblast (NIH/3T3) cells engineered to express CMV driven luciferase with the same retroviral expression vector as 22Rv1-CMVluc and PC3-CMVluc cells (Fig. 4.4C). We also examined MDA.MB.231 cells transiently transfected with either pCDNA3.1-luc (CMV-driven luciferase) or pGL3 (SV40-driven luciferase) (Figure 4.4D). For each of the cell lines engineered to express luciferase under the control of the CMV promoter, optimized doses of paclitaxel induced a significant increase in bioluminescence compared to non-treated controls (Figure 4.4C), though the magnitude of this increase varied among these cell lines. In contrast, MDA.MB.231 cells transiently expressing luciferase under control of the SV40 promoter did not show induction of bioluminescence signal in response to drug treatment as we observed for the 22Rv1 cell line. These data indicate that paclitaxel induces bioluminescence in cells expressing luciferase under the control of the CMV promoter, but not SV40 promoter. This occurs in multiple cell lines and is independent of the method in which the expression vector is introduced to these cells (stably integrated retroviral vector or transient transfection of a plasmid-based vector).

Bioluminescence can be induced by translation-independent and translation- dependent mechanisms

We observed a transient increase in bioluminescence in all three human prostate cancer cell lines using a high dose of staurosporine but only 22Rv1-CMVluc and PC3-

CMVluc cell lines exhibited an increase in bioluminescence in response to lower doses. To test whether the increase in bioluminescence we observed was due to new protein synthesis, possibly *de-novo* luciferase production, we tested the effects of 4μM staurosporine and 60nM staurosporine on 22Rv1-CMVluc cells in the presence or absence of 10ug/mL cycloheximide, a potent translation inhibitor. Figure 4.6A demonstrates that cycloheximide was unable to block the induction in bioluminescence signal by 4μM staurosporine, indicating that the increase in bioluminescence from a 4μM dose of staurosporine does not result from new protein synthesis. In contrast, Figure 4.6B demonstrates that 10μg/ml cycloheximide blocked bioluminescence induction by a 60nM dose of staurosporine at 4hrs and 6hrs post treatment. These data indicate that different doses of staurosporine are able to induce bioluminescence through two independent mechanisms; a translation-independent mechanism (at 4uM staurosporine) and a translation-dependent mechanism (at 60nM staurosporine).

A previous study reported that arsenite treatment of cell lines transfected with CMV expressing constructs induces an increase in transcription from the CMV promoter via activation of cellular stress factors (Bruening, Giasson et al. 1998). 22Rv1-CMVluc and PC3-CMVluc cell lines have been engineered to express luciferase through transduction with a retroviral vector that expresses luciferase from an internal CMV immediate early promoter with its proximal enhancer element (herein referred to as CMV promoter) and contains a CMV/MSV hybrid promoter in the 5' LTR (pQCXIN; BD Biosciences). In contrast, 22Rv1-SV40luc cells are engineered to express luciferase through stable integration of a vector containing SV40 promoter driven luciferase expression. Since we did not observe an increase in bioluminescence in 22Rv1-SV40luc cells treated with varying doses of doxorubicin and paclitaxel or low doses of staurosporine, we reasoned that these agents are able to increase bioluminescence in 22Rv1-CMVluc and PC3-CMVluc cells through a promoter-dependent mechanism. To test this hypothesis, we examined whether the levels of luciferase mRNA and protein

were altered upon staurosporine and doxorubicin treatment (Figure 4.6C, D and Figure 4.7). We treated both 22Rv1-CMVluc and 22Rv1-SV40luc cell lines with either 4μM staurosporine for 1hr, 60nM staurosporine for 6hrs or 400nM doxorubicin for 48 hours. To evaluate the levels of luciferase mRNA, we performed qRT-PCR on RNA prepared from treated and untreated 22Rv1-CMVluc and 22Rv1-SV40luc cells. Figure 4.6C shows that luciferase mRNA levels are significantly increased when 22Rv1-CMVluc cells are treated with 60nM staurosporine. Luciferase mRNA levels were also significantly increased when 22Rv1-CMVluc cells were treated with 400nM doxorubicin (Figure 4.7). However, although bioluminescence intensity was significantly increased in cells treated with 4μM staurosporine, luciferase mRNA levels actually decreased relative to the control 1hr after treatment. Luciferase mRNA levels in staurosporine and doxorubicin-treated 22Rv1-SV40luc cells were not significantly increased compared to untreated control values. These findings indicate that low doses of staurosporine and 400nM doxorubicin upregulate the synthesis of luciferase in cells where its expression is controlled by the CMV promoter. We then prepared lysates from treated and non-treated cells at the same timepoints as above and analyzed luciferase activity in a cell-free assay. Figure 4.6D shows that the levels of luciferase protein in 22Rv1-CMVluc cells are significantly increased to ~300% of control values upon low dose staurosporine treatment. Doxorubicin treatment also induced a significant increase in luciferase protein in 22Rv1-CMVluc cells (Figure 4.7). Strikingly, cell-free luciferase activity was not significantly different in cells treated with 4μM of staurosporine. 22Rv1-SV40luc cells did not show a difference in the levels of luciferase activity compared to non-treated control cells. Taken together, these data indicate an increase in luciferase activity, subsequent to upregulation of the CMV promoter when cells are treated with low doses of staurosporine and 400nM doxorubicin. However, high doses of staurosporine are able to increase bioluminescence by a mechanism that does not involve upregulation of the CMV promoter and is only apparent when luciferase is in intact cells.

Doxorubicin treatment of subcutaneous luciferase expressing xenograft tumors leads to a transient increase in bioluminescence *in vivo*

To test whether we could extend our findings in cell-based assays to tumors *in vivo* we employed a subcutaneous xenograft model. Figure 4.8A shows that a single dose of doxorubicin had a marked effect on tumor growth, with the average tumor volume being 4-fold lower than PBS controls 10 days after treatment. However, Figure 4.8B demonstrates that the bioluminescence signal from the doxorubicin-treated animals was comparable to PBS controls during this period. When bioluminescence is normalized to tumor volume (photons/sec/cm^2/sr/mm^3) there is an increase in bioluminescence in the doxorubicin treated group relative to the PBS controls over a period of 10 days following treatment (Figure 4.8C). Images in Figure 4.8C show examples of animals from these doxorubicin and PBS (day 6 post-treatment) groups where it is clear that the smaller tumor (50mm^3) in the doxorubicin-treated animal is emitting a bioluminescence signal comparable to the larger tumor (220mm^3) in a PBS-treated animal. Figure 4.8C also demonstrates that the bioluminescence increase is transient. 23 days after treatment, both groups displayed similar normalized values. This normalized value is modestly lower than when treatment commenced, possibly due to necrosis in these tumors or decreased efficiency in light penetration as the tumors grow larger. In contrast, normalized bioluminescence signals were similar throughout the time course among doxorubicin and PBS-treated mice bearing xenografts derived from 22Rv1-SV40luc cells (Figure 4.9). Thus, these results parallel our observations of doxorubicin-induced increase in bioluminescence signal from CMV-driven luciferase *in vitro*.

Inhibition of the p38MAPK pathway blocks doxorubicin and staurosporine induced bioluminescence in 22Rv1-CMVluc cells.

The CMV promoter is complex and contains numerous binding sites for transcription factors such as Sp-1, CREB/ATF, and NFκB, among others which are regulated by a variety of cell signaling pathways [REF]. To determine which pathway(s) might be responsible for our observations, we screened several small molecule inhibitors of the NFκB, JNK, and p38 MAPK pathways for their ability to block doxorubicin-induced bioluminescence in 22Rv1-CMVluc cells. Only the p38 MAPK inhibitor SB203580 was able to block bioluminescence induced by doxorubicin and staurosporine in 22Rv1-CMVluc cells. Figure 4.10A shows that a 30 μM dose of SB203580 was able to block ~95% of the bioluminescence induction by doxorubicin (at 48hrs) or low dose staurosporine (at 24hrs) in 22Rv1-CMVluc cells. We were also able to block 95% of the bioluminescence induction by paclitaxel in PC3-CMVluc cells. Another p38MAPK inhibitor, SB202190 also significantly blocked bioluminescence induction by doxorubicin and paclitaxel in 22Rv1-CMVluc cells, though to a lesser degree than SB203580. These data suggest that p38 MAPK is activated upon doxorubicin, paclitaxel and low dose staurosporine treatment and is able to upregulate the CMV promoter. To determine whether SB203580 was able to block the bioluminescence induction through inhibiting upregulation of the CMV promoter we also prepared RNA from the treated cells and performed qRT-PCR for luciferase mRNA. Figure 4.10B demonstrates that doxorubicin treatment alone induced a 5-fold increase in luciferase mRNA but addition of the SB203580 was able to block this increase. Finally, to measure activation of p38MAPK we performed western blotting for phosphorylated p38MAPK from 22Rv1-CMVluc cells treated with doxorubicin. Figure 4.10C demonstrates that p38MAPK becomes phosphorylated when cells are treated with doxorubicin. Taken together, these results indicate that treatment with low dose staurosporine, doxorubicin and paclitaxel

induces a p38 MAPK stress response that is responsible for the observed upregulation of the CMV promoter and increased bioluminescence signal.

Discussion

We found that the treatment of prostate cancer cell lines which stably express firefly luciferase from a CMV promoter with apoptosis-inducing agents (AR-siRNAs, staurosporine, doxorubicin, paclitaxel and trichostatin A) induced a transient increase in bioluminescence even as these cells were undergoing apoptosis. Of these treatments, only a high dose of staurosporine (4μM) was capable of producing this same result in prostate cancer cells stably expressing luciferase under the control of the SV40 promoter. Lower doses of staurosporine (60nM and 250nM) were only capable of inducing bioluminescence in CMV luciferase expressing cells. Furthermore, cycloheximide treatment of cells expressing CMV-driven luciferase abrogated the induction of bioluminescence elicited by low doses (60nM) of staurosporine, while co-treatment of cycloheximide with high doses of staurosporine (4μM) was unable to block bioluminescence induction; thus, we concluded that the high dose staurosporine induces bioluminescence through a promoter-independent mechanism and does not require new protein synthesis. We also observed a transient induction of bioluminescence in other, non-prostate cancer cell lines stably expressing CMV-driven luciferase. Further investigations revealed that doxorubicin treatment of 22Rv1 cells induced luciferase mRNA expression from the CMV promoter as well as increased production of luciferase protein as measured by in vitro luciferase assay, concomitant with increased bioluminescence signal. These findings in cultured cells were extended *in vivo*; treatment of mice bearing 22Rv1 xenografts with CMV-, but not SV40-driven, luciferase with doxorubicin also resulted in a transient increase in bioluminescence when normalized to tumor volume. This observation resulted from the maintenance of relatively steady mean

bioluminescence values in tumors that were dramatically decreasing in volume in response to doxorubicin treatment; while control tumors maintained a consistent relationship between tumor volume and bioluminescence signal.

We considered several possibilities to explain these observations: (1) these agents result in the production of reactive oxygen species that affect the redox-sensitive bioluminescence reaction; (2) apoptosis results in the temporal increase in cytosolic ATP levels, increasing bioluminescence; (3) the expression of the luciferase enzyme was increased. A previous study by Zamaraeva et al. reported a transient increase in bioluminescence from staurosporine, tumor necrosis factor-α-, and etoposide-treated cell lines expressing luciferase under the control of the SV40 promoter (pGL3 control vector, Promega) (Zamaraeva, Sabirov et al. 2005). This group argued that cells undergoing apoptosis exhibit an increase in cytosolic ATP, with little increase in total cellular ATP, which rapidly and transiently results in increased bioluminescence. Using the same high dose of staurosporine we showed that the induction of bioluminescence is independent of promoter status and *de-novo* protein synthesis. Therefore it is possible that ATP compartmentalization or other effects on luciferase reaction components may be influencing the light generating reaction and driving the increase in bioluminescence. We also demonstrate that lower doses of staurosporine are able to increase bioluminescence by a mechanism that is not explained by an increase in cytosolic ATP. Our data show that this alternative mechanism is dependent upon *de novo* protein synthesis, and that the increase in bioluminescence observed is due to upregulation of the CMV promoter. Thus, we conclude that under the sets of conditions studied, induction of bioluminescence occurs through two independent mechanisms: 1) a promoter-independent mechanism,, not requiring new protein synthesis and 2) a promoter-dependent mechanism which requires *de novo* protein synthesis and is associated with an increase in the steady state levels of luciferase mRNA and protein.

The CMV immediate early promoter with its proximal enhancer is commonly employed to achieve high level protein expression in mammalian cells (Stinski 1999). However, this element is also known to be responsive to a variety of stimuli that activate various signaling pathways, including NFκB and p38 MAP kinases, among others, which are involved in viral replication (Johnson, Huong et al. 2000; Chen and Stinski 2002). As a consequence of this biology, when the CMV promoter is used to drive expression of heterologous proteins, factors which engage those pathways such as inflammatory cytokines or cell stress-related molecules may alter the expression of proteins under its control (Ramanathan, Hasko et al. 2005). Previous studies have shown that the CMV promoter activity is increased by NFκB activation (Sambucetti, Cherrington et al. 1989; Prosch, Staak et al. 1995). Since chemotherapeutic drugs have been shown to activate the NFκB pathway in some cell types, we were surprised to find that specific inhibitors of this pathway did not block CMV-driven bioluminescence induction in doxorubicin- and paclitaxel-treated prostate cancer cell lines. Rather, our studies indicated that activation of the p38 MAPK pathway was responsible for activation of the CMV promoter. Consistent with our findings, Bruening et al. reported that a p38 MAPK inhibitor completely blocked arsenite-induced up regulation of the CMV promoter (Bruening, Giasson et al. 1998). Previous studies have demonstrated that p38 MAPK is activated upon treatment with doxorubicin and paclitaxel (Bacus, Gudkov et al. 2001; Grethe, Coltella et al. 2006). These studies also showed that inhibition of p38 MAPK reduced doxorubicin- and paclitaxel-induced apoptosis, demonstrating an important role for p38 MAPK in the apoptotic process. More recently, Reinhardt et al. also demonstrated the importance of p38 MAPK activation in cell cycle checkpoint function after DNA damage (Reinhardt, Aslanian et al. 2007). We were able to block ~95% of the bioluminescence induction by doxorubicin and paclitaxel in 22Rv1 cells using a specific inhibitor of p38 MAPK. p38 MAPK activates the transcription factors CREB, ATF-2, and ETS-1, all of which have binding sites within the CMV proximal enhancer and are required for optimal

HCMV replication. However, paclitaxel but not doxorubicin, induced bioluminescence in PC-3 cells indicating that this response may be cell-type specific and/or dependent on the genetic status of the cell type. Together these results highlight the complex regulation of the CMV promoter in response to various cytokines, chemotherapeutics and other stress-inducing stimuli and suggest the likelihood that factors other than p38MAPK may regulate expression from this promoter, both positively and negatively, in response to different treatments, physiologic contexts, or in a cell-type specific manner.

Given that the CMV promoter has long been known to be responsive to various stress-sensing pathways, it is not surprising that the chemotherapeutic agents employed in this study (which also engage similar pathways) would induce luciferase expression driven by the CMV promoter. Therefore, this information is highly relevant for designing and interpreting studies involving bioluminescence to assess tumor response to chemotherapeutics in mouse models. Indeed, in the original paper describing BLI, the potential problematic aspects of agents that affected constitutive promoters driving luciferase expression were noted (Contag, Spilman et al. 1997). We recapitulated our *in vitro* observations in a subcutaneous tumor model. In response to chemotherapeutic agent doxorubicin, 22Rv1-CMVluc xenografts demonstrated tumor regression as evaluated by traditional volume measurements. However, during a period of 3-10 d following a single dose of doxorubicin (8mg/kg; i.v.) these tumors exhibited bioluminescence signals comparable to PBS-treated control tumors. Effectively, this treatment changed the relationship between viable cell number and light output following treatment. The duration of elevated bioluminescence was longer *in vivo* than *in vitro,* >10d versus <4d, respectively. This could be due to differences in drug exposure in tumors versus *in vitro* culture conditions or other mechanisms such as inflammation in the regressing tumor. In contrast, the light output from 22Rv1-SV40luc xenografts did not appreciably change as a function of tumor volume following doxorubicin treatment even though these tumors also responded by a decrease in tumor volume, arguing that the

increased bioluminescence signal in 22Rv1-CMVluc xenografts did not result from a drug-induced effect on the tumor microenvironment. Thus, these *in vivo* findings mirrored our *in vitro* findings, suggesting that doxorubicin-treatment induces a p38 MAPK-dependent increase in luciferase expression from the CMV-promoter in 22Rv1-CMVluc xenografts.

These findings demonstrate that caution is warranted in the design and interpretation of experiments involving BLI to assess tumor response to chemotherapeutics in mouse models. A previous study showed that paclitaxel treatment (10mg/kg/d; i.p.) of PC-3 xenografts expressing luciferase under the control of the CMV-promoter resulted in decreased tumor weight in intramuscular primary tumors but luciferase activity measured in homogenates from these tumors was not significantly different from control treated animals (El Hilali, Rubio et al. 2005). This led the authors to suggest that paclitaxel was exerting its effects primarily on the tumor stroma, leading to reduced tumor weight. Our results suggest an alternative possibility that these results may be explained by paclitaxel upregulation of luciferase expression driven by the CMV promoter in these tumors. Thus, care should be taken to evaluate possible effects of drug treatment on luciferase expression with *in vitro* studies and to correlate BLI results with alternative measures of tumor growth. To the extent that specific mechanisms can be related to the regulation of the CMV promoter in tumor cells *in vivo*, this liability might also be useful as a pharmacodynamic marker of drug effect. Specific bioluminescent reporters have already been used successfully in mice to evaluate drug effects in mice, for example (Gross and Piwnica-Worms 2005). Although the SV40 promoter was not influenced by some drug treatments in our experiments, we are reluctant to conclude that this will be the case with other treatments in other contexts. The SV40 promoter-driven luciferase has been used successfully to measure the response to chemotherapy in several previous studies e.g. (Rehemtulla, Stegman et al. 2000; Jenkins, Yu et al. 2003). In the case of studies involving the CMV-promoter, the induction of bioluminescence may not

have been observed due to the cell lines or treatments involved or chosen imaging timepoints may not have captured a transient increase in bioluminescence signal (Buchhorn, Seidl et al. 2007). Treatments that dramatically and rapidly reduce tumor burden would be expected to mask any potential upregulation in the CMV-promoter, though in this case BLI may underestimate drug efficacy. Future studies involving BLI of tumor response to therapy should account for other effects on quantitation *in vivo* such as changes in O_2 levels and pharmacokinetics of luciferin delivery to tumors, both of which may be affected by treatment and have the potential to modify the resultant signal. BLI has become an important tool for the development of sophisticated animal models of cancer and other diseases, as well as providing quantitative assessments of response to therapeutic interventions and we expect this to continue. However, our studies underscore the fact that a biological process, the luciferase-mediated light generating reaction, is required to generate a signal in this imaging modality. Therefore, one should carefully consider how other biological processes or agents extrinsic to the light generating reaction may potentially affect the signal generated.

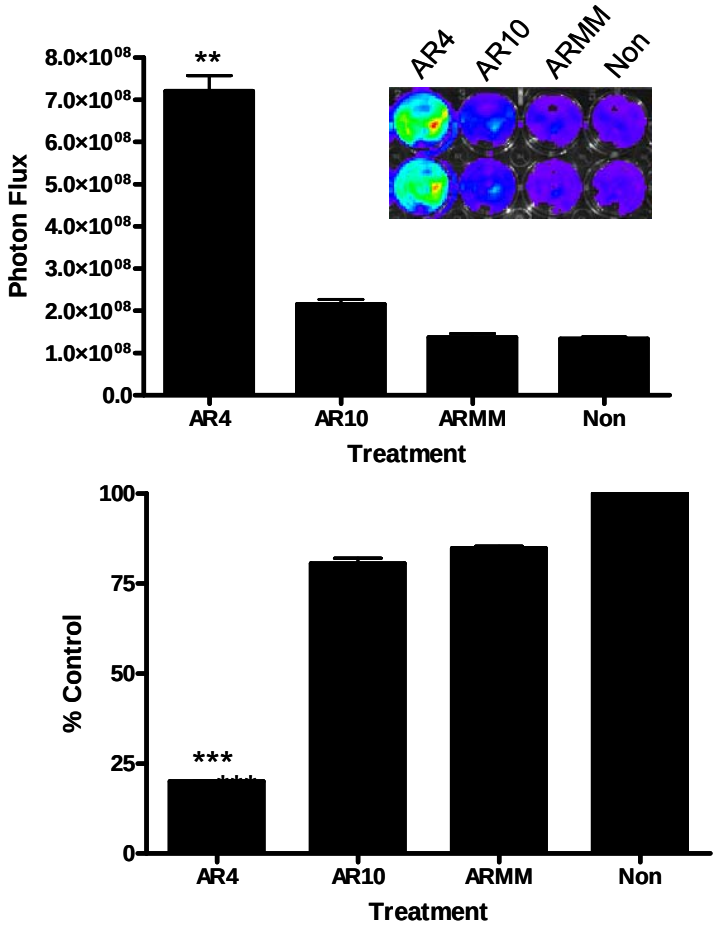

Figure 4.1: AR siRNAs induce an increase in bioluminescence in 22Rv1 cells that is inversely correlated with cell viability. (A) Cells were treated with AR4, AR10, ARMM or left untreated (Non) and assayed for bioluminescence 3 days post treatment. Bioluminescence intensity increases in AR4 and AR10 treated cells. Image is of bioluminescence overlay from the IVIS100. (B) Cell viability assay of treatment groups. AR4 significantly reduced cell viability in 22Rv1 cells 3 days post treatment. Significant differences between treatment groups denoted by asterisks; **p<0.01, ***p<0.001

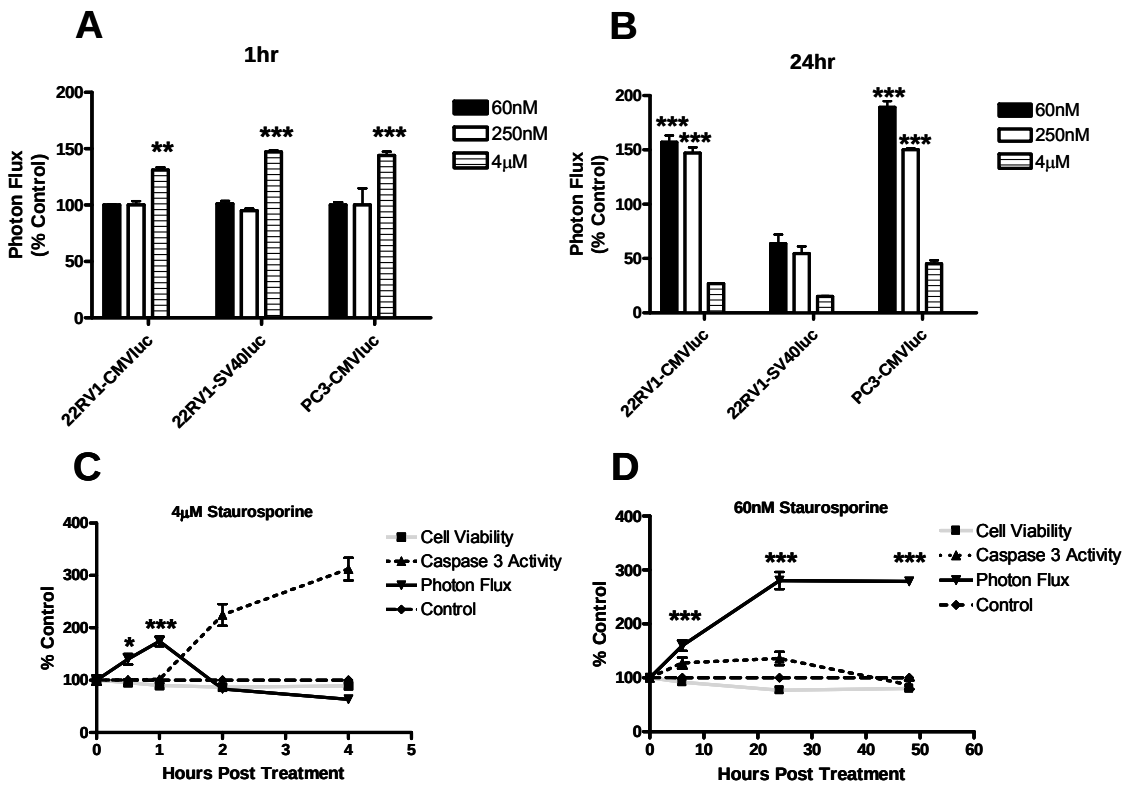

Figure 4.2: Staurosporine induces a transient increase in bioluminescence in luciferase expressing prostate carcinoma cells. 22Rv1-CMVluc, 22Rv1-SV40luc and PC3-CMVluc cells were treated with varying doses of staurosporine for up to 24h. Y-axes in *A* and *B* represent bioluminescence signal as photon flux (photons/sec/cm^2/sr) expressed as % vehicle control. *A*, 4μM staurosporine induces a rapid increase in bioluminescence in all three cell lines after 1 hr of treatment. *B*, 60nM and 250nM staurosporine treated 22Rv1-CMVluc and PC3-CMVluc cells exhibit an increase in bioluminescence after 24hrs which was not evident in 22Rv1-SV40luc cells. *C*, Representative time course of 22Rv1-CMVluc cells treated with 4μM staurosporine demonstrating that at this high dose the bioluminescence increase is transient and precedes induction of apoptosis (caspase 3 activity). *D*, Representative timecourse of 22Rv1-CMVluc cells treated with 60nM staurosporine demonstrating that at this low dose the bioluminescence increase accompanies induction of apoptosis (caspase 3 activity) and a loss in cell viability. Significant increases in photon flux relative to controls are denoted by asterisks; *p<0.05, **p<0.01 ***p<0.001.

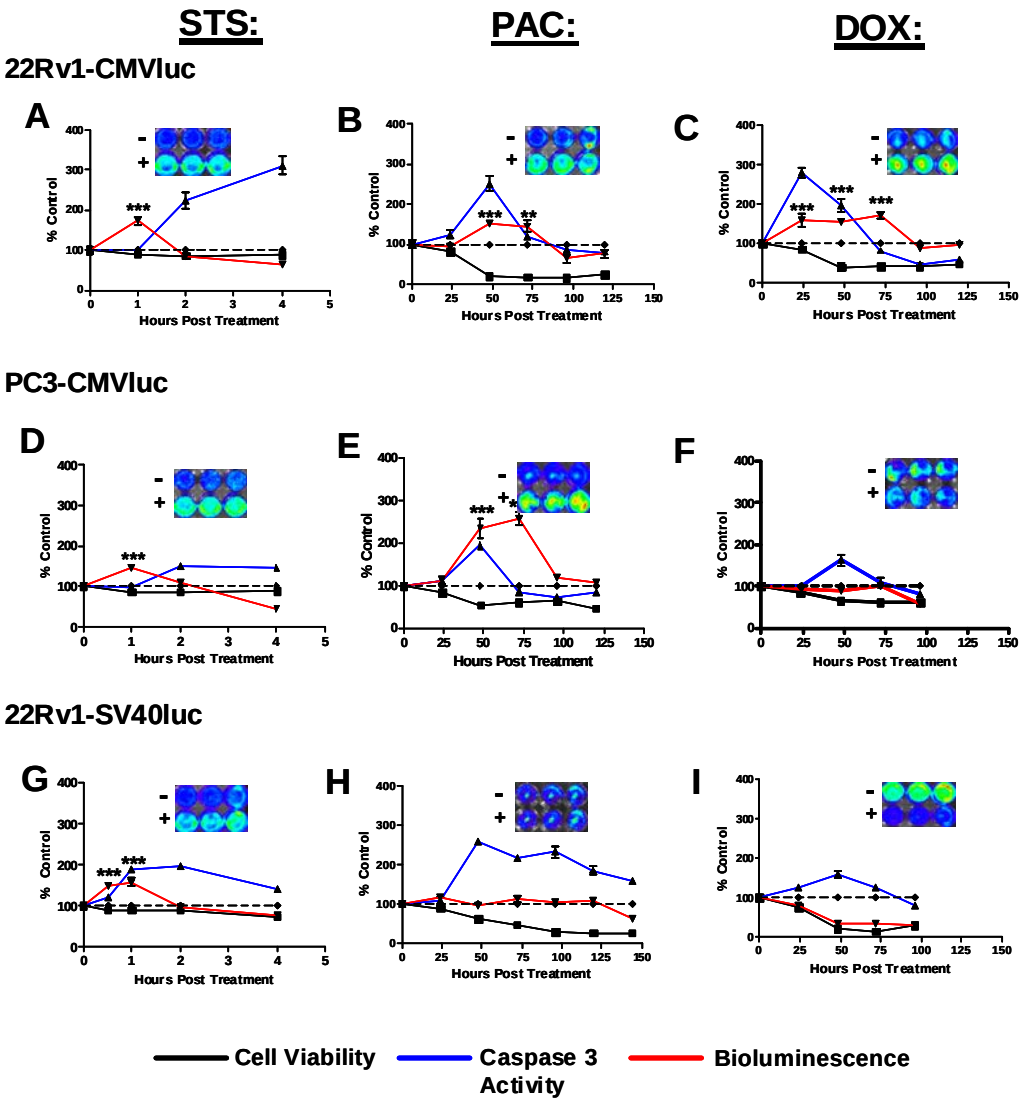

Figure 4.3: Doxorubicin, staurosporine and paclitaxel induce a transient increase in bioluminescence in luciferase expressing prostate carcinoma cells. 22Rv1-CMVluc, PC3-CMVluc, and 22Rv1–SV40luc cells were treated with either 4 µmol/L of staurosporine (STS) for 4 h; 90 nmol/L paclitaxel (PAC) for 6 days; or doxorubicin (DOX) (400 nmol/L in 22RV1-CMVluc and 22RV1-SV40luc and 700nmol/L in PC3-CMVluc cells) for 5 days. Bioluminescent images, caspase-3 activation assays and cell viability assays were performed daily throughout the time course for each treatment. The Y axis represents the percent of control values for each parameter being measured. Staurosporine induces a rapid and significant increase in bioluminescence in all three cell lines after 1 h of treatment, after which signal begins to decline as cells die (*A*, *D*, *G*). Paclitaxel induces a significant increase in bioluminescence in both CMVluc lines from 24 - 48 h; after 75 h, bioluminescence signal begins to decline as cells lose viability and die (*B*, *E*, *H*). Doxorubicin induces a significant increase in bioluminescence only in 22Rv1-CMVluc cells (C) at 24 h; after 75 h, signal begins to decline as cells die (*C*,*F*,*I*). Significant increases in photon flux relative to controls are denoted by asterisks; **p<0.01 ***p<0.001

TABLE 1	Dose (nM)	Cell Line	Cell Viability ± SEM	Caspase 3 Activity ± SEM	Photon Flux ± SEM
Doxorubicin	400	22RV1.Luc.1.17	21± 2.3 *	158 ± 8.6 †	36 ± 1.6
	400	22RV1.Luc.PN2	39 ± 10.8 *	196 ± 16.6 †	170 ± 9.0 ‡
	700	PC3.Luc.PN2	65.7 ± 5.2 *	132 ± 11.8 †	87.8 ± 7.3
Paclitaxel	90	22RV1.Luc.1.17	45 ± 7.2 *	257 ± 0.5 †	95 ± 3.4
	90	22RV1.Luc.PN2	21 ± 0.8 *	251 ± 17.9 †	153 ± 2.3 ‡
	90	PC3.Luc.PN2	55 ± 3.7 *	194 ± 7.4 †	238 ± 2.3 ‡

Table 4.1: **Doxorubicin and paclitaxel-induced increase in bioluminescence is accompanied by an induction of apoptosis and a loss in cell viability**. Table shows effects of chemotherapeutic agents on bioluminescence, cell viability and apoptosis in CMV-Luc and SV40-Luc cell lines.

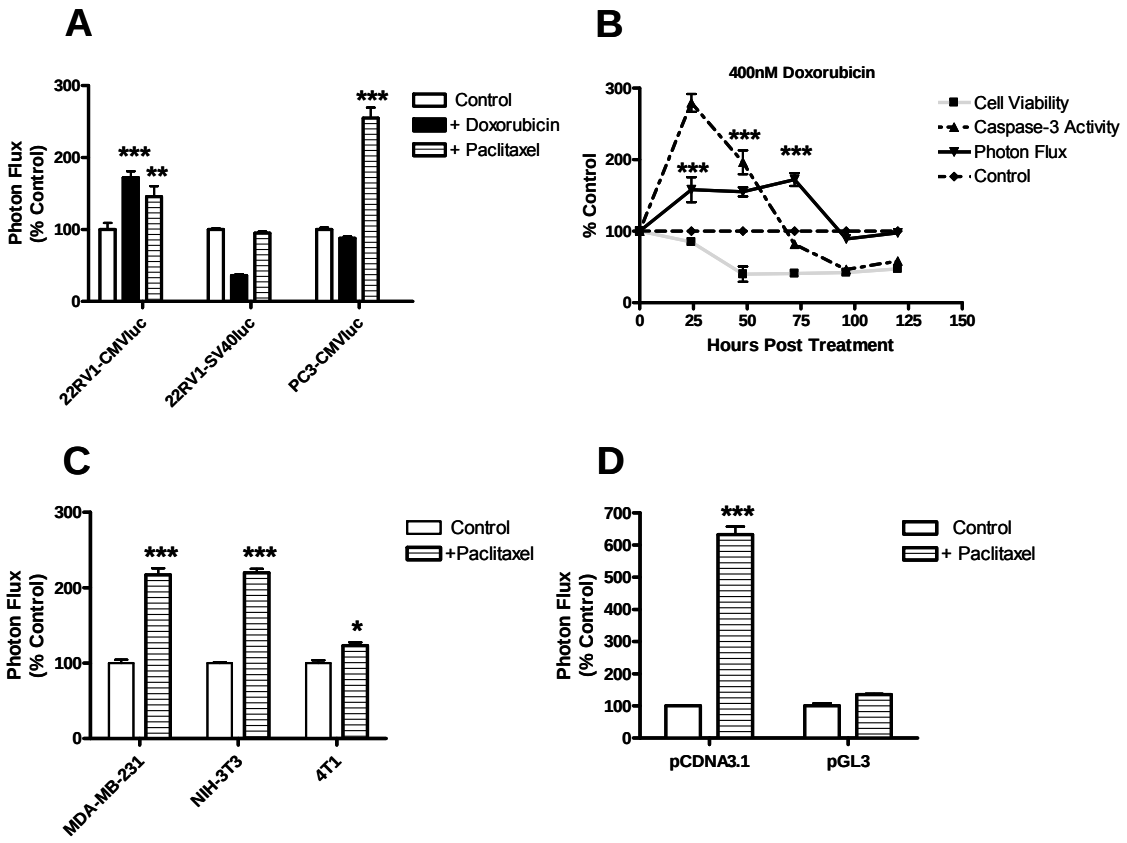

Figure 4.4: Chemotherapeutics doxorubicin and paclitaxel induce a transient increase in bioluminescence in 22Rv1-CMVluc and PC3-CMVluc cells but not 22Rv1-SV40luc cells. Luciferase expressing cell lines were treated with chemotherapeutics doxorubicin and paclitaxel. Y-axes in *A* and *C* represent bioluminescence as photon flux (photons/sec/cm^2/sr) expressed as % untreated control after 48hrs. *A*, 400nM doxorubicin and 90nM paclitaxel treated 22Rv1-CMVluc cells and 90nM paclitaxel treated PC3-CMVluc cells induced a transient increase in bioluminescence which was not evident at any dose in 22Rv1-SV40luc cells. *B*, Representative time course of 400nM doxorubicin-treated 22Rv1-CMVluc cells demonstrating that the bioluminescence increase is transient and accompanies an induction of apoptosis (caspase 3 activity) and loss in cell viability (WST assay). *C*, Paclitaxel treatment induces an increase in bioluminescence in non-prostate carcinoma cell lines expressing luciferase under the control of the CMV promoter. *D*, Paclitaxel induces bioluminescence in MDA.MB.231 cells transiently transfected with pCDNA3.1 (CMV-Luc) but not pGL3 (SV40-Luc). Significant increases in photon flux relative to controls are denoted by asterisks; *p<0.05, **p<0.01, ***p<0.001.

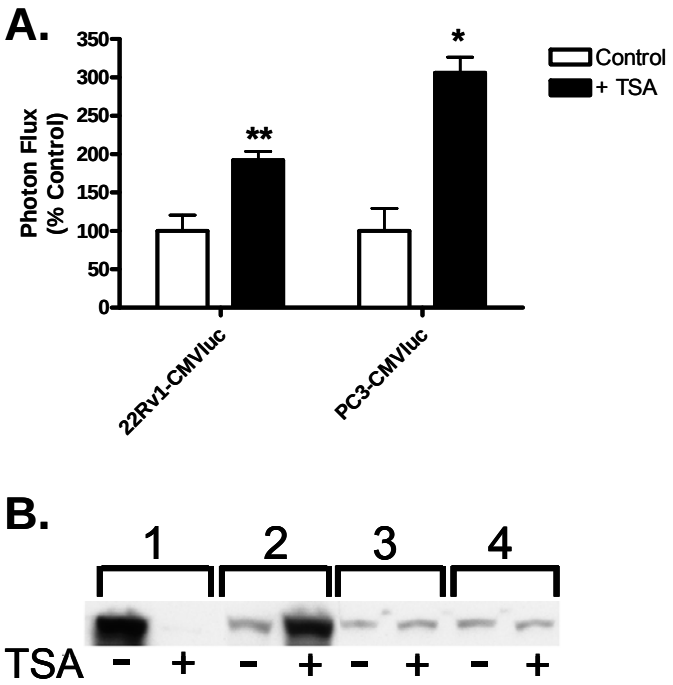

Figure 4.5: Trichostatin-A (TSA) induces bioluminescence and AR gene expression in cells engineered to express luciferase and AR from the CMV promoter. *A*, 22Rv1-CMVluc and PC3-CMVluc cells were treated with 100 ng/mL TSA for 48 h and bioluminescence values (photons/sec/cm2/sr) were compared to untreated control cells. TSA induces a significant increase in bioluminescence. Significant increases in photon flux relative to controls are denoted by asterisks; *$p<0.05$, **$p<0.01$. B, LNCaP (# 1), PC3-CMV-AR (#2) and two different PC3-SFFV-AR lines (# 3 and 4) were treated for 24h with TSA (400 ng/mL) and expression of AR was examined via western blot. TSA induces AR expression only in cell lines engineered to express AR from the CMV promoter (lane 2).

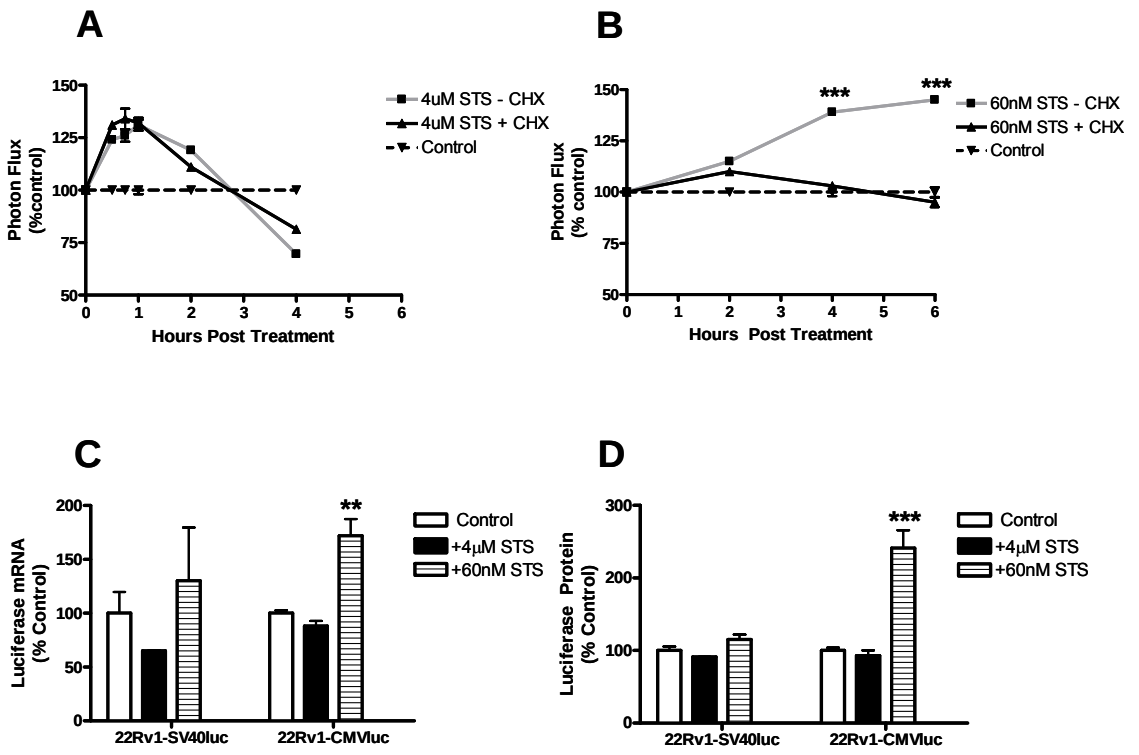

Figure 4.6: Bioluminescence can be induced by translation-independent and translation-dependent mechanisms. 22Rv1-CMVluc cells were pre-treated for 2 hrs with 10μg/ml cycloheximide (CHX) or fresh media and then treated with either (*A*) 4μM staurosporine (STS) or (*B*) 60nM staurosporine (STS) and analyzed for bioluminescence (photon flux; photons/sec/sec/cm^2/sr). Cycloheximide treatment does not block the bioluminescence increase induced using a high 4□M dose of staurosporine but does block the low 60nM dose-induced increase in bioluminescence. Significant increases in photon flux relative to cycloheximide-treated cells are denoted with asterisks; ***p<0.001. *C*, 22Rv1-CMVluc and 22Rv1-SV40luc cells were treated with either 4□M staurosporine for 1hr, 60nM staurosporine for 6hrs or 0.5% DMSO (control) and qRT-PCR was performed for luciferase mRNA. 60nM staurosporine induces an increase in luciferase mRNA in 22Rv1-CMVluc cells but not 22Rv1-SV40luc cells. Significant increases in luciferase mRNA relative to control cells are denoted with asterisks; **p<0.01. *D*, Lysates of treated and untreated cells were analyzed for luciferase activity (see Materials and Methods). 60nM staurosporine significantly increased luciferase activity in 22Rv1-CMVluc cells but not 22Rv1-SV40luc cells. Significant increases in luciferase protein levels relative to controls are denoted by asterisks; ***p<0.001.

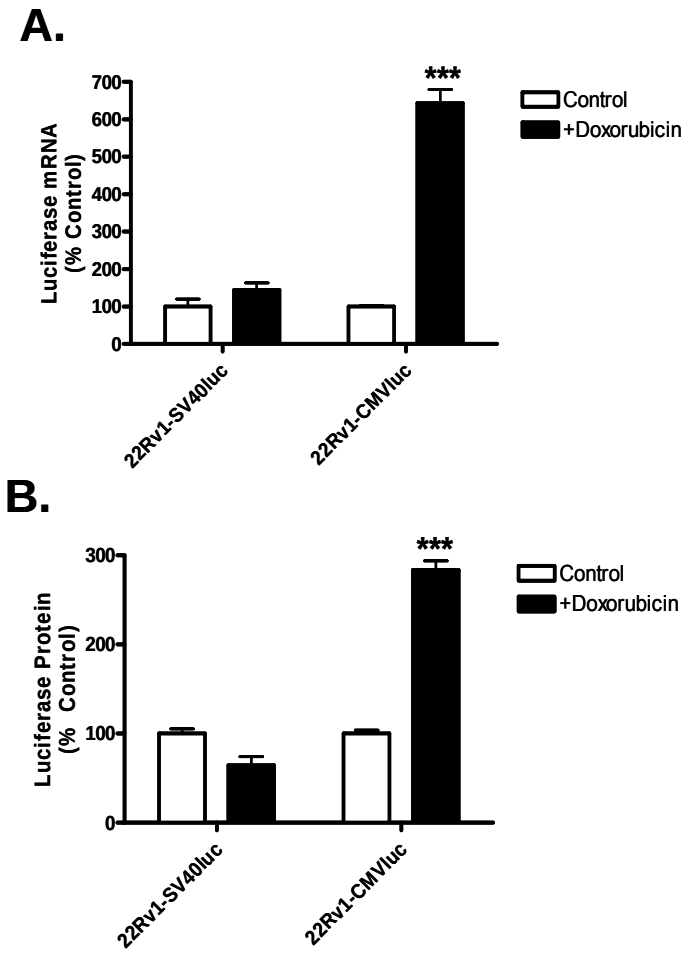

Figure 4.7: Doxorubicin treatment increases luciferase mRNA and protein in 22Rv1-CMVluc cells but not 22Rv1-SV40luc cells. 22Rv1-CMVluc and 22Rv1-Sv40luc cells were either treated with 400 nmol/L doxorubicin or left untreated for 48 h. *A*, RNA was prepared from treated and untreated cells and qRT-PCR was performed for luciferase mRNA. Doxorubicin treatment significantly increased luciferase mRNA levels in 22Rv1-CMVluc cells but not 22Rv1-SV40 luc cells. *B*, Cell lysates from above were also analyzed for luciferase protein using an *in vitro* luciferase activity assay (see material and methods). Doxorubicin treatment significantly increased luciferase protein in 22Rv1-CMVluc cells but not 22Rv1-SV40luc cells. Significant increases in photon flux relative to controls are denoted by asterisks; ***$p<0.001$

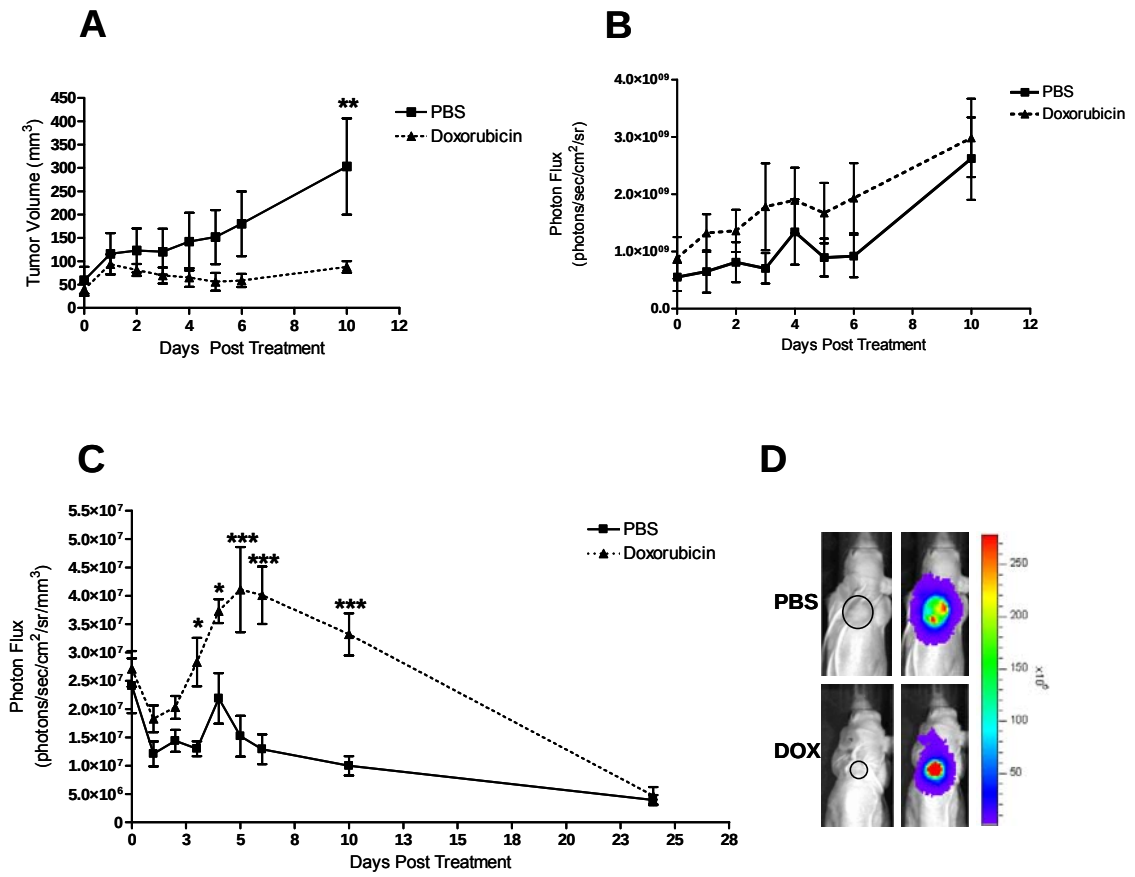

Figure 4.8: Doxorubicin treatment of 22Rv1-CMVluc subcutaneous xenograft tumors leads to a transient increase in luciferase expression *in vivo*. Subcutaneous 22Rv1-CMVluc and 22Rv1-SV40luc xenografts were initiated in *nude* mice (see Materials and Methods). Groups of 6 randomly assigned animals were injected once via the tail vein with either 200µl PBS or 200µl 1mg/ml doxorubicin (8mg/kg). Tumor volumes were recorded and BLI was performed daily for a period of 10 days. *A*, Doxorubicin treatment significantly delayed tumor growth. *B*, Doxorubicin treatment had no effect on bioluminescence intensity (photon flux; photons/sec/cm^2/sr). *C*, When bioluminescence was normalized to tumor volume, (photons/sec/cm^2/sr/mm^3), there was an increase in bioluminescence intensity in the doxorubicin-treated group relative to the PBS controls over a period of 10 days following treatment. At 23 days both groups display similar normalized values demonstrating that the bioluminescence increase is transient. Images in *D* show an example of a doxorubicin-treated and a PBS-treated animal where it is clear that the smaller tumor (50mm^3) in the doxorubicin-treated animal has a bioluminescence intensity comparable to the larger tumor (220mm^3) PBS-treated animal. Significant increases in tumor volume and in normalized photon flux relative to controls are denoted by asterisks;*p<0.05, **p<0.01 ***p<0.001.

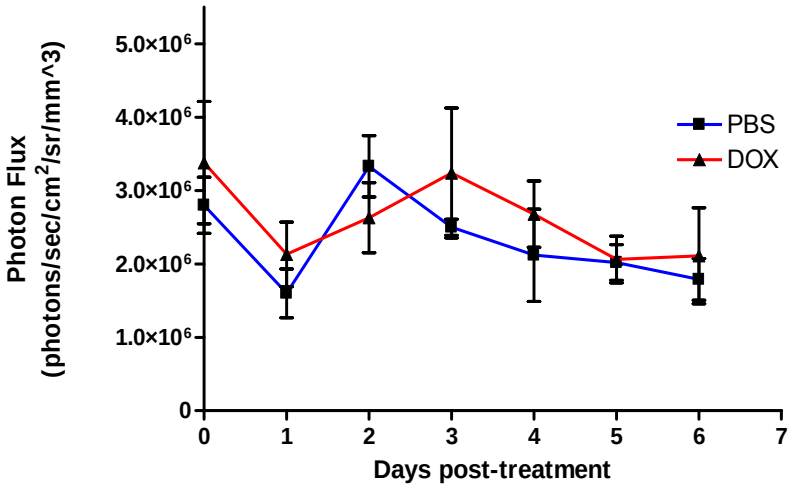

Figure 4.9: Doxorubicin treatment of 22RV1-SV40luc subcutaneous xenograft tumors does not affect luciferase expression *in vivo*. Subcutaneous 22Rv1-Sv40luc xenografts were initiated in *nu/nu* mice (see Materials and Methods). Groups of 6 randomly assigned animals were injected once via the tail vein with either 200µL PBS or 200µl 1mg/mL doxorubicin (8mg/kg). Tumor volumes were recorded and BLI was performed daily for a period of 10 days. The Y axis represents bioluminescence normalized to tumor volume (photons/sec/cm2/sr/mm3). In contrast to the 22Rv1- CMVluc xenografts, the bioluminescent signal of doxorubicin treated 22Rv1–SV40luc cells remained similar to the PBS controls over a period of 6 days following treatment.

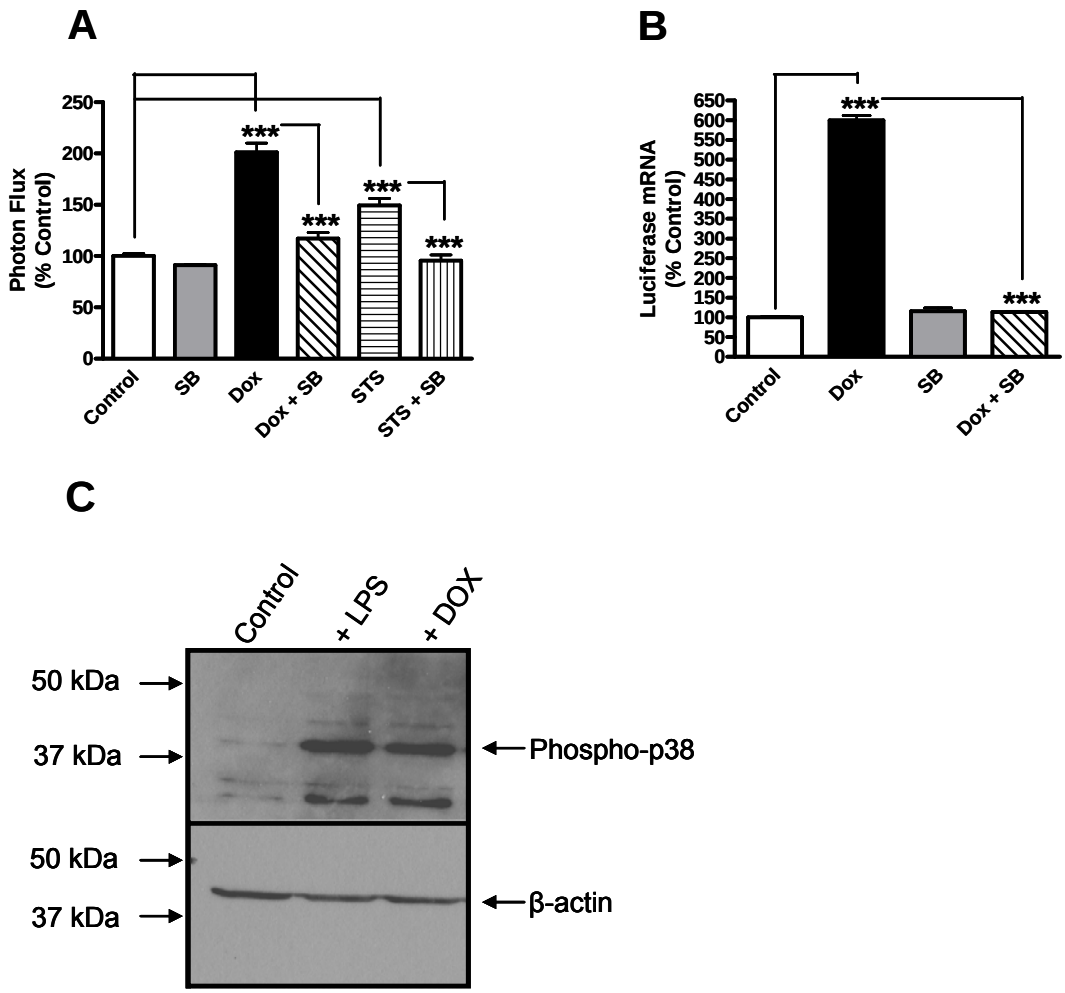

Figure 4.10: Inhibition of the p38MAPK pathway blocks the doxorubicin and staurosporine-induced increase in bioluminescence. 22Rv1-CMVluc cells were treated with vehicle only (Control), 30μM SB203580 only (SB), 400nM doxorubicin only (DOX), 60nM staurosporine only (STS) or a combination of doxorubicin or staurosporine + 30μM SB203580 (DOX + SB and STS + SB). Bioluminescence intensity (photon flux; photons/sec/cm^2/sr) was recorded as % vehicle control after 48hrs of doxorubicin treatment and 24hrs of staurosporine treatment. *A*, SB203580 was able to block 95% of the bioluminescence induction from doxorubicin and staurosporine. *B*, 22Rv1-CMVluc cells were treated as above and qRT-PCR was performed using cDNA from these cells. Doxorubicin induced a significant increase in luciferase transcript levels, and SB203580 blocked this induction. Significant changes in photon flux or luciferase mRNA levels between indicated treatments are denoted by asterisks; ***$p<0.001$. *C*, 22Rv1-CMVluc cells were treated with either LPS, doxorubicin or left untreated and western blotting for phosphorylated p38MAPK (phospho-p38) was performed. Doxorubicin treatment induces phosphorylation of p38MAPK. Immunblotting for β-actin confirms equal protein loading.

CHAPTER V

CHARACTERIZATION OF A NOVEL MOUSE MODEL OF PROSTATE CANCER

Introduction

Prostate cancer is the second leading cause of cancer related deaths in men in the United States and is a complex multifactorial disease that displays heterogeneous growth patterns, making it very difficult to study mechanistically. Despite its high morbidity, some advances have been made in both trying to understand the pathogenesis of prostate cancer and develop effective treatment strategies. Studies have been aided, in part, by the development of animal models of prostate cancer which are now becoming invaluable in our effort to unravel and combat this complex disease (Kasper 2005).

The development of animal models that can closely mimic progression of human prostate cancers is an ongoing effort. Many studies have exploited immortalized human prostate cancer cell lines to model various stages of prostate cancer. Cell lines such as PC3, DU145 and LNCap are routinely injected into immunocompromised mice in an attempt to study processes such as primary tumor growth, metastasis, development of androgen independent prostate cancer and response to therapy (Murillo, Huang et al. 2001; Jenkins, Yu et al. 2003; Ennis, Fultz et al. 2005; Svensson, Barnes et al. 2007). In such models, the route of injection primarily dictates the nature of the study. Primary tumor growth can easily be studied by subcutaneous injection of tumor cells, whereas events during metastasis, such as extravasation, can be studied by inducing dissemination of tumor cells into the vasculature by intra-cardiac injections. The application of small animal imaging has greatly facilitated our ability to efficiently perform such studies (Jenkins, Oei et al. 2003). However, several notable flaws with these xenograft models are apparent. Introducing cultured cell lines into immunocompromised mice limits our

ability to study the influence of the immune system on cancer progression. Furthermore, dynamic interactions between the tumor microenvironment and prostate epithelial cells do not exist in such models. Therefore it is advantageous to study models of prostate cancer that develop spontaneously in genetically defined and immunocompetent animals (Sharpless and Depinho 2006).

The progression of human prostate cancer is a multistep process, beginning with primary tumor formation and ending with metastasis of cancer cells to distant sites. The development of GEM models of prostate cancer to model these events presents a considerable challenge since few models are able to mimic this progression series (Winter, Cooper et al. 2003; Pienta, Abate-Shen et al. 2008). Some models, such as the TRAMP, are able to span the spectrum of pathogenesis thereby enabling us to dissect some of the molecular mechanisms of prostate cancer (Greenberg, DeMayo et al. 1995; Gingrich, Barrios et al. 1997). However, such models have been hampered by biological relevance because phenotypically the lesions that promote prostate cancer are not typically documented in human patients. In an effort to create a more biologically relevant model, Wang *et al* developed a conditional mouse model of prostate cancer in which the *Pten* tumor suppressor gene was exclusively deleted in the prostatic epithelium (Wang, Gao et al. 2003). Histologically, the progression series of prostate cancer in this model was praised for its accurate recapitulation of human prostate cancer. Mice developed prostatatic intraepithelial neoplasms as early as 6 weeks, which eventually progressed to distant metastases. Furthermore, it has been postulated that a stem cell/progenitor cell may be the cancer initiating cell in this model (Wang, Garcia et al. 2006). However, in order to efficiently monitor the progression series and to derive statistically significant data, often post-mortem studies of large cohorts of mice are required. To circumvent this, researchers have employed imaging techniques in an effort to non-invasively monitor tumor progression. For example, the TRAMP mouse was refined by introducing a luciferase reporter allele under control of the human PSA

promoter (Lyons, Lim et al. 2006; Hsieh, Xie et al. 2007). BLI enabled both tumor growth and response to therapy to be visualized over time. Similarly, the *Pten* model of prostate cancer was improved by incorporating a firefly luciferase allele under control of the beta actin promoter (Liao, Zhong et al. 2007). However, the potential of this model was not fully maximized due to variability in tumor kinetics and problems with specificity and sensitivity. To this end we have further improved on the *Pten* model of prostate cancer. We introduced the conditional *ROSA26*-LSL firefly luciferase allele (Safran, Kim et al. 2003) in an attempt to enhance the specificity of this model because the cancer initiating event is now coupled to expression of luciferase from a strong endogenous promoter in the same cell. Furthermore, in order to reduce the variability in tumor kinetics and to create a defined and uniform genetic background we extensively backcrossed this model onto C57BL6 and BALB/c genetic backgrounds and designated mice as either B6-Luc or BALB/c-Luc. We utilized the albino C57BL6 mice (C57BL6TYRC2J) in order to maximize the sensitivity of BLI (Troy, Jekic-McMullen et al. 2004). Consistent with previous studies, we show that progression of prostate cancer from 3-12 weeks is rapid and is correlated with an increase in bioluminescence. However, longitudinal BLI from 12-40 weeks reveals a plateau in bioluminescence signal that is correlated with a halt in cellular proliferation as evidenced by Ki67 staining at necropsy. In contrast to other studies, cancer progression in B6-Luc mice never progressed beyond HGPIN despite a progressive inflammatory response, characterized by myeloid derived suppressor cell (MDSC) recruitment, and focal loss of glycosylated alpha dystroglycan. Differences in progression between our model and others may be related to genetic background (Freeman, Lesche et al. 2006). To address this we are currently characterizing BALB/c-Luc mice to determine whether there are any histological differences in cancer progression. We further demonstrate the utility of this model to monitor response to therapy. Our model may offer advantages in sensitivity and specificity of cancer detection compared to other similar approaches and for the first time

we demonstrate that MDSCs are recruited to prostate cancer in an autochthonous mouse model of prostate cancer.

Materials and Methods

Mouse Strains and Genotyping

All animal procedures were performed with approval from the University of Iowa Animal Care and Use Committee and by the authors' Institutional Review Board. PbCre4+ mice were obtained from obtained from the NIH Mouse Models of Human Cancer Consortium. *Pten* fl/fl mice were obtained from Jackson laboratories. *ROSA26*-LSL-Luc mice were a kind gift from William Kaelin. Mice were intercrossed and backcrossed to C57BL6TYRC2J (Jackson Labs) or BALB/c (Taconic Farms) for 7 generations. Mice were genotyped for PbCre4+, *Pten* and Luciferase using gene specific primers as previously described (Wu, Wu et al. 2001; Lesche, Groszer et al. 2002; Safran, Kim et al. 2003) .

Bioluminescence Imaging

All BLI was performed in an IVIS100 imaging system (Caliper Life Sciences). For BLI of mice, D-luciferin (Gold Biotechnology) was administered to each mouse via intraperitoneal injection at a dose of 150mg/kg. Animals were then anesthetized in a chamber with 3% isoflurane and immediately placed onto the imaging platform while being maintained on 3% isoflurane. Mice were then imaged after 5 min of substrate injection using a 20cm field of view and an exposure time varying from 1sec -1 min. Bioluminescence values were calculated by measuring photon flux (photons/sec) in the region of interest surrounding the bioluminescence signal emanating from the mice.

RNA and protein preparation from tissues

Tissues from B6-Luc mice were removed and either flash frozen in liquid nitrogen for subsequent protein preparation or immediately placed (100mg) into 1ml of TRIZOL (Invitrogen) for RNA preparation. For RNA extraction, samples in TRIZOL were homogenized using a Powergen125 Teflon homogenizer (Fisher Scientific). Samples were then subjected to RNA extraction under manufacturer's conditions. Purified RNA preparations were subjected to DNaseI treatment to remove any contaminating genomic DNA. For protein preparation, frozen tissues were homogenized into a powder using a mortar and pestle. Samples were then suspended in 1X Reporter Lysis Buffer (Buffer RLB, Promega) and frozen overnight at -80°C. Samples were then subjected to three freeze thaw cycles (37°C – LN_2) and centrifuged at 13000rpm for 7.5 min. Supernatants were analyzed for protein quantity using a Biorad (Hercules, California) protein assay using manufacturers conditions.

PCR and luciferase activity assay

RNA samples were subjected to quantitative-RT-PCR as previously described (Svensson, Barnes et al. 2007). Protein samples (150µg) were subjected to an *in vitro* luciferase activity assay as previously described (Svensson, Shey et al. 2008).

Immunofluorescence and antibodies

Mice were sacrificed using CO2 inhalation followed by cervical dislocation and prostates were immediately harvested. Prostates were then fixed in 4% PFA overnight and transferred to 30% Etoh and imbedded in paraffin wax using an automatic tissue processor. Prostate were then embedded into cutting block using a heated plate followed

by cooling at -5C. Sections from blocks were cut at 7uM using a Leica microtome, placed into a heated waterbath (37C) and mounted onto charged (+/+) superfrost slides. Samples were then air dried and left at room temperature until IF was performed. For IF, sections were rehydrated in a series of ethanols (100%-70%) and washed in 1X PBS after being dipped in xylene for 10 mins to remove the paraffin. Following this sections were subjected to antigen retrieval using either citrate buffer or proteinase K treatment. For citrate buffer, sections were immersed in a solution of 0.1M Sodium citrate + 0.01M Citric acid and heated at 95C for 20 mins. Sections were then left to cool in solution at room temp for an additional 20 mins. For proteinase K treatment, sections were immersed in proteinase K(in TE buffer pH 8.0) for 20 mins at 37C. Following antigen retrieval sections were washed in 1X PBS and blocked in donkey block (2% BSA, 0.1% Triton X, 0.1% Tween 20, 1% Donkey serum, PBS) for 1 hr at room temp. Samples were then incubated with primary antibody (in donkey block) overnight at RT at the following dilutions; pAKT473 1:100 (Cell signaling), pS6 1:200 (Cell Signaling), *Pten* 1:100 (Invitrogen), Ki67 1:400 (Novocastra), Chromogranin A 1:100 (Cell Signaling), FOXA2 1:200 (Cell Signaling), IIH6 1:100 (Kind gift from Kevin Campbell), E-Cadherin 1:200 (BD Transduction), keratin 5 1:100 (Cell Signaling).Following this, samples were washed and incubated with secondary antibody in a solution of donkey block + DAPI (1:5000) for 1 hr at RT. Samples were washed in 1X PBS, mounted in fluorgel and visualized on a Leica DM2500 microscope.

Haematoxylin, Eosin and Massons Trichrome staining

For H&E staining, sections were treated as follows: Xylene 5 mins; 100% ethanol 2 X 1 min; 95% ethanol 2 X 1 min; Harris Haematoxylin 45 secs; rinsed in tap water; acid alcohol 1 min; rinse in ddH20; Ammonium water 1 min; rinse in ddH20; rinse 95%

ethanol; Eosin 45 secs; 95% ethanol 1 min; 100% ethanol 2 X 1 min; Xylene 2 mins; Mounted with coverslips with permount-xylene (1:1). Slides were visualized using a Leica DM2500 microscope. Pathological changes in B6-Luc mice were assessed by Michael Cohen M.D. For Massons trichrome staining we sent slides to the Histopathology department at the University of Iowa (Department of Pathology).

Senescence associated β-Galactosidase stain

For SA-BGal staining, prostates were immersed in OCT and flash frozen in liquid nitrogen. 5uM sections were immediately cut on a Leica cryostat and mounted on charged (+/+) superfrost slides. Sections were air dried for 10 mins and then immersed in PBS to remove residual OCT. Sections were then stained for SA-BGal activity using a senescence associated B-Gal assay kit under manufacturers conditions (Cell Signaling). Following staining, sections were counterstained in eosin and mounted in a solution of permount-xylene (1:1) and analyzed using a Leica DM2500 microscope.

2- Deoxyglucose uptake

Mice were injected via lateral tail vein with 200nM of near infrared labeled 2 deoxyglucose (Leica). 48 hrs post injection, prostate tissue was harvested and analyzed for near infrared fluorescence *ex vivo* in an IVIS100 imaging system.

Rapamycin treatment of B6-Luc mice

Rapamycin (LC Laboratories) was reconstituted in 100% ethanol to a concentration of 25mg/ml. It was then further diluted (2.5 mg/ml) in a solution of sterile ddH20 containing 5 % Tween 20 and 5 % PEG400. B6-Luc mice were injected i.p with

either 10mg/kg rapamycin or vehicle control, daily (5 days on 2 days off) for either 3 weeks or continuously throughout the study (~18 weeks). Body weights were routinely monitored to assess toxicity of drug exposure. We did not observe any weight loss or other signs of toxicity in any rapamycin-treated mice.

Castrations of B6-Luc mice

Mice were anesthetized by ketamine/xylazine (80mg/kg ;10 mg/kg i.p); proper anesthetic plane will be judged by lack of response to light paw pinch. A sterile surgical field was prepared on a sterile surgical drape inside of a laminar flow hood. A small section of the scrotum was shaved with #40 clippers posterior to the mid-scapular region. This area was then swabbed with a surgical iodine solution. Using a sterile scalpel blade, a 2 cm ventral midline incision was made in the scrotum, and the skin retracted to expose the tunica. The tunica was pierced, and the opening stretched with blunt forceps. The testes were pushed out by gentle pressure on the pelvic region. The spermatic artery was clamped and cauterized, and the testes were removed. The epididymis, deferential vessels and ductus are replaced in the tunica. Wound clips then closed the incision.

FACS analysis of inflammatory subsets

Prostates lobes were isolotaed and digested in 500ul of collagenase D in RPMI. Tissue was minced using dissecting scissors and then placed at 37C for 1 hr with shaking. Samples were then transferred onto filter top FACS tubes and centrifuged for 5 min @ 1200rpm. Supernatant was discarded and pellet was vortxed. RPMI was added to wash excess collagenase away, samples were centrifuged for 5 min @1200rpm and pellet was vortexed. FC block was then added to the samples and left at 4C for 15 mins. Staining solution was then added directly to cells in the FC block for 30 mins at 4C in the dark.

Cells were then washed with 1 ml RPMI, centrifuged and fixed in stabilization buffer fixative and analyzed vy flow cytometry. Digested spleens were used for compensation.

Results

Generation of a novel model of prostate cancer

In order to generate a novel mouse model of spontaneous prostate cancer we utilized three independent strains of mice (Fig 5.1) 1) Mice containing conditional alleles of *Pten* (Lesche, Groszer et al. 2002) 2) Mice expressing the probasin Cre recombinase transgene (Pb-Cre4+) (Wu, Wu et al. 2001) 3) Mice containing a conditional luciferase reporter allele (*ROSA26*-LSL-Luc) (Safran, Kim et al. 2003). Prostate epithelium specific expression of the Pb-Cre transgene enables recombination of the floxed alleles of *Pten*, thereby inactivating it, coupled to activation of the *ROSA26* luciferase reporter through excision of the transcriptional stop cassette. Because *Pten* deletion is coupled to luciferase expression in the same cell, it facilitates non invasive BLI of cancer progression using an IVIS imaging system. We crossed the three strains together and then backcrossed the triple homozygote to albino C57BL6 (C57BL6TYRC2J) and BALB/c mice for 7 generations to create a homogenous genetic background. We utilized the albino mutants of the C57BL6 strain to enhance the BLI properties in white coat color mice (Troy, Jekic-McMullen et al. 2004) and designated these mice as B6-Luc (C57BL6 backcrossed) or BALB/c-Luc (BALB/c backcrossed).

Bioluminescence in B6-Luc mice is restricted to the prostate

BLI of B6-Luc mice revealed that bioluminescence signal is restricted to the lower abdominal region which was confirmed to be prostatic tissue when samples were

analyzed *ex vivo* (Figure 5.2). We performed RT-PCR for recombined luciferase in an attempt to assess any ectopic expression of the Pb-Cre transgene in peripheral tissues (Figure 5.2B). We detected recombined luciferase in prostate tissue as expected but also detected recombination in testis and seminal vesicle. Ectopic expression of Pb-Cre has been documented previously in both these tissues and is not unexpected given that the probasin promoter is androgen regulated (Wu, Wu et al. 2001). However, the degree of luciferase expression in these tissues was not sufficient to be visualized by BLI. In order to determine recombination of *Pten* we performed immunofluorescence (IF) on fixed prostate sections from 9 week old *Pten* $^{-/-}$ B6-Luc mice. Figure 5.3 reveals that *Pten* is undetectable in most epithelial cells at 9 weeks however we did detect retention of *Pten* expression in some compartments. This may be due to latent activity of cre recombinase in certain lobes or due to an inactivity of the cre transgene in the basal cell compartment as reported in a previous study (Esser, Cohen et al. 2010). Concordant with a loss of *Pten* expression in B6-Luc prostates, we detected expression of phosphorylated AKT ($pAKT^{473}$) in prostate epithelial cells of *Pten* $^{-/-}$ B6-Luc mice (Figure 5.4). Hence, when Pb-Cre becomes expressed in B6-Luc mice it facilitates BLI of prostate specific luciferase expressing cells that have deleted *Pten* and activated pAKT.

BLI of cancer progression in B6-Luc and BALB/c-Luc mice

We performed BLI weekly in *Pten* $^{+/+, +/- \text{ and } -/-}$ B6-Luc and BALB/c-Luc mice from weaning in order to determine whether bioluminescence intensity correlates with cancer progression (Figure 5.5). Furthermore, we wanted to assess any differences in bioluminescence kinetics between B6 and BALB/c mice because *Pten* dependent tumorigenesis was previously shown to be variable in different genetic backgrounds (Freeman, Lesche et al. 2006). Bioluminescence intensity rapidly increased from 3-11 weeks in *Pten* $^{-/-}$ mice compared to *Pten* $^{+/+}$ and *Pten* $^{+/-}$ mice, which displayed a moderate

increase probably due to development and maturation of the prostate during puberty. However, the magnitude of increase in *Pten* $^{-/-}$ suggests that bioluminescence is tightly correlated to the development of prostate cancer in this model, consist with previous studies (Wang, Gao et al. 2003).

To confirm that bioluminescence is correlated with increases in cellular proliferation during these stages we performed IF for the proliferative marker Ki67 in prostate sections from both *Pten* $^{-/-}$ and *Pten* $^{+/+}$ animals (Figure 5.6). We detected a significant increase in Ki67 positive cells in *Pten* $^{-/-}$ animals at 6 and 9 weeks of age. Although we detected a rapid increase in bioluminescence during early cancer progression (3-11 weeks), surprisingly the bioluminescence intensity did not change from 11 weeks on as visualized by a plateau in photon flux in both B6-Luc and BALB/c-Luc mice subjected to longitudinal BLI (Figure 5.4). The plateau in bioluminescence was correlated with a halt in proliferation of the epithelial cells as assessed by Ki67 IF in *Pten* $^{-/-}$ animals (Figure 5.7). Previous studies have documented a cellular senescence response in prostate specific *Pten* null mice (Chen, Trotman et al. 2005). Therefore we performed senescence associated β-Galactosidase staining of frozen prostate sections to assess the degree of cellular senescence in our model (Figure 5.8). Surprisingly we did not detect any β-Gal positive cells in *Pten* $^{-/-}$ animals indicating that the proliferative response is halted in our model, probably due to other reasons. Despite the cessation of proliferation, prostates of *Pten* $^{-/-}$ animals still remain metabolically active as determined by uptake of fluorescently labeled 2-Deoxyglucose (2-DG) (Figure 5.8). Hence, increases in bioluminescence in *Pten* $^{-/-}$ B6-Luc and BALB/c-Luc mice during 3-11 weeks is correlated with increases in proliferation and cell number, however longitudinal BLI suggests that tumor growth is slower than previously reported studies. This may be related to the extensive backcrossing effort compared to other approaches which use mice on mixed genetic backgrounds. Furthermore bioluminescence kinetics in B6-Luc and

BALB/c-Luc mice were very similar, suggesting that bulk cancer progression, assessed by BLI, in both of these genetic backgrounds is similar.

Pathologic changes in *Pten* $^{-/-}$ and *Pten* $^{+/-}$ B6-Luc and BALB/c-Luc mice

In order to assess the degree of pathological changes in B6-Luc and BALB/c-Luc mice we analyzed haematoxylin and eosin (H&E) stained sections of *Pten* $^{+/+}$, *Pten* $^{+/-}$ and *Pten* $^{-/-}$ animals (Figure 5.9A). The development of PIN was evident as early as 6 weeks in *Pten* $^{-/-}$ animals. 9 week old *Pten* $^{-/-}$ mice displayed signs of HGPIN which manifested as a cribriform morphology in the majority of the glands. HGPIN was more evident in dorsal and lateral lobes compared to ventral lobes. At 12 weeks, *Pten* $^{-/-}$ mice had developed an increase in focal stromal cellularity which increased over time, consistent with previous studies (Wang, Gao et al. 2003). This became more obvious when we performed Massons trichrome staining of *Pten* $^{-/-}$ animals (Figure 5.9B). 25 Week old *Pten* -/- display large amounts of collagen fibers in their stroma compared to younger animals. Surprisingly however and in contrast to previous studies, *Pten* $^{-/-}$ B6-Luc animals never progressed beyond a HGPIN, even when we assessed 6 month old animals (Figure 5.9). Prostate glands were always well encapsulated within the basement membrane and we never observed signs of local invasion. Furthermore, we did not observe any signs of metastatic lesions in lymph node, liver and lung tissue. We cannot definitively determine whether the degree of pathological changes are identical in BALB/c-Luc mice because we are in the midst of still analyzing these mice in large enough numbers. However, it does seem that although prostate glands appear to display a similar pathology and HGPIN is clearly evident at 12 weeks, there seems to be an enhanced stromal response at earlier stages in BALB/c-Luc mice which may be due to differences in inflammation between the two strains (arrows in Figure 5.10).

We also report that *Pten* $^{+/-}$ animals develop focal HGPIN with advancing age. The earliest evidence of focal HGPIN was documented in 6 month old animals. Interestingly, in the glands that displayed a HGPIN phenotype, there was a stromal response restricted to that compartment (Figure 5.11A). Furthermore, pAKT^{473} expression was exclusively limited to the glands that had undergone a transformation (Figure 5.11B). *Pten* $^{+/-}$ BALB/c-Luc mice also display phenotypic changes. Furthermore, we were able to visualize spontaneous prostate cancer development in a *Pten* $^{+/-}$ BALB/c-Luc individual animal that had developed a large increase in bioluminescence (Figure 5.12A). Tumor growth in this animal was confirmed at necropsy and was evident as a mass emanating from the dorsal lobe of the prostate. H&E analysis revealed a massive stromal response with some epithelial cells protruding into this compartment (Figure 5.12B).

Pten $^{-/-}$ B6-Luc mice respond to androgen deprivation and develop rare neuoroendocrine features

Androgen deprivation is the first line therapy for treatment of advanced prostate cancers in human patients. Despite initial responsiveness most will relapse into an androgen independent prostate cancer for which there is no cure (discussed earlier in Chapter II). Previous studies have documented development of AIPC in prostate specific *Pten* null mice (Wang, Gao et al. 2003; Liao, Zhong et al. 2007). In order for us to determine whether B6-Luc mice develop AIPC and whether we can monitor this via BLI, we castrated 12 week old *Pten* $^{+/+,+/-}$ and $^{-/-}$ B6-Luc animals and performed BLI weekly to monitor relapse from androgen deprivation (Figure 5.13). *Pten* $^{-/-}$ mice responded to castration as evidenced by a decrease in bioluminescence intensity from 12 weeks. Bioluminescence values decreased ~10 fold and then remained steady for 4 months until the end of the study. Interestingly, because bioluminescence intensity did not increase

from this steady state it suggests that although *Pten* $^{-/-}$ prostates develop castrate resistance, they are not able to proliferate in the absence of androgens in contrast to previous studies. Castration of *Pten* $^{+/-}$ animals led to a decrease in bioluminescence intensity that returned to basal levels after 10 weeks of castration, indicating that castrate resistant cells do not populate their prostates. It was previously demonstrated that castrate resistance develops early in Nkx3.1 *Pten* mutant animals (Gao, Ouyang et al. 2006). To confirm this in our model we castrated *Pten* $^{-/-}$ B6-Luc mice at 3 weeks of age, immediately after weaning. Bioluminescence intensity did not change after castration and remained steady throughout the time course of the study, demonstrating the early emergence of castrate resistance cells that are unable to proliferate in the absence of androgens. In contrast, *Pten* $^{+/+}$ B6-Luc mice displayed a decrease in bioluminescence intensity upon castration after weaning, demonstrating that castrate resistance does not occur in *Pten* $^{+/+}$ cells (Figure 5.14).

Pure neuroendocrine tumors in early stage human prostate cancers are rare (Randolph, Amin et al. 1997). However, advanced hormone refractory prostate cancers contain neuoroendocrine cell types that are associated with poor prognosis and androgen independence (Hirano, Okada et al. 2004). In order for us to determine whether castrate resistant *Pten* $^{-/-}$ B6-Luc mice develop neuoroendocrine differentiation, we performed IF for Chromogranin A and FOXA2 which are two neuoroendocrine markers upregulated in human AIPC and associated with poor prognosis (Isshiki, Akakura et al. 2002; Mirosevich, Gao et al. 2006). Figures 5.15 and 5.16 demonstrate that castrated *Pten* $^{-/-}$ mice contain rare populations of Chromogranin A and FOXA2 positive cells. FOXA2 positive cells were also located in the proximal ducts of *Pten* $^{+/+}$ mice as expected (Fig 5.15). Otherwise, we never detected expression of either Chromogranin A or FOXA2 in non castrated *Pten* $^{-/-}$ animals, suggesting that androgen deprivation induces neuoroendocrine differentiation in a rare subpopulation of cells.

Aged *Pten* $^{-/-}$ B6-Luc display focal loss of glycosylated dystroglycan

Dystroglycan is a transmembrane protein that links the extracellular matrix to the actin cytoskeleton in a number of different tissues and cell types (Henry and Campbell 1996). The function of dystroglycan in muscle tissue is well characterized; however its function in non muscle tissue has not been fully elucidated. We previously demonstrated that loss of dystroglycan in luminal prostate cells did not display an overt phenotype in a conditional knockout animal (Esser, Cohen et al.). However, the lack of phenotype associated with this model may result from inactivity of cre recombinase in the basal cell compartment. Despite the lack of phenotype in the prostate of these mice, dystroglycan expression has shown to be reduced in epithelial cancers including breast and prostate cancer (Henry, Cohen et al. 2001; Muschler, Levy et al. 2002). Furthermore, glycosylation defects of alpha dystroglycan (α-DG) has been implicated as a factor in cancer progression (de Bernabe, Inamori et al. 2009). To determine the glycosylation status of α-DG in B6-Luc mice we performed IF for glycosylated α-DG using an antibody that only recognizes the glycosylated form (IIH6) (Figure 5.17). Six week old *Pten* $^{-/-}$ and *Pten* $^{+/+}$ B6-Luc mice displayed expression of glycosylated α-DG in all of the epithelial cells examined, even in cells that have detached from the basement membrane and filled the luminal space. However, 25 week old *Pten* animals displayed focal loss of glycosylated α-DG expression in cells that had filled the luminal space. Most of the glands that were filled in with cells still retained expression of glycosylated α-DG indicating that loss of its expression is relatively rare. Interestingly, cells that had moved into the centers of the lumens did not retain expression of laminin, a well known binding partner of α-DG. Laminin expression remained confined to the basement membrane and is most likely still produced by the basal cells of the prostate as evidenced by increased keratin 5 (K5) staining in *Pten* $^{-/-}$ animals compared to *Pten* $^{+/+}$ animals. Furthermore, although K5 positive cells mostly remained confined to the outer glandular layer, we also

observed glands that were nearly completely composed of K5 positive cells in *Pten* $^{-/-}$ animals. In contrast, glands from *Pten* $^{+/+}$ animals contain very few K5 positive cells (Figure 5.18). The reasons for increased K5 positive cells in *Pten* $^{-/-}$ animals remains unclear but may relate to differentiation of a transformed stem cell progenitor. Taken together, these data demonstrate that pathologic changes relating to cancer progression may be evident in focal areas of *Pten* $^{-/-}$ animals.

Myeloid derived suppressor cells (MDSCs) are recruited to prostates of *Pten* $^{-/-}$ B6-Luc mice

MDSCs have been shown to accumulate in cancer patients (Buessow, Paul et al. 1984; Young, Newby et al. 1987). Recent studies have identified MDSCs as potent suppressors of tumor immunity and therefore offer a mechanism of how inflammation might promote tumor progression (Ostrand-Rosenberg and Sinha 2009). Mouse tumor models have also been shown to accumulate MDSCs (Youn, Nagaraj et al. 2008), however MDSCs have not been shown to accumulate in any spontaneous mouse models of prostate cancer examined to date. We noticed that *Pten* $^{-/-}$ mice displayed massive signs of inflammation when we analyzed H&E stained prostate sections (Figure 5.9A). In an attempt to characterize the inflammatory subsets we performed FACs analysis of individual digested prostate lobes (Figure 5.19). We stained prostate epithelial cells with multiple antibodies including CD45 to identify all leukocytes, Thy 1.2 as a pan T cell marker and CD11b and Gr-1 to identify MDSCs. As expected, *Pten* $^{-/-}$ mice displayed a significant increase in infiltrating $CD45^+$ cells. Interestingly, when we phenotyped the $CD45^+$ cells we found that the majority of these cells (60-70%) were MDSCs. MDSC infiltration was clearly evident as early as 4 months in *Pten* $^{-/-}$ animals. We did not detect any differences in the percentage of $C45^+$ cells that were either $CD8^+$ or $CD4^+$ between *Pten* $^{-/-}$ and *Pten* $^{+/+}$ B6-Luc mice (Figure 5.16). These data demonstrate that *Pten* $^{-/-}$

animals display significant inflammation in their prostates, characterized mostly by infiltrating MDSCs that might contribute to cancer progression.

Pten $^{-/-}$ B6-Luc mice respond to Rapamycin treatment

PI3K, AKT and many of its downstream effectors such as mTOR are often overexpressed in human cancers (Yuan and Cantley 2008). Therefore, current efforts are focused on developing targeted therapies for the PI3K/AKT pathway (Sarker, Reid et al. 2009). Rapamycin and its rapalogues have shown to be effective in targeting mTOR activity and have shown clinical efficacy in subsets of cancers (Dancey 2006; Easton and Houghton 2006). *Pten* $^{-/-}$ B6-luc offer a unique model to test the effects of preclinical drugs such as rapamycin because they demonstrate aberrant activation of AKT and mTOR, while utilizing non invasive BLI to monitor changes in tumor burden over time. Therefore, they offer a large advantages over xenograft and other spontaneous models of prostate cancer that have not incorporated imaging technology. To test the effects of rapamycin in *Pten* $^{-/-}$ B6-Luc mice we performed daily intra-peritoneal injections of 10mg/kg rapamycin (5 days on 2 days off) for either 3 weeks or continuously throughout the time course of the study (Figure 5.20). Response to daily injections of rapamycin was rapid in treated *Pten* $^{-/-}$ B6-Luc animals, as evidenced by a decrease in bioluminescence intensity 1 week after injection compared to control treated mice. Bioluminescence continued to decrease during the treatment period (3 weeks). However, when mice were taken off treatment, they displayed a rapid increase in bioluminescence which returned to control treated levels after a couple of weeks. Continuous treatment of *Pten* $^{-/-}$ animals with rapamycin led to an initial decrease in bioluminescence, however we observed the development of resistance to rapamycin therapy because prolonged treatment induced a steady increase in bioluminescence intensity. Although continuous treatment did not cause an increase in bioluminescence back to vehicle control levels, the continual steady

increase indicated that response to rapamycin therapy was only transient. mTOR exists in at least two distinct protein complexes in mammalian cells; rapamycin sensitive mTORC1 and rapamycin insensitive mTORC2 (Hara, Maruki et al. 2002; Kim, Sarbassov et al. 2002; Jacinto, Loewith et al. 2004; Sarbassov, Ali et al. 2004). mTORC1 activation results in the phosphorylation of ribosomal protein S6 (pS6). Therefore, we performed IF for pS6 expression in prostate sections from rapamycin treated and vehicle control treated mice (Figure 5.21). Rapamycin treatment led to a reduction in pS6 staining compared to control treated mice. However, pAKT473 expression was not affected by rapamycin treatment demonstrating that rapamycin is unable to inhibit mTORC2 activity, at least during this treatment regimen. Taken together, we demonstrate that B6-Luc mice respond to rapamycin treatment and offer and provide a unique and valuable model that may aid in the development of prostate cancer therapies in a pre clinical setting.

Discussion

Here we describe further improvement on the *Pten* conditional knockout prostate cancer mouse model. We demonstrate that incorporation of the *ROSA26*-LSL-Luc allele facilitates BLI of cancer progression and response to therapy. Furthermore, in this model, bioluminescence is finely tuned to cell number and the proliferative capacity of prostate tumors because the cancer initiating event is coupled to activation of luciferase in the same epithelial cell. Surprisingly and in contrast to previous studies, prostate cancer progression in B6-Luc mice never progressed beyond HGPIN. Despite this, we have demonstrated an increased inflammatory response in *Pten* $^{-/-}$ B6-Luc mice that is characterized by MDSC recruitment. Although MDSCs have been shown to accumulate in a spontaneous mouse model of pancreatic cancer, this is the first evidence to date that describes a similar phenomenon in an autochthonous mouse model of prostate cancer.

BLI of prostate cancer has been described in a number of spontaneous models. Lyons et al generated a modified version of the TRAMP mouse by incorporating a luciferase reporter under control of the human prostate specific antigen promoter (Lyons, Lim et al. 2006). Tumor growth and response to androgen ablation was monitored by BLI. However, prostate tumorigenesis was induced by overexpression of SV40 T antigens in this model and prostate tumors exhibited massive neuoroendocrine differentiation, features that are extremely rare in human prostate cancers. Furthermore, the PSA promoter used to drive luciferase expression is androgen regulated lending to the possibility that luciferase expression may be more correlative with prostatic androgen levels rather than tumor growth per se. Despite a clear response to androgen ablation in this model, it may also cause difficulties in visualizing tumor relapse in this model during castrate levels of androgens. In our model, although probasin is also androgen regulated, Cre recombinase allows the cancer initiating event to be coupled to expression of luciferase in the same cell. Once the genes have undergone recombination, the affected cells no longer require the presence of androgens. Because the recombination event is irreversible, the proliferative capacity is tightly correlated with bioluminescence. We are not the first group to have introduced a luciferase allele into the *Pten* model of prostate cancer (Liao, Zhong et al. 2007). Liao *et al* were the first to describe a model in which a bicistronic transgene harboring both GFP and luciferase reporters under the control of the β-actin promoter was incorporated into this model. Bioluminescence was correlated to tumor growth and response to castration. However, tumor growth and response to castration was variable between individual animals and leaky expression of the reporter was documented. Recombination in skeletal muscle was detected and mice would often present with strong focal bioluminescent signals in the thoracic area, which were never confirmed to be metastatic lesions. The model was also hampered by sensitivity issues, as mice had to be shaved and bladders emptied in order to enhance the bioluminescent signal intensity. Although we did detect some recombination of luciferase in testis and

seminal vesicles bioluminescent signals were never detected in regions outside of the prostate. Furthermore, we took the time to extensively backcross our model unlike the β-actin Luc model which was on a mixed genetic background. In our model, tumor growth kinetics did not vary between individual animals and the white coat color of both B6-Luc and BALB/c-Luc enhanced the bioluminescent signal intensity.

In B6-Luc mice, bioluminescence was tightly correlated with the proliferative capacity of the prostatic epithelial cells, as evidenced by Ki67 staining. We observed a rapid increase in bioluminescence from 3-11 weeks in *Pten* $^{-/-}$ animals that was significantly greater than in control animals. However, longitudinal BLI revealed that bioluminescence intensity did not significantly increase from 11 weeks on. During this time frame, Ki67 levels were not significantly different between *Pten* $^{-/-}$ and *Pten* $^{+/+}$ animals. The reasons for this plateau are yet to be elucidated in this model, however a previous study reported the induction of a p53 mediated senescence response in *Pten* knockout mice (Chen, Trotman et al. 2005). We were unable to identify a senescence response in B6-Luc though us of a senescence associated β-Gal stain, one of the most widely used methods to identify senescence (Dimri, Lee et al. 1995; Reznikoff, Yeager et al. 1996; Serrano, Lin et al. 1997). It is possible that several intrinsic and extrinsic factors may be influencing tumor growth in this model. For example, the tumor microenvironment may not be conducive to facilitate further growth or the epithelial cells may not have gained the additional oncogenic events needed to further proliferate. This second hit model may support the hypothesis that two genetic events are required for progression of prostate cancers to form tumors and invasive adenocarcinomas (Knudson 1971).

The *Pten* conditional model of prostate cancer was previously shown to recapitulate many aspects of the progression series seen in human prostate cancers (Wang, Gao et al. 2003). Mice developed hyperplasia by 4 weeks, PIN by 6 weeks and invasive carcinoma and metastases by 12 weeks of age. Death was also documented in a

small number of animals. Furthermore, prostate epithelial cells were shown to proliferate in castrate levels of androgens. Other groups have not been able to demonstrate metastases in this model although focal signs of microinvasion have still been described (Trotman, Niki et al. 2003). Discrepancies between prostate cancer progression in these studies may be related to the genetic background of the study cohorts (Freeman, Lesche et al. 2006). It was previously demonstrated that *Pten* dependent tumorigenesis is variable in different genetic backgrounds. This study stemmed from a clinical observation in human patients with germline *Pten* mutations. Often the same mutation would present with different symptoms that were characterized by different disorders, such as Cowden syndrome, Lhermite Duclos disease and Banayan Zonana syndrome. This led researchers to assess cancer progression in mice that harbored different *Pten* mutations in different genetic backgrounds. Tumor formation was shown to be dependent on genetic background and independent of the type of mutation (Freeman, D., R. Lesche, et al. 2006). However, prostate tumors were not examined in this study lending the hypothesis that prostate cancer progression is also influenced by genetic background. This may explain the differences in progression between studies. Surprisingly, in our model, prostate cancer never progressed beyond a HGPIN even when animals older than 1 yr were examined. Focal HGPIN was also detected in older *Pten* $^{+/-}$ animals. We did not detect any signs of micro invasion or evidence of metastases in *Pten* $^{-/-}$ animals. We are currently assessing the degree of pathologic changes in BALB/c-Luc mice do determine whether there are any differences in progression between the two strains. Future studies may be aimed at identifying genetic modifiers of prostate cancer progression.

Despite loss of the proliferative response and 'milder' phenotype of this model compared to others, we still see evidence of focal loss of glycosylated α-DG in *Pten* $^{-/-}$ mice. In younger *Pten* $^{-/-}$ animals, glands that presented with HGPIN still retained expression of glycosylated α-DG. However, we demonstrated that older (~6 month) animals display focal loss of glycosylated α-DG. The functional consequences of this are

unknown, however it is well described that the interactions between epithelial cells and their basement membrane is compromised during cancer progression. Dystroglycan is a membrane receptor that mediates interactions between cells and basement membranes in a variety of cell types. Loss of dystroglycan expression has been reported in prostate cancers (Henry, Cohen et al. 2001) and recent studies have identified the importance of dystroglycan ligand binding in epithelial cancers (de Bernabe, Inamori et al. 2009). Although the basement membrane appears intact in older *Pten* $^{-/-}$ animals, it is possible that focal areas of epithelial cells are detaching from their ECM in an attempt to become invasive. Future studies may be aimed at targeted disruption of the basement membrane in an attempt to assess invasion in this model.

The link between inflammation and cancer has long been appreciated (Balkwill and Mantovani 2001). Epidemiological data show strong correlations between inflammation and cancer incidence and experimental data supports a causative relationship between chronic inflammation and cancer onset and progression (Coussens and Werb 2002; Mantovani, Allavena et al. 2008). Inflammation can promoter tumor progression through a number of mechanisms such as inducing DNA damage through increased production of ROS, and promoting proliferation and angiogenesis through production of chemokines, cytokines and angiogenic factors like VEGF (Ellis and Hicklin 2008). There is also evidence that inflammation can inhibit the development of cancer by immunoserveliance mechanisms that can recognize and eliminate cancer cells. Dysfunctional anti-tumor immunity also positively affects tumor development. A major culprit in this scenario is the production of MDSCs that are able to inhibit both innate and adaptive immunity (Gabrilovich and Nagaraj 2009). MDSCs have been shown to accumulate at tumor sites in cancer patients and experimental animals of cancer (Buessow, Paul et al. 1984; Young, Newby et al. 1987; Clark, Hingorani et al. 2007; Zhao, Obermann et al. 2009) but their accumulation in mouse models of spontaneous prostate cancer has not been assessed to date. We have shown for the first time that

prostates of *Pten* $^{-/-}$ B6-Luc mice display a progressive increase in MDSC recruitment. MDSCs comprised the majority of CD45+ cells and were found to accumulate in all four lobes of the prostate in older *Pten* $^{-/-}$ animals and as early as 2 months in the dorsal lobes. MDSCs were not found to accumulate in healthy wildtype mice. MDSCs can suppress antitumor immunity through a variety of different mechanisms including T cell and NK cell suppression, induction of regulatory T cells and limiting antigen presentation by dendritic cells (Gabrilovich and Nagaraj 2009). Future studies are aimed at assessing the functionality of infiltrating MDSCs in B6-Luc mice by analyzing the production of arginase, iNOS, IL12 and IL10. In this context, B6-Luc mice will facilitate the evaluation of novel therapies that are able to target and render MDSCs nonfunctional, in turn providing the opportunity to examine the role of immunomodulators in prostate cancer progression.

The generation of GEM models of prostate cancer has greatly facilitated our understanding of the molecular mechanisms underlying progression of AIPC. Androgen independent prostate cancer represents a late stage and lethal event of prostate cancer for which there is no cure. Previous studies using conditional *Pten* $^{-/-}$ mice demonstrated that prostate epithelial cells were able to proliferate in the absence of androgens after castration, implicating a role for *Pten* in the development of AIPC. Castrated *Pten* $^{-/-}$ prostate tumors also remained AR positive, however the role of AR during AIPC in this model is still unclear. Studies using Nkx3.1, *Pten* mutant mice have implicated a role for the AR in the development of AIPC. Castrated prostates also displayed strong activation of the Erk Mitogen activated protein kinase (MAPK) pathway which has also been implicated in human disease (Gao, Ouyang et al. 2006). Furthermore, prostate epithelial cells were found to develop androgen independent phenotypes well before they displayed a cancer phenotype (Gao, Ouyang et al. 2006). We found that castration of *Pten* $^{-/-}$ B6-Luc mice at weaning induced a similar effect because, in contrast to *Pten* $^{+/+}$ animals, bioluminescence intensity did not decrease after castration indicating that castrate

resistance has already developed. However, when we castrated 11 week old animals we found that prostate epithelial cells were unable to proliferate in the absence of androgens although a large population of castrate resistant cells remained. Similar work using the β-actin luc *Pten* $^{-/-}$ model has demonstrated that prostate tumors under go a relapse after castration and are able to proliferate as evidenced by increasing bioluminescence intensity 7-28 weeks after castration (Liao, Zhong et al. 2007). Discrepancies between the studies may be related to time of castration and genetic background of the study cohorts.

Another feature of AIPC is the increased number of neuroendocrine cells observed in patients. Focal neuroendocrine differentiation (NED) represents a common feature of prostate cancer whereas pure NE cell tumors are extremely rare (Randolph, Amin et al. 1997; Hirano, Okada et al. 2004). Because higher numbers of NE cells are associated with increased neoplastic progression rates, the phenomenon of NED is of great oncological interest. However, their origin is unknown and little is known about the pathophysiology of NED. We have shown that castrated *Pten* $^{-/-}$ B6-Luc prostates contain rare number of neuroendocrine cells that express chromogranin A and Foxa2, two common markers used to identify NE cells in human prostate cancers.

The development of therapeutic strategies for prostate cancer has been hampered by the lack of relevant animal models. We have highlighted the primary advantages of B6-Luc mice for preclinical drug development. B6-Luc mice display aberrant activation of the AKT/mTOR signaling pathway which is commonly activated in human prostate cancers. Furthermore, B6-Luc mice contain a luciferase reporter allele that enables BLI of response to therapy, as evidenced by rapamycin treatment of *Pten* $^{-/-}$ animals. 3 week rapamycin treatment caused a transient decrease in bioluminescence, however, continuous rapamycin treatment was ineffective in further reducing bioluminescence levels, probably due to the development of rapamycin resistance. Consequently, B6-Luc mice may be useful to dissect apart the mechanistic basis for rapamycin resistant prostate cancers which are currently a large clinical problem. It is increasingly recognized that the

mechanism of action of rapamycin may not be sufficient for achieving a robust anti cancer effect due to its failure to inhibit mTORC2 (Shor, Gibbons et al. 2009). Rapamycin is an mTORC1 specific inhibitor and its effects on the activity of mTORC2 are somewhat controversial. Recent data has demonstrated that expression of mTORC2 is critical for the development of *Pten* $^{-/-}$ prostate cancer, highlighting mTORC2 as an attractive therapeutic target (Guertin and Sabatini 2009; Guertin, Stevens et al. 2009). mTORC2 inhibitors are currently being developed as are Dual TOR kinase inhibitors in an attempt to simultaneously inhibit both mTORC1 and mTORC2 activity (Yu, Shi et al.; Feldman, Apsel et al. 2009; Garcia-Martinez, Moran et al. 2009; Yu, Toral-Barza et al. 2009). B6-Luc mice will provide an excellent high throughput model for screening the efficacy of lead compounds. Furthermore, B6-Luc mice could aid the general development of prostate cancer therapeutics because they should facilitate large scale screening of many compounds that might possess anti tumorigenic properties.

The primary advantages of B6-Luc mice as a GEM model of prostate cancer can be appreciated from the above discussion. The lack of invasive adenocarcinoma and failure of *Pten* $^{-/-}$ prostates to progress to androgen independence are the primary limitations of this model. However, at the same time, the benign phenotype associated with these mice may allow us to manipulate them in an attempt to accelerate or advance disease progression beyond a HGPIN. Possibilities ranging from genetic to environmental affects on disease progression can easily be assessed in a high throughput manner in this model. Taken together, we believe that B6-Luc mice provide an invaluable opportunity to dissect the mechanisms of prostate cancer progression and will aid in the development of therapies in a preclinical setting.

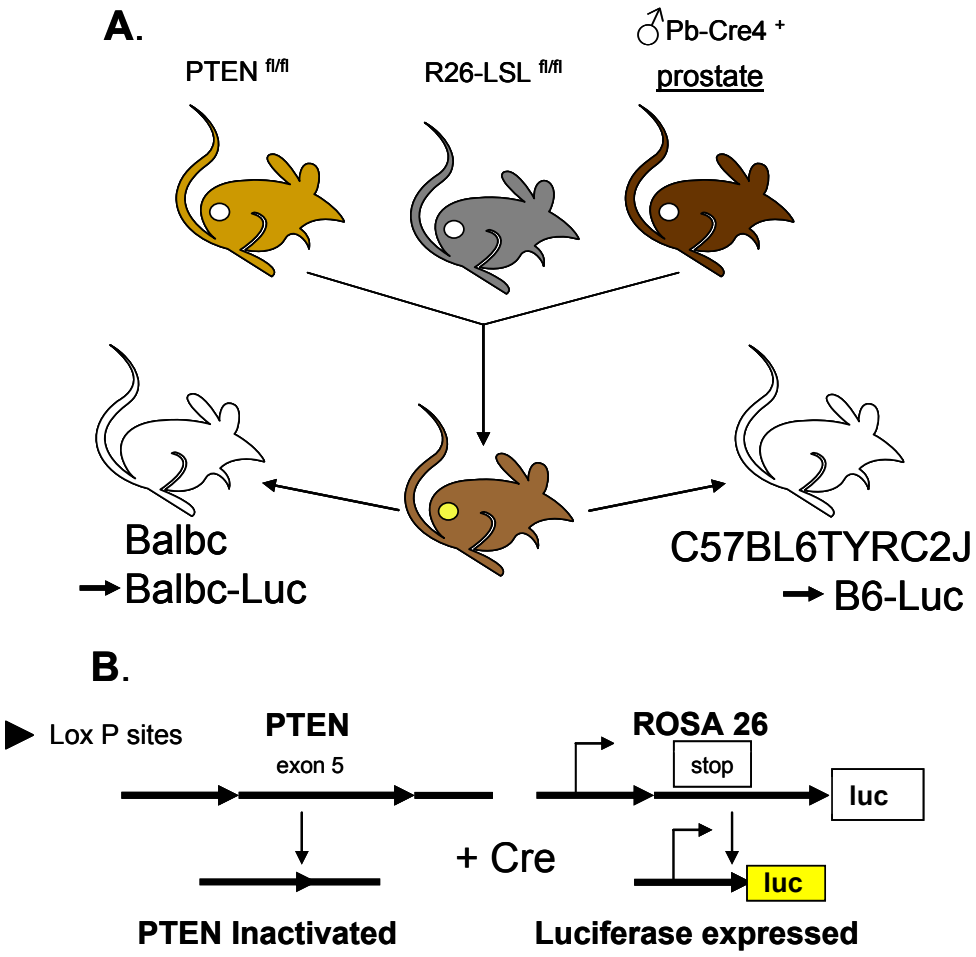

Figure 5.1: Generating a novel mouse model of spontaneous prostate cancer. (A) We intercrossed three independent strains of mice to generate a model of prostate cancer that incorporates a luciferase reporter allele and then the triple homozygote was backcrossed to C57B6TYRC2J or BALB/c mice for 7 generations to create a uniform genetic background. Backcrossed mice were designated as B6-Luc and BALB/c-Luc. (B) Cre-recombinase, under control of the probasin promoter, is expressed exclusively in the prostatic epithelium where it simultaneously inactivates *Pten* and activates luciferase in the same cell.

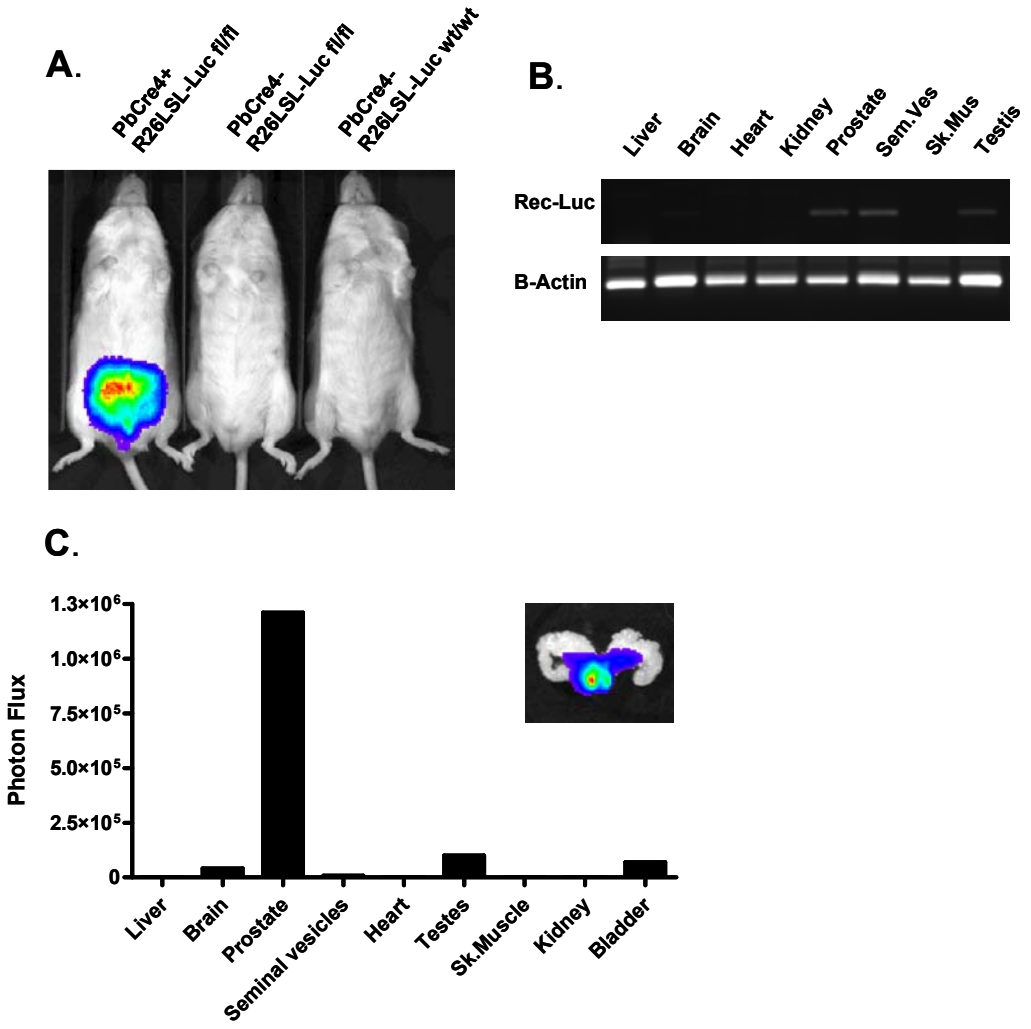

Figure 5.2: Prostate specific bioluminescence in B6-Luc mice. (A) B6-Luc mice were injected with luciferin and imaged in an IVIS100. Bioluminescence emanates from the lower abdominal region of a PbCre+, R26-LSL-Luc fl/fl animal but not from PbCre- animals. Signal was confirmed to be prostate tissue when analyzed *ex vivo* (inset image in C). (B) PCR for recombined luciferase demonstrating that recombination is detected in prostate, seminal vesicles and testis. (C) Luciferase assay of protein lysates demonstrating that only prostate tissue is capable of producing a bioluminescence signal.

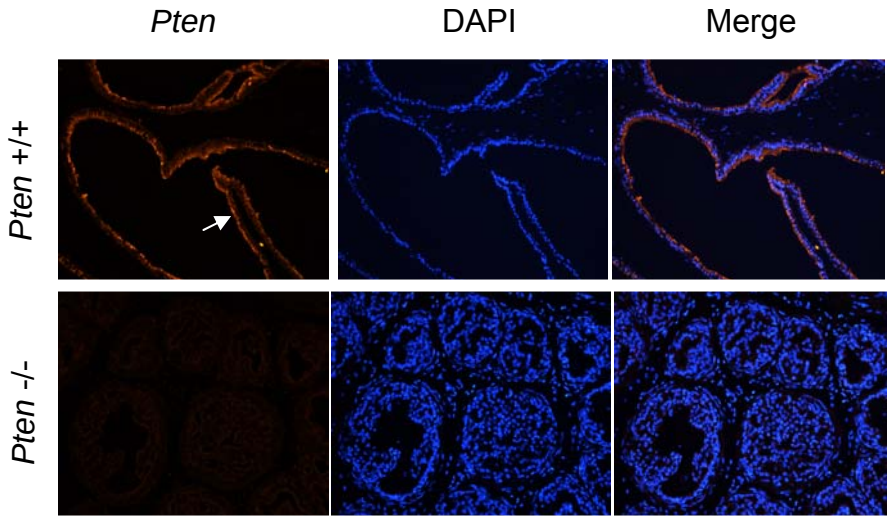

Figure 5.3: Loss of *Pten* expression in epithelial cells of *Pten* -/- B6-Luc mice. Immunofluorescence analysis of *Pten* expression in lateral lobes *Pten* -/- and *Pten* +/+ B6-Luc mice demonstrates that *Pten* expression is lost in the epithelium of *Pten* -/- animals. Arrow in top panel denotes apical location of *Pten* expression in the epithelium.

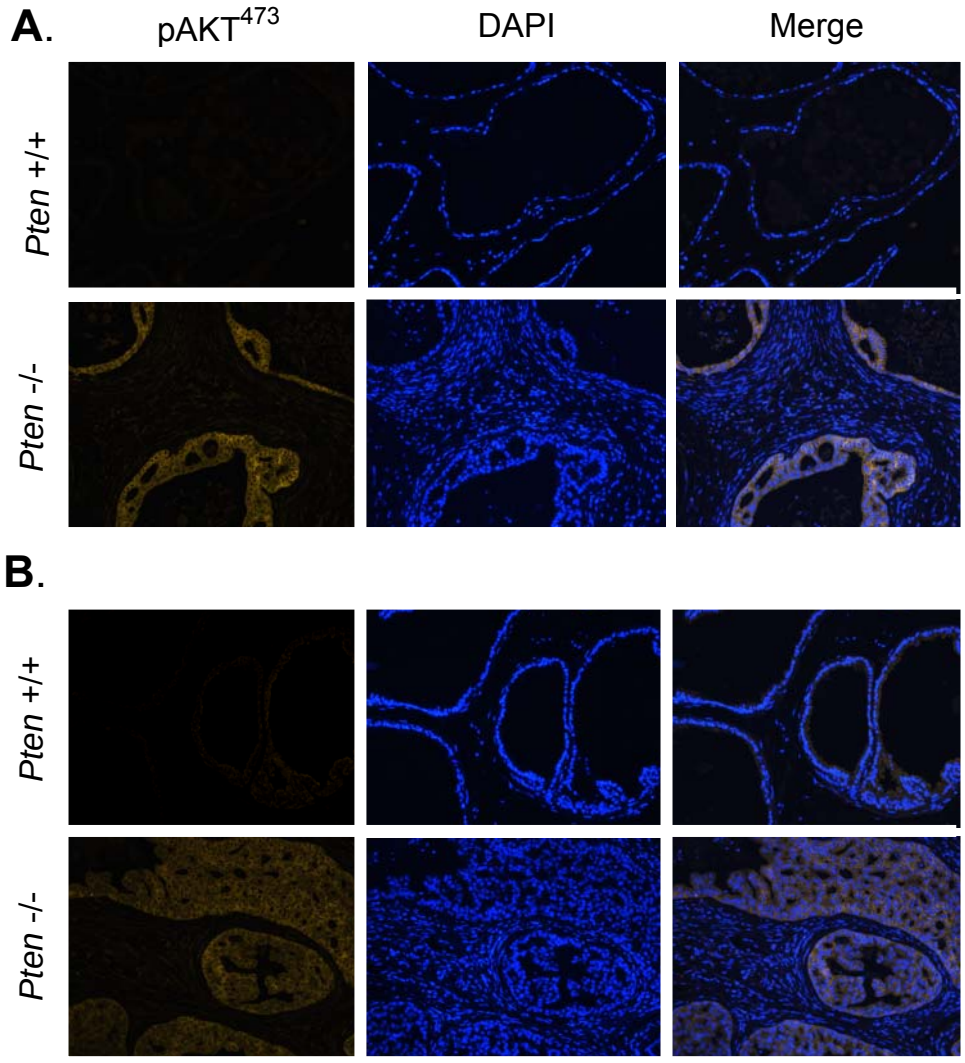

Figure 5.4: Induction of pAKT473 in *Pten* -/- B6-Luc mice. Immunofluorescence analysis for expression of pAKT473 in lateral lobes (A) and ventral lobes (B) of *Pten* -/- and *Pten* +/+ B6-Luc mice demonstrates induction of pAKT473 expression exclusively in *Pten* -/- animals.

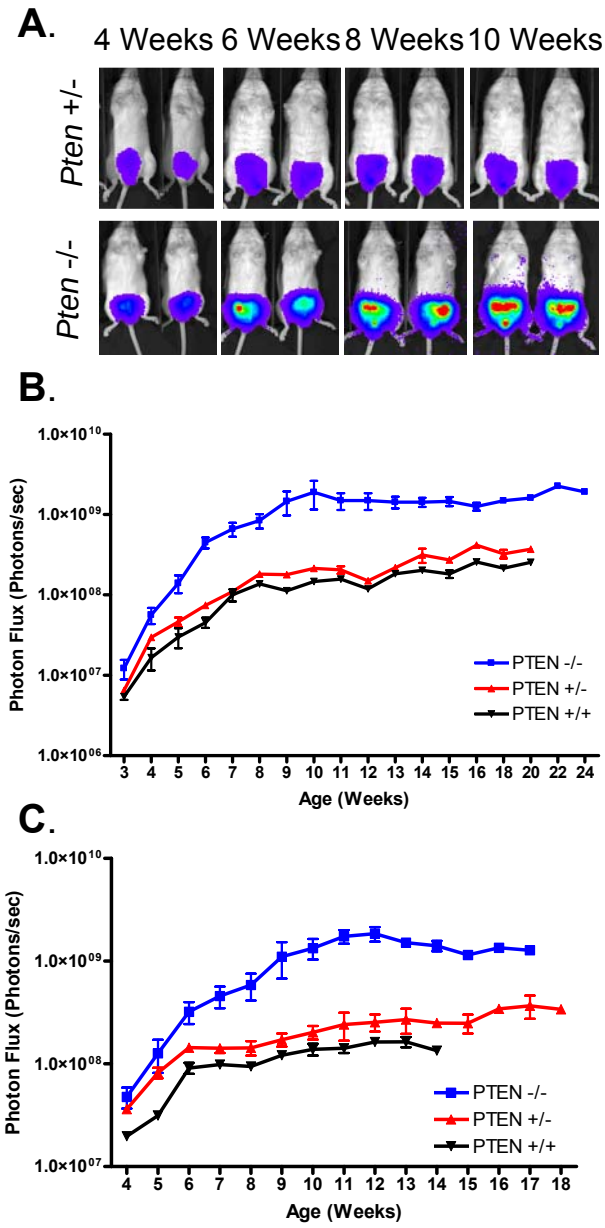

Figure 5.5: Bioluminescence imaging of prostate cancer progression in B6-Luc and BALB/c-Luc mice. (A) BLI of *Pten* +/- and *Pten* -/- B6-Luc mice to monitor cancer progression reveals that prostates in *Pten* -/- mice display increased signal intensity compared to *Pten* +/- animals. (B) Quantification of bioluminescence intensity plotted over age of animal reveals a rapid increase in bioluminescence from 3-11 weeks in B6-Luc mice and BALB/c-Luc mice (C). Y axis represents bioluminescence intensity measured as photon flux (photons/sec).

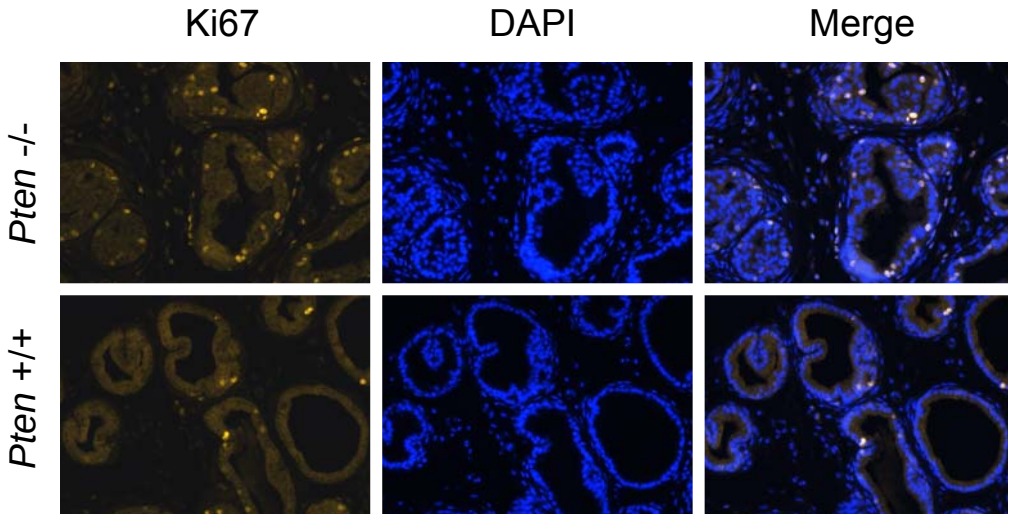

Figure 5.6: Ki67 positive proliferative levels in 6 week old B6-Luc mice. Immunofluorescence for Ki67 in lateral lobes (A) and dorsal lobes (B) of 6 week old *Pten* -/- and *Pten* +/+ B6-Luc mice demonstrates increased proliferation in epithelial cells of *Pten* -/- animals.

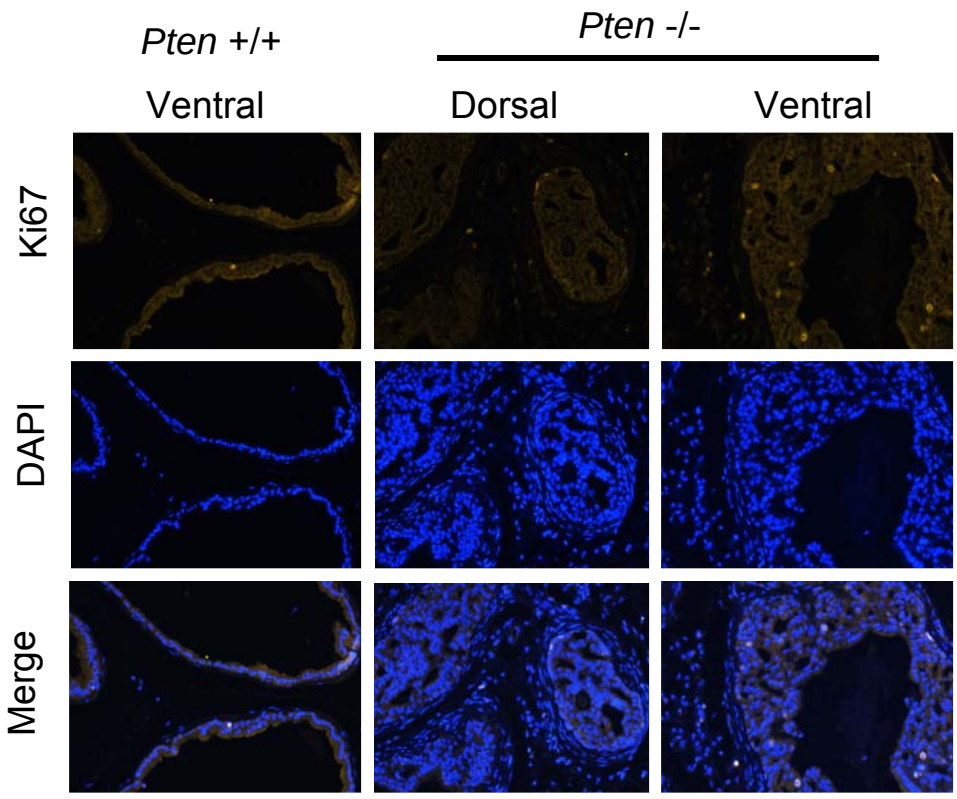

Figure 5.7: Ki67 positive proliferation levels in 25 week old B6-Luc mice:
Immunofluorescence analysis for Ki67 in *Pten* +/+ and *Pten* -/- B6-Luc mice demonstrates that proliferation of epithelial cells in *Pten* -/- mice has stopped at 25 weeks.

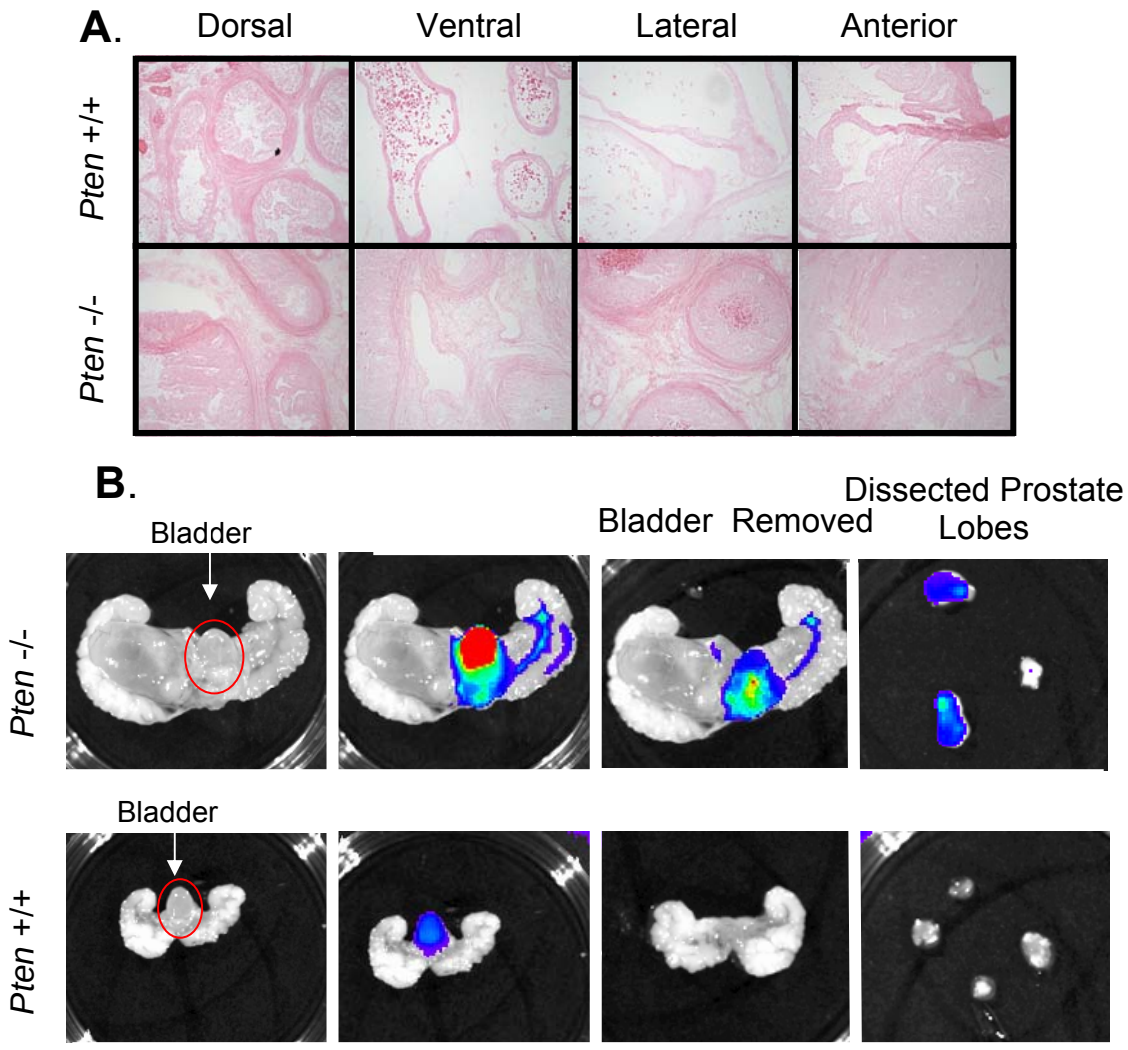

Figure 5.8: Senescence associated β-Gal activity and metabolic activity of B6-Luc mice. (A) SA- β-Gal staining of *Pten* -/- and *Pten* +/+ mice reveals no senescent positive cells in B6-Luc mice. (B) B6-Luc mice were injected with NIR labeled 2-DG and prostates were analyzed for metabolic activity by examining prostate specific uptake of the dye. We removed the bladders of mice due to retention of the dye in this tissue. Only prostates of *Pten* -/- mice are metabolically active as evidenced by uptake of 2-DG when dissected prostate lobes were examined *ex vivo*.

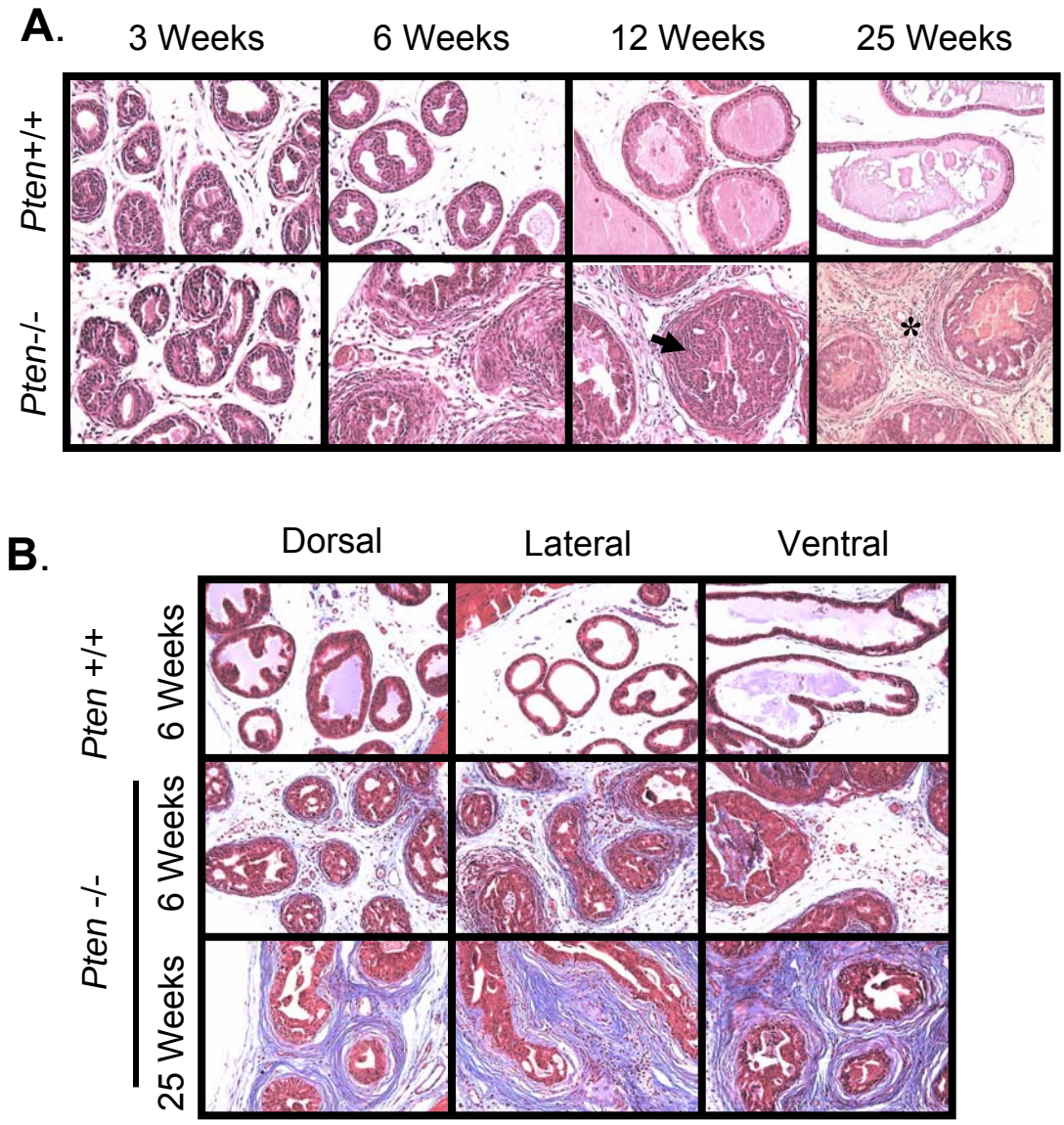

Figure 5.9: Pathologic changes in *Pten* -/- B6-Luc mice. (A) H&E staining of prostate sections from *Pten* -/- and *Pten* +/+ B6-Luc mice demonstrates the progressive pathological changes in *Pten* -/- animals. HGPIN is evident at 12 weeks (arrow) and the desmoplastic stromal response increases in older animals (asterisk). (B) Massons trichrome stain demonstrates increased numbers of collagen fibers in 25 week old *Pten* -/- animals.

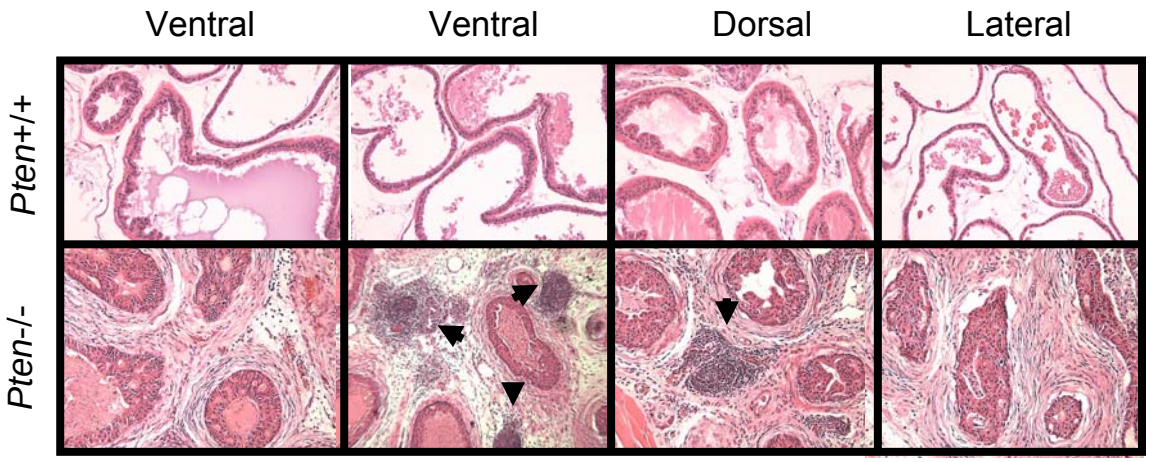

Figure 5.10: Pathologic changes in *Pten* -/- BALBC/c-Luc mice. H&E staining of prostate sections from *Pten* -/- and *Pten* +/+ BALBC/c-Luc mice demonstrates the progressive pathological changes in *Pten* -/- animals. *Pten* -/- prostates display an intense stromal response with large numbers of inflammatory cells infiltrating the tissue (arrows)

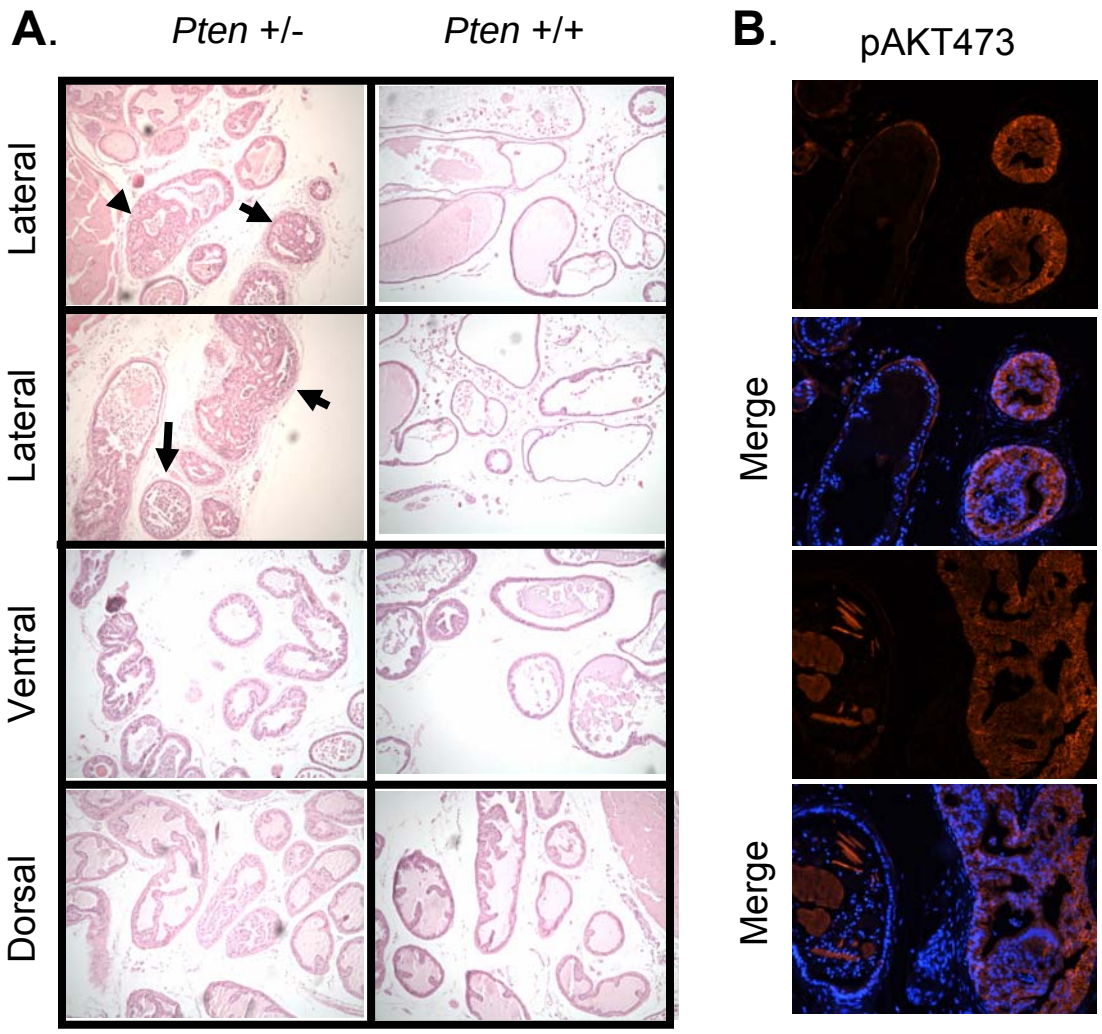

Figure 5.11: Focal HGPIN is evident in 6 month old *Pten* +/- B6-Luc mice. (A) H&E staining of prostate sections from 6 month old *Pten* +/- and *Pten* +/+ B6-Luc mice demonstrates focal areas of HGPIN in *Pten* +/- animals (arrows). (B) IF for pAKT expression in *Pten* +/- prostates demonstrates that pAKT is expressed exclusively in epithelial cells that are transformed.

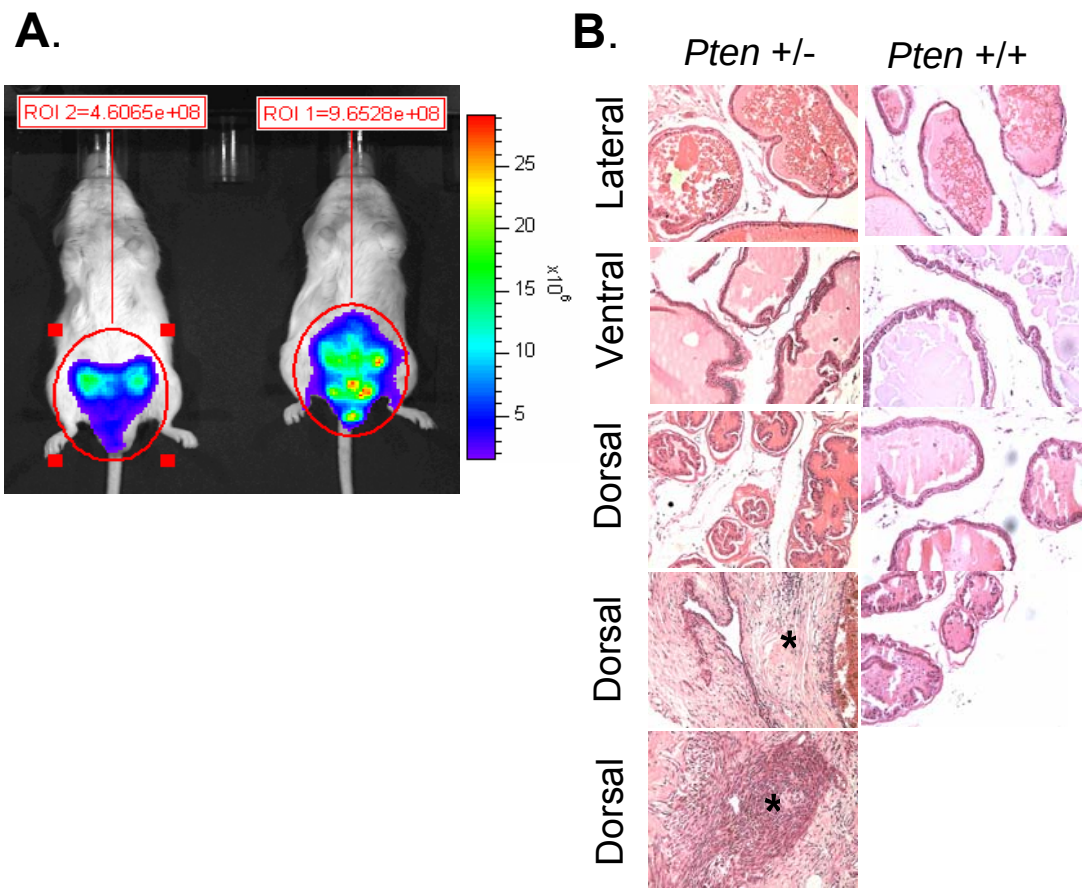

Figure 5.12: Spontaneous tumor development in 18 month old *Pten* +/- BALBC/c-Luc mice. (A) BLI of *Pten* +/- BALBC/c-Luc mice reveals a 2 fold increase in bioluminescence in an individual animal. (B) H&E staining of prostate sections from this individual revealed a large tumor in the dorsal lobe. There was no evidence of transformation in any of the other lobes. The tumor possessed an intense stromal response (asterisk) and also contained glands that were invading into the surrounding stromal tissue (asterisk).

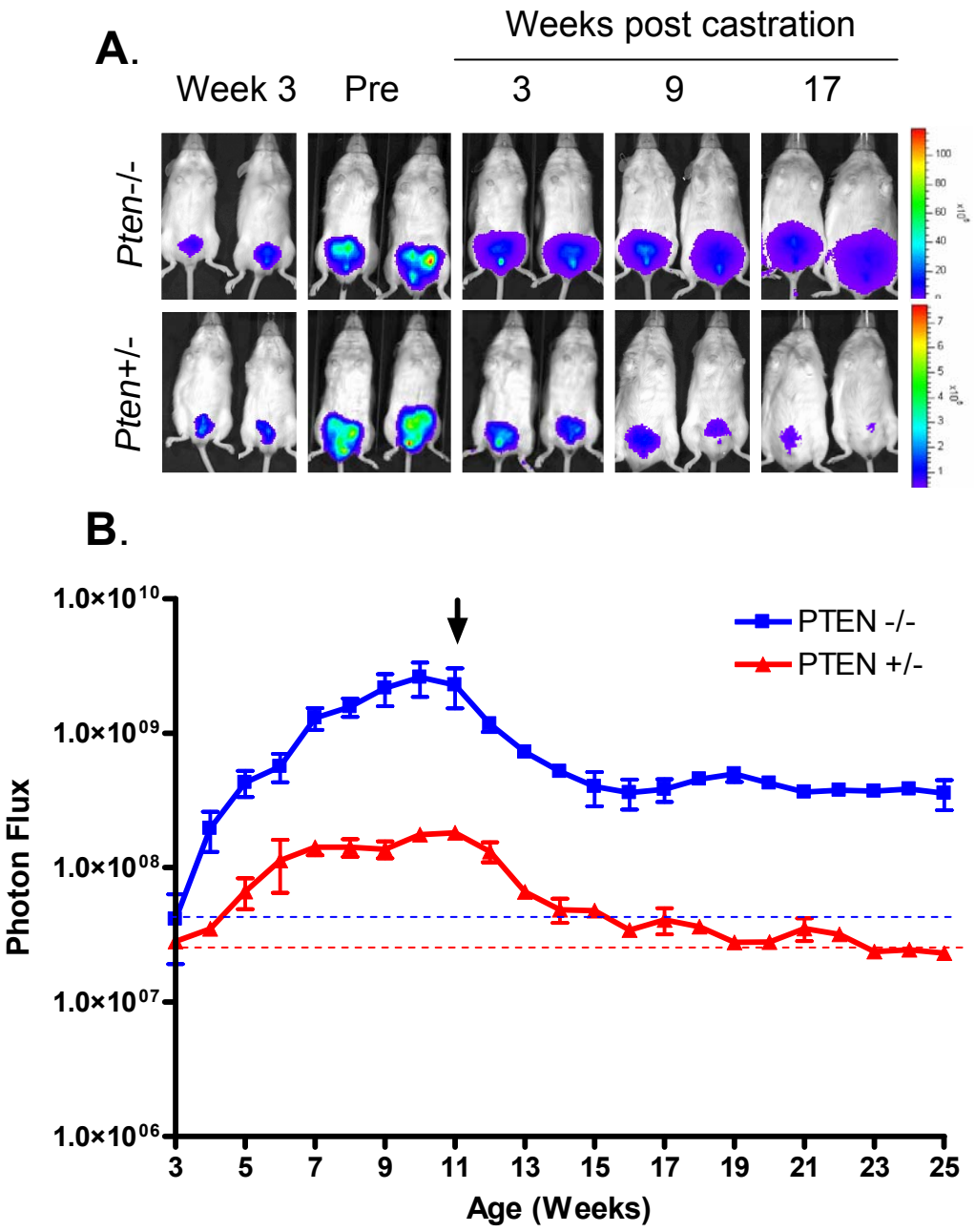

Figure 5.13: Response to castration and development of castrate resistance in B6-Luc mice. (A) *Pten* -/- and *Pten* +/- B6-Luc mice were imaged weekly and castrated at 11 weeks. Mice were then serially imaged weekly to monitor response to castration. (B) Bioluminescence was quantified and represented as photon flux over time. Bioluminescence intensity in *Pten* -/- animals remains 10 fold over basal levels compared to *Pten* +/- which has returned to baseline (hashed red line).

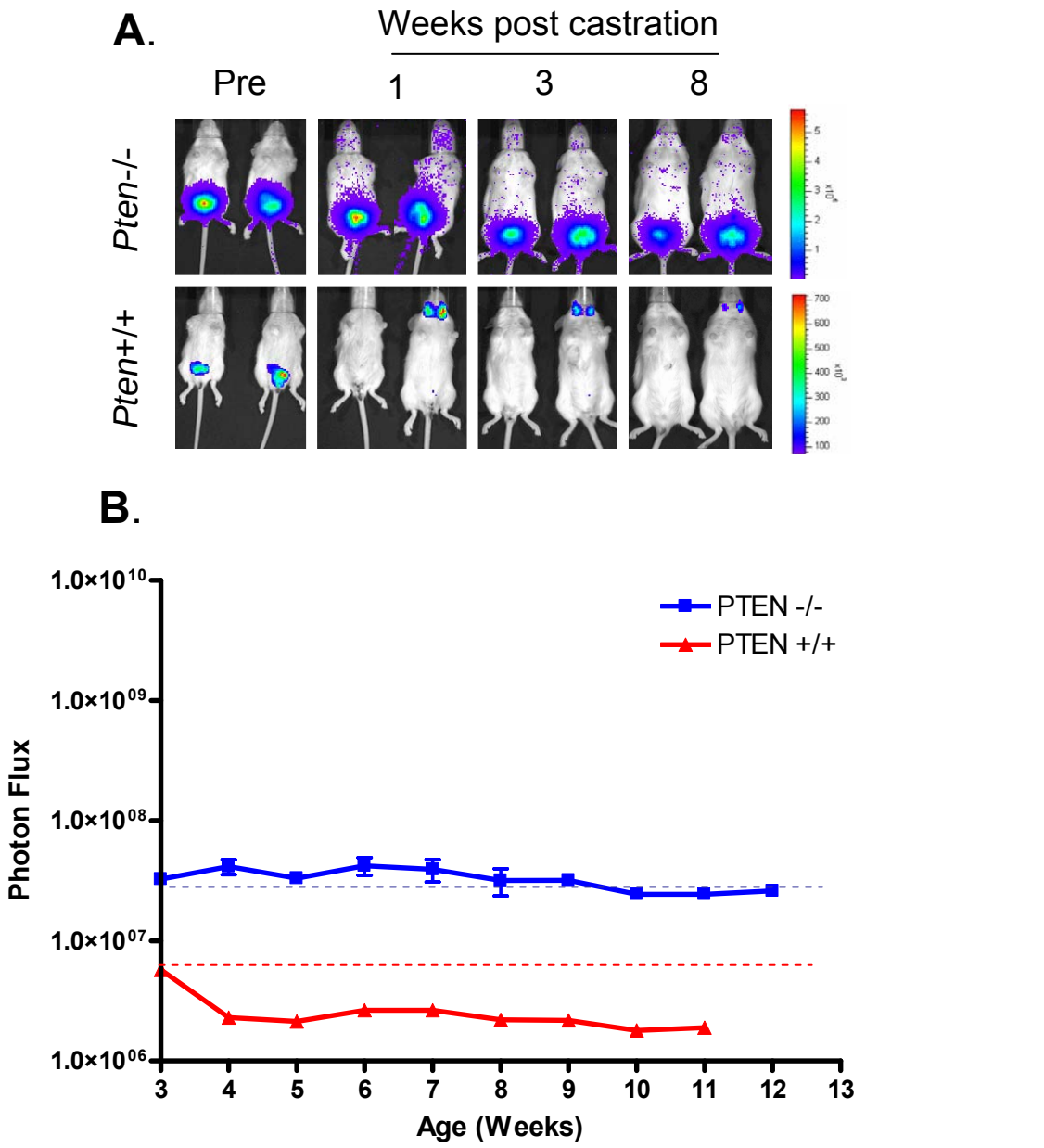

Figure 5.14: Early emergence of castrate resistance in B6-Luc mice. (A) *Pten* -/- and *Pten* +/+ B6-Luc mice were castrated at weaning (3 weeks) and serially imaged for bioluminescence weekly. (B) Quantification of bioluminescence reveals that bioluminescence intensity does not change in *Pten* -/- animals and decreases in *Pten* +/+ animals.

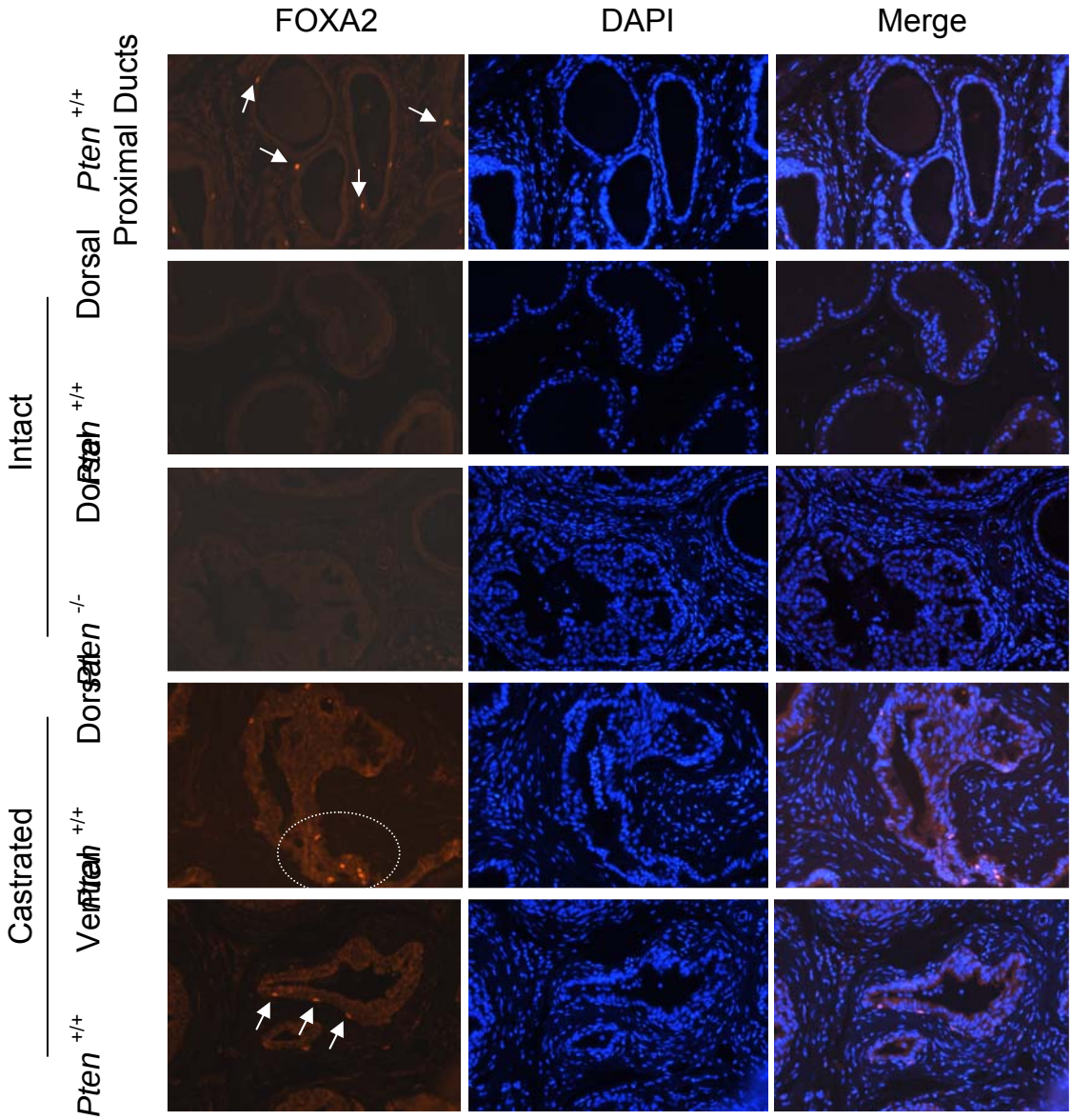

Figure 5.15: Localization of FOXA2 positive cells in castrate resistant B6-Luc mice. IF for FOXA2 expression in *Pten* +/+, intact *Pten* -/- and castrated *Pten* -/- animals. FOXA2 positive cells are detected in the proximal ducts of *Pten* +/+ animals (arrows). FOXA2 positive cells are only found in castrated *Pten* -/- animals (hashed circle and arrows)

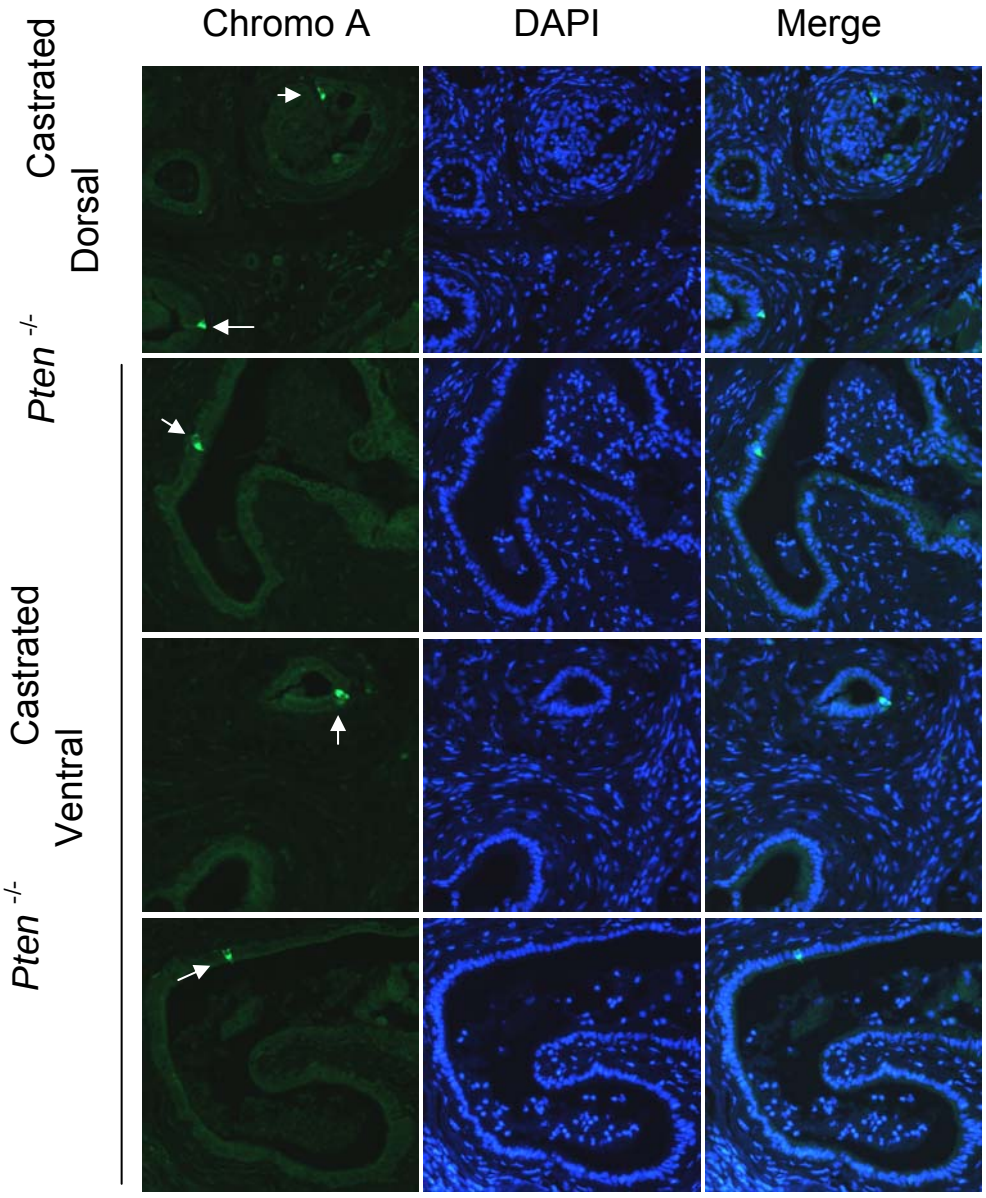

Figure 5.16: Localization of Chromogranin A positive cells in castrate resistant B6-Luc mice. IF for Chromogranin A expression in castrated *Pten* -/- animals. Chromogranin A positive cells are detected in dorsal and lateral lobes of castrated *Pten* -/- animals (arrows)

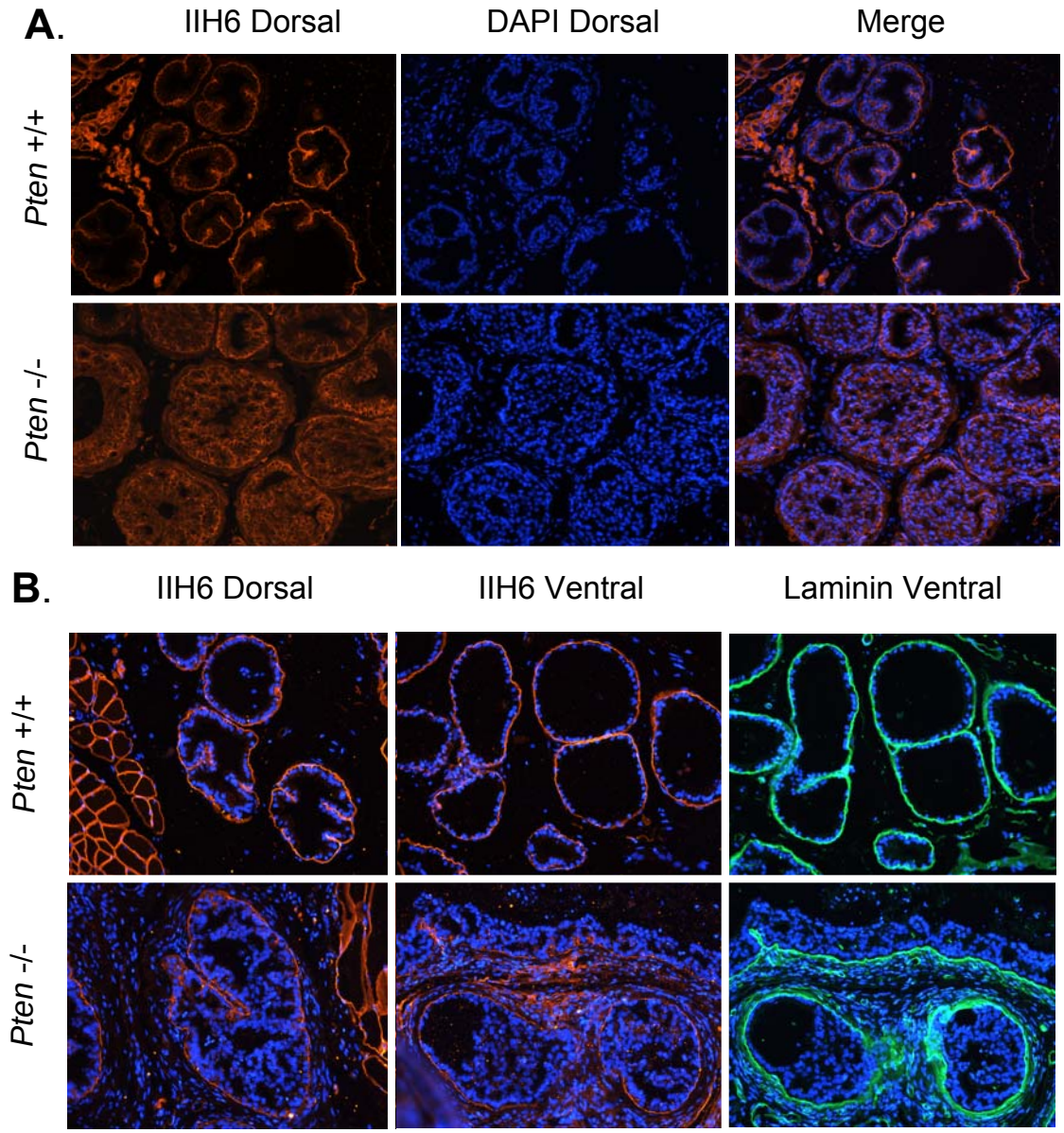

Figure 5.17: Focal loss of glycosylated α-DG expression in B6-Luc mice. (A) IF for glycosylated α-DG expression in 6 week old *Pten* +/+ and *Pten* -/- B6-Luc mice. Glycosylated α-DG expression is detected in all epithelial cells examined. (B) Focal loss of α-DG is detected in epithelial cells of 25 week old *Pten* -/- animals. Laminin expression remains confined to the basement membrane.

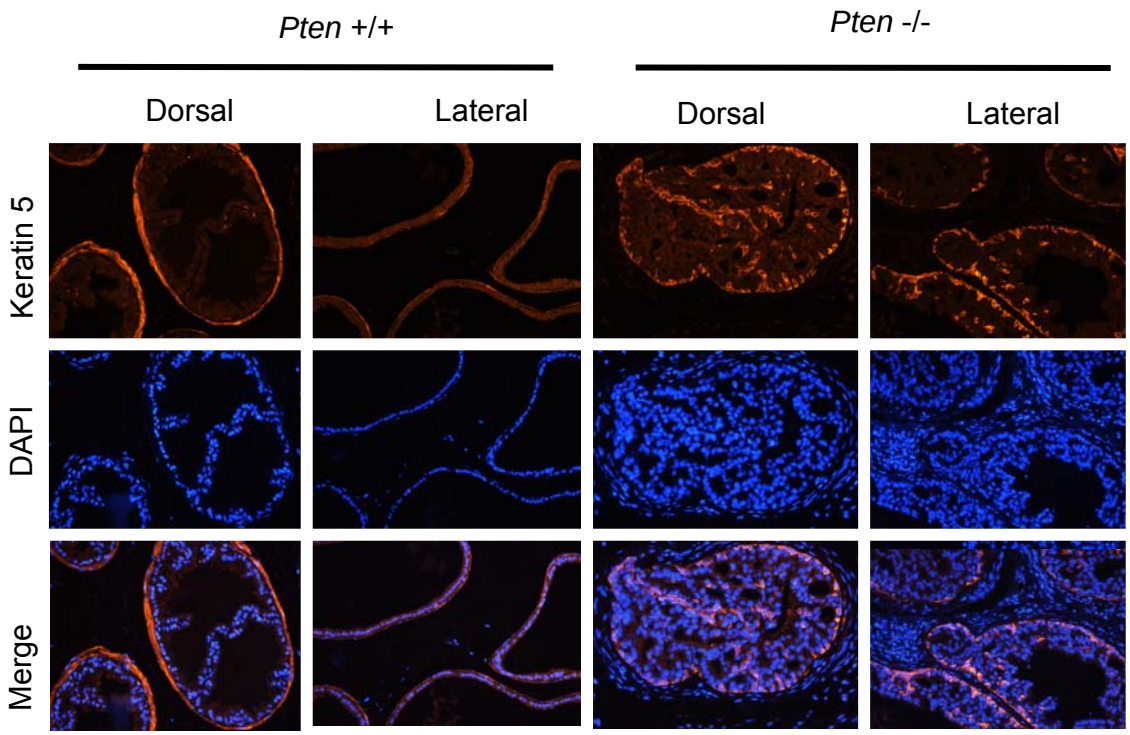

Figure 5.18: Increased numbers of basal cells in *Pten* -/- B6-Luc mice. IF for K5 expression in 25 week old *Pten* +/+ and *Pten* -/- B6-Luc mice. K5 positive basal cells are extremely rare in *Pten* +/+ prostates. Non specific basement membrane staining is seen in dorsal lobes of *Pten* +/+ prostates. K5 positive cells are abundant in *Pten* -/- prostates and localize to the basal layer of the glands. K5 positive cells are also found in the centers of the lumens.

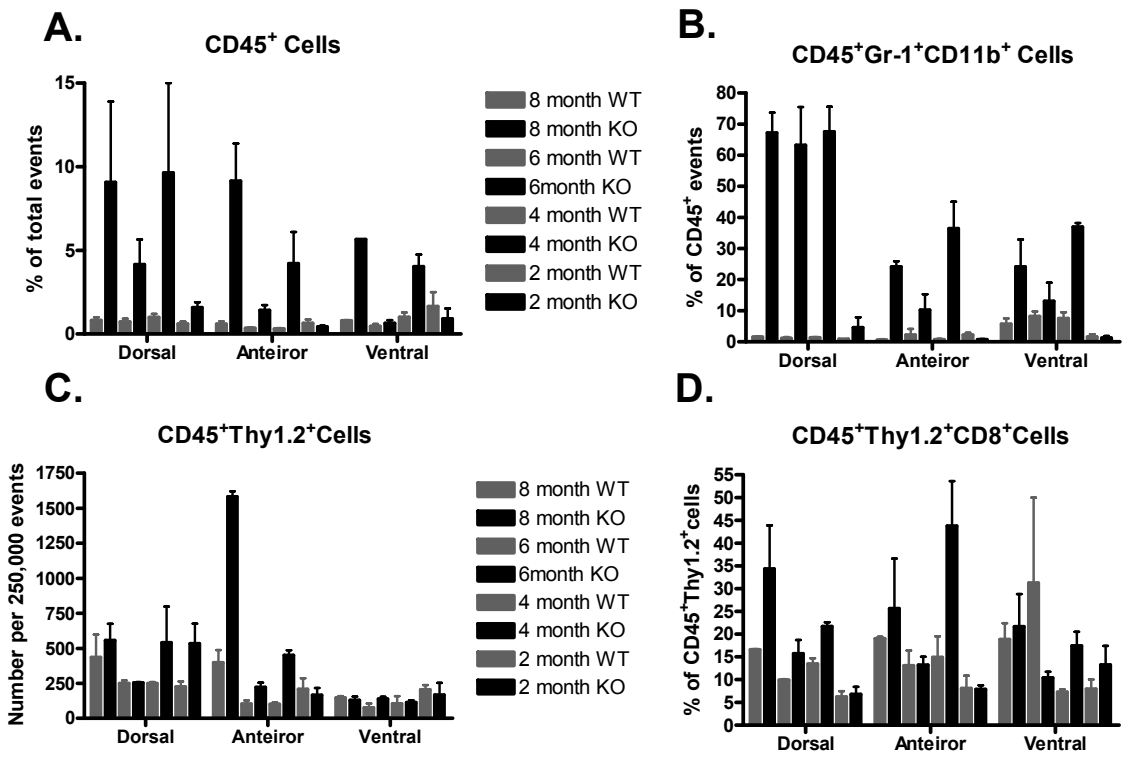

Figure 5.19: MDSCs are recruited to the prostate lobes of *Pten* -/- B6-Luc mice. (A) Flow cytometry cell counts for C45+ cells demonstrates increased infiltration of CD45+ cells in *Pten* -/- prostates over time. (B) Flow cytometry analysis of MDSC (Gr-1+, CD11b+) cells gated on CD45+ cells demonstrates increased infiltration of MDSCs in *Pten* -/- prostates. (C) Absolute numbers of CD45+ Thy1.2+ T cells (D) Percentage of CD45+ Thy1.2+ cells that are CD8+

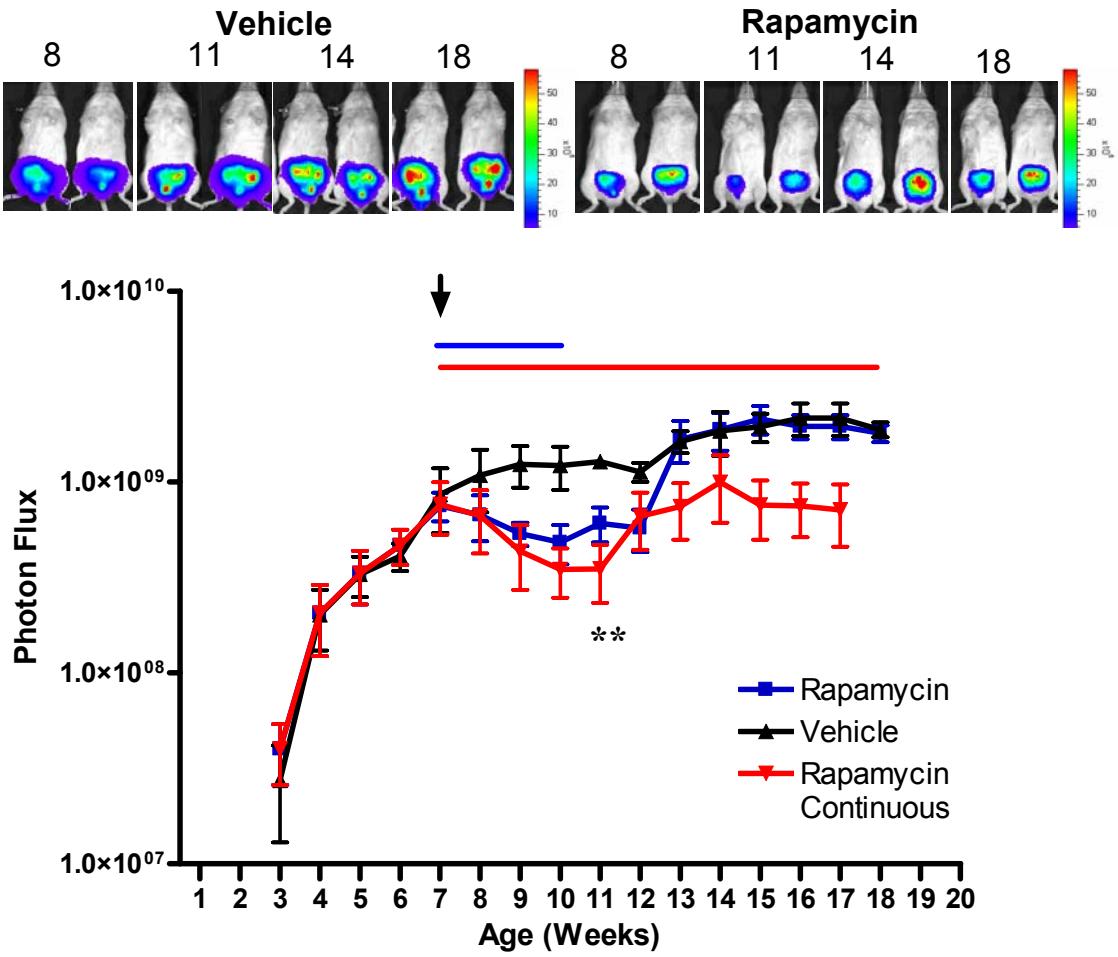

Figure 5.20: *Pten* -/- B6-Luc respond to rapamycin therapy. *Pten* -/- mice were treated with rapamycin or vehicle control at 7 weeks for either 3 weeks or continuously and serially imaged for bioluminescence. *Pten* -/- respond to therapy as evidence by decreases in bioluminescence. Significant changes in photon flux between indicated treatments are denoted by asterisks; **p<0.005

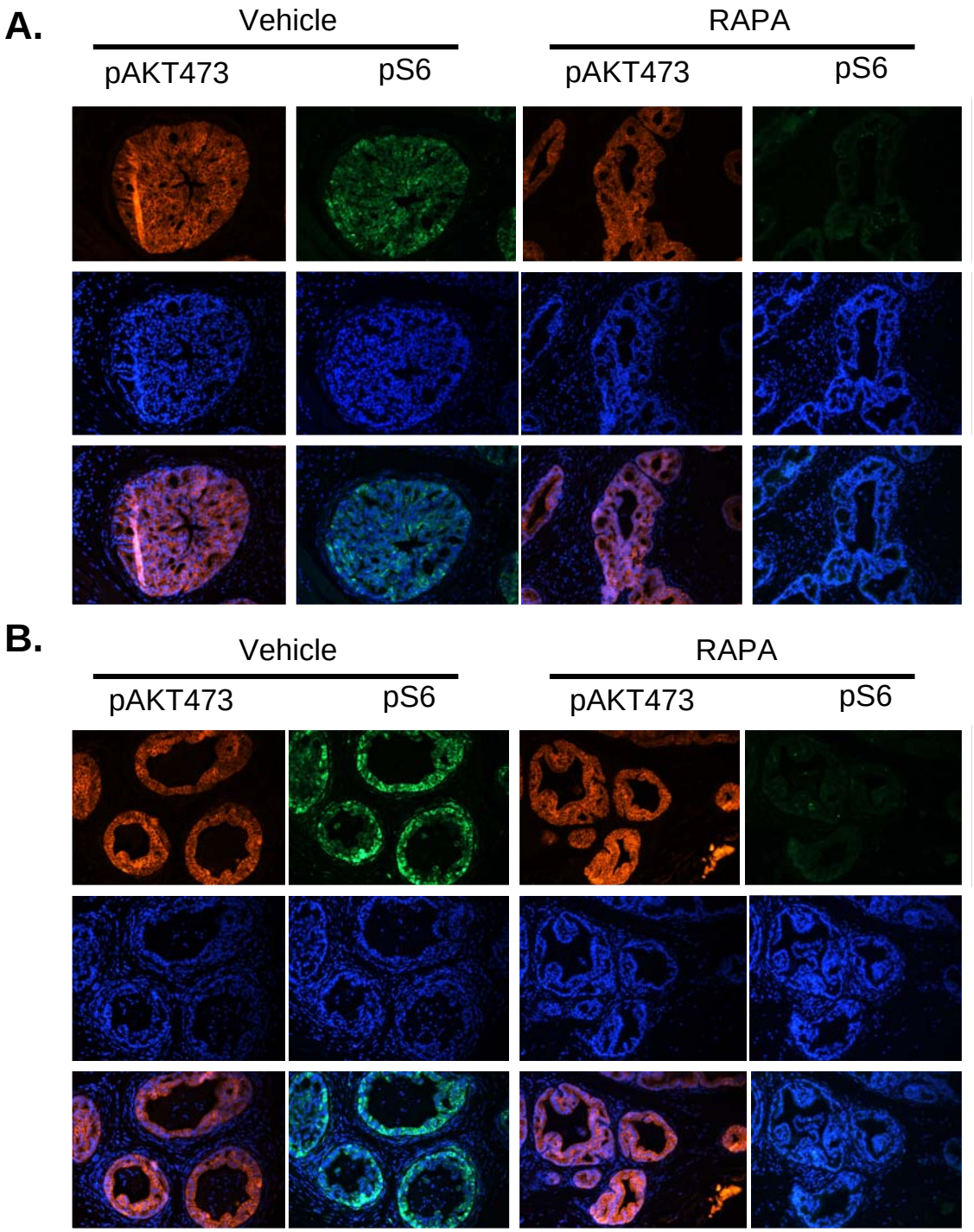

Figure 5.21: Rapamycin reduces pS6 expression in PTEN -/- B6-Luc mice. IF for pS6 and pAKT473 in dorsal lobes (A) and lateral lobes (B) of vehicle and rapamycin treated mice. Rapamycin treatment reduces pS6 but not pAKT473 expression in PTEN -/- prostates.

Experiment	No. of Mice
BLI of Pten -/-	10
BLI of Pten +/-	4
BLI of Pten +/+	4
H&E staining of Pten -/-	3 per age group
H&E staining of Pten +/-	3 per age group
H&E staining of Pten +/+	3 per age group
Castrations	3 per genotype
MDSC flow cytometry	3 per age group
Rapamycin treatment	3 per genotype

Table 5.2: Table showing numbers of mice used for each experiment.

CHAPTER VI

DIET INDUCED OBESITY AND PROSTATE CANCER PROGRESSION

Introduction

One in six men in the USA will be diagnosed with prostate cancer in their lifetime, making it the most common cancer in men (Jemal, Siegel et al. 2009). Prostate cancer is a complex disease making it very difficult to predict whether a prostate cancer will become clinically aggressive in an individual (Gittes 1991). Identifying the risk factors and mechanisms behind prostate cancer progression are of utmost importance in order to prevent the onset or to the treat the disease. Various established risk factors have been identified for prostate cancer (Hsing and Chokkalingam 2006). Recent data has indicated that obesity is linked to prostate cancer and may promote a more aggressive tumor and worsen prognosis, thereby increasing the risk of mortality (Freedland and Aronson 2004).

Obesity is a major health problem that is estimated to affect over 30% of adults in the US population (Freedland and Aronson 2005). Furthermore, according to the World Health Organization (WHO), more than 1 billion adults are overweight globally. Obesity is associated with a number of disorders including cardiovascular disease, type 2 diabetes and osteoarthritis (Haslam and James 2005). A number of large scale epidemiological studies have highlighted that obesity results in a significant increase in cancer risk and relative risk of cancer related death (Percik and Stumvoll 2009). Obesity has been linked to a number of cancers including those of breast, colon, liver and prostate. The relationship between obesity and risk of developing certain cancers, such as hepatocellular carcinoma, is well established, however data on whether obesity acts as a risk factor for prostate cancer development are controversial (Freedland and Platz 2007).

Several large studies have found an increased body mass index (BMI) in adulthood to be associated with an increased risk of developing prostate cancer while others have shown no association (Andersson, Wolk et al. 1997; Giovannucci, Rimm et al. 1997; Veierod, Laake et al. 1997; Lee, Sesso et al. 2001). More of a consensus comes from large scale epidemiological studies that have linked obesity to risk of death from prostate cancer. Obesity has been consistently associated with higher tumor grade, stage and prostate cancer metastasis. In one study, men were more than twice as likely to die from prostate cancer if they were obese (Gong, Agalliu et al. 2007). Higher BMI has also been associated with higher biochemical failure rates after radical prostatectomy (Amling, Riffenburgh et al. 2004; Freedland, Aronson et al. 2004; Strom, Wang et al. 2005). Moreover, studies have found that obesity in adolescence can increase the risk of dying from prostate cancer (Wright, Chang et al. 2007). These epidemiological studies demonstrate that obesity is clearly associated with increased risk of dying from prostate cancer. However, the mechanisms of how obesity drives prostate cancer progression have not been elucidated.

Studying the mechanisms of prostate cancer progression in humans is difficult; therefore appropriate animal models are necessary. Unfortunately, experiments testing the effects of obesity on prostate cancer progression in reliable animal models are lacking. Several studies have evaluated the role of obesity in other cancers. Dietary and genetic obesity was recently demonstrated to act as a liver tumor promoter in mice (Park, Lee et al.).Obesity promoted hepatocellular carcinoma development and was dependent on enhanced production of IL-6 and TNF-α which induced a chronic inflammatory response and activation of STAT3. It is surprising that so few studies have evaluated the role of obesity in prostate cancer progression. To date, most of the studies have focused on the influence of dietary components with an emphasis on calorie intake and how caloric restriction might be palliative to prostate cancer. Dietary fat intake has garnered much attention due to its association with prostate cancer and obesity; however, its

effects on prostate cancer in animal models have been mixed. Discrepancies between these data may be related to differences in cell lines and mouse strains used in the studies. Furthermore, the majority of studies are performed in xenograft models of prostate cancer which have several notable flaws. Because the relationship between obesity and prostate cancer may be complex, suitable animal models that can recapitulate the progression series of human carcinomas are needed. Moreover, the wealth of epidemiological data clearly warrants the use of reliable animal models to validate and dissect apart the direct effects of obesity on prostate cancer progression. Biologically relevant animals that facilitate the cost effective and high throughput assessment of obesity on cancer progression are invaluable for these needs. To this end, we have developed a novel mouse (B6-Luc) based on the *Pten* prostate cancer model, that specifically lends itself to such a study (discussed in Chapter V). We incorporated a firefly luciferase reporter allele so that we could monitor prostate cancer progression over time using BLI. The advantages of BLI are its low cost, ease of use, sensitivity and high throughput capability (Gross and Piwnica-Worms 2005). Using B6-Luc we attempted to assess the effects of diet induced obesity on prostate cancer progression. Diet induced obesity promoted an increased inflammatory response in the prostate, characterized by increased expression of IL-6 and IL-1β but had not effect on prostate cancer progression. Future studies are underway utilizing larger numbers of B6-Luc mice in an attempt to, for the first time, assess the role of obesity on prostate cancer progression in a relevant mouse model and derive statistically significant data.

Materials and Methods

Mouse Strains and Genotyping

All animal procedures were performed with approval from the University of Iowa Animal Care and Use Committee and by the authors' Institutional Review Board. PbCre4+ were obtained from obtained from the NIH Mouse Models of Human Cancer Consortium . *Pten* fl/fl mice were obtained from Jackson laboratories. *ROSA26*-LSL-Luc mice were a kind gift from William Kaelin. Mice were intercrossed and backcrossed to C57BL6TYRC2J (Jackson Labs) or BALB/c (Taconic Farms) for 7 generations. Mice were genotyped for PbCre4+, *Pten* and Luciferase using gene specific primers as previously described (Wu, Wu et al. 2001; Lesche, Groszer et al. 2002; Safran, Kim et al. 2003). In order to create the study cohorts (PbCre4+, R26-LSL-Luc fl/wt, *Pten* fl/wt) we crossed triple homozygous B6-Luc males to C57BL6TYRC2J females to generate the mice at a frequency of 25%.

Bioluminescence Imaging

All BLI was performed in an IVIS100 imaging system (Caliper Life Sciences). Mice underwent BLI weekly from 3 - 20 weeks and then bi-weekly in an attempt to monitor prostate cancer progression For BLI, D-luciferin (Gold Biotechnology) was administered to each mouse via intraperitoneal injection at a dose of 150mg/kg. Animals were then anesthetized in a chamber with 3% isoflurane and immediately placed onto the imaging platform while being maintained on 3% isoflurane. Mice were then imaged after 5 min of substrate injection using a 20cm field of view and an exposure time varying from 10sec -1 min. Bioluminescence values were calculated by measuring photon flux

(photons/sec) in the region of interest surrounding the bioluminescence signal emanating from the mice.

Diet induced obesity

Mice were assigned either a regular rodent chow diet (Harlan Teklad) or high fat diet (composed of 24% protein, 41% carbohydrate and 24% fat; 45% KCal from fat, Reseacrh Diets Inc) ad libitum from 6 weeks of age and maintained on their diets for the duration of the study. Body weights were recorded everytime BLI was performed to assess the degree of diet induced obesity.

Plasma biomarker analysis

Blood from 15 weeks old animals was collected via a submandibular cheek punch into EDTA coated vacutainers (BD Biosciences). Blood was then centrifuged for 10 mins @13000rpm, plasma was collected and subjected to ELISAs for leptin (Crytsal Chemical), IGF-1 (RnD Systems), Insulin (Crystal Chemical) and Testosterone (Cayman Chemical) according to manufacturers conditions.

Histological and immunfluorscence assays

Prostates were fixed in 4% PFA overnight and transferred to 30% Etoh and embedded in paraffin wax using an automatic tissue processor. Prostate were then embedded into cutting blocks using a heated plate followed by cooling at -5C. Sections from blocks were cut at 7uM using a Leica microtome, placed into a heated waterbath (37C) and mounted onto charged (+/+) superfrost slides. Samples were then air dried and left at room temperature until IF was performed. For IF, sections were rehydrated in a series of ethanols (100%-70%) and washed in 1X PBS after being dipped in xylene for 10

mins to remove the paraffin. Following this sections were subjected to antigen retrieval using citrate buffer as follows. Sections were immersed in a solution of 0.1M Sodium citrate + 0.01M Citric acid and heated at 95C for 20 mins. Sections were then left to cool in solution at room temp for an additional 20 mins. Following antigen retrieval sections were washed in 1X PBS and blocked in donkey block (2% BSA, 0.1% Triton X, 0.1% Tween 20, 1% Donkey serum, PBS) for 1 hr at room temp. Samples were then incubated with primary antibody (in donkey block) overnight at RT at the following dilutions; pAKT473 1:100 (Cell signaling), Ki67 1:400 (Novocastra). Following primary Ab treatment, samples were washed and incubated with secondary antibody in a solution of donkey block + DAPI (1:5000) for 1 hr at RT. Samples were washed in 1X PBS, mounted in fluorgel and visualized on a Leica microscope.

For H&E staining, sections were treated as follows: Xylene 5 mins; 100% ethanol 2 X 1 min; 95% ethanol 2 X 1 min; Harris Haematoxylin 45 secs; rinsed in tap water; acid alcohol 1 min; rinse in ddH20; Ammonium water 1 min; rinse in ddH20; rinse 95% ethanol; Eosin 45 secs; 95% ethanol 1 min; 100% ethanol 2 X 1 min; Xylene 2 mins; Mounted with coverslips with permount-xylene (1:1). Slides were visualized using a Leica . . microscope

Results

Generation of study cohorts

In an attempt to model biologically relevant prostate cancer we developed an animal model based on the prostate specific *Pten* mutant described previously [REF]. We further improved on this model by incorporating a firefly luciferase reporter allele that becomes activated simultaneously to deletion of *Pten* (for complete animal model characterization see Chapter V). Furthermore, we extensively backcrossed our model

onto the albino C57BL6 genetic background. The primary advantages of B6-Luc mice are that BLI enables cost effective high throughput analysis of prostate cancer progression in a model that is biologically relevant. Furthermore, the C57BL6 strain has a well characterized metabolic profile which will facilitate the study. We have previously described the development of focal HGPIN in *Pten* $^{+/-}$ B6-Luc mice. Because these mice develop pre neoplastic lesions that never progress to carcinomas they provide an excellent background to test the effects of diet induced obesity on prostate cancer progression. In order to generate study *Pten* $^{+/-}$ study cohorts we crossed a triple homozygous B6-Luc male (PbCre+, R26LSL-Luc $^{fl/fl}$, *Pten* $^{fl/fl}$) to wildtype C57BL6TYRC2J females (Figure 6.1). From this cross we were able to generate PbCre+, R26LSL-Luc $^{fl/wt}$, *Pten* $^{fl/wt}$ study cohort males at a frequency of 25%. Study cohorts underwent BLI weekly from weaning (3 weeks) and at 6 weeks were randomized based on bioluminescence intensity values and assigned into their treatment groups.

High fat diet induces obesity in B6-Luc mice

Study cohorts were assigned either a standard rodent chow diet (Harlan Teklad) or high fat diet containing 60% of calories from fat (Research diets). Diets were initiated when mice had reached 6 weeks of age and mice were maintained on their specific diet throughout the 12 month duration of the study. We monitored body weights weekly to assess the degree of weight gain in control vs high fat fed mice (Figure 6.2A-C). Significant increases in weight gain became apparent at 12 weeks of age to the point where mice on high fat diets were on average 15g heavier than control fed mice at the end of the study. Although the extent of obesity can not be assessed in mice due to the inability to measure BMI, mice fed high fat diets clearly contained larger amounts of intra-abdominal adipose tissue which is a standard measurement for obesity in rodents (Figure 6.2D).

Diet induced obesity increases levels of plasma biomarkers

Obesity has been shown to alter circulating levels of a number of adipokines, hormones and growth factors in both human patients and experimental animal models. Leptin, one of the most well studied adipokines that is increased in obesity, is produced almost exclusively by adipocytes and its role in energy intake and expenditure is well defined (Jequier 2002). Obesity is also associated with increased levels of insulin resulting in chronic hyperinsulinemia and insulin resistance . Growth factors such as IGF-1 have also shown to be increased in obesity. Testosterone levels are found to be decreased in obesity which may be related to leptin levels because a strong inverse association between the two has been described (Luukkaa, Pesonen et al. 1998). In order to assess the plasma levels of these biomarkers we collected blood from control fed and high fat fed mice, extracted the plasma and performed ELISAs for leptin, insulin, IGF-1 and testosterone (Figure 6.3). As expected, plasma levels of leptin were significantly higher in high fat fed mice. Insulin production was also increased demonstrating that obese mice may also be developing insulin resistance and type 2 diabetes. We did not detect any significant differences in the plasma levels of IGF-1 and insulin between control and high fat fed mice. These data demonstrate similarities in diet induced obesity in B6-Luc compared to human patients.

Bioluminescence intensity is not significantly different between control vs high fat fed B6-Luc mice

We performed BLI bi-weekly in an attempt to assess differences in prostate cancer progression between control and high fat fed mice (Figure 6.4). Although bioluminescence intensity was greater in high fat fed mice at the end of the study, the magnitude was not significantly different. Bioluminescence intensity displayed a

progressive increase in both groups as mice aged, indicating that prostates were continuously growing overtime. Interestingly we noticed that one particular animal on a high fat diet (#1480) presented with an enhanced bioluminescence signal, at 6 months of age, that was greater than its counterparts (Figure 6.4B). Shortly after imaging this animal was found dead in its cage, however, we were able to harvest prostate tissue and prepare sections for analysis (Figure 6.5). We also euthanized a control fed animal to use as a control for the subsequent assays. We performed H&E staining of prostate sections and noticed a striking difference in the stromal compartment of the dorsal lobes of the high fat fed individual (Figure 6.5A). The stromal response was similar to the desmoplasia seen in *Pten* $^{-/-}$ B6-Luc animals, which present with increased collagen deposition and inflammation. Unfortunately, because this animal was found dead, we were unable to perform FACS analysis to assess differences in inflammatory subsets. However, the H&E sections clearly demonstrate an inflammatory response that is exclusive to the dorsal lobe. Because bioluminescence intensity was increased in this individual, we also performed IF for Ki67 to assess the level of proliferation (Figure 6.5B). Ki67 levels were increased in the dorsal prostate of the high fat fed animal compared to control fed, however pAKT levels were unchanged between the two.

Diet induced obesity enhances production of pro-inflammatory cytokines

We were encouraged by the data from mouse #1480 but decided to complete the study before sacrificing and analyzing more mice due to the small number of animals enrolled in the study. When the study cohorts reached 12 months of age we euthanized the mice and prepared their prostates for histological analysis. H&E staining of both control and high fat fed mice revealed that focal HGPIN was evident in all mice (Figure 6.6A). We also noticed an increased stromal response that was exclusive to the areas that had undergone a transformation (Figure 6.6). Globally, this stromal response appeared to

be more intense in the prostates of mice fed high fat diets. Interestingly, the dorsal lobes of high fat fed mouse #1481 presented with a large stromal response although there appeared to be no minimal pathological changes in the epithelium. Obesity was previously shown to act as bona fida liver tumor promoter by inducing a chronic inflammatory state through production of IL6, IL1-β and TNF (Park, Lee et al.). We performed qRT-PCR from prostate RNA for these pro-inflammatory mRNAs and found that expression of IL6 and IL1-β was significantly upregulated in high fat fed mice (Figure 6.5B). These data indicate that obesity might promote an inflammatory state in the prostate through enhanced production of pro-inflammatory cytokines. Next we assessed the degree of pathological changes to the prostatic epithelium. High fat fed mouse #1479 displayed large areas of focal HGPIN, accompanied by a stromal response, which were exclusive to the entire lateral lobe. Similarly control fed mouse #1477 presented with a large areas of HGPIN in the same region. We performed IF for pAKT expression and Ki67 to assess any differences in proliferation between control vs high fat fed mice (Figure 6.6). pAKT473 expression was limited to the areas of HGPIN in all cases. We did not detect any significant differences in Ki67 levels between the groups indicating that diet induced obesity has not increased the proliferation status in B6-Luc mice. Taken together, data from this study has revealed ambiguous results. The small number of animals enrolled in this study makes it challenging to interpret the data and difficult to derive statistically significant data. Future studies are underway with larger cohort sizes in an attempt to assess the effects of diet induced obesity in a more intricate and efficient manner.

Discussion

We have demonstrated the feasibility of studying the relationship between obesity and prostate cancer progression in B6-Luc mice. B6-Luc mice fed a high fat diet gained significantly more weight than control fed mice and displayed elevated plasma levels of

leptin and insulin, two of the most commonly altered hormones in obese human patients. B6-Luc mice presented with focal HGPIN at the end of the study, although it is difficult to determine whether obesity influenced the progression rate of HGPIN due to the small numbers of animals used. However, we have demonstrated that in a rare case, high fat diet did promote an early stromal response and enhanced epithelial cell proliferation in the prostate. Furthermore, diet induced obesity resulted in enhanced production of pro-inflammatory cytokines IL-6 and IL1-β in the prostates of high fat fed B6-Luc mice. Data from this study is encouraging and warrants the need for larger cohorts in order to derive statistically significant data.

In this study, we attempted to bridge the gap in knowledge from clinical epidemiological findings to an experimental model. The majority of epidemiological literature suggests that obesity is clearly associated with increased risk of dying from prostate cancer. Several large prospective cohort studies are notable. The American Cancer Society enrolled 816,268 patients for longitudinal cancer studies, known as Cancer Prevention Studies I and II (CPS-I and CPS-II) (Rodriguez, Patel et al. 2001). Men were followed for 13 yrs in CPS-I and 14 years for CPS-II. During this time there were 5212 prostate cancer deaths. Both studies reported that obese men were significantly more likely to die from prostate cancer with a 27% and 21% increased risk relative to normal weight men. Furthermore, it was shown that severely obese men were at an even greater risk of death from prostate cancer (34% higher risk). Similarly, the NIH-AARP Diet and Health Study examined BMI and weight change in relation to prostate cancer incidence and mortality in 287760 men aged 50-71 at the time of enrollment (Wright, Chang et al. 2007). Higher BMI was associated with significantly reduced prostate cancer incidence, conversely however, a significant elevation in prostate cancer mortality was observed at higher BMI levels. Interestingly, adult weight gain also significantly increased the risk of dying from prostate cancer. Obese men are also more likely to experience cancer recurrence after surgery and have lower chances of cure after

radiation therapy for prostate cancer (Strom, Kamat et al. 2006). We attempted to validate these large scale epidemiological studies in an experimental animal model of prostate cancer designed in our laboratory. However, we were unable to conclusively determine the effects of obesity on cancer progression in mice. We are currently repeating similar experiments using larger numbers of study cohorts. If we are able to deduce that obesity accelerates prostate cancer progression in this model, future experiments will be aimed at trying to determine the mechanism/s involved.

Despite the clear link between obesity and prostate cancer mortality, the underlying mechanisms are poorly understood. Obesity leads to a number of changes in hormone production, growth factor signaling and inflammatory responses (Bastard, Maachi et al. 2006). For example, decreased levels of testosterone are a common feature of obesity, lending a hypothesis as to why obesity, in some cases, obesity may be protective against the development of prostate cancer. However, decreased testosterone levels might augment the development of androgen independent prostate cancer, the most aggressive and lethal stage of the disease. Insulin resistance in obesity results in elevated levels of insulin. Elevated insulin levels have been postulated as one of the key metabolic changes that link obesity with mortality from many different types of cancer (Boyd 2003). A recent study found that men who had a BMI >25 and high C peptide concentrations (a marker of insulin blood levels) had quadruple the risk of dying from prostate cancer compared with men who had lower BMI and lower C peptide concentrations (Ma, Li et al. 2008). Increased adiposity during obesity results in elevated levels of leptin production. Increased serum leptin levels have been associated with larger and higher grade prostate tumors (Stattin, Soderberg et al. 2001; Saglam, Aydur et al. 2003). Furthermore, leptin has been shown to act as a mitogen for prostate cancer cells (Onuma, Bub et al. 2003; Somasundar, Yu et al. 2003). Other adipokines, such as TNF, IL-6 and IL-1β have been associated with obesity and may promote an inflammatory state that might contribute to prostate cancer progression. TNF and IL-6 were recently

shown to promoter liver tumor progression by inducing a chronic inflammatory state in hepatocellular carcinoma in mice (Park, Lee et al.). The link between inflammation and cancer is well established and because inflammation is generally associated with obesity it would seem plausible that such a mechanism might promote prostate cancer progression. We have demonstrated that obesity induced an inflammatory response prior to the onset of PIN in a rare case within this study. Furthermore, the prostates from high fat fed mice generally had an increased stromal response compared to control fed mice which were characterized by enhanced production of IL-6 and IL-1β. It would be interesting to characterize the absolute numbers of inflammatory cells between the two groups and to phenotype the subsets to determine which inflammatory cells might be more prevalent. Current studies are aimed at addressing these questions in our lab.

To our knowledge, this is one of the first reports that has examined the effects of diet induced obesity on prostate cancer progression in a spontaneous mouse model. The majority of studies have focused on dietary composition and caloric intake in animal models of prostate cancer. An isocaloric low fat diet was found to slow prostate tumor growth, which may be mediated through modulation of the insulin/IGF axis (Ngo, Barnard et al. 2003). A low fat diet also delayed the transition from PIN to invasive carcinoma in another mouse model of prostate cancer (Kobayashi, Barnard et al. 2008). The scarceness of direct studies of obesity on prostate cancer progression might be related to the lack of animal models that are suitable for such studies. The majority of experiments performed to date were done in xenograft models of prostate cancer. Because prostate cancer progression and obesity are complex diseases, xenograft models might not possess key features of each disease to be able to successfully determine the relationship between the two. B6-Luc mice possess a number of key advantages over existing mouse models of prostate cancer (discussed in Chapter V) and particularly lend themselves to lengthy studies that require longitudinal assessment of cancer progression. Furthermore, obesity has been extensively studied on the C57BL6 background making

the metabolic profile of this strain more characterized than others. With such a model we will be able to better understand the mechanistic basis between obesity and prostate cancer and at the same time develop a model that will facilitate the development of therapeutic interventions in the same context.

In our model, B6-Luc mice display signs of focal HGPIN with aging. However, the majority of the prostate epithelium remains healthy and data regarding whether HGPIN is a precursor for carcinoma is controversial. Epidemiological studies have validated that obesity can accelerate prostate cancer in patients with established disease but its effects on prostate cancer development are mixed. Therefore it is possible that obesity is not able to accelerate the development or promote the progression of HGPIN in B6-Luc mice and requires a more developed prostate cancer as a model with which to manipulate. We have previously characterized *Pten* homozygous (*Pten* $^{-/-}$) mutant B6-Luc mice that develop HGPIN with 100% penetrance and display progressive changes in the stromal compartment. *Pten* $^{-/-}$ B6-Luc mice may provide a more suitable model to examine the effects of obesity on prostate cancer progression and because of this, future studies are aimed at utilizing these mice in such studies.

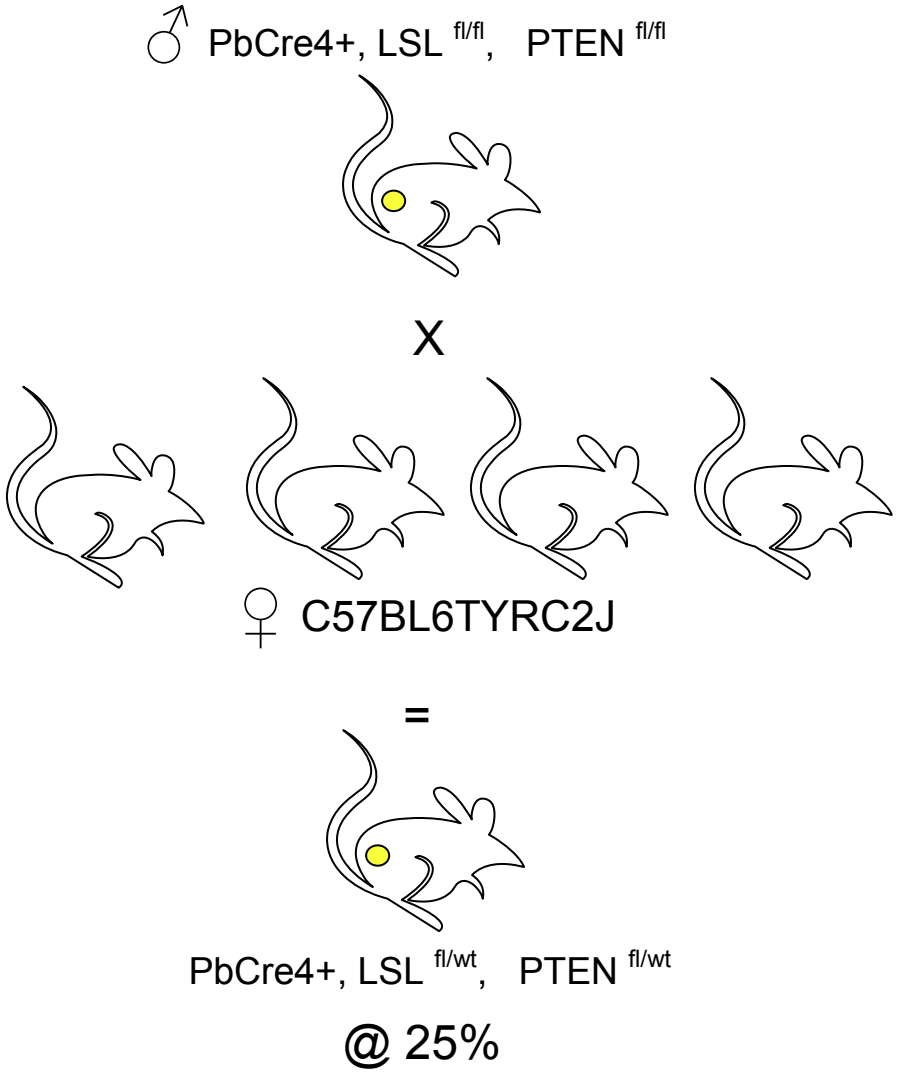

Figure 6.1: Generation of B6-Luc study cohorts. We crossed PbCre+, LSL fl/fl, PTEN fl/fl males to C57BL6TYRC2J females in an effort to generate the PbCre+, LSL fl/wt, PTEN fl/wt study cohorts at a 25% frequency.

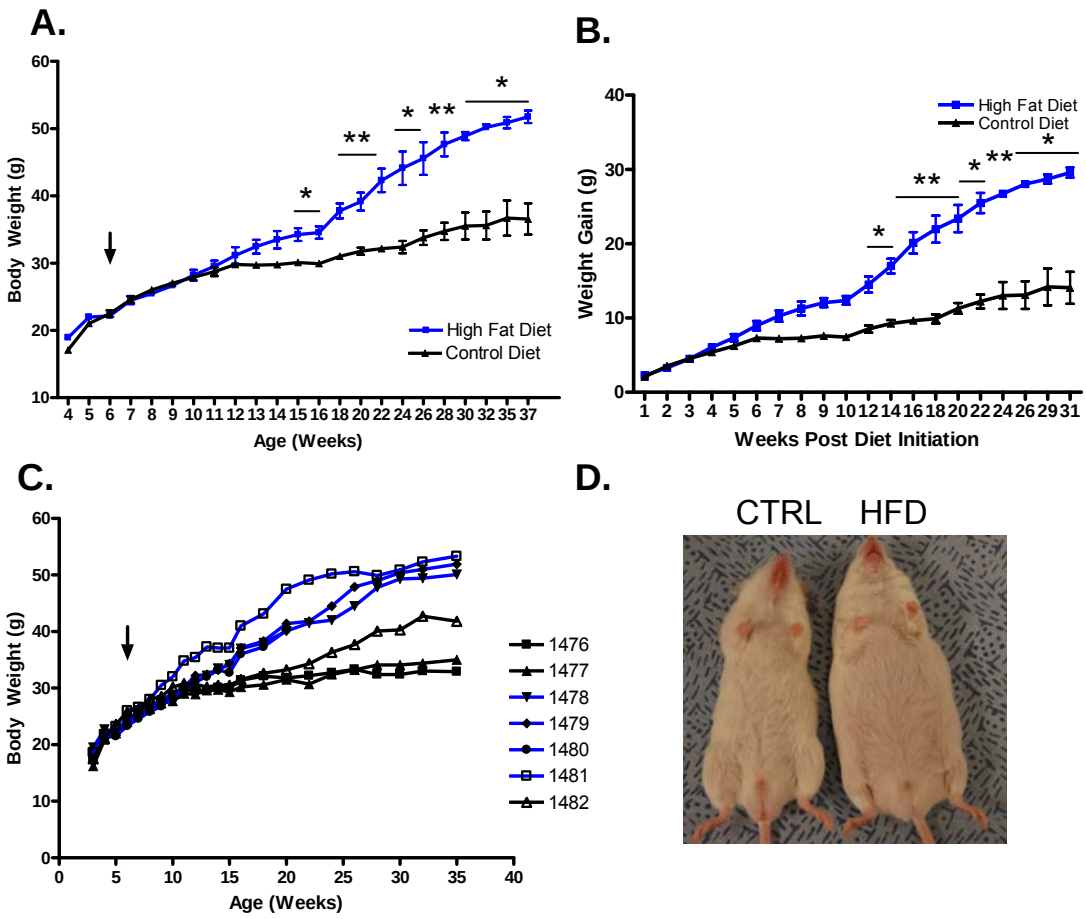

Figure 6.2: Diet induced obesity in B6-Luc mice. (A) Body weights of B6-Luc mice fed either control diet or high fat diet ad libitum from 6 weeks of age. (B) Average weight gain of control fed and high fat fed mice during the study. High fat fed mice gained significantly more weight than control fed mice. (C) Individual weight gains of study cohorts. Blue lines represent mice fed a high fat diet. (D) Photo images of control fed (CTRL) and high fat fed (HFD) mice shows that HFD mice have significantly more abdominal fat than CTRL fed mice. Significant increases in photon flux relative to controls are denoted by asterisks; *$p<0.05$, **$p<0.01$

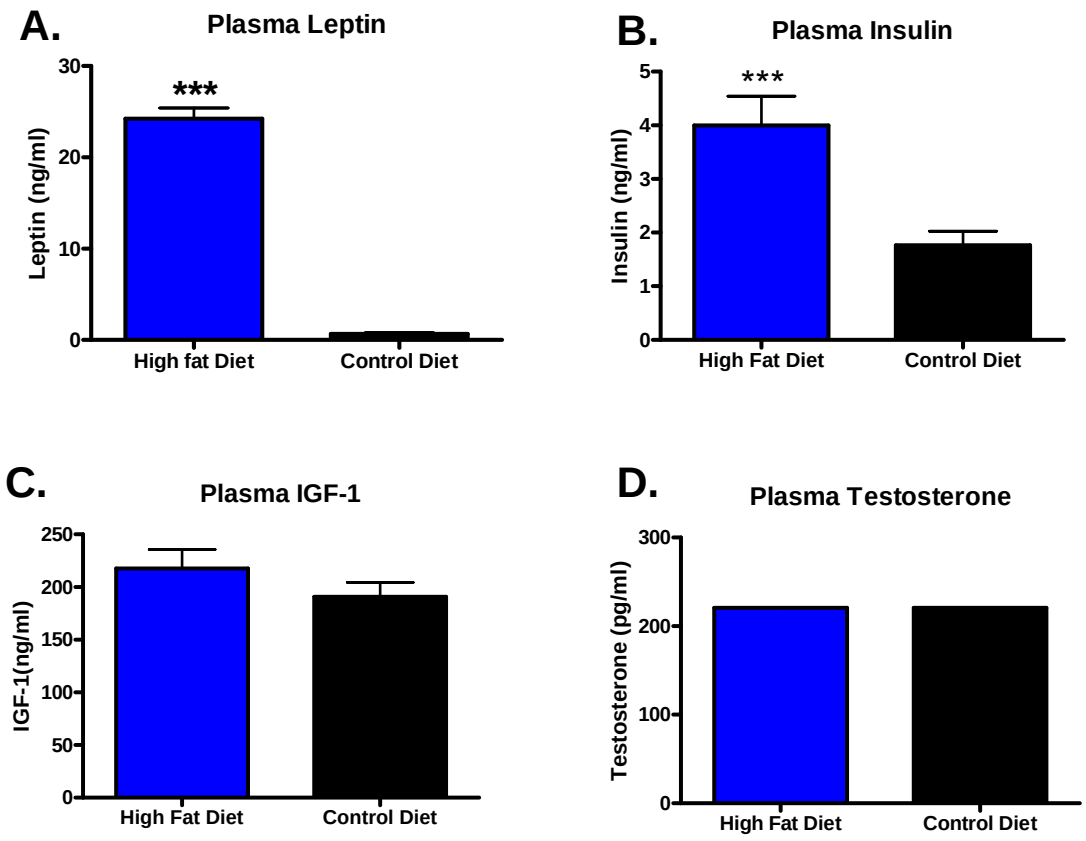

Figure 6.3: High fat diet increases plasma leptin and insulin levels in B6-Luc mice. ELISAs for leptin (A), Insulin (B), IGF-1 (C) and Testosterone (D) at 9 weeks post diet initiation. Plasma leptin and insulin are significantly increased in B6-Luc mice fed a high fat diet.

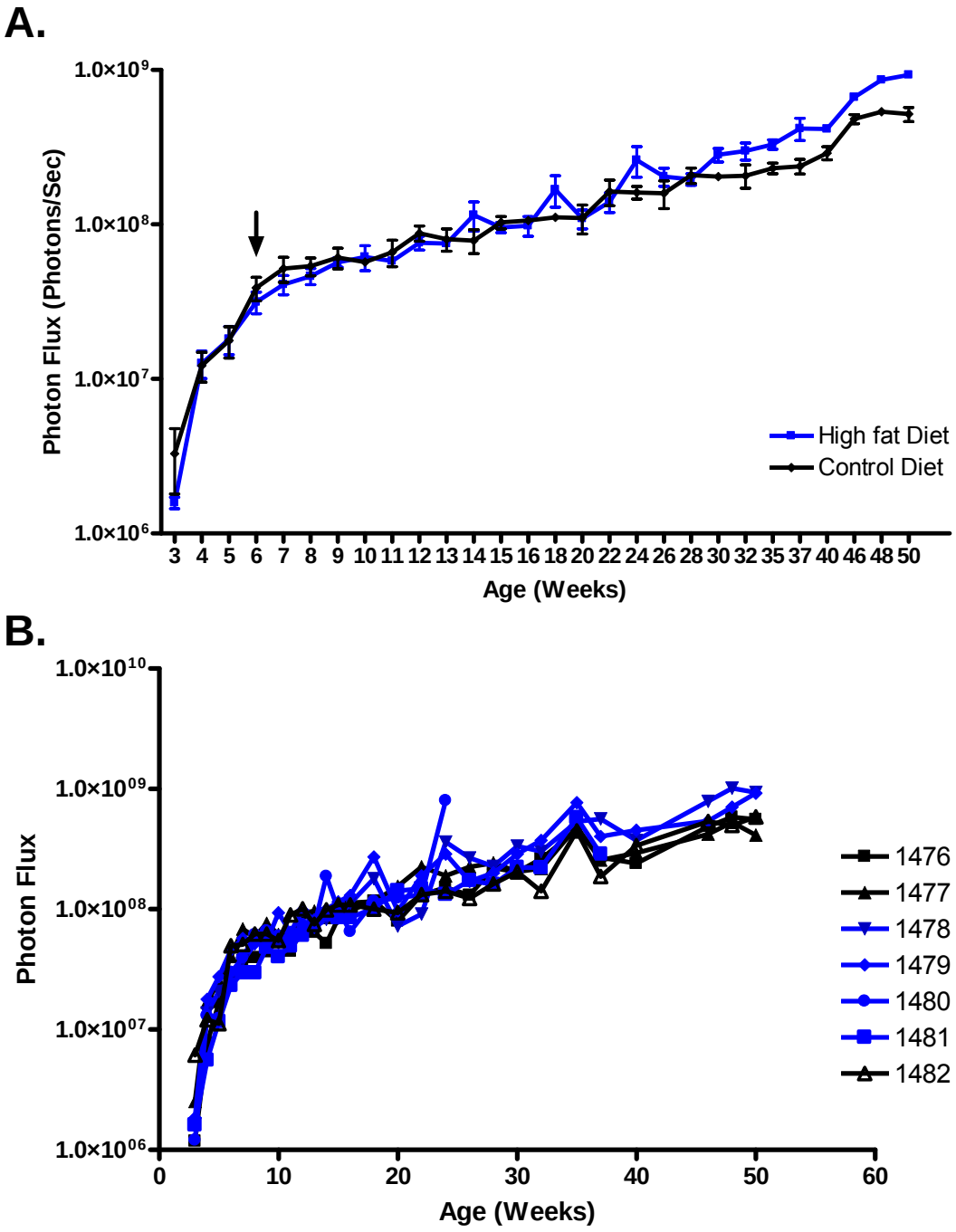

Figure 6.4: BLI of prostate cancer progression in high fat fed and control B6-Luc mice. (A) BLI quantification of prostate cancer progression in PTEN +/- B6-Luc mice fed either high fat diet or control diet. Bioluminescence intensity is not significantly different between study cohorts. (B) BLI quantification of individual animals reveals an increase in a single animal (#1480) fed a high fat diet at 24 weeks.

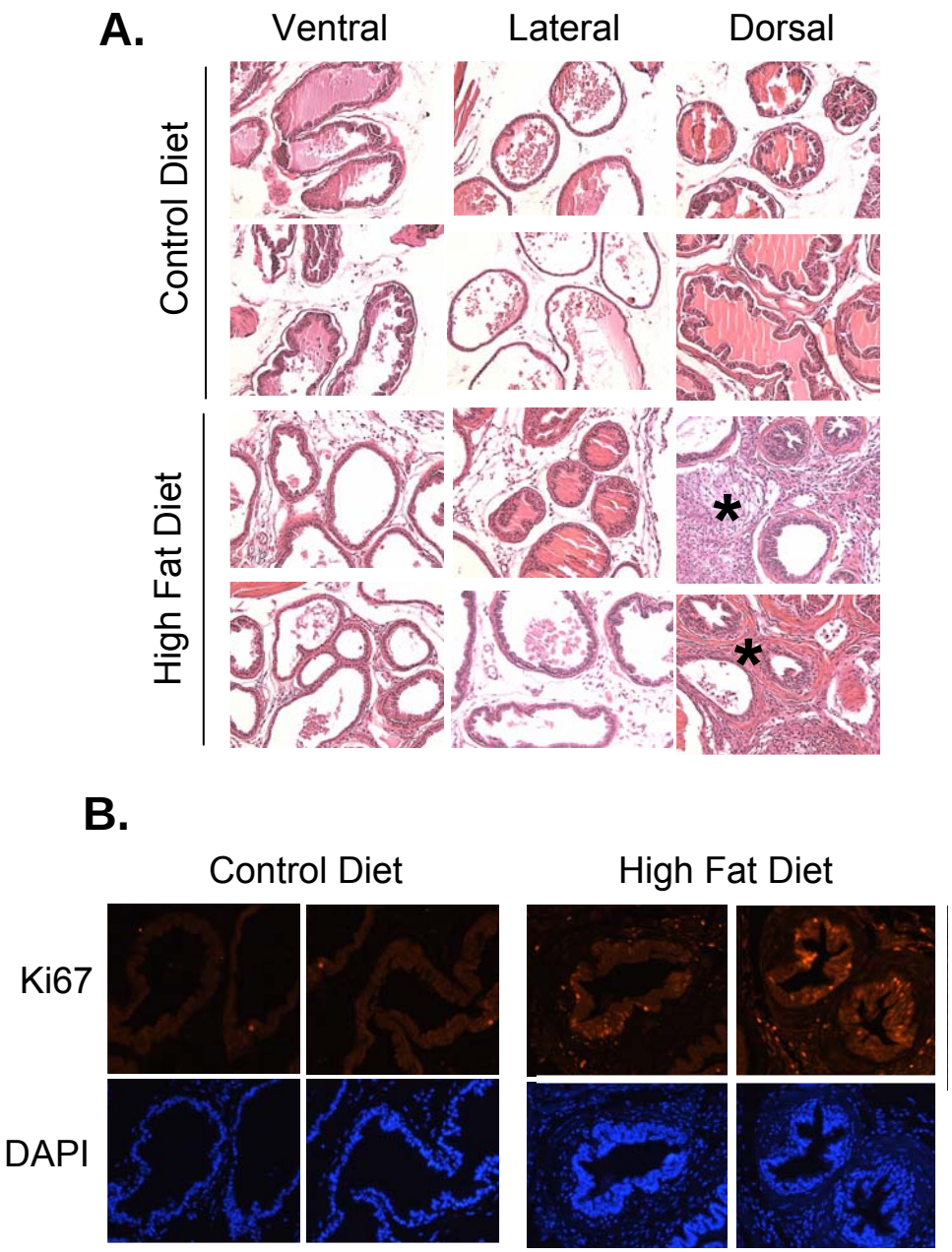

Figure 6.5: Increased stromal response and epithelial cell proliferation in high fat fed mouse #1480. (A) H&E staining of prostates fom a control fed and high fat fed B6-Luc mouse. High fat diet induced an increased stromal response in the dorsal lobes (asterix). A milder stromal response was also detected in the ventral lobes. (B) IF for Ki67 in dorsal lobes of the same control fed and high fat fed mice. High fat diet induced an increase in proliferation in the dorsal lobes as evidenced by increased Ki67 expression.

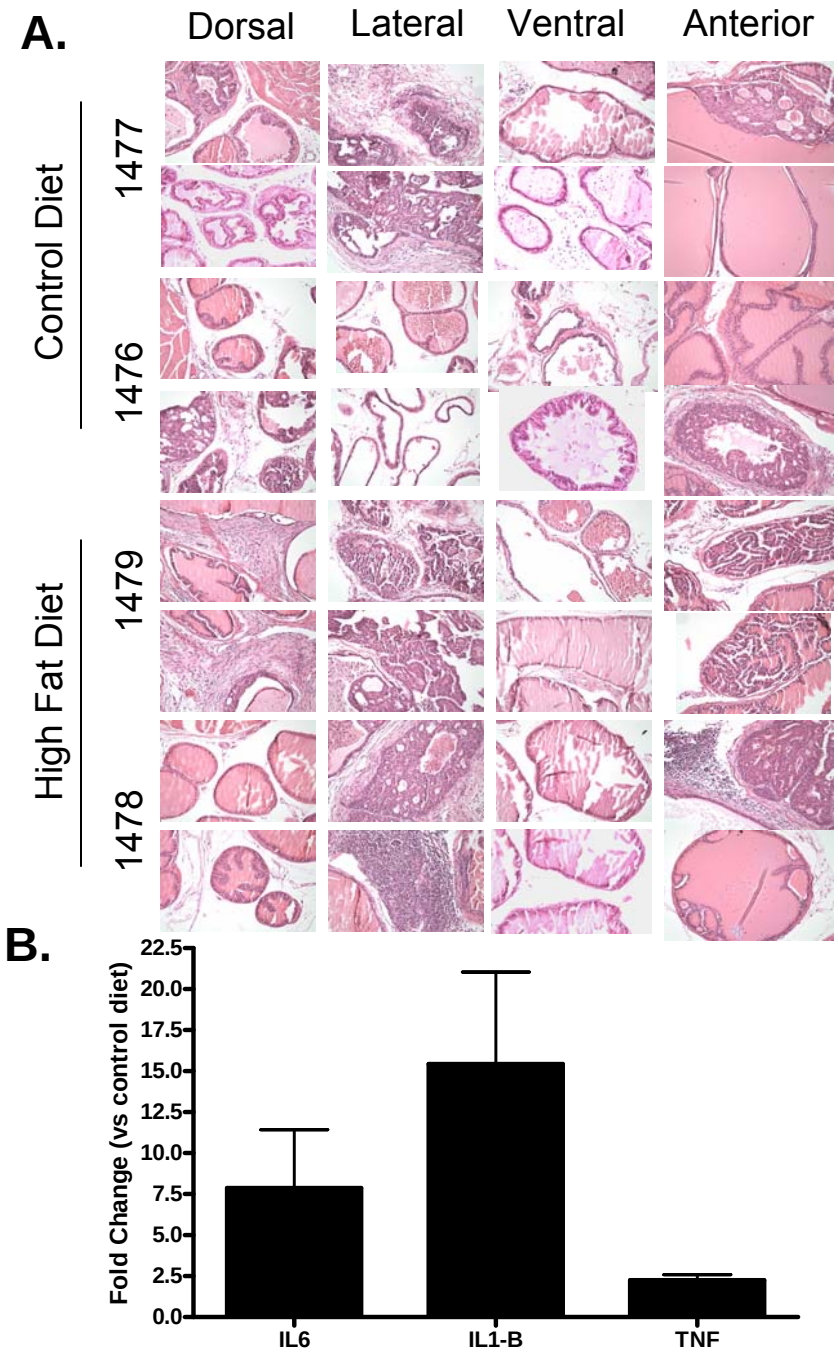

Figure 6.6: Increased expression of IL-6 and IL-1β in diet induced obesity. (A) H&E staining of prostates from control fed and high fat fed B6-Luc mice at 12 months. Focal HGPIN is evident in control fed and high fat fed mice. Diet induced obesity had no obvious effects on histological prostate cancer progression. (B) Quantitative RT-PCR for IL-6, IL-1β and TNF in control fed vs. high fat fed B6-Luc mice represented as fold change over control diet. Diet induced obesity increases the levels of IL-6 and IL-1β mRNA in prostates of B6-Luc mice.

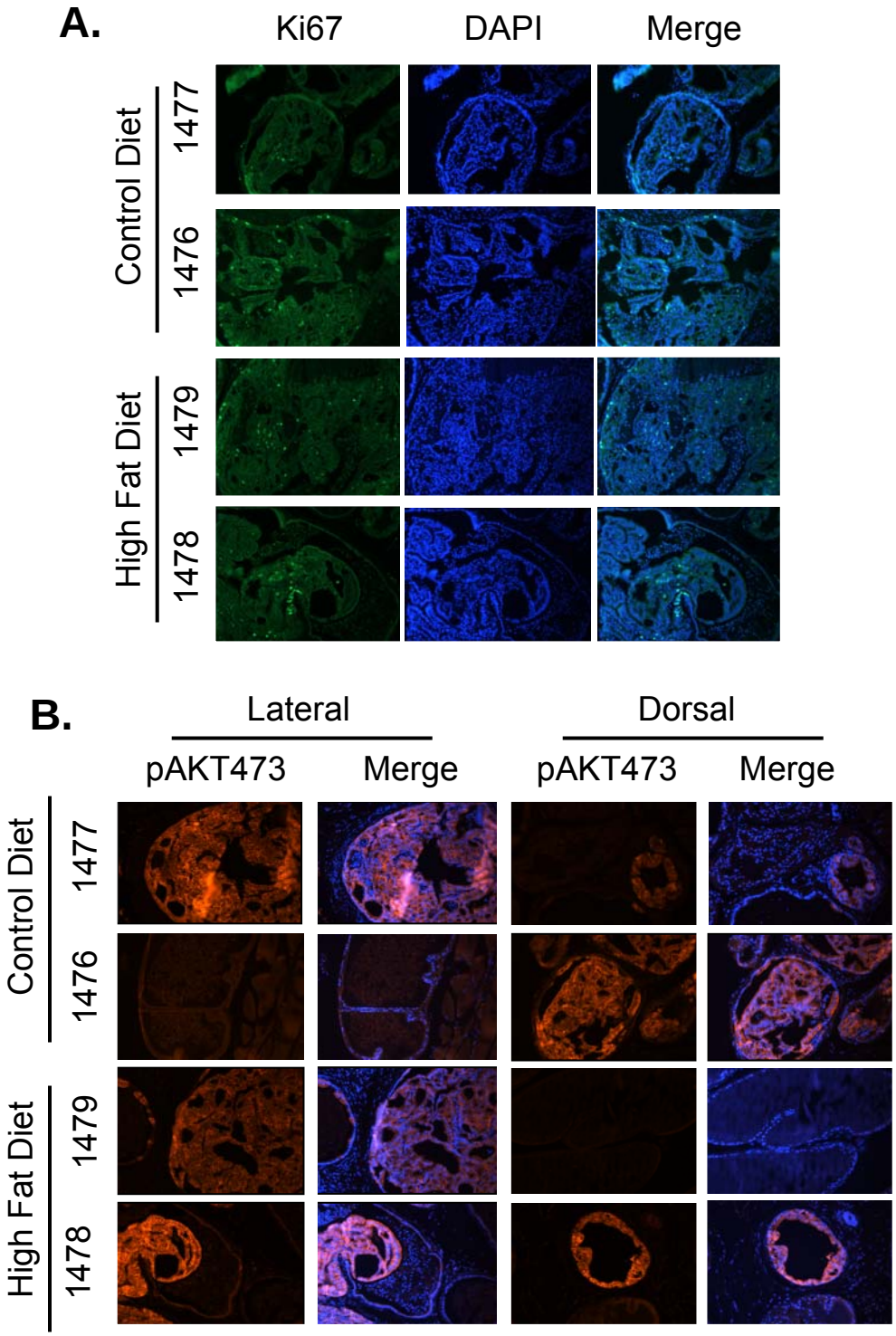

Figure 6.7: No differences in Ki67 or pAKT473 expression in diet induced obesity. (A) IF for Ki67 in prostates of control fed and high fat fed mice at 12 months. Ki67 expression levels are similar between the treatment groups. (B) pAKT473 expression in the same study cohorts. pAKT473 expression was confined to the areas of HGPIN and was not different between the treatment groups.

CHAPTER VII

SUMMARY AND FUTURE DIRECTIONS

My thesis projects were quite diverse and spanned both ends of the prostate cancer spectrum; from progression of the disease, to therapy for advanced cancer. We began by investigating the efficacy of siRNA mediated inhibition of the AR for advanced prostate cancer. siRNA therapeutics represent an exciting new class of drugs with the potential to overcome many existing problems associated with traditional chemotherapeutic approaches. We developed a panel of siRNAs targeting the AR and chemically modified the most potent ones to enhance their pharmacokinetic and pharmacodynamic properties in *vivo*. Although we utilized modified siRNAs with phosphothiorate backbones and 2'OMe nucleotides to improve nuclease resistance, we did not examine these specific properties. To determine this we could simply examine their degradation in the presence of nucleases *in vitro*. Furthermore, we did not examine whether the *in vivo* administered siRNAs induced an interferon response in host animals. To address this concern we could simply isolate blood from injected study cohorts and assess the levels of IL-12 and IFN-γ via an ELISA. We were able to demonstrate that AR inhibition in cell culture caused an induction of apoptosis and loss of cell viability, providing a proof of concept of AR targeted therapy. However, recent studies have identified that inhibiting AR expression via siRNAs induces PI3K activation of AKT and anti-apoptotic signaling which is mediated by calcium/calmodulin dependent kinase II (CAMKII) (Rokhlin, Taghiyev et al. 2007). This may represent an important mechanism by which prostate cancer cells are able to escape apoptosis after inhibition of the AR. Obviously this presents a problem for AR targeted siRNA therapy and warrants a re-evaluation of AR therapies for prostate cancer. To circumvent this problem it may be desirable to use a dual therapy where both AR and CAMKII are effectively inhibited. A

combination therapy of AR siRNAs and CAMKII inhibitors, such as KN-93, might provide a more powerful means to target AIPC. However, KN-93 was recently shown to mediate reduction in L type calcium channels and was also responsible for generating ROS (Rokhlin, Guseva et al.). The development of other more specific CAMKII inhibitors may demonstrate the efficacy of CAMKII inhibition in prostate cancers.

We were only able to demonstrate efficacy of liposomal siRNAs in the absence of any transfection reagents. Previous studies have demonstrated the need for cellular receptors and extracellular chaperone proteins for cholesterol and atelocollagen particle uptake (Wolfrum, Shi et al. 2007). We did not examine whether the prostate cancer cells used in this study expressed either the LDL or HDL receptor or collagen receptors. The fact that neither cholesterol nor atelocollagen were able to enter prostate cancer cells *in vitro* was a major hindrance to their efficacy *in vivo*. If we were able to demonstrate efficacy of cholesterol uptake in prostate cancer cells we may be able to enhance the process by starving the cells of endogenous cholesterol to the point where they would need to receive it from their extracellular environment. This could be accomplished by using one of the statins, a very well characterized class of drugs commonly used to lower cholesterol levels in human patients. Mevastatin is well tolerated *in vivo* with well profiled pharmacokinetic and pharmacodynamic properties making it feasible to treat mice, which have been implanted with prostate carcinoma cells, with this drug to facilitate the inhibition of endogenous cholesterol production and uptake of cholesterol from the serum.

Despite the fact that liposomal siRNAs were effective *in vitro*, they failed to inhibit tumor growth and improve survival in our pre clinical animal model of prostate cancer. These data highlight delivery of liposomal siRNAs as the main hurdle to its success. Liposomes are one the most well studied siRNA delivery systems for liver delivery and have been utilized in mice and non human primates (Love, Mahon et al.; Zimmermann, Lee et al. 2006; Svensson, Shey et al. 2008). The synthesis and screening

of novel lipidoid materials has led to the identification of a number of liposomal siRNA delivery vehicles (Semple, Akinc et al.). Furthermore, various formulation parameters have been optimized to maximize efficiency and minimize toxicity *in vivo* (Akinc, Goldberg et al. 2009). Improved liposomal formulations were found to dramatically enhance liver specific silencing of multiple target genes in multiple species providing proof of concept validation of liposomal siRNA therapy for liver disorders. In our study, it is unclear whether liposomal AR-siRNAs were effective at inhibiting liver specific tumor growth in our animal model. To address this it would be feasible to direct tumor growth to the liver by injecting the spleens of mice with prostate carcinoma cells. Injecting spleens will distribute the cells into the hepatic portal vein which drains to the liver. Prostate cancer cells would then invade the liver and form tumors similar to metastatic lesions. Mice could then be treated with Lipo si-AR and their efficacy of liver specific tumor inhibition could be easily assessed in an identical manner to our study. Such a study would provide a proof of concept and strengthen the pre clinical development of liposomal siRNAs for liver cancers.

We have also documented a problem with using BLI to monitor response to therapy in our animal model. We have shown that cells expressing CMV driven luciferase exhibit increases in bioluminescence intensity as they are undergoing apoptosis and losing viability. Therefore, any potential effects of systemically delivered AR siRNAs might be masked by bioluminescence, our primary readout of tumor response. However, we have shown that the induction of bioluminescence is transient. Furthermore, we are able to assess survival of treated mice at our endpoint analysis, circumventing some of the problems associated with this assay.

Clearly the main hurdle to efficacy of therapy in this study was delivery and uptake of the siRNAs to tumors at disseminated sites. The formulations that were used in this study were not designed to target any specific cell types or tumor antigens, thus making them suboptimal for such a study. Prostate cancer cells express a number of cell

surface markers that are attractive for siRNA targeting. Furthermore, it would be beneficial to use a targeting molecule that is preferentially taken up by prostate cancer cells. One such molecule is testosterone. As discussed earlier, prostate cancers require testosterone and even though late stage AIPC cancers do not, they are still able to take it up from the extracellular environment. Thus, an attractive approach to systemic siRNA therapy would be to conjugate siRNA duplexes to a testosterone molecule. Furthermore, the testosterone molecule could be rendered inactive; circumventing the problems associated with systemic testosterone injections.

To examine additional properties of systemically delivered siRNAs, we developed FLASH mice in an attempt to further assess siRNA biodistribution and pharmacodynamics. We chose to specifically focus on the liposomal siRNA formulation because it had shown most promise in our earlier studies. We demonstrated that FLASH mice could be successfully used in a facile screen to assess the tissue distribution and potency of systemically delivered liposomal siRNAs. A single bolus injection of si-Luc was able to significantly reduce luciferase expression in the livers of FLASH mice for 14 days. Si-Luc was not able to significantly reduce luciferase expression in any other tissues that we examined, demonstrating the therapeutic potential for liposomal siRNAs for liver disorders. The liver is an important organ with a number of potential therapeutic targets and efforts are currently focused on developing liposomal siRNA based therapies for a number of these including hypercholesteremia and liver cancers. We were initially interested to determine whether we could monitor efficacy of si-Luc non invasively over time in FLASH mice. However, the ubiquitous and strong levels of luciferase expression masked any reduction in luciferase expression from the livers of mice treated with si-Luc. Therefore, the optimal method of visualizing si-Luc efficacy was through the use of an *in vitro* luciferase activity assay which we developed. However, it would be possible to generate mice that only had liver specific luciferase expression. This could be accomplished easily in our mice through the injection of an adenovirus expressing cre

recombinase (Ad-cre) into FLASH mice that are negative for the Pbcre transgene. An intravenous tail vein injection of Ad-cre would be expected to direct cre recombinase expression primarily to the liver. Provided that cre expression in the liver was constant and uniform, mice could then be administered with si-Luc and imaged non invasively for liver specific bioluminescence intensity.

As mentioned earlier, we have shown that cells expressing CMV driven luciferase exhibit increases in bioluminescence intensity as they are undergoing apoptosis and losing viability. We decided to characterize this further. We found that treatment of cancer cell lines expressing luciferase under control of the CMV promoter with apoptosis inducing agents resulted in a transient increase in bioluminescence which was positively correlated with apoptosis and inversely correlated with cell viability. In contrast, similar treatment of cell lines expressing luciferase under control of the SV40 promoter did not exhibit this result. Additionally, we found that low doses of staurosporine induced bioluminescence in CMV- but not SV40-driven luciferase cell lines, while high doses elicited induction in both; indicating promoter-dependent and –independent mechanisms of bioluminescence induction. The promoter-dependent increase in bioluminescence intensity from CMV-driven luciferase was a result of induction of luciferase mRNA and protein expression that was dependent on the p38MAPK pathway. Inhibiting the p38MAPK pathway blocked the bioluminescence induction by apoptosis inducing agents. It is still unclear why high doses of staurosporine were able to induce bioluminescence in SV40 cell lines. There are a number of potential explanations for this result. Staurosporine treatment of cell lines might increase the intracellular levels of ATP and/or O2, both of which are essential rate limiting components of the light generating reaction. Alternatively, luciferin delivery to the cell lines might be altered by treatment. Recent data suggests that luciferin uptake within cells is modulated by expression of the ATP binding cassette (ABC) family transporter ABCG2/BCRP (Zhang, Bressler et al. 2007). Therefore, STS treatment may effect ABCG2/BCRP expression which in turn will

influence the bioluminescent light generating reaction and the resultant signal. Our study also raises another interesting question. How accurate are the data from studies that have utilized BLI in transgenic animal models? *In vivo*, many different promoters, from tissue specific to ubiquitous, have been used to drive luciferase expression (Lyons, Lim et al. 2006; Svensson, Shey et al. 2008). It seems logical that endogenous promoters are both positively and negatively regulated by a number of factors that could be potentially altered due to drug treatments or other events. Indeed, this has been the basis for many studies that have used luciferase expression as a readout of cellular processes, ranging from apoptosis to cytokine signaling (Carlsen, Moskaug et al. 2002; Laxman, Hall et al. 2002). Our studies highlight the need for important controls and consideration into how processes extrinsic to the bioluminescent reaction might affect the signal generated.

The second part of my thesis centered on the progression of prostate cancer. We began by developing and characterizing a novel mouse model of prostate cancer that was based on the prostate specific *Pten* mutant previously characterized (Wang, Gao et al. 2003). While we are not the first to develop a spontaneous model of prostate cancer that utilizes BLI, we believe that our model offers several advantages over those previously described. 1) Sensitivity: The white coat color in our model increases the sensitivity of bioluminescence compared to darker coat colors (Troy, Jekic-McMullen et al. 2004). Additionally, *ROSA26* is a popular promoter for driving high level protein expression in animals (Soriano 1999; Safran, Kim et al. 2006); 2) Specificity: expression of luciferase derives from the endogenous *ROSA26* promoter as opposed to a transgene and is coupled to *Pten* inactivation in the same cell; 3) Biological relevance: *Pten* is frequently mutated in human prostate cancers and the *Pten* conditional mutant was previously characterized to recapitulate many aspects of human prostate cancer. 4) Tumor kinetics: We extensively backcrossed our model onto both C57BL6 and BALB/c backgrounds which should reduce variability in tumor formation between individual animals.

In B6-Luc mice we demonstrated that bioluminescence was tightly correlated to the proliferative capacity of the prostatic epithelial cells. In *Pten* $^{-/-}$ B6-Luc mice, bioluminescence increase was rapid from 3-11 weeks. However, from 11 weeks onward, bioluminescence intensity did not significantly increase and was correlated with low Ki67 levels. The bioluminescence kinetics were identical in both strains of mice used in this study. These data suggest that prostate cancer growth in this model is slow. We performed SA βGal staining to assess whether the senescence response induced in a previous *Pten* mutant was evident in our model. We did not detect any senescent positive cells using this assay. However, we were unable to use a positive tissue control lending to the possibility that either the assay was not performed correctly or the reagents were bad. However, previous studies utilizing prostate specific *Pten* mutant mice have not documented the induction of a senescence response either (Mulholland, Xin et al. 2009). Interestingly, many studies have been performed in these particular mice and none have reported the slow growing phenotype that we observe in this model. Furthermore, tumor growth and response to therapy using ultrasound has been described in *Pten* $^{-/-}$ mice (Zhang, Zhu et al. 2009). It is possible that the BLI aspect of our model offers us the first opportunity to visualize the true biology of *Pten* $^{-/-}$ prostate cancer in this context. To confirm that prostate tumors were not growing throughout the longitudinal time course we weighed the individual lobes of *Pten* $^{-/-}$ and *Pten* $^{+/+}$ at various timepoints. The majority of prostatic weight gain came from the anterior lobes as a result of severe fluid build up over time. Although the dorsal, lateral and ventral lobes did increase in weight, a large part of this is attributed to increases in the stromal compartment as individual ducts become 'glued' together in older animals. There is the possibility, however unlikely, that the bioluminescence intensity is an artifact of *Pten* deletion. We have not assessed whether a *Pten* $^{-/-}$ epithelial cell is expressing identical amounts of luciferase as a *Pten* $^{+/+}$ cell. Furthermore, and as discussed previously, it is possible that other factors extrinsic to the light generating reaction are affected in a *Pten* dependent manner. We are currently

attempting to perform laser capture micro-dissection of epithelial cells to determine the level of luciferase mRNA in said cell types. Furthermore, we can isolate MEFS from *Pten* fl/fl and *Pten* wt/wt animals, infect them with cre and then examine the effects on bioluminescence intensity to address our concerns. However, the fact that bioluminescence correlated with Ki67 levels and the fact that we can monitor response to therapy with both castration and rapamycin treatment suggests that the bioluminescence model is performing as expected. Therefore, these data raise a very interesting question. Why do the epithelial cells fail to proliferate at later timepoints? The answer to this question might shed some light as to why most human prostate cancers develop at a vary slow rate. Therefore, *Pten* $^{-/-}$ B6-Luc mice might possess key features of indolent human prostate cancers and at the same time will offer insight into a mechanistic basis. We are currently interested in the role of the stromal compartment during prostate cancer progression. Previous studies have identified a critical role for stromatogenesis to support the progression of many cancers (Cunha, Hayward et al. 2003). Recent studies have shown an important role for matrix stiffening to support the neoplastic progression of breast cancers (Paszek, Zahir et al. 2005; Levental, Yu et al. 2009). Matrix stiffening, from integrin clustering and collagen crosslinking, induces focal adhesions and activates Rac, Rho and ERK dependent signaling cascades to facilitate tumor growth and invasion. However, it is possible the matrix stiffening may also be detrimental to tumor growth. A highly stiff matrix might antagonize tumor growth by assembly of multiple stable focal adhesions resulting in encapsulated tumors that never become invasive. We noticed that prostate glands of *Pten* $^{-/-}$ B6-Luc mice were well encapsulated. Although epithelial cells would often fill the lumens we did not observe any evidence of local invasion. Furthermore, we noticed an increase in collagen deposition over time in *Pten* $^{-/-}$ prostates, as evidenced by Massons trichrome staining. We hypothesize a space filling model, in *Pten* $^{-/-}$ B6-Luc mice, where the epithelial cells are able to fill the luminal space but are constrained from additional growth and invasion due to exogenous forces from stromal

matrix stiffening. To begin to assess this we will analyze epithelial cell number (DAPI positive nuclei) and basement membrane perimeter measurements in *Pten* $^{-/-}$ and *Pten* $^{+/+}$ prostates and express them as a ratio. We expect that basement membrane measurements should remain similar between *Pten* $^{-/-}$ and *Pten* $^{+/+}$ mice, cell number however should be significantly increased in *Pten* $^{-/-}$ prostates. This will provide initial evidence that cells are able to fill the lumens but are not able to overcome the space constraint and expand the ducts. Future experiments would then be aimed at manipulating matrix stiffness in an attempt to alter prostate cancer progression, from growth to invasion. Matrix stiffness is one potential explanation for the phenotype observed in B6-Luc mice. Another might by the second hit hypothesis which states that additional genetic alterations that favor tumor growth are required for cancer progression. The *Pten* $^{-/-}$ mouse has been used in conjunction with other mutants to assess whether second mutations are able to accelerate disease. For example, Nkx3.1 null mice and p53 null mice were combined with *Pten* $^{-/-}$ mice and found to accelerate disease progression. In this context, it would be interesting to induce such mutations in B6-Luc mice to assess the effects on tumor growth via BLI. We would expect that tumor growth should be accelerated which will be correlated to greater increases in bioluminescence intensity. It would also be interesting to see whether bioluminescence values still plateau, or whether tumors just continued to grow exponentially.

We have shown that *Pten* $^{-/-}$ B6-Luc prostates display an increased inflammatory response that is characterized by MDSC infiltration. This is the first report that has described the recruitment of MDSCs in a spontaneous model of prostate cancer. MDSCs comprised the majority of CD45+ cells. Interestingly, we did not see significant increases in CD8+ T cell infiltration in *Pten* $^{-/-}$ prostates compared to *Pten* $^{+/+}$. This may be related to MDSC recruitment, because MDSCs possess T cell suppressive functions through a variety of mechanisms (Gabrilovich and Nagaraj 2009). Future studies are aimed at assessing the functionality of recruited MDSCs. This could be accomplished by

measuring the expression levels of iNOS and arginase by qRT-PCR, two important suppressors of T cell activity. We would compare prostate specifc iNOS and arginase expression to those of the spleen to validate that only infiltrating MDSCs in the prostate are functional. Additionally we could perform a T cell suppression assay where we would isolate prostate specific MDSCs and examine their ability to inhibit T cell activity in a cytotoxic T lymphocyte assay *in vitro*. Additionally, it would also be interesting to augment the endogenous antitumor immunity of *Pten* $^{-/-}$ prostates by inhibiting the suppressive functions of MDSCs. This could be accomplished through the use of phosphodiesterase 5 (PDE5) inhibitors which have been shown to down regulate arginase 1 and NOS2, thereby reducing the suppressive machinery of MDSCs (Serafini, Meckel et al. 2006). We could simply treat *Pten* $^{-/-}$ B6-Lu mice with PDE5 inhibitors such as sildenafil and tadalafil and monitor the effects of progression using via BLI.

To further assess the role of inflammation on prostate cancer progression we aim to utilize a mouse model of prostatitis in conjunction with B6-Luc mice. Prostate ovalbumin transgenic mice (POET), developed by Tim Ratliff (University of Purdue), are a mouse strain in which a robust prostatic inflammatory response can be induced by the adoptive transfer of ovalbumin specific T cells. We aim to cross POET mice to B6-Luc mice, induce prostatic inflammation and assess its effects on prostate cancer progression. Interestingly, in the induced POET-3 *Pten* +/- mice, a large number of MDSCs accumulate in the prostates (Figure 7.1). Furthermore, in some preliminary studies, we induced inflammation in POET-3 *Pten* $^{+/-}$ B6-Luc animals and noticed a robust inflammatory response that results in loss of tissue architecture and proliferation of the prostatic epithelium in anterior and dorsal lobes (Figure 7.2). We did not see any pathological changes in induced POET-3 *Pten* $^{+/+}$ mice. Future studies are aimed at assessing the effects of chronic inflammation in *Pten* $^{-/-}$ and *Pten* $^{+/-}$ B6-Luc mice.

We have also demonstrated the utility of B6-Luc mice as a preclinical model for prostate cancer therapy. *Pten* $^{-/-}$ B6-Luc mice responded transiently to rapamycin

treatment, as evidenced by reductions in bioluminescence and pS6 expression. Interestingly, when mice were taken off treatment, bioluminescence intensity increased back to the exact levels of the control treated mice. These data are further support for our space filling hypothesis which states that once the ducts get filled with epithelial cells they become space constrained and static. Rapamycin is able to inhibit the growth of a number of epithelial cells during the treatment period, however once they are relieved of this inhibition, the cells are able to repopulate and fill the ducts. We also described the development of rapamycin resistance in B6-Luc mice. Continuous treatment with rapamycin resulted in a slow but steady increase in bioluminescence intensity over time. Although pS6 expression was reduced by rapamycin treatment, pAKT743 expression was not. These data indicate an important role of mTORC2 in prostate cancer and demonstrate that rapamycin, in this treatment setting, is unable to inhibit the functions of mTORC2. The limited effectiveness of rapamycin can be explained by its biochemical mechanism. Rapamycin acts through an allosteric mechanism that requires binding to its intracellular receptor, FKBP12, for inhibition of mTORC1 (Choi, Chen et al. 1996). However, this does not block all the functions of mTORC1. Furthermore, mTORC1 negative feedback can enhance PI3K-AKT activity, contributing to rapamycin resistance (Carracedo, Ma et al. 2008; Carracedo and Pandolfi 2008). To further explore the therapeutic potential of targeting mTOR in cancer a strong interest exists in trying to develop selective dual kinase inhibitors of mTORC1 and mTORC2 (Yu, Shi et al.; Feldman, Apsel et al. 2009; Garcia-Martinez, Moran et al. 2009; Yu, Toral-Barza et al. 2009). Some of these TOR kinase inhibitors have proven to be substantially more effective than rapamycin and are able to target the rapamycin resistance outputs of mTORC1 and mTORC2 (Feldman, Apsel et al. 2009). We are interested in assessing the efficacy of dual TOR kinase inhibitors in B6-Luc mice which will facilitate their pharmacodynamic assessment. Furthermore, the lack of available biologically relevant animal models is a huge hindrance to the successful general development of most

chemotherapeutic agents (Sharpless and Depinho 2006). Therefore, B6-Luc will be invaluable for testing many of the novel drugs targeted for prostate cancer.

The etiology of prostate cancer is complex. Relatively few established risk factors have been identified. We are interested in trying to determine some of the risk factors that might promote the progression of prostate cancers from indolent to life threatening. One recently identified risk factor in this context is obesity, which has been associated with prostate cancer mortality. We attempted to assess the effects of obesity on prostate cancer progression using B6-Luc mice heterozygous for *Pten* deletion (*Pten* $^{+/-}$). We chose *Pten* $^{+/-}$ mice because they develop focal HGPIN that never progresses to an adenocarcinoma. Therefore we wanted to examine whether diet induced obesity could enhance their cancer progression to a more aggressive phenotype. We demonstrate that obesity did not affect prostate cancer progression but induced an inflammatory response in the prostates which was characterized by increased expression of the pro-inflammatory cytokines IL-6 and IL1- β. Interestingly, IL-6 and IL1-β have been identified as the cytokines involved in inducing MDSC infiltration. Mice inoculated with tumor cells secreting either IL-1 β or IL-6 developed significantly higher levels of MDSC as compared with control mice (Song, Krelin et al. 2005; Bunt, Sinha et al. 2006; Bunt, Yang et al. 2007). Future studies are aimed at characterizing the obesity induced inflammatory phenotype by performing flow cytometry for a number of immune cell subsets. There are no previous studies linking obesity to enhanced MDSC production, making these studies novel and highly relevant. We are also assessing whether obesity can promote the progression of prostate cancer in *Pten* $^{-/-}$ B6-Luc mice (Figure 7.3). Thus far we have seen no significant increases in bioluminescence between high fat fed and control fed mice.

Obesity is a complex disease that is influenced by a number of factors (Weinsier, Hunter et al. 1998). Along with influence of diet on obesity, obesity also has a large genetic component (Farooqi and O'Rahilly 2006). There a number of genetic mouse models of obesity currently available. Naturally occurring mutants and genetically

modified mice have been used successfully to study obesity (Carroll, Voisey et al. 2004). An alternative to our study would be to create a genetic mouse model of obesity that spontaneously developed prostate cancer. Obesity models such as the obese mouse (ob/ob) or diabetic mouse (db/db) could be used in this context (Zhang, Proenca et al. 1994; Tartaglia, Dembski et al. 1995). We could simply cross ob/ob or db/db mice to B6-Luc mice to generate such a model. Disadvantages of such an approach primarily involve lack of leptin production or signaling in these models. However, alternative mechanisms that might contribute to prostate cancer could still be evaluated in a genetically defined and spontaneous model.

The mechanistic basis for obesity induced prostate cancer progression in humans is yet to be elucidated. I had previously described some of the prevailing hypotheses involving hormones such as testosterone, insulin and leptin. We became interested on the effects of leptin on prostate cancer due to the association of leptin and higher grade tumors and evidence that leptin acts as a mitogen *in vitro* (Onuma, Bub et al. 2003; Somasundar, Yu et al. 2003). We are currently attempting to determine the role of leptin in prostate cancer progression. We have determined that leptin receptor expression is evident at the mRNA level in both mouse and human prostate tissue (Figure 7.4). Leptin treatment of a panel of prostate cancer cells moderately accelerated growth of PC3 and BPH1 cells *in vitro* (Figure 7.4). Leptin may facilitate prostate cancer progression by exerting indirect effects on the tumor microenvironment. To study the effects of leptin on prostate cancer progression *in vivo* we constructed an adeno-associated virus (AAV) that expresses murine leptin from the human alpha anti-trypsin promoter and apolipoprotein E enhancer (ApoEHAAT). We performed specific restriction digests to ensure that recombination of the ITRs had not occurred during the final cloning step (Figure 7.5A). We then transfected hepatocyte cells (HEPG2) with the FBGR-leptin construct to determine its efficiency *in vitro* (Figure 7.5B). FBGR-Leptin was then utilized for AAV8-Leptin construction at the University of Iowa Gene Therapy facility. Injection of

AAV8-Leptin into mice should direct leptin expression to liver hepatocytes. Stable integration of the AAV via the inverted terminal repeats (ITR) should facilitate constant leptin production *in vivo*. We injected mice with 10^12 vg of either AAV-Leptin or AAV-control and assessed plasma levels of leptin at various timepoints (Figure 7.5C). Although we were able to achieve increases in plasma leptin we did not achieve the desirable anticipated levels. Once we are able to optimize the dose for injection, we plan to assess the effects of elevated leptin production during the early stages of prostate cancer progression in B6-Luc mice.

In conclusion, we have examined multiple aspects of prostate cancer. We have developed an animal model that will aid in the general development of siRNA therapeutics. Additionally, we have developed an animal model of prostate cancer that will enable us to dissect the molecular basis for prostate cancer progression. Finally, B6-Luc mice will also aid in the general development and optimization of novel therapies for prostate cancer.

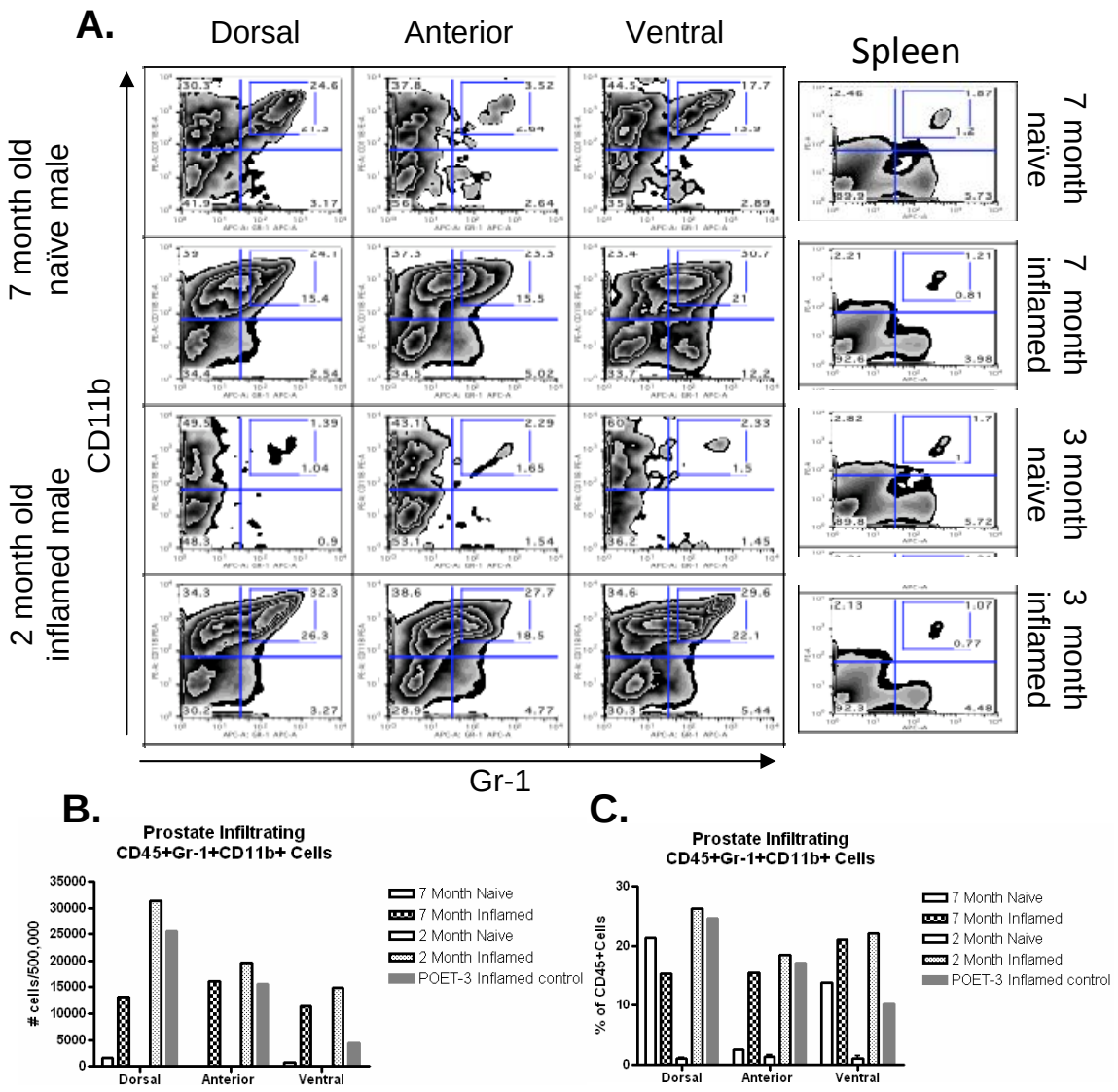

Figure 7.1: **Recruitment of MDSCs in prostates of aged POET-3 PTEN +/- mice & increased infiltration during acute prostatitis.** Prostates were harvested from 7 month old POET-3 PTEN +/-mice heterozygous for PTEN 6 days after adoptive transfer of pre-activated OT-I cells (inflamed) or naïve control mice and prostate lobes were stained for analysis of infiltrating MDSCs (CD45+ Gr-1+CD11b+ cells). (A) Flow cytometry plots gated on CD45+ cells. (B) Absolute number of MDSCs in prostate lobes. (C) Percentage of CD45+ cells that are MDSCs.

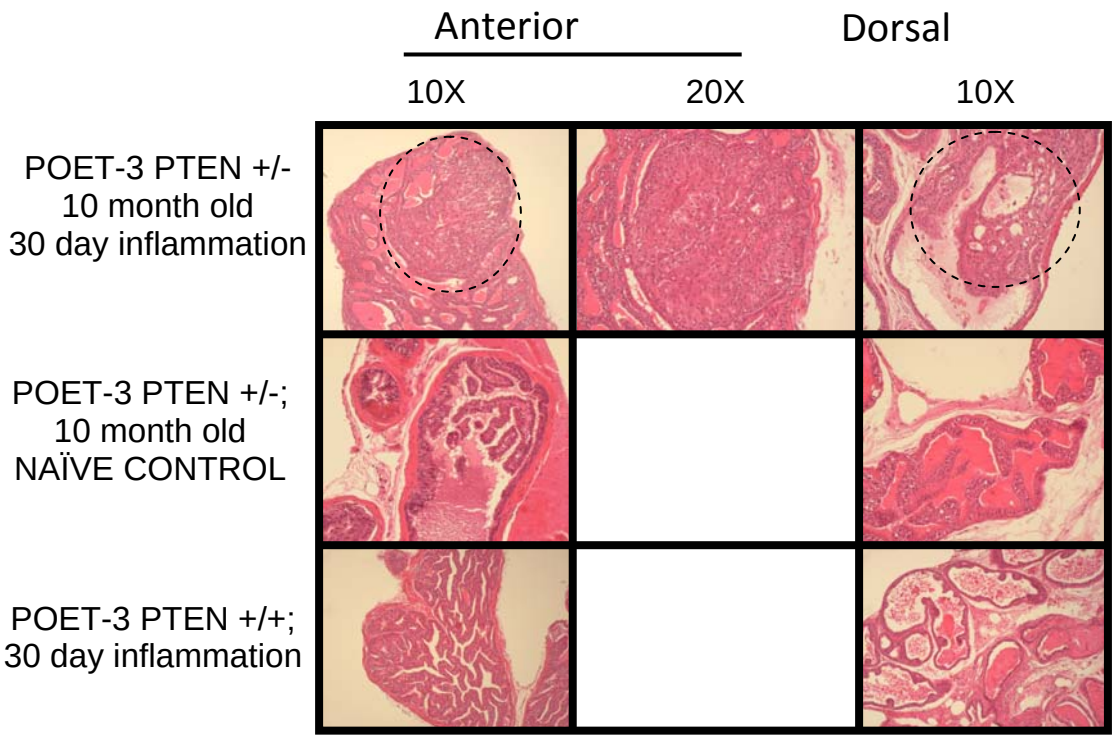

Figure 7.2: **Pathological changes in prostates of induced POET-3 PTEN +/- mice.** Prostates were harvested from 10 month old POET-3 PTEN +/- or PTEN +/+ mice 30 days after adoptive transfer of pre-activated OT-I cells (inflamed) or naïve control mice and analyzed for pathologic changes. 30 day inflammation in PTEN +/- mice induced epithelial cell proliferation and pathological changes in anterior and dorsal lobes (hashed circle). No pathologic changes were detected in 30 day inflamed PTEN +/+ mice.

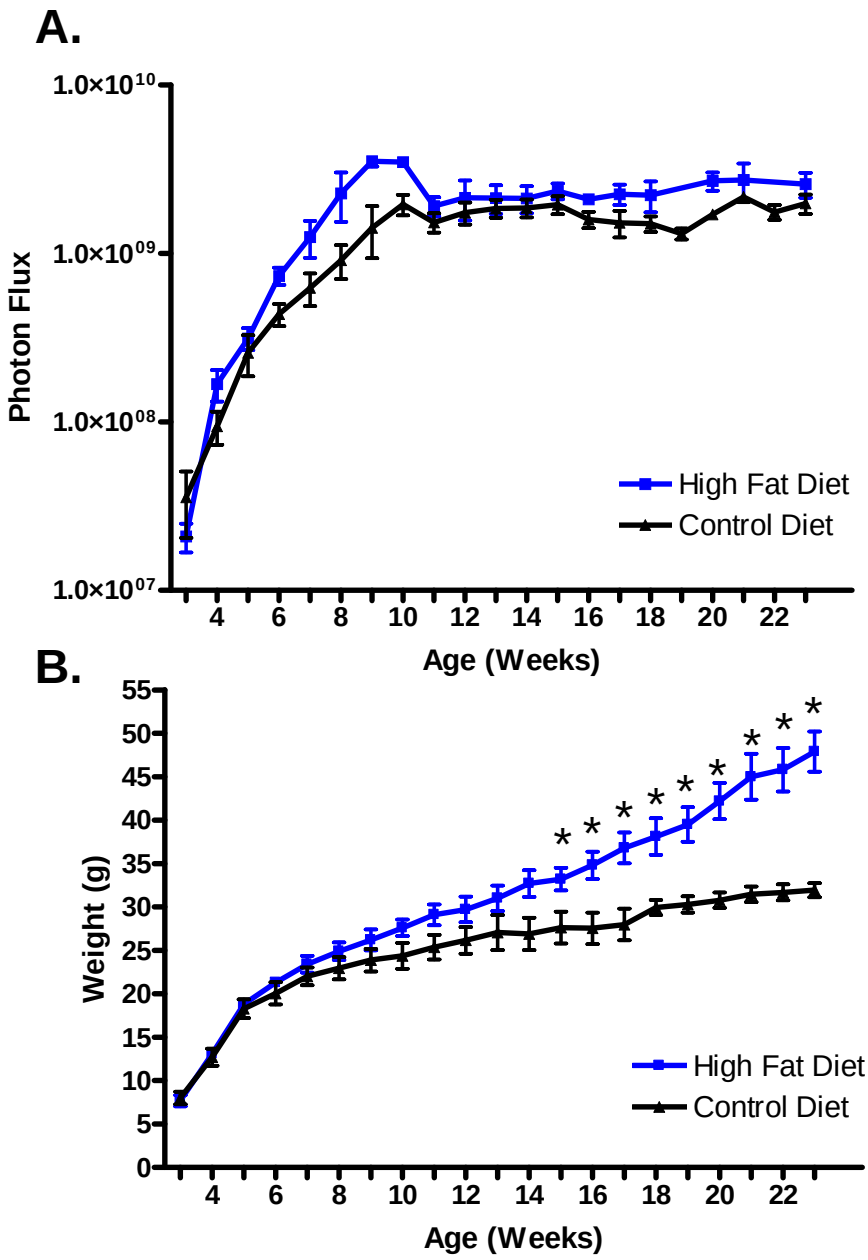

Figure 7.3: **BLI of prostate cancer progression during diet induced obesity in PTEN -/- B6-Luc animals.** (A) PTEN -/- mice were fed either control diet or high fat diet from weaning and imaged for prostate cancer progression. Diet induced obesity did not affect bioluminescence intensity. (B) Mice fed high fat diet gained significantly more weight than control fed mice. Significant differences in body weight denoted by asterisks; *p<0.05

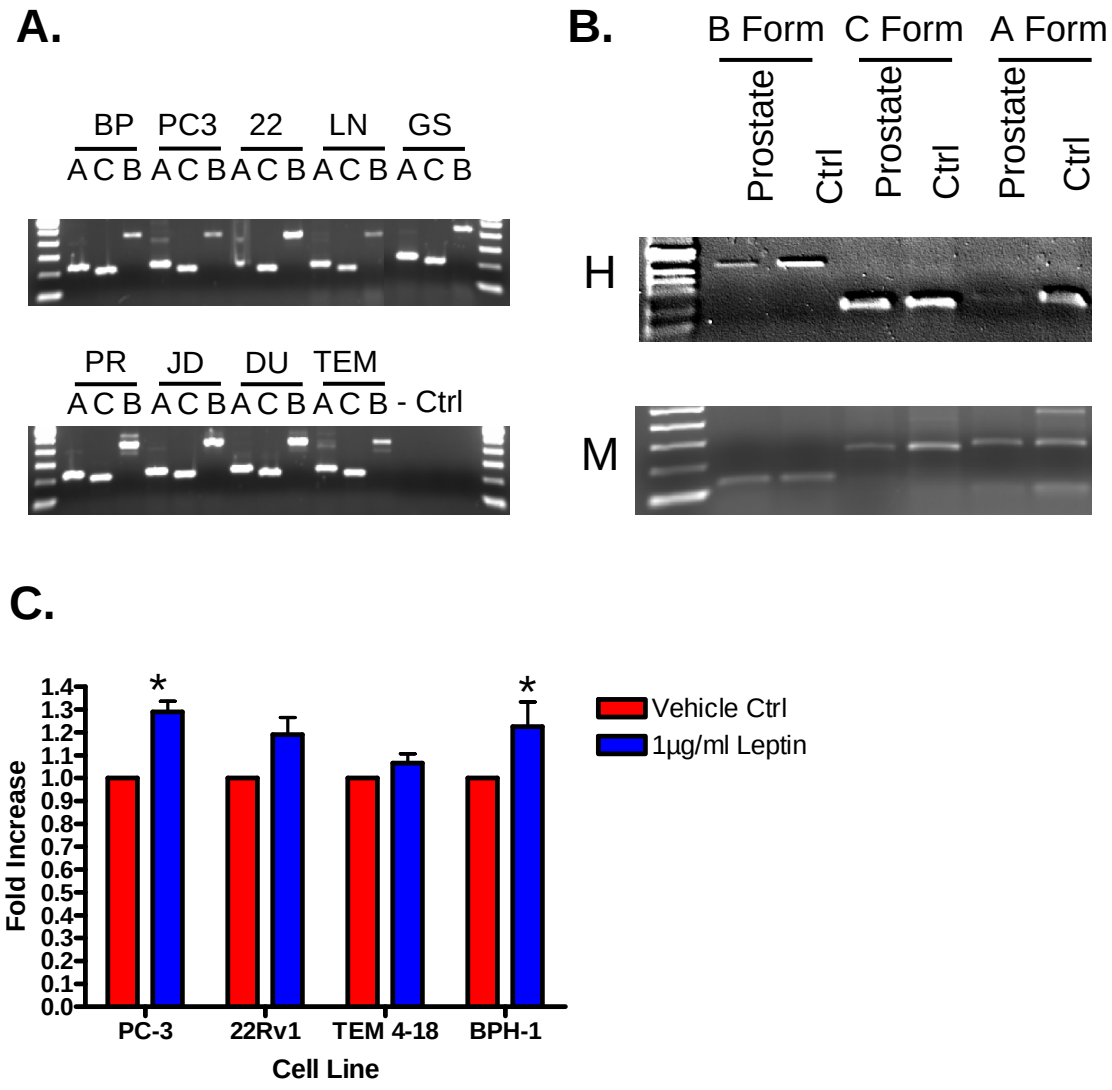

Figure 7.4: **Leptin receptor mRNA expression and effects of leptin on prostate cancer cell growth.** (A) PCR analysis for Leptin receptor mRNA expression (A,B and C forms) in BPH1 (BP), PC3, 22Rv1 (22), LNCap (LN), GS683 (GS), PREC (PR), JD33 (JD), DU145 (DU) and TEM418 (TEM) prostate cancer cells. All receptor isoforms are expressed at the mRNA level. (B) mRNA leptin receptor expression in human (H) and mouse (M) prostate tissue. All isoforms are expressed in both human and mouse tissue. (C) Effects of leptin on growth of prostate cancer cells *in vitro*. Leptin has moderate growth promoting properties on PC3 and BPH1 cells 5 days after treatment. Data represented as fold change of leptin treatment vs vehicle control. Significant increases in growth denoted by asterisks; *p<0.05, **p<0.01

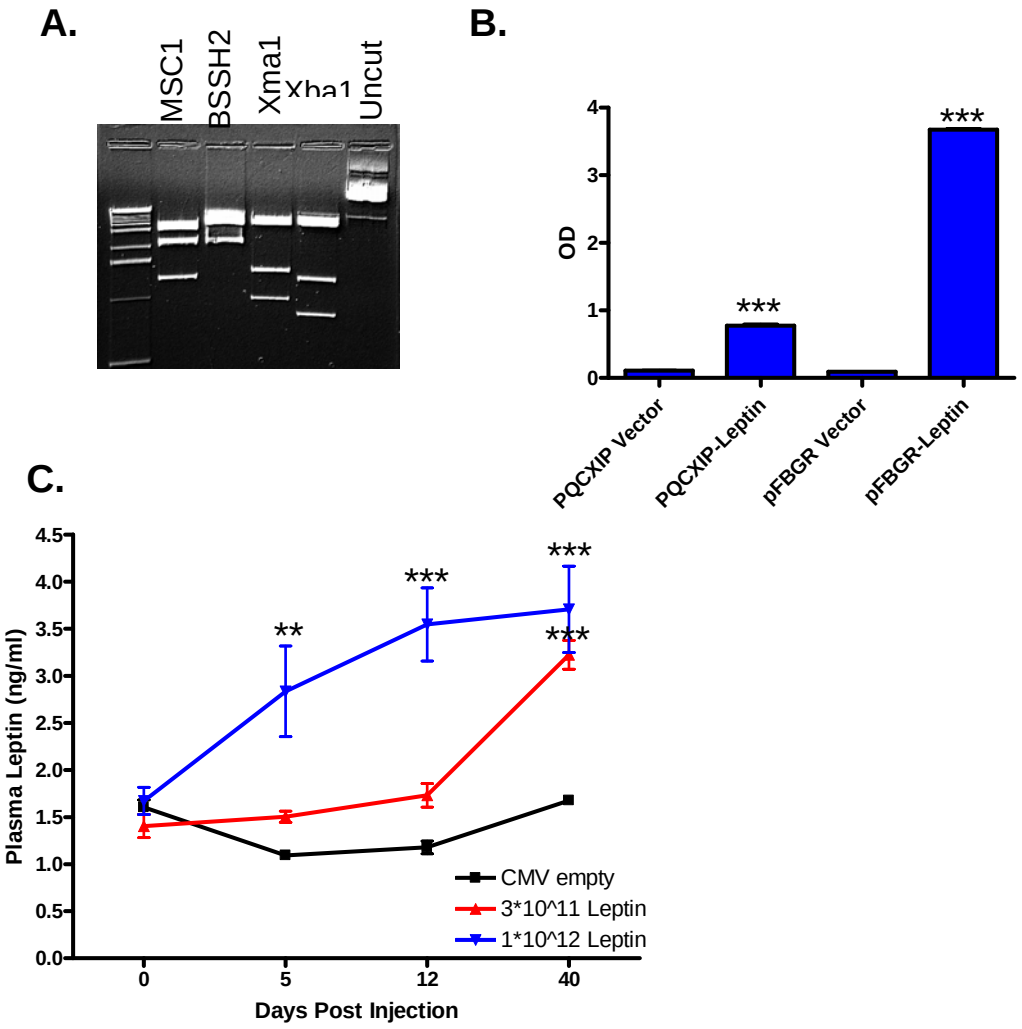

Figure 7.5: **Construction and efficacy of AAV8-Leptin *in vitro* and *in vivo*.** (A) Restriction digest analysis of pFBGR-Leptin. Product sizes were as expected indicating that no ITR recombination ad occurred. (B) HEPGS cells were transfected with pQXIP-Leptin, pFBGR-Leptin or vector controls and analyzed for leptin production by ELISA. Leptin.. Transfection of pFBGR-Leptin significantly increased HEPG2 leptin production. (C) SCID mice were injected with either 3*10^11, 1*10^12vg AAV8-leptin or 1*10^12vg CMV empty and analyzed for plasma leptin levels. AAV8-Leptin significantly increased plasma leptin levels compared to CMV empty. Significant increases in leptin levels relative to controls are denoted by asterisks *p<0.05, **p<0.01, ***p<0.001

REFERENCES

Akinc, A., M. Goldberg, et al. (2009). "Development of lipidoid-siRNA formulations for systemic delivery to the liver." Mol Ther **17**(5): 872-9.

Akinc, A., A. Zumbuehl, et al. (2008). "A combinatorial library of lipid-like materials for delivery of RNAi therapeutics." Nat Biotechnol **26**(5): 561-9.

Ameres, S. L., J. Martinez, et al. (2007). "Molecular basis for target RNA recognition and cleavage by human RISC." Cell **130**(1): 101-12.

Amling, C. L., R. H. Riffenburgh, et al. (2004). "Pathologic variables and recurrence rates as related to obesity and race in men with prostate cancer undergoing radical prostatectomy." J Clin Oncol **22**(3): 439-45.

Andersson, S. O., A. Wolk, et al. (1997). "Body size and prostate cancer: a 20-year follow-up study among 135006 Swedish construction workers." J Natl Cancer Inst **89**(5): 385-9.

Attar, R. M., C. H. Takimoto, et al. (2009). "Castration-resistant prostate cancer: locking up the molecular escape routes." Clin Cancer Res **15**(10): 3251-5.

Bacus, S. S., A. V. Gudkov, et al. (2001). "Taxol-induced apoptosis depends on MAP kinase pathways (ERK and p38) and is independent of p53." Oncogene **20**(2): 147-55.

Bairati, I., F. Meyer, et al. (1998). "Dietary fat and advanced prostate cancer." J Urol **159**(4): 1271-5.

Balkwill, F. and A. Mantovani (2001). "Inflammation and cancer: back to Virchow?" Lancet **357**(9255): 539-45.

Bastard, J. P., M. Maachi, et al. (2006). "Recent advances in the relationship between obesity, inflammation, and insulin resistance." Eur Cytokine Netw **17**(1): 4-12.

Baumjohann, D. and M. B. Lutz (2006). "Non-invasive imaging of dendritic cell migration in vivo." Immunobiology **211**(6-8): 587-97.

Behlke, M. A. (2006). "Progress towards in vivo use of siRNAs." Mol Ther **13**(4): 644-70.

Bernstein, E., A. A. Caudy, et al. (2001). "Role for a bidentate ribonuclease in the initiation step of RNA interference." Nature **409**(6818): 363-6.

Birmingham, A., E. M. Anderson, et al. (2006). "3' UTR seed matches, but not overall identity, are associated with RNAi off-targets." Nat Methods **3**(3): 199-204.

Bitko, V., A. Musiyenko, et al. (2005). "Inhibition of respiratory viruses by nasally administered siRNA." Nat Med **11**(1): 50-5.

Boese, Q., D. Leake, et al. (2005). "Mechanistic insights aid computational short interfering RNA design." Methods Enzymol **392**: 73-96.

Borley, N. and M. R. Feneley (2009). "Prostate cancer: diagnosis and staging." Asian J Androl **11**(1): 74-80.

Boyd, D. B. (2003). "Insulin and cancer." Integr Cancer Ther **2**(4): 315-29.

Bridge, A. J., S. Pebernard, et al. (2003). "Induction of an interferon response by RNAi vectors in mammalian cells." Nat Genet **34**(3): 263-4.

Bruening, W., B. Giasson, et al. (1998). "Activation of stress-activated MAP protein kinases up-regulates expression of transgenes driven by the cytomegalovirus immediate/early promoter." Nucleic Acids Res **26**(2): 486-9.

Buchanan, G., N. M. Greenberg, et al. (2001). "Collocation of androgen receptor gene mutations in prostate cancer." Clin Cancer Res **7**(5): 1273-81.

Buchhorn, H. M., C. Seidl, et al. (2007). "Non-invasive visualisation of the development of peritoneal carcinomatosis and tumour regression after (213)Bi-radioimmunotherapy using bioluminescence imaging." Eur J Nucl Med Mol Imaging.

Buessow, S. C., R. D. Paul, et al. (1984). "Influence of mammary tumor progression on phenotype and function of spleen and in situ lymphocytes in mice." J Natl Cancer Inst **73**(1): 249-55.

Bumcrot, D., M. Manoharan, et al. (2006). "RNAi therapeutics: a potential new class of pharmaceutical drugs." Nat Chem Biol **2**(12): 711-9.

Bunt, S. K., P. Sinha, et al. (2006). "Inflammation induces myeloid-derived suppressor cells that facilitate tumor progression." J Immunol **176**(1): 284-90.

Bunt, S. K., L. Yang, et al. (2007). "Reduced inflammation in the tumor microenvironment delays the accumulation of myeloid-derived suppressor cells and limits tumor progression." Cancer Res **67**(20): 10019-26.

Calle, E. E., C. Rodriguez, et al. (2003). "Overweight, obesity, and mortality from cancer in a prospectively studied cohort of U.S. adults." N Engl J Med **348**(17): 1625-38.

Cao, Y. A., M. H. Bachmann, et al. (2005). "Molecular imaging using labeled donor tissues reveals patterns of engraftment, rejection, and survival in transplantation." Transplantation **80**(1): 134-9.

Cao, Y. A., A. J. Wagers, et al. (2004). "Shifting foci of hematopoiesis during reconstitution from single stem cells." Proc Natl Acad Sci U S A **101**(1): 221-6.

Carlsen, H., J. O. Moskaug, et al. (2002). "In vivo imaging of NF-kappa B activity." J Immunol **168**(3): 1441-6.

Carracedo, A., L. Ma, et al. (2008). "Inhibition of mTORC1 leads to MAPK pathway activation through a PI3K-dependent feedback loop in human cancer." J Clin Invest **118**(9): 3065-74.

Carracedo, A. and P. P. Pandolfi (2008). "The *Pten*-PI3K pathway: of feedbacks and cross-talks." Oncogene **27**(41): 5527-41.

Carroll, L., J. Voisey, et al. (2004). "Mouse models of obesity." Clin Dermatol **22**(4): 345-9.

Chan, R., K. Lok, et al. (2009). "Prostate cancer and vegetable consumption." Mol Nutr Food Res **53**(2): 201-16.

Chen, C. D., D. S. Welsbie, et al. (2004). "Molecular determinants of resistance to antiandrogen therapy." Nat Med **10**(1): 33-9.

Chen, J. and M. F. Stinski (2002). "Role of regulatory elements and the MAPK/ERK or p38 MAPK pathways for activation of human cytomegalovirus gene expression." J Virol **76**(10): 4873-85.

Chen, Z., L. C. Trotman, et al. (2005). "Crucial role of p53-dependent cellular senescence in suppression of Pten-deficient tumorigenesis." Nature **436**(7051): 725-30.

Choi, J., J. Chen, et al. (1996). "Structure of the FKBP12-rapamycin complex interacting with the binding domain of human FRAP." Science **273**(5272): 239-42.

Choung, S., Y. J. Kim, et al. (2006). "Chemical modification of siRNAs to improve serum stability without loss of efficacy." Biochem Biophys Res Commun **342**(3): 919-27.

Clark, C. E., S. R. Hingorani, et al. (2007). "Dynamics of the immune reaction to pancreatic cancer from inception to invasion." Cancer Res **67**(19): 9518-27.

Colabufo, N. A., V. Pagliarulo, et al. (2008). "Bicalutamide failure in prostate cancer treatment: involvement of Multi Drug Resistance proteins." Eur J Pharmacol **601**(1-3): 38-42.

Contag, C. H. (2000). "Use of reporter genes for optical measurements of neoplastic disease in vivo." Neoplasia **2**(1-2): 41-52.

Contag, C. H., S. D. Spilman, et al. (1997). "Visualizing gene expression in living mammals using a bioluminescent reporter." Photochem Photobiol **66**(4): 523-31.

Coussens, L. M. and Z. Werb (2002). "Inflammation and cancer." Nature **420**(6917): 860-7.

Culig, Z., A. Hobisch, et al. (1994). "Androgen receptor activation in prostatic tumor cell lines by insulin-like growth factor-I, keratinocyte growth factor, and epidermal growth factor." Cancer Res **54**(20): 5474-8.

Cunha, G. R., S. W. Hayward, et al. (2003). "Role of the stromal microenvironment in carcinogenesis of the prostate." Int J Cancer **107**(1): 1-10.

Dancey, J. E. (2006). "Therapeutic targets: MTOR and related pathways." Cancer Biol Ther **5**(9): 1065-73.

Dassie, J. P., X. Y. Liu, et al. (2009). "Systemic administration of optimized aptamer-siRNA chimeras promotes regression of PSMA-expressing tumors." Nat Biotechnol **27**(9): 839-49.

de Bernabe, D. B., K. Inamori, et al. (2009). "Loss of alpha-dystroglycan laminin binding in epithelium-derived cancers is caused by silencing of LARGE." J Biol Chem **284**(17): 11279-84.

de Fougerolles, A., H. P. Vornlocher, et al. (2007). "Interfering with disease: a progress report on siRNA-based therapeutics." Nat Rev Drug Discov **6**(6): 443-53.

Delatour, N. L. and K. T. Mai (2008). "Positive predictive value of high-grade prostatic intraepithelial neoplasia in initial core needle biopsies of prostate adenocarcinoma--a study with complete sampling of hemi-prostates with corresponding negative biopsy findings." Urology **72**(3): 623-7.

Dimri, G. P., X. Lee, et al. (1995). "A biomarker that identifies senescent human cells in culture and in aging skin in vivo." Proc Natl Acad Sci U S A **92**(20): 9363-7.

Drake, J. M., C. L. Gabriel, et al. (2005). "Assessing tumor growth and distribution in a model of prostate cancer metastasis using bioluminescence imaging." Clin Exp Metastasis **22**(8): 674-84.

Drake, J. M., G. Strohbehn, et al. (2009). "ZEB1 Enhances Transendothelial Migration and Represses the Epithelial Phenotype of Prostate Cancer Cells." Mol Biol Cell.

Easton, J. B. and P. J. Houghton (2006). "mTOR and cancer therapy." Oncogene **25**(48): 6436-46.

Edinger, M., Y. A. Cao, et al. (2003). "Revealing lymphoma growth and the efficacy of immune cell therapies using in vivo bioluminescence imaging." Blood **101**(2): 640-8.

Edinger, M., T. J. Sweeney, et al. (1999). "Noninvasive assessment of tumor cell proliferation in animal models." Neoplasia **1**(4): 303-10.

Edwards, B. K., E. Ward, et al. "Annual report to the nation on the status of cancer, 1975-2006, featuring colorectal cancer trends and impact of interventions (risk factors, screening, and treatment) to reduce future rates." Cancer **116**(3): 544-73.

El Hilali, N., N. Rubio, et al. (2005). "Different effect of paclitaxel on primary tumor mass, tumor cell contents, and metastases for four experimental human prostate tumors expressing luciferase." Clin Cancer Res **11**(3): 1253-8.

Elbashir, S. M., J. Harborth, et al. (2001). "Duplexes of 21-nucleotide RNAs mediate RNA interference in cultured mammalian cells." Nature **411**(6836): 494-8.

Ellis, L. M. and D. J. Hicklin (2008). "VEGF-targeted therapy: mechanisms of anti-tumour activity." Nat Rev Cancer **8**(8): 579-91.

Ennis, B. W., K. E. Fultz, et al. (2005). "Inhibition of tumor growth, angiogenesis, and tumor cell proliferation by a small molecule inhibitor of c-Jun N-terminal kinase." J Pharmacol Exp Ther **313**(1): 325-32.

Esser, A. K., M. B. Cohen, et al. "Dystroglycan is not required for maintenance of the luminal epithelial basement membrane or cell polarity in the mouse prostate." Prostate.

Farooqi, S. and S. O'Rahilly (2006). "Genetics of obesity in humans." Endocr Rev **27**(7): 710-18.

Feldman, B. J. and D. Feldman (2001). "The development of androgen-independent prostate cancer." Nat Rev Cancer **1**(1): 34-45.

Feldman, M. E., B. Apsel, et al. (2009). "Active-site inhibitors of mTOR target rapamycin-resistant outputs of mTORC1 and mTORC2." PLoS Biol **7**(2): e38.

Fire, A., S. Xu, et al. (1998). "Potent and specific genetic interference by double-stranded RNA in Caenorhabditis elegans." Nature **391**(6669): 806-11.

Foster, F. S., P. N. Burns, et al. (2000). "Ultrasound for the visualization and quantification of tumor microcirculation." Cancer Metastasis Rev **19**(1-2): 131-8.

Freedland, S. J. and W. J. Aronson (2004). "Examining the relationship between obesity and prostate cancer." Rev Urol **6**(2): 73-81.

Freedland, S. J. and W. J. Aronson (2005). "Obesity and prostate cancer." Urology **65**(3): 433-9.

Freedland, S. J., W. J. Aronson, et al. (2004). "Impact of obesity on biochemical control after radical prostatectomy for clinically localized prostate cancer: a report by the Shared Equal Access Regional Cancer Hospital database study group." J Clin Oncol **22**(3): 446-53.

Freedland, S. J. and E. A. Platz (2007). "Obesity and prostate cancer: making sense out of apparently conflicting data." Epidemiol Rev **29**: 88-97.

Freeman, D., R. Lesche, et al. (2006). "Genetic background controls tumor development in *Pten*-deficient mice." Cancer Res **66**(13): 6492-6.

Freeman, K. W., B. E. Welm, et al. (2003). "Inducible prostate intraepithelial neoplasia with reversible hyperplasia in conditional FGFR1-expressing mice." Cancer Res **63**(23): 8256-63.

Friedrich, G. and P. Soriano (1991). "Promoter traps in embryonic stem cells: a genetic screen to identify and mutate developmental genes in mice." Genes Dev **5**(9): 1513-23.

Gabrilovich, D. I. and S. Nagaraj (2009). "Myeloid-derived suppressor cells as regulators of the immune system." Nat Rev Immunol **9**(3): 162-74.

Gao, H., X. Ouyang, et al. (2006). "Combinatorial activities of Akt and B-Raf/Erk signaling in a mouse model of androgen-independent prostate cancer." Proc Natl Acad Sci U S A **103**(39): 14477-82.

Gao, H., X. Ouyang, et al. (2006). "Emergence of androgen independence at early stages of prostate cancer progression in nkx3.1; pten mice." Cancer Res **66**(16): 7929-33.

Gao, X., M. P. LaValley, et al. (2005). "Prospective studies of dairy product and calcium intakes and prostate cancer risk: a meta-analysis." J Natl Cancer Inst **97**(23): 1768-77.

Garcia-Martinez, J. M., J. Moran, et al. (2009). "Ku-0063794 is a specific inhibitor of the mammalian target of rapamycin (mTOR)." Biochem J **421**(1): 29-42.

Gillies, R. J., Z. M. Bhujwalla, et al. (2000). "Applications of magnetic resonance in model systems: tumor biology and physiology." Neoplasia **2**(1-2): 139-51.

Gingrich, J. R., R. J. Barrios, et al. (1997). "Androgen-independent prostate cancer progression in the TRAMP model." Cancer Res **57**(21): 4687-91.

Giovannucci, E., E. B. Rimm, et al. (2003). "Body mass index and risk of prostate cancer in U.S. health professionals." J Natl Cancer Inst **95**(16): 1240-4.

Giovannucci, E., E. B. Rimm, et al. (1997). "Height, body weight, and risk of prostate cancer." Cancer Epidemiol Biomarkers Prev **6**(8): 557-63.

Gittes, R. F. (1991). "Carcinoma of the prostate." N Engl J Med **324**(4): 236-45.

Gleason, D. F. and G. T. Mellinger (1974). "Prediction of prognosis for prostatic adenocarcinoma by combined histological grading and clinical staging." J Urol **111**(1): 58-64.

Gong, Z., I. Agalliu, et al. (2007). "Obesity is associated with increased risks of prostate cancer metastasis and death after initial cancer diagnosis in middle-aged men." Cancer **109**(6): 1192-202.

Greenberg, N. M., F. DeMayo, et al. (1995). "Prostate cancer in a transgenic mouse." Proc Natl Acad Sci U S A **92**(8): 3439-43.

Gregory, C. W., R. T. Johnson, Jr., et al. (2001). "Androgen receptor stabilization in recurrent prostate cancer is associated with hypersensitivity to low androgen." Cancer Res **61**(7): 2892-8.

Grethe, S., N. Coltella, et al. (2006). "p38 MAPK downregulates phosphorylation of Bad in doxorubicin-induced endothelial apoptosis." Biochem Biophys Res Commun **347**(3): 781-90.

Gronberg, H. (2003). "Prostate cancer epidemiology." Lancet **361**(9360): 859-64.

Gross, S. and D. Piwnica-Worms (2005). "Real-time imaging of ligand-induced IKK activation in intact cells and in living mice." Nat Methods **2**(8): 607-14.

Gross, S. and D. Piwnica-Worms (2005). "Spying on cancer: molecular imaging in vivo with genetically encoded reporters." Cancer Cell **7**(1): 5-15.

Gu, Z. and M. Cole (2007). Transgenic *ROSA26*-lucifrease mice for bioluminescent imaging. US, Genentech, Inc.

Guertin, D. A. and D. M. Sabatini (2009). "The pharmacology of mTOR inhibition." Sci Signal **2**(67): pe24.

Guertin, D. A., D. M. Stevens, et al. (2009). "mTOR complex 2 is required for the development of prostate cancer induced by Pten loss in mice." Cancer Cell **15**(2): 148-59.

Haggman, M. J., J. A. Macoska, et al. (1997). "The relationship between prostatic intraepithelial neoplasia and prostate cancer: critical issues." J Urol **158**(1): 12-22.

Hara, K., Y. Maruki, et al. (2002). "Raptor, a binding partner of target of rapamycin (TOR), mediates TOR action." Cell **110**(2): 177-89.

Haslam, D. W. and W. P. James (2005). "Obesity." Lancet **366**(9492): 1197-209.

Henry, M. D. and K. P. Campbell (1996). "Dystroglycan: an extracellular matrix receptor linked to the cytoskeleton." Curr Opin Cell Biol **8**(5): 625-31.

Henry, M. D., M. B. Cohen, et al. (2001). "Reduced expression of dystroglycan in breast and prostate cancer." Hum Pathol **32**(8): 791-5.

Henry, M. D., S. Wen, et al. (2004). "A prostate-specific membrane antigen-targeted monoclonal antibody-chemotherapeutic conjugate designed for the treatment of prostate cancer." Cancer Res **64**(21): 7995-8001.

Hewitt, J. E. (2009). "Abnormal glycosylation of dystroglycan in human genetic disease." Biochim Biophys Acta **1792**(9): 853-61.

Hirano, D., Y. Okada, et al. (2004). "Neuroendocrine differentiation in hormone refractory prostate cancer following androgen deprivation therapy." Eur Urol **45**(5): 586-92; discussion 592.

Hornung, V., M. Guenthner-Biller, et al. (2005). "Sequence-specific potent induction of IFN-alpha by short interfering RNA in plasmacytoid dendritic cells through TLR7." Nat Med **11**(3): 263-70.

Hsieh, C. L., Z. Xie, et al. (2007). "Non-invasive bioluminescent detection of prostate cancer growth and metastasis in a bigenic transgenic mouse model." Prostate **67**(7): 685-91.

Hsing, A. W. and A. P. Chokkalingam (2006). "Prostate cancer epidemiology." Front Biosci **11**: 1388-413.

Huang, C., W. Y. Ma, et al. (1997). "Blocking activator protein-1 activity, but not activating retinoic acid response element, is required for the antitumor promotion effect of retinoic acid." Proc Natl Acad Sci U S A **94**(11): 5826-30.

Huffman, D. M., M. S. Johnson, et al. (2007). "Cancer progression in the transgenic adenocarcinoma of mouse prostate mouse is related to energy balance, body mass, and body composition, but not food intake." Cancer Res **67**(1): 417-24.

Huggins, C. (1967). "Endocrine-induced regression of cancers." Science **156**(3778): 1050-4.

Huggins, C. (1967). "Endocrine-induced regression of cancers." Cancer Res **27**(11): 1925-30.

Huggins, C. and C. V. Hodges (1972). "Studies on prostatic cancer. I. The effect of castration, of estrogen and androgen injection on serum phosphatases in metastatic carcinoma of the prostate." CA Cancer J Clin **22**(4): 232-40.

Isaacs, J. T. (1999). "The biology of hormone refractory prostate cancer. Why does it develop?" Urol Clin North Am **26**(2): 263-73.

Isshiki, S., K. Akakura, et al. (2002). "Chromogranin a concentration as a serum marker to predict prognosis after endocrine therapy for prostate cancer." J Urol **167**(2 Pt 1): 512-5.

Jacinto, E., R. Loewith, et al. (2004). "Mammalian TOR complex 2 controls the actin cytoskeleton and is rapamycin insensitive." Nat Cell Biol **6**(11): 1122-8.

Jackson, A. L., S. R. Bartz, et al. (2003). "Expression profiling reveals off-target gene regulation by RNAi." Nat Biotechnol **21**(6): 635-7.

Jackson, A. L., J. Burchard, et al. (2006). "Widespread siRNA "off-target" transcript silencing mediated by seed region sequence complementarity." Rna **12**(7): 1179-87.

Jemal, A., R. Siegel, et al. (2009). "Cancer statistics, 2009." CA Cancer J Clin **59**(4): 225-49.

Jenkins, D. E., Y. Oei, et al. (2003). "Bioluminescent imaging (BLI) to improve and refine traditional murine models of tumor growth and metastasis." Clin Exp Metastasis **20**(8): 733-44.

Jenkins, D. E., S. F. Yu, et al. (2003). "In vivo monitoring of tumor relapse and metastasis using bioluminescent PC-3M-luc-C6 cells in murine models of human prostate cancer." Clin Exp Metastasis **20**(8): 745-56.

Jequier, E. (2002). "Leptin signaling, adiposity, and energy balance." Ann N Y Acad Sci **967**: 379-88.

John, M., R. Constien, et al. (2007). "Effective RNAi-mediated gene silencing without interruption of the endogenous microRNA pathway." Nature **449**(7163): 745-7.

Johnson, R. A., S. M. Huong, et al. (2000). "Activation of the mitogen-activated protein kinase p38 by human cytomegalovirus infection through two distinct pathways: a novel mechanism for activation of p38." J Virol **74**(3): 1158-67.

Kaneko, K., M. Yano, et al. (2001). "Detection of peritoneal micrometastases of gastric carcinoma with green fluorescent protein and carcinoembryonic antigen promoter." Cancer Res **61**(14): 5570-4.

Kasper, S. (2005). "Survey of genetically engineered mouse models for prostate cancer: analyzing the molecular basis of prostate cancer development, progression, and metastasis." J Cell Biochem **94**(2): 279-97.

Kasper, S., P. C. Sheppard, et al. (1998). "Development, progression, and androgen-dependence of prostate tumors in probasin-large T antigen transgenic mice: a model for prostate cancer." Lab Invest **78**(3): 319-33.

Kawata, H., N. Ishikura, et al. "Prolonged treatment with bicalutamide induces androgen receptor overexpression and androgen hypersensitivity." Prostate.

Kim, D., C. F. Hung, et al. (2007). "Monitoring the trafficking of adoptively transferred antigen- specific CD8-positive T cells in vivo, using noninvasive luminescence imaging." Hum Gene Ther **18**(7): 575-88.

Kim, D. H., D. D. Sarbassov, et al. (2002). "mTOR interacts with raptor to form a nutrient-sensitive complex that signals to the cell growth machinery." Cell **110**(2): 163-75.

Klein, E. A., J. Ciezki, et al. (2009). "Outcomes for intermediate risk prostate cancer: are there advantages for surgery, external radiation, or brachytherapy?" Urol Oncol **27**(1): 67-71.

Knudson, A. G., Jr. (1971). "Mutation and cancer: statistical study of retinoblastoma." Proc Natl Acad Sci U S A **68**(4): 820-3.

Kobayashi, N., R. J. Barnard, et al. (2008). "Effect of low-fat diet on development of prostate cancer and Akt phosphorylation in the Hi-Myc transgenic mouse model." Cancer Res **68**(8): 3066-73.

Krek, A., D. Grun, et al. (2005). "Combinatorial microRNA target predictions." Nat Genet **37**(5): 495-500.

Labrie, F., A. Dupont, et al. (1982). "New hormonal therapy in prostatic carcinoma: combined treatment with an LHRH agonist and an antiandrogen." Clin Invest Med **5**(4): 267-75.

Landen, C. N., Jr., A. Chavez-Reyes, et al. (2005). "Therapeutic EphA2 gene targeting in vivo using neutral liposomal small interfering RNA delivery." Cancer Res **65**(15): 6910-8.

Laxman, B., D. E. Hall, et al. (2002). "Noninvasive real-time imaging of apoptosis." Proc Natl Acad Sci U S A **99**(26): 16551-5.

Lee, I. M., H. D. Sesso, et al. (2001). "A prospective cohort study of physical activity and body size in relation to prostate cancer risk (United States)." Cancer Causes Control **12**(2): 187-93.

Lee, K. H., S. S. Byun, et al. (2003). "Cell uptake and tissue distribution of radioiodine labelled D-luciferin: implications for luciferase based gene imaging." Nucl Med Commun **24**(9): 1003-9.

Lesche, R., M. Groszer, et al. (2002). "Cre/loxP-mediated inactivation of the murine Pten tumor suppressor gene." Genesis **32**(2): 148-9.

Leung, G., I. F. Benzie, et al. (2002). "No effect of a high-fat diet on promotion of sex hormone-induced prostate and mammary carcinogenesis in the Noble rat model." Br J Nutr **88**(4): 399-409.

Levental, K. R., H. Yu, et al. (2009). "Matrix crosslinking forces tumor progression by enhancing integrin signaling." Cell **139**(5): 891-906.

Liao, C. P., C. Zhong, et al. (2007). "Mouse models of prostate adenocarcinoma with the capacity to monitor spontaneous carcinogenesis by bioluminescence or fluorescence." Cancer Res **67**(15): 7525-33.

Love, K. T., K. P. Mahon, et al. "Lipid-like materials for low-dose, in vivo gene silencing." Proc Natl Acad Sci U S A **107**(5): 1864-9.

Luker, G. D., C. M. Pica, et al. (2003). "Imaging 26S proteasome activity and inhibition in living mice." Nat Med **9**(7): 969-73.

Luker, G. D., V. Sharma, et al. (2002). "Noninvasive imaging of protein-protein interactions in living animals." Proc Natl Acad Sci U S A **99**(10): 6961-6.

Lukka, H., T. Waldron, et al. (2006). "Maximal androgen blockade for the treatment of metastatic prostate cancer--a systematic review." Curr Oncol **13**(3): 81-93.

Luo, M. C., D. Q. Zhang, et al. (2005). "An efficient intrathecal delivery of small interfering RNA to the spinal cord and peripheral neurons." Mol Pain **1**: 29.

Luukkaa, V., U. Pesonen, et al. (1998). "Inverse correlation between serum testosterone and leptin in men." J Clin Endocrinol Metab **83**(9): 3243-6.

Lyons, S. K., E. Lim, et al. (2006). "Noninvasive bioluminescence imaging of normal and spontaneously transformed prostate tissue in mice." Cancer Res **66**(9): 4701-7.

Lyons, S. K., R. Meuwissen, et al. (2003). "The generation of a conditional reporter that enables bioluminescence imaging of Cre/loxP-dependent tumorigenesis in mice." Cancer Res **63**(21): 7042-6.

Ma, J., H. Li, et al. (2008). "Prediagnostic body-mass index, plasma C-peptide concentration, and prostate cancer-specific mortality in men with prostate cancer: a long-term survival analysis." Lancet Oncol **9**(11): 1039-47.

Ma, R. W. and K. Chapman (2009). "A systematic review of the effect of diet in prostate cancer prevention and treatment." J Hum Nutr Diet **22**(3): 187-99; quiz 200-2.

Mackinnon, A. C., B. C. Yan, et al. (2009). "Molecular biology underlying the clinical heterogeneity of prostate cancer: an update." Arch Pathol Lab Med **133**(7): 1033-40.

MacLaren, D. C., S. S. Gambhir, et al. (1999). "Repetitive, non-invasive imaging of the dopamine D2 receptor as a reporter gene in living animals." Gene Ther **6**(5): 785-91.

Magheli, A. and A. L. Burnett (2009). "Erectile dysfunction following prostatectomy: prevention and treatment." Nat Rev Urol **6**(8): 415-27.

Majumder, P. K., J. J. Yeh, et al. (2003). "Prostate intraepithelial neoplasia induced by prostate restricted Akt activation: the MPAKT model." Proc Natl Acad Sci U S A **100**(13): 7841-6.

Mandl, S., C. Schimmelpfennig, et al. (2002). "Understanding immune cell trafficking patterns via in vivo bioluminescence imaging." J Cell Biochem Suppl **39**: 239-48.

Mantovani, A., P. Allavena, et al. (2008). "Cancer-related inflammation." Nature **454**(7203): 436-44.

Marcelli, M., M. Ittmann, et al. (2000). "Androgen receptor mutations in prostate cancer." Cancer Res **60**(4): 944-9.

Maroulakou, I. G., M. Anver, et al. (1994). "Prostate and mammary adenocarcinoma in transgenic mice carrying a rat C3(1) simian virus 40 large tumor antigen fusion gene." Proc Natl Acad Sci U S A **91**(23): 11236-40.

Matranga, C., Y. Tomari, et al. (2005). "Passenger-strand cleavage facilitates assembly of siRNA into Ago2-containing RNAi enzyme complexes." Cell **123**(4): 607-20.

McDonnell, T. J., P. Troncoso, et al. (1992). "Expression of the protooncogene bcl-2 in the prostate and its association with emergence of androgen-independent prostate cancer." Cancer Res **52**(24): 6940-4.

McKenna, N. J., R. B. Lanz, et al. (1999). "Nuclear receptor coregulators: cellular and molecular biology." Endocr Rev **20**(3): 321-44.

McNamara, J. O., 2nd, E. R. Andrechek, et al. (2006). "Cell type-specific delivery of siRNAs with aptamer-siRNA chimeras." Nat Biotechnol **24**(8): 1005-15.

McNeal, J. E. (1988). "Normal histology of the prostate." Am J Surg Pathol **12**(8): 619-33.

Melder, R. J., L. L. Munn, et al. (2002). "Systemic distribution and tumor localization of adoptively transferred lymphocytes in mice: comparison with physiologically based pharmacokinetic model." Neoplasia **4**(1): 3-8.

Mellinger, G. T., D. Gleason, et al. (1967). "The histology and prognosis of prostatic cancer." J Urol **97**(2): 331-7.

Merglen, A., F. Schmidlin, et al. (2007). "Short- and long-term mortality with localized prostate cancer." Arch Intern Med **167**(18): 1944-50.

Merrimen, J. L., G. Jones, et al. (2009). "Multifocal high grade prostatic intraepithelial neoplasia is a significant risk factor for prostatic adenocarcinoma." J Urol **182**(2): 485-90; discussion 490.

Minakuchi, Y., F. Takeshita, et al. (2004). "Atelocollagen-mediated synthetic small interfering RNA delivery for effective gene silencing in vitro and in vivo." Nucleic Acids Res **32**(13): e109.

Mirosevich, J., N. Gao, et al. (2006). "Expression and role of Foxa proteins in prostate cancer." Prostate **66**(10): 1013-28.

Mulholland, D. J., L. Xin, et al. (2009). "Lin-Sca-1+CD49fhigh stem/progenitors are tumor-initiating cells in the Pten-null prostate cancer model." Cancer Res **69**(22): 8555-62.

Murillo, H., H. Huang, et al. (2001). "Role of PI3K signaling in survival and progression of LNCaP prostate cancer cells to the androgen refractory state." Endocrinology **142**(11): 4795-805.

Muschler, J., D. Levy, et al. (2002). "A role for dystroglycan in epithelial polarization: loss of function in breast tumor cells." Cancer Res **62**(23): 7102-9.

Nakamura, H., S. S. Siddiqui, et al. (2004). "RNA interference targeting transforming growth factor-beta type II receptor suppresses ocular inflammation and fibrosis." Mol Vis **10**: 703-11.

Napoli, C., C. Lemieux, et al. (1990). "Introduction of a Chimeric Chalcone Synthase Gene into Petunia Results in Reversible Co-Suppression of Homologous Genes in trans." Plant Cell **2**(4): 279-289.

Ngo, T. H., R. J. Barnard, et al. (2003). "Effect of isocaloric low-fat diet on human LAPC-4 prostate cancer xenografts in severe combined immunodeficient mice and the insulin-like growth factor axis." Clin Cancer Res **9**(7): 2734-43.

Ochiya, T., Y. Takahama, et al. (1999). "New delivery system for plasmid DNA in vivo using atelocollagen as a carrier material: the Minipellet." Nat Med **5**(6): 707-10.

Onuma, M., J. D. Bub, et al. (2003). "Prostate cancer cell-adipocyte interaction: leptin mediates androgen-independent prostate cancer cell proliferation through c-Jun NH2-terminal kinase." J Biol Chem **278**(43): 42660-7.

Ostrand-Rosenberg, S. and P. Sinha (2009). "Myeloid-derived suppressor cells: linking inflammation and cancer." J Immunol **182**(8): 4499-506.

Pal, A., A. Ahmad, et al. (2005). "Systemic delivery of RafsiRNA using cationic cardiolipin liposomes silences Raf-1 expression and inhibits tumor growth in xenograft model of human prostate cancer." Int J Oncol **26**(4): 1087-91.

Park, E. J., J. H. Lee, et al. "Dietary and genetic obesity promote liver inflammation and tumorigenesis by enhancing IL-6 and TNF expression." Cell **140**(2): 197-208.

Park, Y., P. N. Mitrou, et al. (2007). "Calcium, dairy foods, and risk of incident and fatal prostate cancer: the NIH-AARP Diet and Health Study." Am J Epidemiol **166**(11): 1270-9.

Parkin, D. M., P. Pisani, et al. (1999). "Global cancer statistics." CA Cancer J Clin **49**(1): 33-64, 1.

Paszek, M. J., N. Zahir, et al. (2005). "Tensional homeostasis and the malignant phenotype." Cancer Cell **8**(3): 241-54.

Patel, A. R. and E. A. Klein (2009). "Risk factors for prostate cancer." Nat Clin Pract Urol **6**(2): 87-95.

Percik, R. and M. Stumvoll (2009). "Obesity and cancer." Exp Clin Endocrinol Diabetes **117**(10): 563-6.

Petrylak, D. P., C. M. Tangen, et al. (2004). "Docetaxel and estramustine compared with mitoxantrone and prednisone for advanced refractory prostate cancer." N Engl J Med **351**(15): 1513-20.

Pfaffl, M. W. (2001). "A new mathematical model for relative quantification in real-time RT-PCR." Nucleic Acids Res **29**(9): e45.

Pienta, K. J., C. Abate-Shen, et al. (2008). "The current state of preclinical prostate cancer animal models." Prostate **68**(6): 629-39.

Prosch, S., K. Staak, et al. (1995). "Stimulation of the human cytomegalovirus IE enhancer/promoter in HL-60 cells by TNFalpha is mediated via induction of NF-kappaB." Virology **208**(1): 197-206.

Qiu, S., C. M. Adema, et al. (2005). "A computational study of off-target effects of RNA interference." Nucleic Acids Res **33**(6): 1834-47.

Radu, C. G., C. J. Shu, et al. (2008). "Molecular imaging of lymphoid organs and immune activation by positron emission tomography with a new [18F]-labeled 2'-deoxycytidine analog." Nat Med **14**(7): 783-8.

Rajala, M. W. and P. E. Scherer (2003). "Minireview: The adipocyte--at the crossroads of energy homeostasis, inflammation, and atherosclerosis." Endocrinology **144**(9): 3765-73.

Ramanathan, M., G. Hasko, et al. (2005). "Analysis of signal transduction pathways in macrophages using expression vectors with CMV promoters: a cautionary tale." Inflammation **29**(2-3): 94-102.

Rand, T. A., K. Ginalski, et al. (2004). "Biochemical identification of Argonaute 2 as the sole protein required for RNA-induced silencing complex activity." Proc Natl Acad Sci U S A **101**(40): 14385-9.

Rand, T. A., S. Petersen, et al. (2005). "Argonaute2 cleaves the anti-guide strand of siRNA during RISC activation." Cell **123**(4): 621-9.

Randolph, T. L., M. B. Amin, et al. (1997). "Histologic variants of adenocarcinoma and other carcinomas of prostate: pathologic criteria and clinical significance." Mod Pathol **10**(6): 612-29.

Rehemtulla, A., L. D. Stegman, et al. (2000). "Rapid and quantitative assessment of cancer treatment response using in vivo bioluminescence imaging." Neoplasia **2**(6): 491-5.

Rehemtulla, A., N. Taneja, et al. (2004). "Bioluminescence detection of cells having stabilized p53 in response to a genotoxic event." Mol Imaging **3**(1): 63-8.

Reich, S. J., J. Fosnot, et al. (2003). "Small interfering RNA (siRNA) targeting VEGF effectively inhibits ocular neovascularization in a mouse model." Mol Vis **9**: 210-6.

Reinhardt, H. C., A. S. Aslanian, et al. (2007). "p53-deficient cells rely on ATM- and ATR-mediated checkpoint signaling through the p38MAPK/MK2 pathway for survival after DNA damage." Cancer Cell **11**(2): 175-89.

Reznikoff, C. A., T. R. Yeager, et al. (1996). "Elevated p16 at senescence and loss of p16 at immortalization in human papillomavirus 16 E6, but not E7, transformed human uroepithelial cells." Cancer Res **56**(13): 2886-90.

Rodriguez, C., A. V. Patel, et al. (2001). "Body mass index, height, and prostate cancer mortality in two large cohorts of adult men in the United States." Cancer Epidemiol Biomarkers Prev **10**(4): 345-53.

Rokhlin, O. W., N. V. Guseva, et al. "KN-93 inhibits androgen receptor activity and induces cell death irrespective of p53 and Akt status in prostate cancer." Cancer Biol Ther **9**(3): 224-35.

Rokhlin, O. W., A. F. Taghiyev, et al. (2007). "Calcium/calmodulin-dependent kinase II plays an important role in prostate cancer cell survival." Cancer Biol Ther **6**(5): 732-42.

Rokhlin, O. W., A. F. Taghiyev, et al. (2002). "TRAIL-DISC formation is androgen-dependent in the human prostatic carcinoma cell line LNCaP." Cancer Biol Ther **1**(6): 631-7.

Roy-Burman, P., H. Wu, et al. (2004). "Genetically defined mouse models that mimic natural aspects of human prostate cancer development." Endocr Relat Cancer **11**(2): 225-54.

Rudin, M., M. Rausch, et al. (2005). "Molecular imaging in drug discovery and development: potential and limitations of nonnuclear methods." Mol Imaging Biol **7**(1): 5-13.

Safran, M., W. Y. Kim, et al. (2003). "Mouse reporter strain for noninvasive bioluminescent imaging of cells that have undergone Cre-mediated recombination." Mol Imaging **2**(4): 297-302.

Safran, M., W. Y. Kim, et al. (2006). "Mouse model for noninvasive imaging of HIF prolyl hydroxylase activity: assessment of an oral agent that stimulates erythropoietin production." Proc Natl Acad Sci U S A **103**(1): 105-10.

Saglam, K., E. Aydur, et al. (2003). "Leptin influences cellular differentiation and progression in prostate cancer." J Urol **169**(4): 1308-11.

Sakr, W. A., D. J. Grignon, et al. (1996). "Age and racial distribution of prostatic intraepithelial neoplasia." Eur Urol **30**(2): 138-44.

Sakr, W. A. and A. W. Partin (2001). "Histological markers of risk and the role of high-grade prostatic intraepithelial neoplasia." Urology **57**(4 Suppl 1): 115-20.

Sambucetti, L. C., J. M. Cherrington, et al. (1989). "NF-kappa B activation of the cytomegalovirus enhancer is mediated by a viral transactivator and by T cell stimulation." Embo J **8**(13): 4251-8.

Sarbassov, D. D., S. M. Ali, et al. (2004). "Rictor, a novel binding partner of mTOR, defines a rapamycin-insensitive and raptor-independent pathway that regulates the cytoskeleton." Curr Biol **14**(14): 1296-302.

Sarker, D., A. H. Reid, et al. (2009). "Targeting the PI3K/AKT pathway for the treatment of prostate cancer." Clin Cancer Res **15**(15): 4799-805.

Scatena, C. D., M. A. Hepner, et al. (2004). "Imaging of bioluminescent LNCaP-luc-M6 tumors: a new animal model for the study of metastatic human prostate cancer." Prostate **59**(3): 292-303.

Scher, H. I. (2003). "Prostate carcinoma: defining therapeutic objectives and improving overall outcomes." Cancer **97**(3 Suppl): 758-71.

Schroeder, T., H. Yuan, et al. (2005). "Spatial heterogeneity and oxygen dependence of glucose consumption in R3230Ac and fibrosarcomas of the Fischer 344 rat." Cancer Res **65**(12): 5163-71.

Semple, S. C., A. Akinc, et al. "Rational design of cationic lipids for siRNA delivery." Nat Biotechnol **28**(2): 172-6.

Serafini, P., K. Meckel, et al. (2006). "Phosphodiesterase-5 inhibition augments endogenous antitumor immunity by reducing myeloid-derived suppressor cell function." J Exp Med **203**(12): 2691-702.

Serrano, M., A. W. Lin, et al. (1997). "Oncogenic ras provokes premature cell senescence associated with accumulation of p53 and p16INK4a." Cell **88**(5): 593-602.

Severi, G., D. R. English, et al. (2006). "Re: Prospective studies of dairy product and calcium intakes and prostate cancer risk: a meta-analysis." J Natl Cancer Inst **98**(11): 794-5; author reply 795.

Shah, K., C. H. Tung, et al. (2005). "In vivo imaging of S-TRAIL-mediated tumor regression and apoptosis." Mol Ther **11**(6): 926-31.

Shariat, S. F., P. T. Scardino, et al. (2008). "Screening for prostate cancer: an update." Can J Urol **15**(6): 4363-74.

Sharpless, N. E. and R. A. Depinho (2006). "The mighty mouse: genetically engineered mouse models in cancer drug development." Nat Rev Drug Discov **5**(9): 741-54.

Shirodkar, S. P., T. A. Kishore, et al. (2009). "The risk and prophylactic management of bladder cancer after various forms of radiotherapy." Curr Opin Urol **19**(5): 500-3.

Shor, B., J. J. Gibbons, et al. (2009). "Targeting mTOR globally in cancer: thinking beyond rapamycin." Cell Cycle **8**(23): 3831-7.

Singh, M. and L. Johnson (2006). "Using genetically engineered mouse models of cancer to aid drug development: an industry perspective." Clin Cancer Res **12**(18): 5312-28.

Somasundar, P., A. K. Yu, et al. (2003). "Differential effects of leptin on cancer in vitro." J Surg Res **113**(1): 50-5.

Song, E., P. Zhu, et al. (2005). "Antibody mediated in vivo delivery of small interfering RNAs via cell-surface receptors." Nat Biotechnol **23**(6): 709-17.

Song, Q., M. Wang, et al. (2002). "[Effect of propofol on protecting Rhesus macaques from reperfusion lung injury during hemorrhagic shock and resuscitation]." Zhonghua Yi Xue Za Zhi **82**(17): 1203-6.

Song, X., Y. Krelin, et al. (2005). "CD11b+/Gr-1+ immature myeloid cells mediate suppression of T cells in mice bearing tumors of IL-1beta-secreting cells." J Immunol **175**(12): 8200-8.

Song, Z., X. Wu, et al. (2002). "Fibroblast growth factor 8 isoform B overexpression in prostate epithelium: a new mouse model for prostatic intraepithelial neoplasia." Cancer Res **62**(17): 5096-105.

Soriano, P. (1999). "Generalized lacZ expression with the *ROSA26* Cre reporter strain." Nat Genet **21**(1): 70-1.

Soutschek, J., A. Akinc, et al. (2004). "Therapeutic silencing of an endogenous gene by systemic administration of modified siRNAs." Nature **432**(7014): 173-8.

Spitz, M. R., R. D. Currier, et al. (1991). "Familial patterns of prostate cancer: a case-control analysis." J Urol **146**(5): 1305-7.

Sriprasad, S., M. R. Feneley, et al. (2009). "History of prostate cancer treatment." Surg Oncol **18**(3): 185-91.

Stattin, P., S. Soderberg, et al. (2001). "Leptin is associated with increased prostate cancer risk: a nested case-referent study." J Clin Endocrinol Metab **86**(3): 1341-5.

Stinski, M. F. (1999). Cytomegalovirus promoter for expression in mammalian cells. Gene expression systems: using nature for the art of expression. J. F. Fernandez and J. P. Hoeffler. San Diego, CA, Academic Press**:** 211-233.

Strom, S. S., A. M. Kamat, et al. (2006). "Influence of obesity on biochemical and clinical failure after external-beam radiotherapy for localized prostate cancer." Cancer **107**(3): 631-9.

Strom, S. S., X. Wang, et al. (2005). "Obesity, weight gain, and risk of biochemical failure among prostate cancer patients following prostatectomy." Clin Cancer Res **11**(19 Pt 1): 6889-94.

Svensson, R. U., J. M. Barnes, et al. (2007). "Chemotherapeutic agents up-regulate the cytomegalovirus promoter: implications for bioluminescence imaging of tumor response to therapy." Cancer Res **67**(21): 10445-54.

Svensson, R. U., M. R. Shey, et al. (2008). "Assessing siRNA pharmacodynamics in a luciferase-expressing mouse." Mol Ther **16**(12): 1995-2001.

Sweeney, T. J., V. Mailander, et al. (1999). "Visualizing the kinetics of tumor-cell clearance in living animals." Proc Natl Acad Sci U S A **96**(21): 12044-9.

Takeshita, F., Y. Minakuchi, et al. (2005). "Efficient delivery of small interfering RNA to bone-metastatic tumors by using atelocollagen in vivo." Proc Natl Acad Sci U S A **102**(34): 12177-82.

Tannock, I. F., R. de Wit, et al. (2004). "Docetaxel plus prednisone or mitoxantrone plus prednisone for advanced prostate cancer." N Engl J Med **351**(15): 1502-12.

Taplin, M. E., G. J. Bubley, et al. (1995). "Mutation of the androgen-receptor gene in metastatic androgen-independent prostate cancer." N Engl J Med **332**(21): 1393-8.

Tartaglia, L. A., M. Dembski, et al. (1995). "Identification and expression cloning of a leptin receptor, OB-R." Cell **83**(7): 1263-71.

Thakker, D. R., F. Natt, et al. (2004). "Neurochemical and behavioral consequences of widespread gene knockdown in the adult mouse brain by using nonviral RNA interference." Proc Natl Acad Sci U S A **101**(49): 17270-5.

Tjuvajev, J. G., R. Finn, et al. (1996). "Noninvasive imaging of herpes virus thymidine kinase gene transfer and expression: a potential method for monitoring clinical gene therapy." Cancer Res **56**(18): 4087-95.

Trotman, L. C., M. Niki, et al. (2003). "Pten dose dictates cancer progression in the prostate." PLoS Biol **1**(3): E59.

Troy, T., D. Jekic-McMullen, et al. (2004). "Quantitative comparison of the sensitivity of detection of fluorescent and bioluminescent reporters in animal models." Mol Imaging **3**(1): 9-23.

Uprichard, S. L., B. Boyd, et al. (2005). "Clearance of hepatitis B virus from the liver of transgenic mice by short hairpin RNAs." Proc Natl Acad Sci U S A **102**(3): 773-8.

Veierod, M. B., P. Laake, et al. (1997). "Dietary fat intake and risk of prostate cancer: a prospective study of 25,708 Norwegian men." Int J Cancer **73**(5): 634-8.

Visakorpi, T., E. Hyytinen, et al. (1995). "In vivo amplification of the androgen receptor gene and progression of human prostate cancer." Nat Genet **9**(4): 401-6.

Vooijs, M., J. Jonkers, et al. (2002). "Noninvasive imaging of spontaneous retinoblastoma pathway-dependent tumors in mice." Cancer Res **62**(6): 1862-7.

Wallace, D. M., G. D. Chisholm, et al. (1975). "T.N.M. classification for urological tumours (U.I.C.C.) - 1974." Br J Urol **47**(1): 1-12.

Walsh, P. C., H. Lepor, et al. (1983). "Radical prostatectomy with preservation of sexual function: anatomical and pathological considerations." Prostate **4**(5): 473-85.

Wang, S., J. Gao, et al. (2003). "Prostate-specific deletion of the murine Pten tumor suppressor gene leads to metastatic prostate cancer." Cancer Cell **4**(3): 209-21.

Wang, S., A. J. Garcia, et al. (2006). "Pten deletion leads to the expansion of a prostatic stem/progenitor cell subpopulation and tumor initiation." Proc Natl Acad Sci U S A **103**(5): 1480-5.

Wehrman, T. S., G. von Degenfeld, et al. (2006). "Luminescent imaging of beta-galactosidase activity in living subjects using sequential reporter-enzyme luminescence." Nat Methods **3**(4): 295-301.

Weinsier, R. L., G. R. Hunter, et al. (1998). "The etiology of obesity: relative contribution of metabolic factors, diet, and physical activity." Am J Med **105**(2): 145-50.

Welch, H. G. and P. C. Albertsen (2009). "Prostate cancer diagnosis and treatment after the introduction of prostate-specific antigen screening: 1986-2005." J Natl Cancer Inst **101**(19): 1325-9.

West, D. W., M. L. Slattery, et al. (1991). "Adult dietary intake and prostate cancer risk in Utah: a case-control study with special emphasis on aggressive tumors." Cancer Causes Control **2**(2): 85-94.

Weydert, C. J., A. K. Esser, et al. (2009). "Endothelin-1 inhibits prostate cancer growth in vivo through vasoconstriction of tumor-feeding arterioles." Cancer Biol Ther **8**(8): 720-9.

Willmann, J. K., N. van Bruggen, et al. (2008). "Molecular imaging in drug development." Nat Rev Drug Discov **7**(7): 591-607.

Wilsbacher, L. D., S. Yamazaki, et al. (2002). "Photic and circadian expression of luciferase in mPeriod1-luc transgenic mice invivo." Proc Natl Acad Sci U S A **99**(1): 489-94.

Winter, S. F., A. B. Cooper, et al. (2003). "Models of metastatic prostate cancer: a transgenic perspective." Prostate Cancer Prostatic Dis **6**(3): 204-11.

Wolfrum, C., S. Shi, et al. (2007). "Mechanisms and optimization of in vivo delivery of lipophilic siRNAs." Nat Biotechnol **25**(10): 1149-57.

Wright, M. E., S. C. Chang, et al. (2007). "Prospective study of adiposity and weight change in relation to prostate cancer incidence and mortality." Cancer **109**(4): 675-84.

Wu, J. C., G. Sundaresan, et al. (2001). "Noninvasive optical imaging of firefly luciferase reporter gene expression in skeletal muscles of living mice." Mol Ther **4**(4): 297-306.

Wu, X., J. Wu, et al. (2001). "Generation of a prostate epithelial cell-specific Cre transgenic mouse model for tissue-specific gene ablation." Mech Dev **101**(1-2): 61-9.

Wurdinger, T., C. Badr, et al. (2008). "A secreted luciferase for ex vivo monitoring of in vivo processes." Nat Methods **5**(2): 171-3.

Xie, F. Y., M. C. Woodle, et al. (2006). "Harnessing in vivo siRNA delivery for drug discovery and therapeutic development." Drug Discov Today **11**(1-2): 67-73.

Youn, J. I., S. Nagaraj, et al. (2008). "Subsets of myeloid-derived suppressor cells in tumor-bearing mice." J Immunol **181**(8): 5791-802.

Young, H. H. (1905). "VIII. Conservative Perineal Prostatectomy: The Results of Two Years' Experience and Report of Seventy-Five Cases." Ann Surg **41**(4): 549-57.

Young, M. R., M. Newby, et al. (1987). "Hematopoiesis and suppressor bone marrow cells in mice bearing large metastatic Lewis lung carcinoma tumors." Cancer Res **47**(1): 100-5.

Yu, K., C. Shi, et al. "Beyond rapalog therapy: preclinical pharmacology and antitumor activity of WYE-125132, an ATP-competitive and specific inhibitor of mTORC1 and mTORC2." Cancer Res **70**(2): 621-31.

Yu, K., L. Toral-Barza, et al. (2009). "Biochemical, cellular, and in vivo activity of novel ATP-competitive and selective inhibitors of the mammalian target of rapamycin." Cancer Res **69**(15): 6232-40.

Yuan, T. L. and L. C. Cantley (2008). "PI3K pathway alterations in cancer: variations on a theme." Oncogene **27**(41): 5497-510.

Zamaraeva, M. V., R. Z. Sabirov, et al. (2005). "Cells die with increased cytosolic ATP during apoptosis: a bioluminescence study with intracellular luciferase." Cell Death Differ **12**(11): 1390-7.

Zambrowicz, B. P., A. Imamoto, et al. (1997). "Disruption of overlapping transcripts in the ROSA beta geo 26 gene trap strain leads to widespread expression of beta-galactosidase in mouse embryos and hematopoietic cells." Proc Natl Acad Sci U S A **94**(8): 3789-94.

Zhang, W., J. Zhu, et al. (2009). "Inhibition of tumor growth progression by antiandrogens and mTOR inhibitor in a Pten-deficient mouse model of prostate cancer." Cancer Res **69**(18): 7466-72.

Zhang, Y., J. P. Bressler, et al. (2007). "ABCG2/BCRP expression modulates D-Luciferin based bioluminescence imaging." Cancer Res **67**(19): 9389-97.

Zhang, Y., R. Proenca, et al. (1994). "Positional cloning of the mouse obese gene and its human homologue." Nature **372**(6505): 425-32.

Zhao, F., S. Obermann, et al. (2009). "Increase in frequency of myeloid-derived suppressor cells in mice with spontaneous pancreatic carcinoma." Immunology **128**(1): 141-9.

Zimmermann, T. S., A. C. Lee, et al. (2006). "RNAi-mediated gene silencing in non-human primates." Nature.